NASA CONTRACTOR REPORT

NASA CR-1230



# ANALYTICAL AND EXPERIMENTAL STUDY OF THE DYNAMICS OF A SINGLE-TUBE COUNTERFLOW BOILER

*by H. L. Hess, J. R. Hooper, and S. L. Organ*

*Prepared by*
UNITED AIRCRAFT CORPORATION
East Hartford, Conn.
*for Lewis Research Center*

NATIONAL AERONAUTICS AND SPACE ADMINISTRATION • WASHINGTON, D. C. • FEBRUARY 1969

# ANALYTICAL AND EXPERIMENTAL STUDY OF THE DYNAMICS OF A SINGLE-TUBE COUNTERFLOW BOILER

By H. L. Hess, J. R. Hooper, and S. L. Organ



Prepared under Contract No. NAS 3-9420 by
UNITED AIRCRAFT CORPORATION
East Hartford, Conn.

for Lewis Research Center

NATIONAL AERONAUTICS AND SPACE ADMINISTRATION

For sale by the Clearinghouse for Federal Scientific and Technical Information
Springfield, Virginia 22151 – CFSTI price $3.00

## FOREWORD

This report was prepared by the Pratt & Whitney Aircraft Division of United Aircraft Corporation, East Hartford, Connecticut, to describe work conducted during the period from June 28, 1966 to August 27, 1967 in fulfillment of Contract NAS3-9420, A Boiler Dynamics Investigation. This contract consisted of a study of the transient response characteristics of a single-tube counterflow boiler. This boiler was designed to simulate one of the tubes of a typical boiler for a Rankine-cycle space powerplant.

Both analytical and experimental investigations were conducted. The experimental investigations were performed using a facility designed and built by Pratt & Whitney Aircraft which used water as the working fluid and was designed to simulate many fluid flow and heat transfer aspects of a space power conversion system.

The analytical work described in this report was performed by H. L. Hess, J. R. Hooper, and D. Reitsma, while the experimental work was performed by J. R. Hooper and S. E. Organ. Technical management was provided by H. G. Hurrell and technical assistance by A. A. Schoenberg and P. A. Thollot of the Lewis Research Center, National Aeronautics and Space Administration.

# ABSTRACT

An analytical and experimental study of a single-tube counterflow boiler was conducted. The boiler geometry simulated one of the tubes of a typical boiler for a Rankine-cycle space powerplant.

Steady-state, frequency-response, and step-response tests were conducted using water as the working fluid. The frequency-response and step-response tests were conducted by perturbing the boiling-fluid flow rate at the inlet to the boiler. Experimental transfer functions were obtained from the frequency-response test results.

A linearized analysis of the boiler dynamics was performed to derive a theoretical expression for the boiling-fluid exit pressure transfer function. A comparison was made between the theoretical and experimental transfer functions.

TABLE OF CONTENTS

TABLE OF CONTENTS (Cont'd)

# LIST OF FIGURES

# LIST OF FIGURES (Cont'd)

## LIST OF TABLES

# I. SUMMARY

An experimental and analytical investigation was conducted to study the steady-state and dynamic characteristics of a single-tube counterflow boiler. The purpose of the investigation was to determine the factors influencing the dynamic stability of this type of boiler and to provide information useful for developing dynamic stability criteria. The boiler was designed to simulate one tube of a typical Rankine-cycle space powerplant boiler. It was constructed and tested under this contract. The tests were performed on an experimental facility which simulated a nuclear Rankine-cycle power system. Water was employed as the working fluid in all three loops of the test system to facilitate testing. Three types of tests were performed: steady-state, frequency-response, and step-response. These tests showed how the steady-state and dynamic performance of the boiler varied as a function of the primary systemvariables. The steady-state tests also provided information useful in formulating an analysis of the boiler dynamics, while the frequency-response tests provided experimental data with which to evaluate the theoretical predictions of this analysis.

The experimental investigation indicated that the factors having strong influence on the boiler dynamics are reflected in the conditions of the boiling fluid at the boiler exit. During the testing three types of exit conditions were observed:

1) Dry superheated vapor
2) A nonequilibrium mist containing superheated vapor and liquid droplets,
3) A mist containing saturated vapor and liquid droplets.

In general, as the exit conditions changed in the direction from dry superheated vapor to wet saturated conditions, the result was a lower amplitude and a greater phase lag in boiler pressure and temperature responses, when perturbed at a given frequency by the boiling-fluid flow rate. General conclusions relating this frequency-response characteristic to dynamic stability were precluded by the presence of several pronounced resonances. The frequency-response tests did indicate, however, that instabilities arising from dynamic interactions between the boiler and the feed system could present a potential problem. This resulted from the fact that the amplitude of the frequency response of the boiler inlet pressure was relatively large at the 180-degree phase lag point for several test conditions. One such unstable condition was observed during the testing. In addition a second unstable condition was also observed during the testing. This instability can probably be attributed to dynamic interactions occurring within the boiler itself.

A linearized analysis of the boiler dynamics was performed. The result was an expression for the transfer function between the exit pressure and the inlet flow rate of the boiling fluid. This expression indicated that there were at least 22 different parameters that were significant in describing the dynamic behavior of the boiler. Agreement was found between the trends displayed by the experimental data and the theoretical predictions of the analysis. However, close

quantitative agreement between the theory and the experimental data, particularly in the frequency range where 180-degree phase lag occurs, was not obtained. Further development of the analysis appears desirable in order to develop a more useful analytical tool for predicting the stability of the dynamic interactions between the boiler and feed system.

## II. INTRODUCTION

Instabilities in boiling systems are very common and have been observed for many years. Unstable conditions in a Rankine-cycle powerplant can seriously impair the performance of the system and can, in some cases, cause actual destruction of equipment. Nuclear Rankine-cycle space powerplants such as SNAP-8, must operate continuously for 10,000 hours in deep space without a failure. As a consequence, the detrimental effects of unstable boiler operation cannot be tolerated by such a system. In the development of these powerplants, it is therefore desirable to be able to predict the stability of the boiler in the early design stages. This requires a fundamental understanding of both the causes of boiler instabilities and the physical processes involved.

A review of the literature on boiler stability, Reference 1*, indicates that many different types of instabilities have been observed. In general, these instabilities are very complex in nature and very difficult to analyze. Reference 1 indicates that the task of fully understanding boiler instabilities is still in its early stages.

An important class of boiler instabilities results from the dynamic characteristics of the boiler. These instabilities can result from dynamic interactions between the boiler and other components of the powerplant such as the boiler feed system. These instabilities can also result from dynamic interactions between the thermal and hydraulic processes occuring within the boiler itself. The work presented in this report studied the dynamic characteristics of a boiler having a geometry typical of the type employed in Rankine-cycle space powerplants. The purpose of the study was to provide fundamental information that would be employed in the development of methods for predicting the dynamic stability of this type of boiler.

The work performed under this contract followed both experimental and analytical approaches. A single-tube counterflow boiler employing a flow geometry which simulated one of the tubes of a typical space powerplant boiler was designed and constructed. The boiler was tested on an experimental facility which simulated a nuclear Rankine-cycle system. Water was used as the working fluid to facilitate testing. Three types of tests were performed: steady-state, frequency-response, and step-response.

The use of frequency-response techniques is based on the hypothesis that for small-amplitude disturbances the boiler, which is a non-linear device, can be treated as a linear element. The dynamics of the boiler can then be studied in

*See Page 92 for numbered list of references

terms of the manner in which it responds to small-amplitude perturbations imposed on the controllable variables. Since most boiler instabilities manifest themselves in the form of hydraulic disturbances, the boiling-fluid flow rate at the inlet to the boiler was selected as the variable to be perturbed. Frequency-response techniques have previously been employed successfully in the study of once-through boilers. These techniques were used in studies conducted at the NASA Lewis Research Center [2,3].

In the analytical approach a simplified linearized analysis of the dynamics of the boiler was performed. The result was a theoretical expression for the transfer function between the exit pressure and the inlet flow rate of the boiling fluid. A comparison was made between the frequency response predicted by this theoretical expression and the experimental frequency-response test results.

## III. TEST APPARATUS AND OPERATING PROCEDURES

The tests were conducted on a highly-instrumented boiler designed to simulate a single tube of a typical boiler for a nuclear Rankine-cycle space powerplant. The boiler was of a counterflow configuration and employed swirl flow-inducing devices typical of space powerplant boilers. However, unlike space powerplant boilers, the test boiler was of a single-tube construction. This was done to eliminate the type of boiler instabilities that result from multitube configurations.

The boiler was operated as part of a test system designed to simulate a nuclear Rankine-cycle powerplant. Water rather than a liquid metal was used as the working fluid to facilitate testing. This test system is a modified form of the transient simulator used in previous NASA contracts and described in Reference 4.

This section contains a detailed description of the boiler and its internal instrumentation, a description of the test rig including its instrumentation and controls, and a discussion of the operating procedures employed during both the steady-state and the dynamic tests.

### A. Description of Boiler

The construction of the boiler is shown in Figure 1. The boiler employed a single-tube counterflow configuration. The boiler tube and shell were fabricated from dimensionally selected 316 stainless-steel tubing. The boiler tube had an outside diameter of 0.625 inch and a wall thickness of 0.035 inch, while the boiler shell had an outside diameter of 0.875 inch and a wall thickness of 0.049 inch. The overall heat-transfer length was 10 feet.

Spacers on the boiler tube allowed it to be accurately centered in the shell during assembly. Machined fittings were employed at each end of the boiler. At the boiling-fluid exit both boiler and shell tubes were brazed to the fitting. At the inlet end the shell was brazed to the fitting, but the boiler tube was sealed with an O-ring packing nut arrangement which allowed for expansion and contraction of the boiler tube during operation.

The heating fluid was pressurized water which flowed through the annular passage between the boiler tube and the shell. Water was also used as the boiling fluid. As the boiling fluid entered the boiler tube, a swirl-flow pattern was induced by a close-fitting spirally-machined plug inserted into the inlet end of the boiler tube. The purpose of the swirl-flow pattern was to increase the heat-transfer coefficient of the boiling fluid. After the boiling fluid left the plug, a spirally-wound wire brazed inside the boiler tube maintained the swirl-flow pattern over the remaining length of the boiler.

The boiler employed extensive internal instrumentation to permit measurement of the axial temperature profiles of both the heating and boiling fluids. Fine wire thermocouples were mounted in the heating-fluid passage, the spiral-flow passage formed between the machined plug and the boiler tube, and along the tube axis downstream of the plug. The thermocouples used to measure the boiling-fluid temperature downstream of the plug were mounted on a probe of 0.250 inch outside diameter which was spaced concentrically with the axis of the boiler tube.

The positions of the spirally-machined plug and the thermocouple probe inside the boiler are shown in Figure 1. The following paragraphs present a more detailed description of the plug, the probe, and the boiler instrumentation. A discussion of thermal and hydraulic calculations employed in the design of this boiler is presented in Appendix 1.

1. Spiralled Plug Insert

A photograph of the spirally-machined plug insert is shown in Figure 2. The plug was fabricated from 316 stainless-steel stock. The plug length was 2.15 feet while the pitch of the spiral was 0.4 inch. The width of the spiral thread was 0.040 inch. The tolerance between the plug and the tube was held to within 0.002 inch to maintain a fit that would prevent leakage around the spiral thread.

A 0.310-inch passage was gun drilled through the spiralled-plug insert to carry the leads of the instrumentation. This passage was sealed at the downstream end by a cylindrical plug induction-brazed in place. This cylindrical plug was located one inch from the end of the passage to provide a centering recess for the thermocouple probe (see Figure 1). A tube of 0.375 inch outside diameter two feet long was brazed to the other end of the passage to act as a conduit for the instrumentation leads. An instrumentation junction block was attached to the end of this conduit as shown in Figure 2. Sealing between the conduit and the boiler tube was obtained by use of the heat exchanger tee shown in Figure 2. The heat exchanger tee also provided the inlet fitting for the boiling-fluid flow.

Instrumentation for the spiralled-plug insert consisted of eight thermocouples and a pressure tap. The thermocouples were positioned at equal lengths along the spiral path while the pressure tap was located near the downstream end of the insert. The holes drilled through the wall of the spiralled-plug insert to accommodate the thermocouples were inclined at an angle of 40 degrees from the axis of the insert, to avoid sharp bends that might break the thermocouple leads.

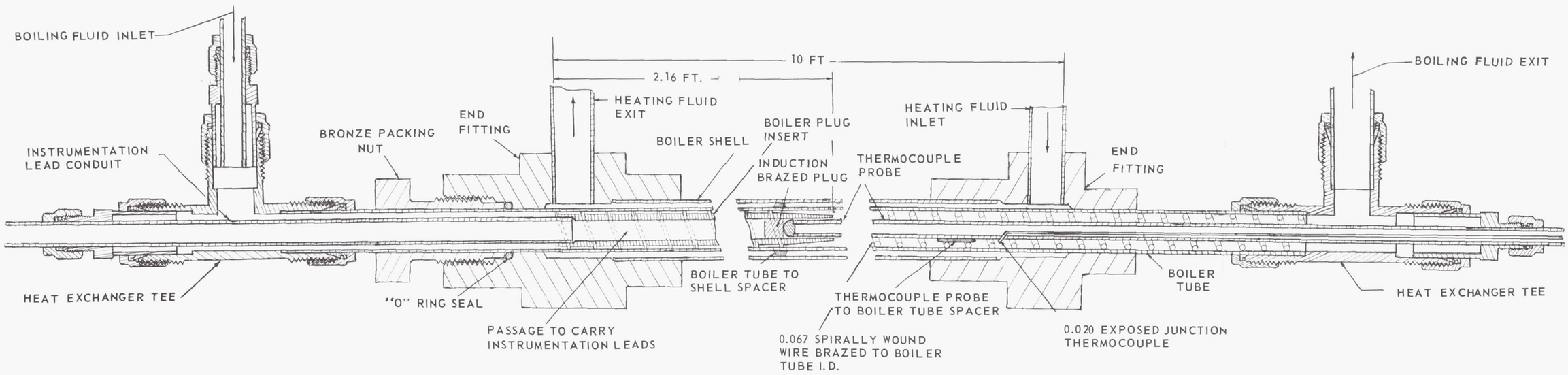


TABLE OF BOILER TUBE DIMENSIONS

BOILER SHELL 0.875"OD 0.049" WALL
BOILER TUBE 0.625"OD 0.035" WALL
BOILER PROBE 0.250"OD 0.049" WALL
INSTRUMENTATION LEAD CONDUIT
0.375OD 0.035" WALL
HEATER LOOP INLET TO BOILER
0.500"OD 0.049" WALL
HEATER LOOP EXIT FROM BOILER
0.625"OD 0.049" WALL

Figure 1 Sectional View of Boiler

Preceding Page Blank

2. Thermocouple Probe

The thermocouple probe was a nine-foot length of 316 stainless-steel tubing with an outside diameter of 0.250 inch and a wall thickness of 0.049 inch. Five thermocouples were mounted along the length of the thermocouple probe in the manner shown in Figure 1. The thermocouple junctions protruded into the fluid stream while the thermocouple leads were conducted along the inside of the probe. The holes for the thermocouples were drilled at an angle of 40 degrees from the probe axis.

Spacers were brazed to the probe at two-foot intervals. These spacers insured that the probe would be centered inside the boiler tube. One end of the probe was braze sealed. This end fitted into the centering recess of the plug. The length of the probe that projected into the boiler was 7.85 feet. Sealing between the boiler tube and the probe was accomplished by using a heat exchanger tee. The heat exchanger tee also provided the exit fitting for the boiling-fluid flow.

3. Boiler Instrumentation

Instrumentation was provided to measure the internal temperature distribution of the heating fluid and the boiling fluid. Provision was also made to measure the pressure of the boiling fluid at one location inside the boiler. Temperatures inside the boiler were measured with 0.020-inch chromel-alumel sheathed thermocouples. The wire diameter of the thermocouple was 3-4 mils. Two types of immersion thermocouples were used: one type where the junction was sealed within the sheath, and another type where the junction was exposed directly to the fluid. The exposed type of thermocouple provided a much faster response to changes in temperature.

In the boiler shell there were 20 immersion thermocouples with sealed junctions to measure the temperature of the heating fluid. Thermocouple positions are presented in Table 1, Appendix 4. The immersion length of the thermocouples was 0.250 inch. The thermocouple junction was centered in the annular passage between the boiler tube and the shell. A stainless-steel sheath having an outside diameter of 0.050 inch extended from the shell to the junction block of the thermocouple to protect the thermocouples from damage. Brazing was used to secure the thermocouples in position.

In the boiler tube there were thirteen exposed junction thermocouples to measure the boiling fluid temperature. Eight were located in the plug and five in the thermocouple probe (see Table 1 for the exact locations). In the plug the thermocouple wire was bent along the contour of the spiral passage and centered in the passage. This provided sufficient immersion depth to eliminate conduction errors. The probe thermocouples were also bent in the direction

of the boiler axis for the same purpose. Because of the nature of the exposed junction thermocouples they could not be brazed in position. Instead, they were sealed and positioned with a high-temperature resin. The thermocouple leads were brought out through the probe and plug and attached to junction blocks welded to the ends of the conduit tubes. This method prevented unnecessary movement and subsequent leakage around the junctions. These thermocouples installed inside of the boiler were very effective in measuring temperature distributions of both fluids. The temperature distributions provided a clear indication of the processes occurring within the boiler as discussed in Section IV below.

A static-pressure tap was located near the downstream end of the spiralled-plug insert in an effort to measure the static pressure of the boiling fluid in this region. The tap was approximately 0.016 inch in diameter. Hypodermic tubing with an outside diameter of 0.020 inch was used to connect the tap with a fitting on the instrumentation junction block shown in Figure 2. A tube 0.250 inch in outside diameter was used to connect this fitting with a Heise Bourdon-tube gage located in the control room. This pressure tap, however, did not provide satisfactory measurements. It took such an extremely long time to respond to changes in the system pressure that it could not be employed even for steady-state measurements. This problem may have resulted from plugging of the hypodermic tubing or from the small inside diameter of the tubing itself.

### B. Description of Test System

The test system was originally designed to simulate a nuclear Rankine-cycle space powerplant. It was composed of three separate fluid loops; the heater loop, the power loop, and an open coolant loop. Heat was added to the system by an electrical heater and removed from the system by the use of city water. The working fluid in all loops was water.

The test system was provided with controls that were capable both of holding the conditions of the steady-state tests within close tolerances, and imposing the perturbations required by the dynamic tests. The test system was also provided with instrumentation which had both the accuracy and the fast response required by the two types of tests.

Figure 3 is a photograph showing the boiler mounted on the test stand as well as some of the power-loop instrumentation. The test system is shown schematically in Figure 4 and is described in detail in the following paragraphs.

#### 1. Description of Fluid Loops

Heater loop - This was a liquid loop which transferred energy from an electrical heat source to the boiler shell. Pressurization of the loop allowed

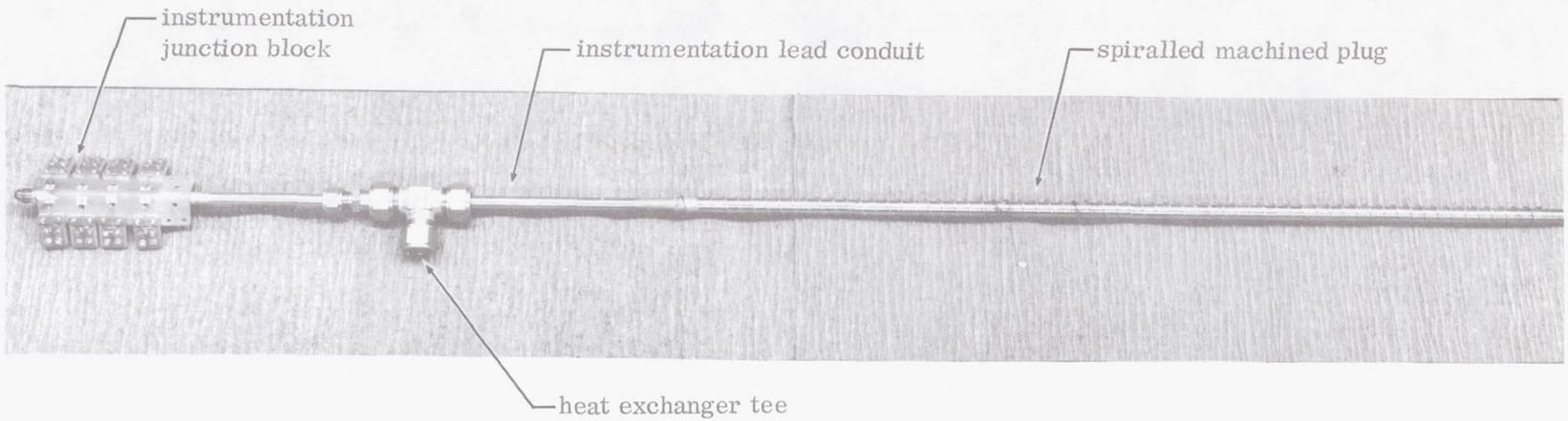


Figure 2 Photograph of Spiralled Plug Insert X-23889

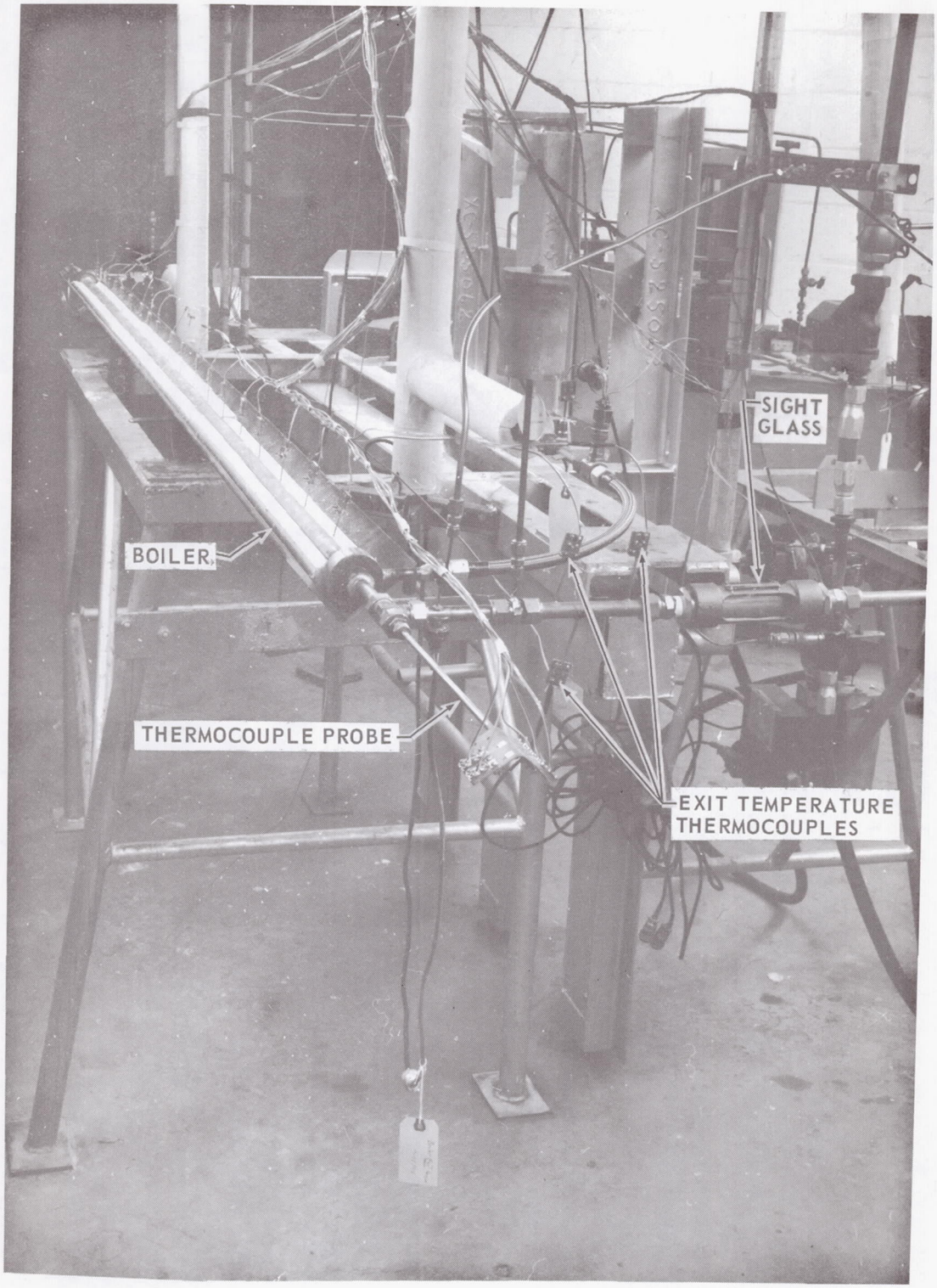


Figure 3 Photograph of Test System X-23893

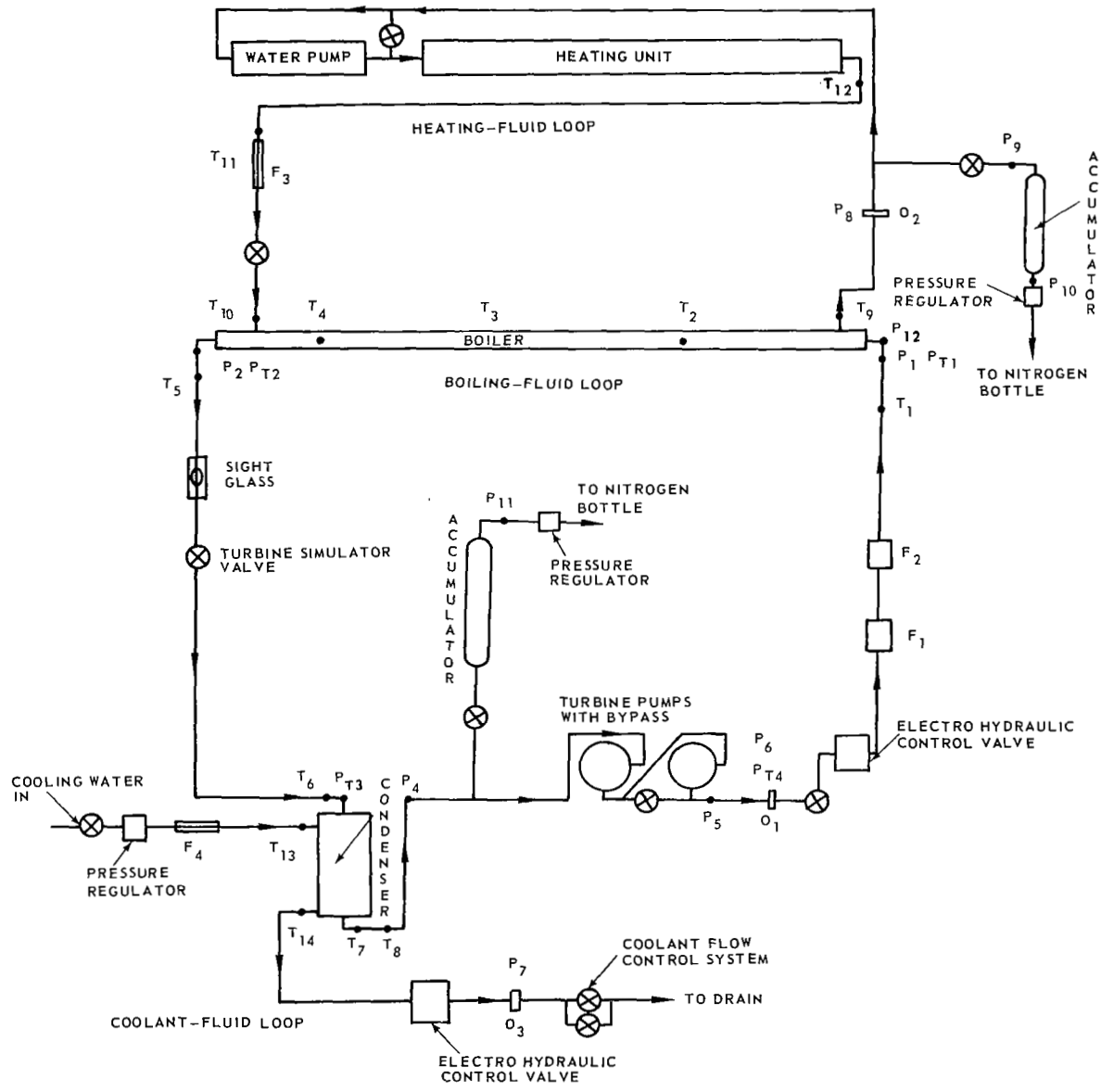


NOTE: SEE TABLE 2 FOR DESCRIPTION OF INSTRUMENTATION AT EACH LOCATION SUCH AS $P_7$, $F_4$, ETC.

Figure 4 Schematic Diagram of Test System

temperatures of 450°F to be reached without vaporization of the fluid. The electrical heat source used is shown in Figure 5. It consisted of 19 calrods 0.496 inch in diameter and six feet long, distributed in circular patterns and encased in Schedule 40 stainless-steel pipe. The pumping power for the heater loop was provided by a Dean Brothers centrifugal pump. A bypass valve around the pump assisted in flow regulation.

Power Loop - This was a two-phase loop in which the boiling fluid was evaporated and recondensed. The fluid was vaporized in the boiler and then passed through a valve which simulated the choked-flow condition and pressure-drop characteristics of flow through a turbine. However, the valve extracted no energy from the system. The fluid then entered a condenser where it was condensed and subcooled. The condensed fluid was returned to the boiler through two Aurora Model B-4-7 turbine pumps connected in series. Flow control in this loop was maintained using a bypass around one of the pumps and an electrohydraulic valve. The bypass permitted control of the pressure-versus-flow characteristics of the pump system. The electrohydraulic valve permitted feedback control of the inlet flow to the boiler.

Coolant Loop - This was an open loop which extracted heat from the boiling fluid by coolant water flowing over the condenser tubes. The coolant water was supplied to this loop directly from the city water supply. The condenser was a single Ross RCF-7M300-8C8 heat exchanger mounted in a vertical position. Both the boiling fluid and the coolant fluid entered at the top of the unit. The boiling fluid flow was downward through 56 condensing tubes. Baffles in the coolant side directed the coolant flow across the condensing tubes. Boiler-inlet temperature was controlled by adjusting the coolant-loop flow rate.

### 2. Rig Instrumentation

Rig instrumentation consisted of temperature, pressure, and flow-sensing devices. Thermocouples were used for temperature measurement; pressure transducers and Bourdon-tube gages for pressure measurements; and turbine-type flowmeters for flow measurements. All instrument locations are shown in the schematic diagram of Figure 4 and identified in Table 2. This table contains a description of each instrument, its accuracy and response time. The instrumentation employed in the dynamic testing was selected to have response times sufficiently fast to detect all significant effects.

Temperatures were measured with chromel-alumel sheathed thermocouples with sealed junctions. These thermocouples were installed with an immersion depth of 10-12 diameters to minimize measurement errors. All rig thermocouples were installed in duplicate. One permitted visual readings through a Brown model 156 readout potentiometer. The other was connected to the recording oscillograph through a thermocouple translator.

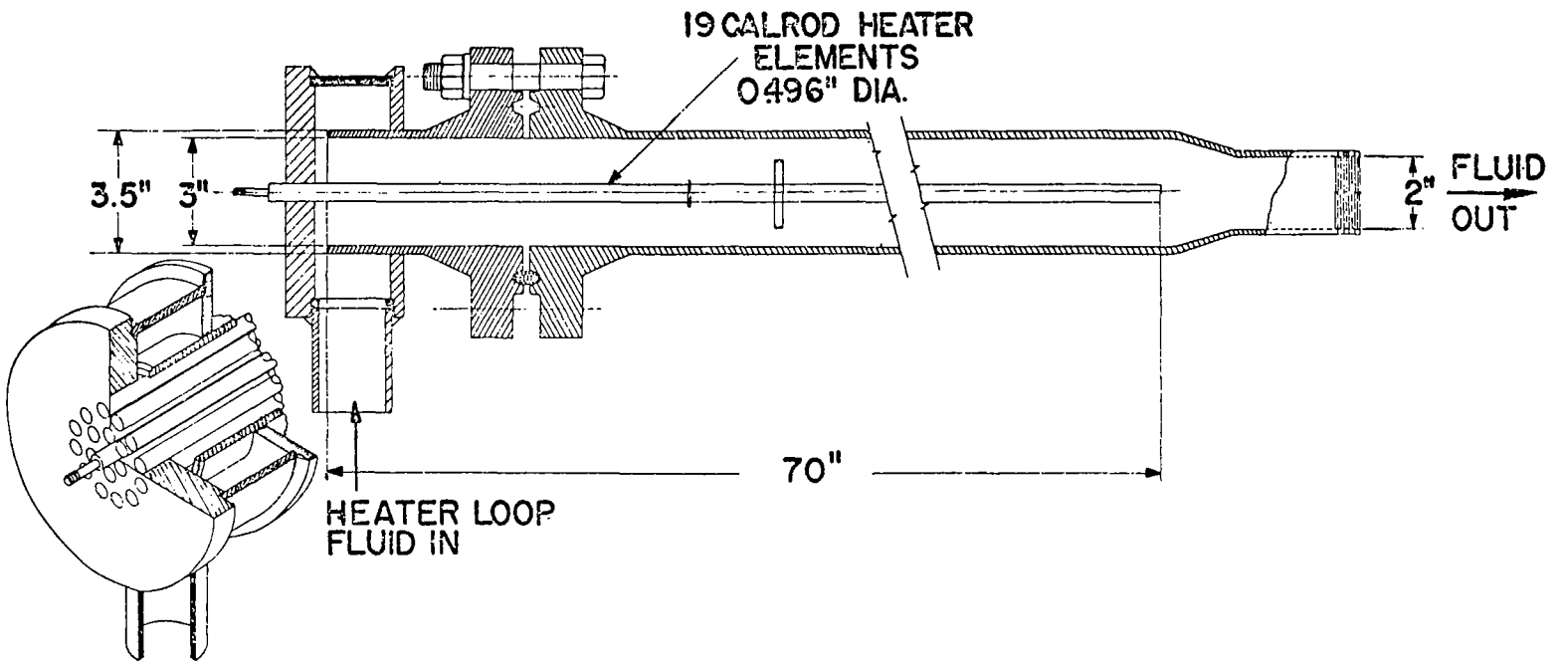


Figure 5 Calrod Heater

Measurements of the boiling-fluid pressure were made using both Bourdon-tube gages and strain-gage type pressure transducers. The Bourdon-tube gages were used for the steady-state measurements. The pressure at the inlet and exit to the boiler were made using Heise Bourdon-tube gages. These gages had an accuracy of ± 0.1 percent of full range and were mounted in the control room at the same height as the pressure taps to reduce gravitational effects. Due to the length of the lines from the pressure taps to the gages, valves were provided at the pressure taps to shut off these lines during the dynamic testing. This prevented these lines from acting as accumulators which might alter the system dynamics. All Bourdon-tube gages were calibrated periodically to insure their accuracy.

Pressure sensing during the dynamic tests was accomplished with strain-gage pressure transducers. The signal from the transducer was fed into preamplifiers which in turn were connected to the recording oscillograph. At the boiler exit the strain-gage face of the transducer was mounted flush with the boiler exit tube. This resulted in virtually no lag between the time a boiling-fluid pressure change occurred and the time it was sensed by the transducer. In mounting all other transducers, the length of line between the fluid and the strain-gage face was kept as short as rig mounting permitted, to maximize the response of the sensing unit.

Flow measurement in the power loop was taken with two Potter Model 60-4115 microflowmeters connected in series. One of these flowmeters provided the feedback signal for the electrohydraulic control valve. It also provided the signal source for the flowmeter frequency counter used to make visual readings during the steady-state tests. The second flowmeter was connected through a preamplifier to the recording oscillograph. Both flowmeters were calibrated over the operating flow range of the test system.

Turbine-type flowmeters were also used in the coolant and heater loops. Signals from these flowmeters were linked through a preamplifier to the recording oscillograph. In addition, these flowmeters were connected through a switching arrangement to a flowmeter frequency counter for visual readings. The switching arrangement allowed the flow in both loops to be monitored during rig operation. These flowmeters were calibrated in the operating range and corrected for temperature when necessary.

A Jacoby-Tarbox sight glass was mounted in the line between the boiler and the turbine simulator valve to permit visual inspection of the condition of the vapor leaving the boiler.

### 3. Control Systems

Control of flow, temperature, and pressure was necessary for operation of the rig. Hand valves and electrohydraulic valves were employed for flow control. Regulation of electrical power input to the heater and regulation of coolant flow provided the methods of temperature control. Pressures were regulated by the use of accumulators and the turbine simulator valve.

The flow rate in the heater loop was set by the bypass valve on the heater-loop pump. Fine adjustment was accomplished manually by the use of a Jenkins stainless-steel steam valve located at the heater-loop inlet to the boiler.

Flow in the power loop was controlled by an Annin electrohydraulic feedback control valve. The complete unit consisted of an Annin flow control valve, a hydraulic actuator with a Moog Model 73-167 servo valve, and an Annin electronic controller. Flow was set by adjusting a reference voltage. It was maintained by electronically comparing the reference to a feedback voltage produced by a turbine flowmeter upstream of the valve. Differences between these voltages resulted in an error signal. Changes in the valve position were then determined by the integral of the error signal over time. In the external control mode an external reference signal was fed into the controller. In the case of frequency-response tests, the external signal was generated by a Wavetek frequency generator. With this unit sinusoidal frequencies as low as 0.0015 cps could be fed into the controller.

The temperature of the boiling fluid at the inlet to the boiler was controlled by regulating the flow in the coolant loop. A feedback control system employing an electrohydraulic valve in the coolant loop was originally used to control this temperature. However, since this temperature responded very slowly to the system dynamics, it was found that adequate control could be obtained manually. This was done using a 0.5-inch gate valve in parallel with a 27-turn needle valve. A pressure regulator upstream of the flowmeter and condenser prevented pressure fluctuations due to city water demand changes.

The temperature of the heating fluid entering the boiler was controlled with a West Model JSB-6 controller which regulated the electrical power into the heater. This unit provided proportional control over a limited range of variation. It consisted of a photocell circuit connected to a meter reading the output of a thermocouple which was located in the exit line from the heater. Magnetic amplifiers increased the output of the photoelectric circuit to a large saturable-core reactor which directly controlled the power input to the calrods in the heater.

Pressure regulators on the heater loop and power loop controlled the system preload. System pressure level was varied by increasing or decreasing the nitrogen pressure to the accumulator bladders. The boiler exit pressure was set by changing the position of the turbine simulator valve.

C. Operation of Test System

The following paragraphs describe the operation of the test system in performing the steady-state, frequency-response, and step-response tests required under the contract. The discussion includes a description of the startup, test, and shutdown procedures for the different types of tests.

1. Steady-State Test Procedures

a. Startup

At the beginning of each week of testing, the heater and power loops were recharged with a fresh inventory of distilled deareated water to minimize the accumulation of contaminants and dissolved gasses in the working fluids.

At the beginning of each day of steady-state testing, the test system was started and the following nominal operating condition was established:

Nominal Operating Condition

| | |
|---|---|
| boiling-fluid flow rate | 45 lb/hr |
| boiling-fluid inlet temperature | 140°F |
| boiling-fluid exit pressure | 65 psia |
| heating-fluid flow rate | 770 lb/hr |
| heating-fluid inlet temperature | 410°F |

Data was then recorded at this condition and compared with the results of previous tests at this same condition to determine if the boiler was performing properly.

b. Steady-State Tests

After the boiler performance at the nominal operating condition was checked, steady-state testing was initiated. These tests were performed at the 34 operating points presented in Table 3.

As can be seen in Table 3, each steady-state test condition was specified by constant values of the following primary variables: boiling-fluid flow rate W, boiling-fluid inlet temperature $T_{in}$, heating-fluid flow rate $W_H$, heating-fluid

inlet temperature $T_{H\ in}$, and either boiling-fluid exit pressure $P_{out}$, or the setting of the turbine simulator valve. The following tolerances were applied to these variables in holding a specific test condition.

| | |
|---|---|
| boiling-fluid flow rate | ±0.5 lb/hr |
| boiling-fluid inlet temperature | ±4°F |
| boiling-fluid exit pressure | ±0.5 psi |
| heating-fluid flow rate | ±1.8% |
| heating-fluid inlet temperature | ±1°F |

After a test condition was established in the system, a period of approximately 30 minutes was taken to allow a steady state to be achieved. Data was then taken in the following manner. First a short oscillograph recording was made of the variables listed in Table 4. Then all temperature, pressure, and flow measurements were read manually. Finally a second oscillograph was made. A comparison between the two oscillograph recordings made it possible to determine if a steady state existed while the data was being read.

The following criteria were used in judging the acceptability of a test point:

1) Primary variables held within the specified tolerances,

2) Existence of steady state as indicated by the oscillograph recordings, and

3) System heat balances that checked within 7 percent.

c. Shutdown

After a series of steady-state tests was completed, the nominal operating conditions were re-established and the data checked to determine if the boiler performance had deteriorated during the course of the testing. Electric power to the heater was then cut while the fluids continued to be circulated through the loops until the system cooled off. At the end of each week of testing, the system was completely drained to permit preventive maintenance to be performed.

2. Dynamic Test Procedures

Dynamic testing included both frequency-response and step-response tests. These tests were performed at 21 operating conditions specified by the NASA project manager and presented in Table 5.

a. Startup

The startup procedures described for the transient tests were identical to those described above for the steady-state tests. After the boiler performance had been checked at the nominal operating condition, the operating condition was set for the transient tests and a period of approximately 30 minutes was allowed for a steady state to be achieved.

b. Step-Response Tests

Once steady state was achieved, the step-response tests were performed in the following manner. The boiling-fluid flow rate was suddenly increased by approximately 12 percent of its original value while the other primary variables were held constant. The system was then allowed to come to equilibrium. A continuous oscillograph recording was made of the variables listed in Table 4 during the initial step change, and for a period of approximately 30 seconds thereafter. Additional short oscillograph recordings were made at intervals of 1, 2, 3, 5 and 15 minutes until steady state had been achieved.

The system was brought back to the original operating condition. After steady state had been restored, the same procedure was repeated except that the boiling-fluid flow rate was suddenly decreased by 12 percent of its original value.

c. Frequency-Response Tests

After the step-response tests had been completed, the system was returned to the initial operating condition and frequency-response tests were initiated. The frequency-response tests were conducted by imposing a sinusoidal perturbation on the boiling-fluid flow rate while holding the other primary variables constant. This was done by feeding a sinusoidal signal from a Wavetek Model 112 frequency generator into the electronic feedback controller of the electrohydraulic valve in the power loop. The amplitude of this perturbation was approximately ±6 percent of the steady-state value.

Frequency-response tests were run for each operating condition between frequencies of 0.003 and 1.0 cycle per second. At each frequency a period of at least twice the period of oscillation was allowed before the data was recorded. An oscillograph recording was made of the variables listed in Table 4 for a period of two oscillations. A new frequency was set and the procedure repeated until the required number of frequencies was tested.

d. Shutdown

After a series of frequency-response tests was completed, the test system was shut down using the same methods described above for the steady-state tests.

# IV. STEADY-STATE CHARACTERISTICS OF BOILER

Steady-state tests were performed to determine how the overall boiler performance changed as a function of the primary variables, and to study the important processes occurring within the boiler. The resulting information served a number of functions. It gave data with which to evaluate the parameters required for calculating the theoretical transfer function. It gave information as to the actual physical processes occurring within the boiler with which to compare the mathematical model used in the theoretical analysis of the boiler dynamics, and it gave an insight into the boiler operating characteristics which was useful in interpreting the frequency-response test results.

The steady-state tests were performed in accordance with the procedures described in Section III above. These tests were performed at the 34 operating conditions listed in Table 3. Each condition is defined by constant values of the following primary variables.

boiling-fluid flow rate W
boiling-fluid inlet temperature $T_{in}$
heating-fluid flow rate $W_H$
heating-fluid inlet temperature $T_{H\ in}$
boiling-fluid exit pressure $P_{out}$, or turbine simulator valve setting

The test conditions were selected so that each of the primary variables was varied about the nominal operating condition described in Section III above. This nominal condition was selected on the basis of preliminary tests to provide a condition typical of that encountered in Rankine-cycle space powerplants.

The results of these tests indicate that the boiler performance can be categorized by the condition of the boiling fluid at the exit. Over the operating range studied, three types of boiling-fluid exit conditions were observed:

1) Dry superheated vapor,
2) Superheated vapor with saturated liquid, and
3) Saturated vapor with saturated liquid.

The second condition is a nonequilibrium condition. Its existence was determined by the visual observation of liquid droplets in the superheated vapor stream and by the fluctuation in the temperature measurements which resulted when these droplets impinged on the thermocouples at the boiling-fluid exit.

By studying the axial temperature distributions measured inside the boiler, it was possible to discern three different regions within the boiler where different modes of heat transfer from the tube wall to the boiling-fluid predominated:

1) A subcooled region,
2) A boiling region, and
3) A nonequilibrium-superheated region.

This section contains a detailed discussion of three different regions of the boiler. The manner in which the primary variables affect these profiles is then related to the changes observed in the overall boiler performance.

A. Regions within Boiler

The temperature measurements made within the boiling-fluid and heating-fluid streams were plotted against the axial distance from the boiling-fluid inlet for each steady-state test condition. Using these temperature distributions and employing heat balances on sections of the boiler, it was possible to estimate the variation of boiling-fluid quality with axial distance in the two-phase regions.

Typical examples of these temperature and quality distributions are shown in Figures 6 through 9. The different regions of the boiler are apparent from the changes in the slopes of the temperature and quality profiles. For example, it can be seen that the boiling-fluid temperature increases rapidly in the subcooled region as it is heated to its saturation temperature. The slope of the heating-fluid temperature is not very steep, however, indicating a relatively low heat flux. Therefore the primary mode of heat transfer to the boiling fluid is forced convection, although some subcooled boiling may take place.

The saturation temperature is reached at the pinch point where bulk boiling commences. This is the primary mode of heat transfer in the boiling region. The high rate of heat transfer achieved in this region is indicated by the relatively steep slope of the heating-fluid temperature.

In the boiling region, saturation conditions exist and the boiling-fluid temperature is dependent upon the pressure. As a consequence the boiling-fluid temperature is observed in Figures 6 through 9 to decrease with length, due to the

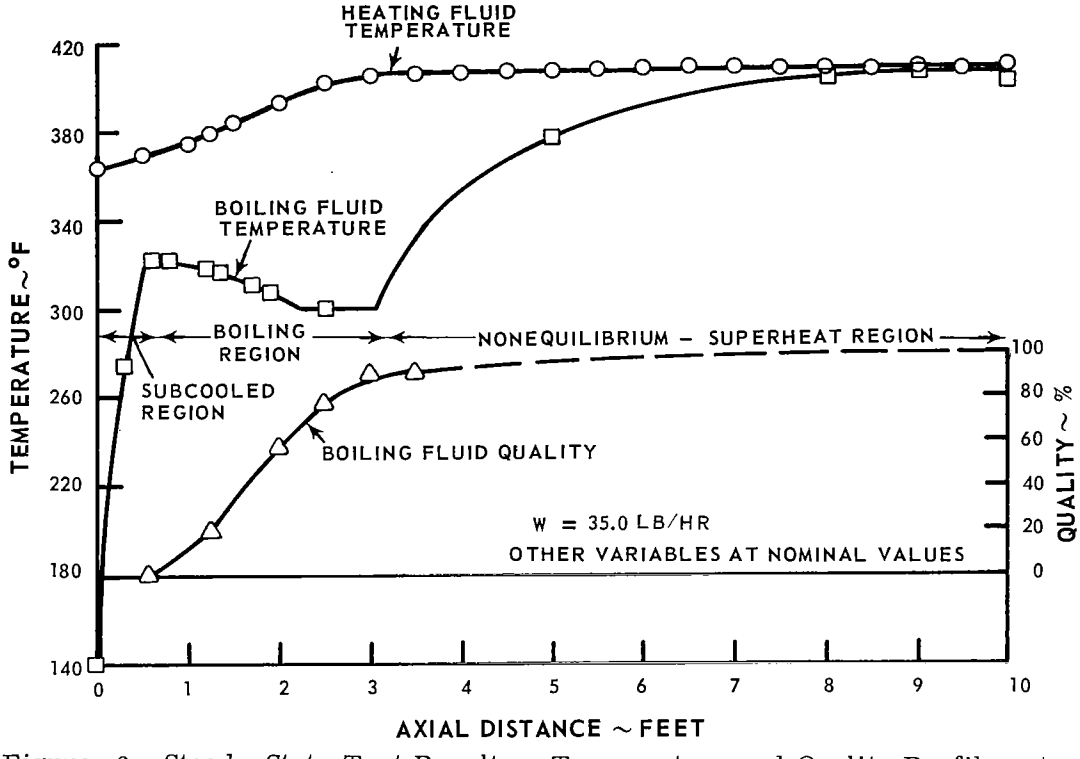


Figure 6 Steady-State Test Results. Temperature and Quality Profiles at Boiling-Fluid Flow Rate of 35.0 lb/hr

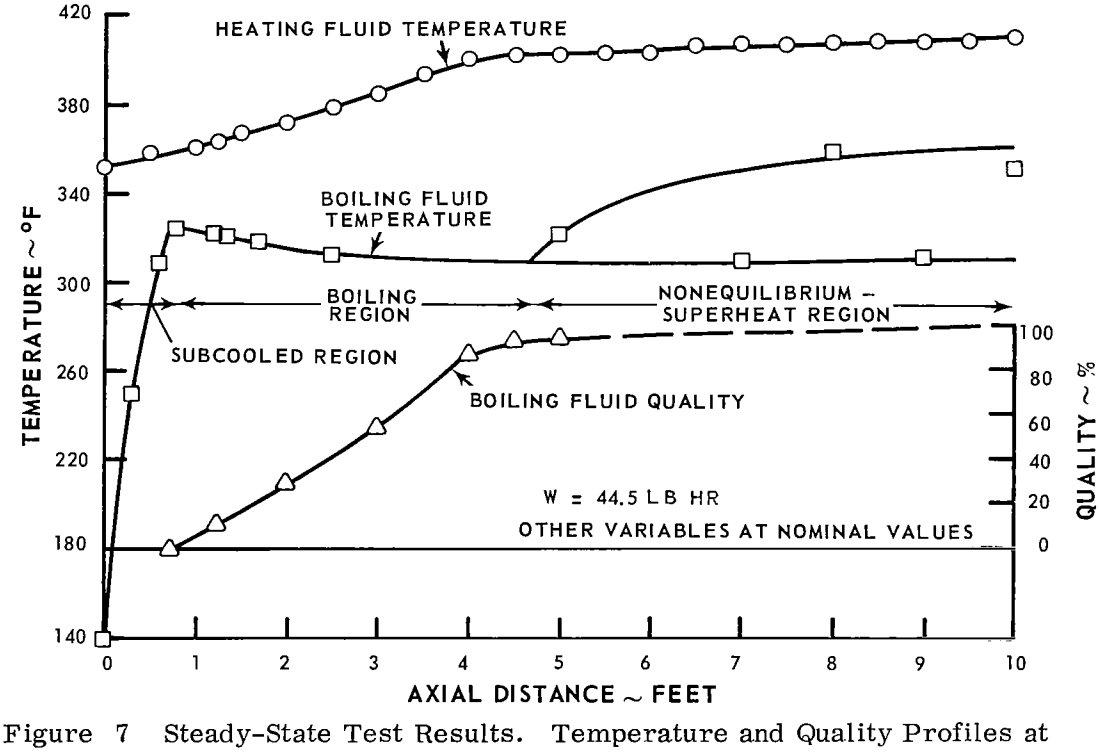


Figure 7 Steady-State Test Results. Temperature and Quality Profiles at Boiling-Fluid Flow Rate of 44.5 lb/hr

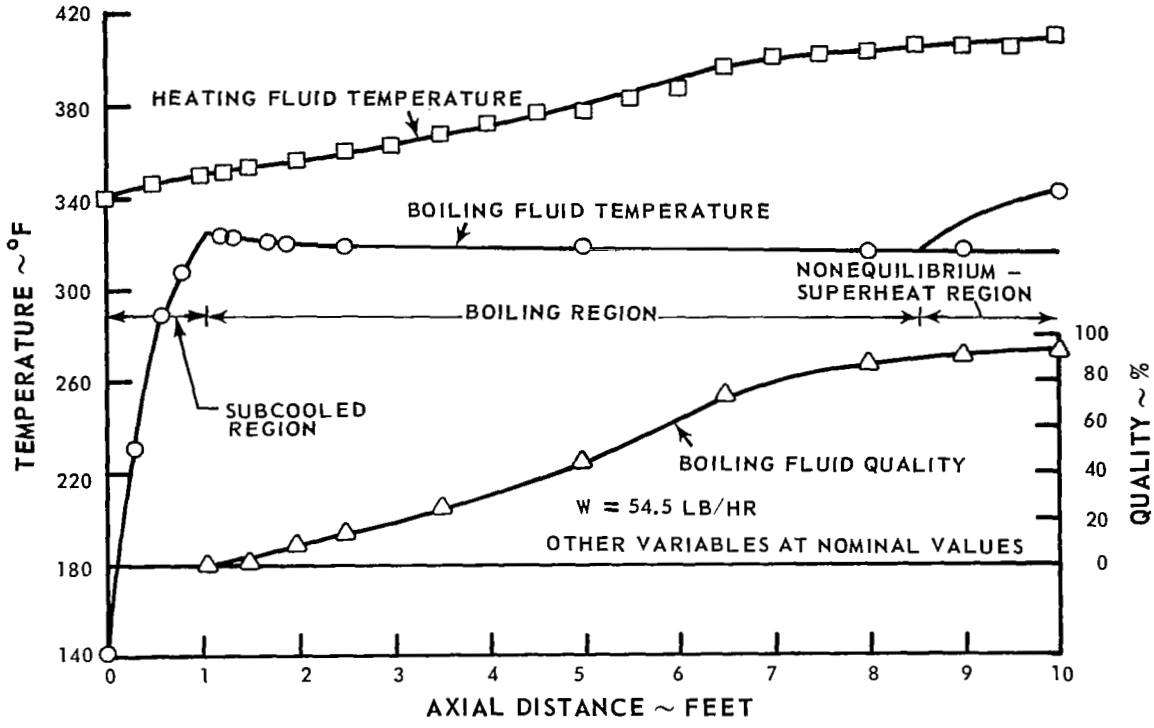


Figure 8 Steady-State Test Results. Temperature and Quality Profiles at Boiling-Fluid Flow Rate of 54.5 lb/hr

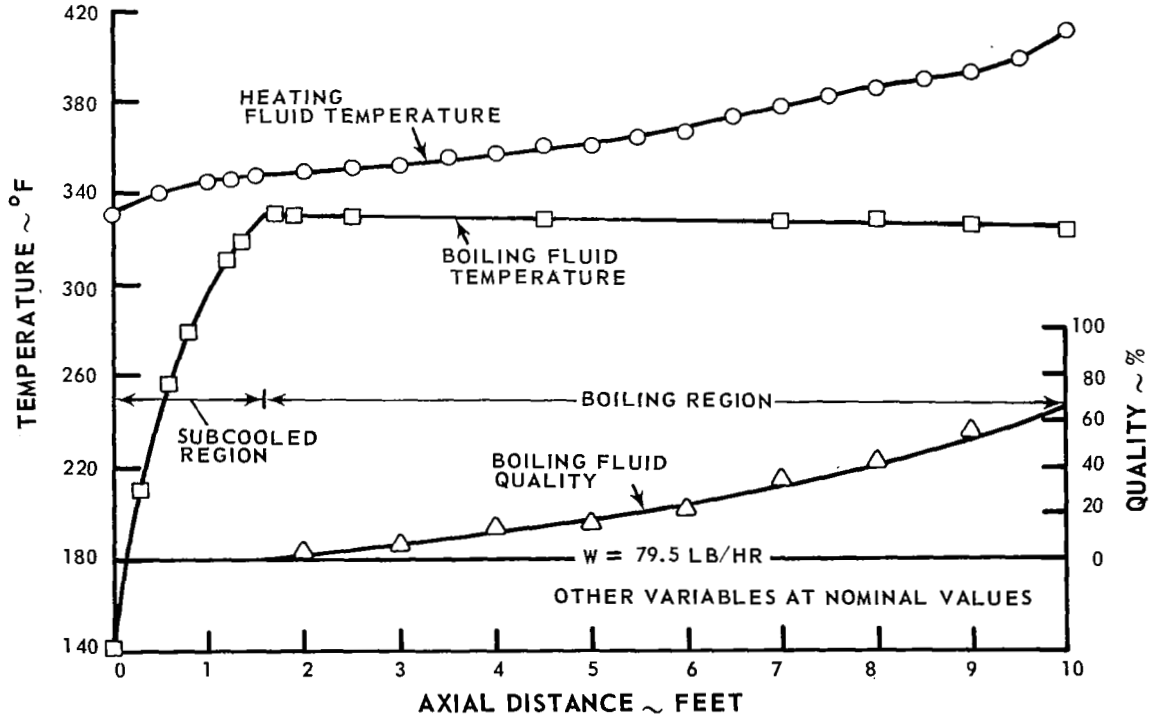


Figure 9 Steady-State Test Results. Temperature and Quality Profiles at Boiling-Fluid Flow Rate of 79.5 lb/hr

decrease in boiling-fluid pressure caused by frictional losses. The steeper slope of the boiling-fluid temperature over the first portion of the boiling region is caused by the boiling fluid flowing through the spiral passage formed by the machined plug, where frictional losses are higher. The boiling fluid is vaporized as it passes through the boiling region, as shown by the increase of quality with length. At a quality of approximately 90 percent, before the evaporation process has been completed, the boiling fluid enters the non-equilibrium-superheat region. In this region, the temperature of the vapor is observed to rise above the saturation temperature and the vapor becomes superheated. However, since the evaporation process was not completed when the boiling fluid entered this region, droplets of saturated liquid can be found dispersed in the superheated vapor. This results in a nonequilibrium state.

Since the evaporation process has not been completed before the vapor becomes superheated there is no clearly defined boundary between the boiling region and the nonequilibrium region, although for purposes of analysis it has been found necessary to define such a boundary. The criteria employed in defining this boundary are discussed in detail in Appendix 3.

Several modes of heat transfer are active in the nonequilibrium-superheat region:

1) Transfer of the heat from the tube wall to the vapor by forced convection,
2) Conduction of heat from the vapor to the liquid droplets, and
3) Transfer of heat by conduction from the tube wall to droplets impinged on the wall.

The low rate of heat transfer indicated by the shallow slope of the heating-fluid temperature in this region indicates that the primary mode of heat transfer is by the forced convection of the vapor.

For the condition illustrated in Figure 6, W=35 lb/hr, the evaporation process is completed shortly after the boiling fluid enters the nonequilibrium-superheat region. This is shown by the fact that none of the thermocouples in this region registered the saturation temperature. The boiling fluid emerges at a temperature only slightly below the heating-fluid inlet temperature and superheated by 117°F. The nonequilibrium effects that occur in this region become more pronounced at higher boiling-fluid flow rates.

The effect of boiling-fluid flow rate on the three regions of the boiler can be seen by comparing Figures 6 through 9 which represent flow rates of 35.0, 44.5, 54.5 and 79.5 lb/hr, respectively. As can be seen, increasing the

boiling-fluid flow rate tends to increase the lengths of the subcooled and boiling regions, while the length of the nonequilibrium-superheat region decreases until the region disappears.

As the boiling-fluid flow rate increases, the evidence of the nonequilibrium effects becomes more noticeable. Figure 7 shows that at 44.5 lb/hr two thermocouples register the saturation temperature, indicating the presence of droplets close to the boiler exit. However, heat balances and visual observation indicate that for this condition the evaporation process is completed before the fluid leaves the boiler. Therefore it leaves as a dry superheated vapor.

Figure 8 indicates at 54.5 lb/hr that the evaporation process has not been completed before the fluid leaves the boiler. As a consequence the boiling-fluid emerges in a nonequilibrium state containing 7 percent saturated liquid and 93 percent vapor superheated by 35°F.

Figure 9 indicates that at a flow rate of 79.5 lb/hr the nonequilibrium-superheat region has disappeared. No superheating of the vapor is observed. The boiling-fluid emerges in a saturated condition at a quality of 65 percent.

B. Effect of Primary Variables on Boiler Performance

The steady-state test data describing the overall performance of the boiler is summarized in Tables 6 through 10. In addition, curves of this data are presented in Figures 10 through 20 to illustrate the effect the primary variables have on boiler performance. The following paragraphs discuss the effect that each of these primary variables has on the performance of the boiler.

1. Effect of Boiling-Fluid Flow Rate

The manner in which the performance of the boiler varies with the boiling-fluid flow rate W is illustrated in Figures 10 and 11. Figure 10a shows the effect of varying W on the different regions of the boiler. The subcooled length $L_{SC}$ and the boiling length $L_B$ represent the axial locations of the boundaries between the regions as measured from the boiling fluid inlet. Figure 10a further illustrates the fact that as W is increased both the subcooled and boiling regions increase in size while the nonquilibrium-superheat region decreases until it disappears.

Figure 10c describes the condition of the boiling fluid at the exit. For boiling-fluid flow rates between 30 and 45 lb/hr, it can be seen that the vapor leaves in a dry superheated condition. Between 45 and 65 lb/hr, however, the exit quality drops below 1.0 while the vapor is still superheated, indicating the co-existence of liquid and superheated vapor in a nonequilibrium state. Above 65 lb/hr saturation conditions exist. There is no vapor superheat and the exit quality is less than one.

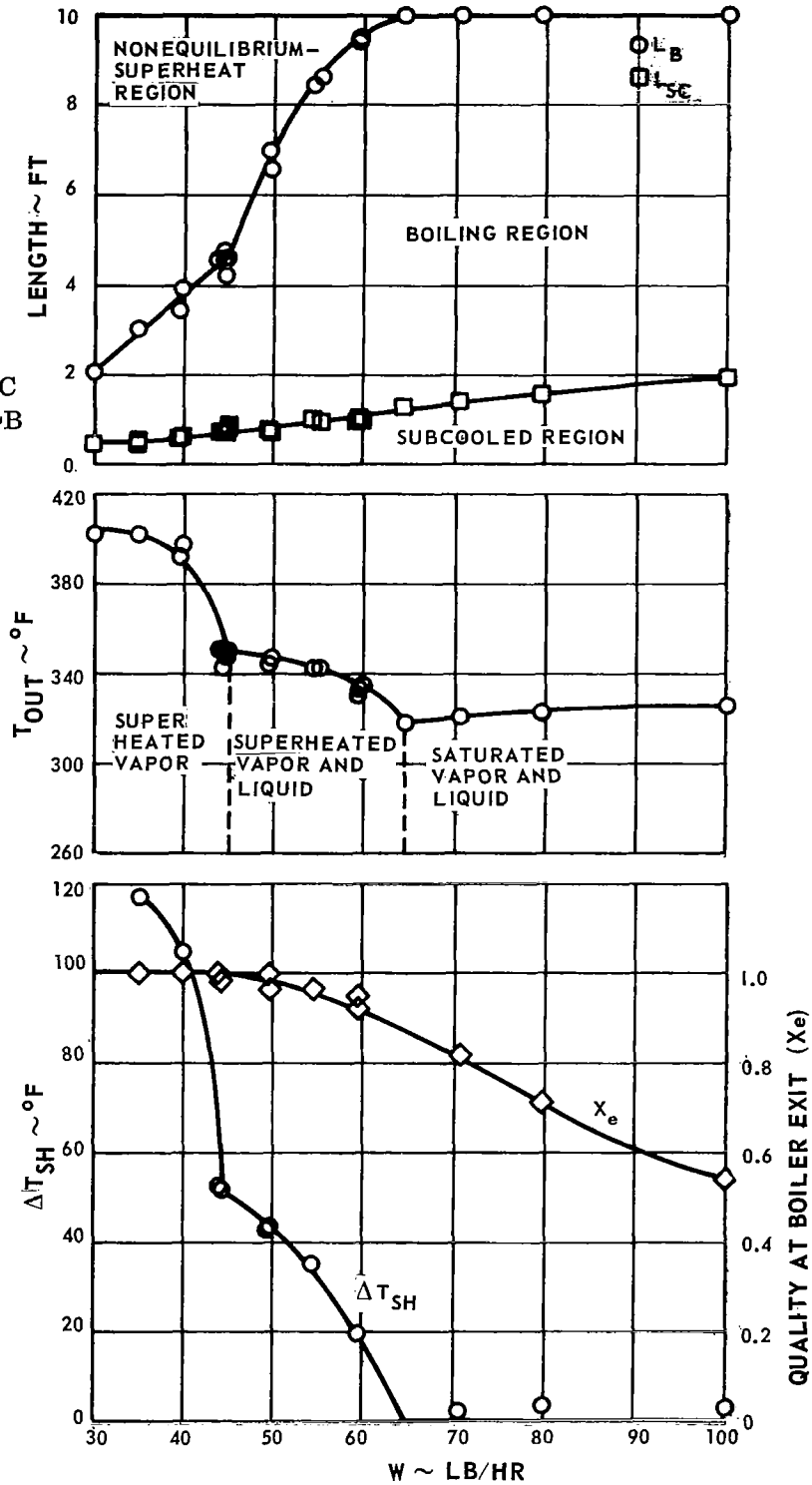


a) Subcooled Length $L_{SC}$ and Boiling Length $L_B$ vs W

b) Boiling-Fluid Exit Temperature $T_{out}$ vs W

c) Boiling-Fluid Superheat $\Delta T_{SH}$ and Exit Quality $X_e$ vs W

Figure 10 Steady-State Test Results. Variation of Boiler Performance with Boiling-Fluid Flow Rate
$W_H$ = 770 lb/hr $T_{H\ in}$ = 410°F $T_{in}$ = 140°F T.S. valve at nominal setting

Figure 10b indicates that the condition of the boiling-fluid at the exit is also reflected in the boiling-fluid exit temperature, since this data exhibits a different curvature for each different exit condition.

Figure 11a illustrates the variation of the boiling-fluid exit pressure $P_{out}$ with W. When the boiling fluid emerges in a dry superheated condition $P_{out}$ is related to flow rate and temperature and pressure through the following relation for flow through a choked restriction.

$$\frac{W\sqrt{T_{out}}}{P_{out}} = \frac{A_{choked}}{\sqrt{\frac{\gamma}{R}\left(\frac{2}{\gamma+1}\right)^{\frac{\gamma+1}{\gamma-1}}}} \qquad (1)$$

For a given turbine simulator valve setting, this equation indicates that the parameter $W\sqrt{T_{out}}/P_{out}$ is approximately constant for a limited range of temperature variation. Also, it can be seen that for a limited range of temperature variation, $P_{out}$ is approximately proportional to W. However, when liquid is intermixed with the vapor, Equation (1) no longer holds and the parameter $W\sqrt{T_{out}}/P_{out}$ becomes a function of exit quality $X_e$. The variation of this parameter with $X_e$ for the condition where the turbine simulator valve setting was held constant is illustrated in Figure 12. The strong departure of the curve in Figure 11a from linearity above 60 lb/hr results from the large percentage of liquid in the flow.

One of the more significant effects of varying W on boiler performance is illustrated in Figure 11b where boiling-fluid pressure drop $\Delta P_B$ is plotted as a function of W. The negative slope in the curve exhibited for flows between 30 and 85 lb/hr is of particular interest in studying the stability of multitube boilers. This negative slope characteristic can lead to the static type of boiler instability, discussed in Section VI below, when the pressure at the exit of the boiling tube is independent of flow rate. This can occur in a multitube boiler where the pressure in the exit header is insensitive to the flow fluctuations in the individual tubes.

The negative slope exhibited in the $\Delta P_B$ curve is the result of a very complex interaction between the boiler geometry, the hydrodynamics of the flow in the three different regions, and the shift in the location of the boundaries of these regions as W is varied. An excellent discussion of the factors influencing $\Delta P_B$ and the manner in which they interact to produce the negative pressure gradient can be found in Reference 5. The mathematical analysis presented in this reference has shown very good agreement with the boiling-fluid pressure drop data presented in this section, as shown in Figures 5 and 6 of the reference.

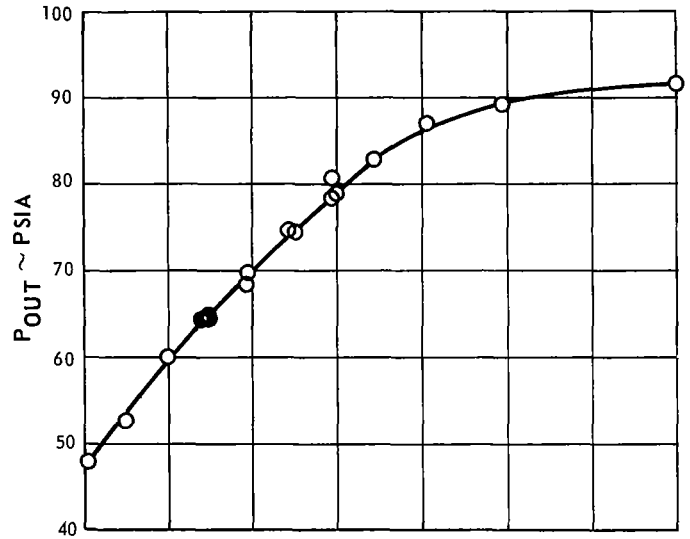


a) Boiling-Fluid Exit Pressure vs W

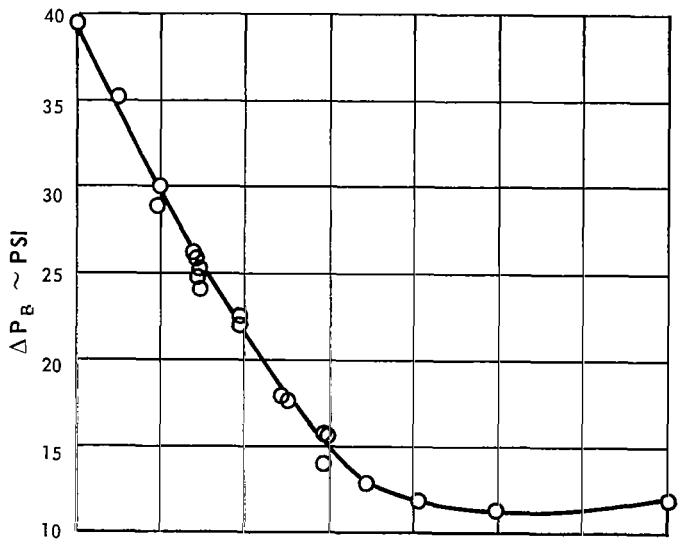


b) Boiling-Fluid Pressure Drop vs W

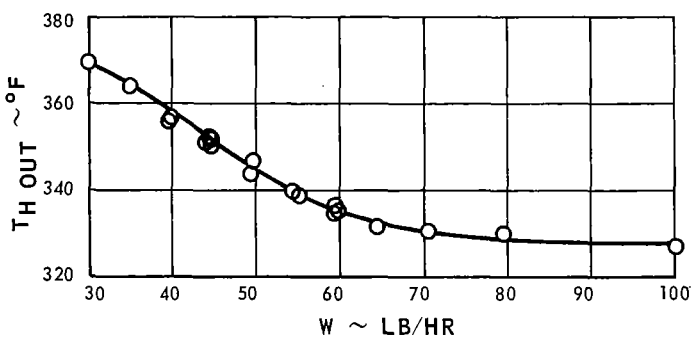


c) Heating-Fluid Exit Temperature vs W

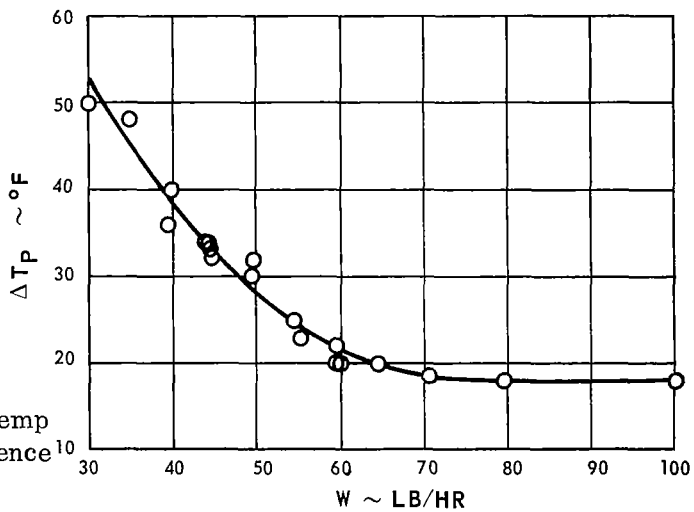


d) Pinch-Point Temperature Difference vs W

Figure 11 Steady-State Test Results. Variation of Boiler Performance with Boiling-Fluid Flow Rate
$W_H$ = 770 lb/hr $T_{H\ in}$ = 410°F $T_{in}$ = 140°F T.S. valve at nominal setting

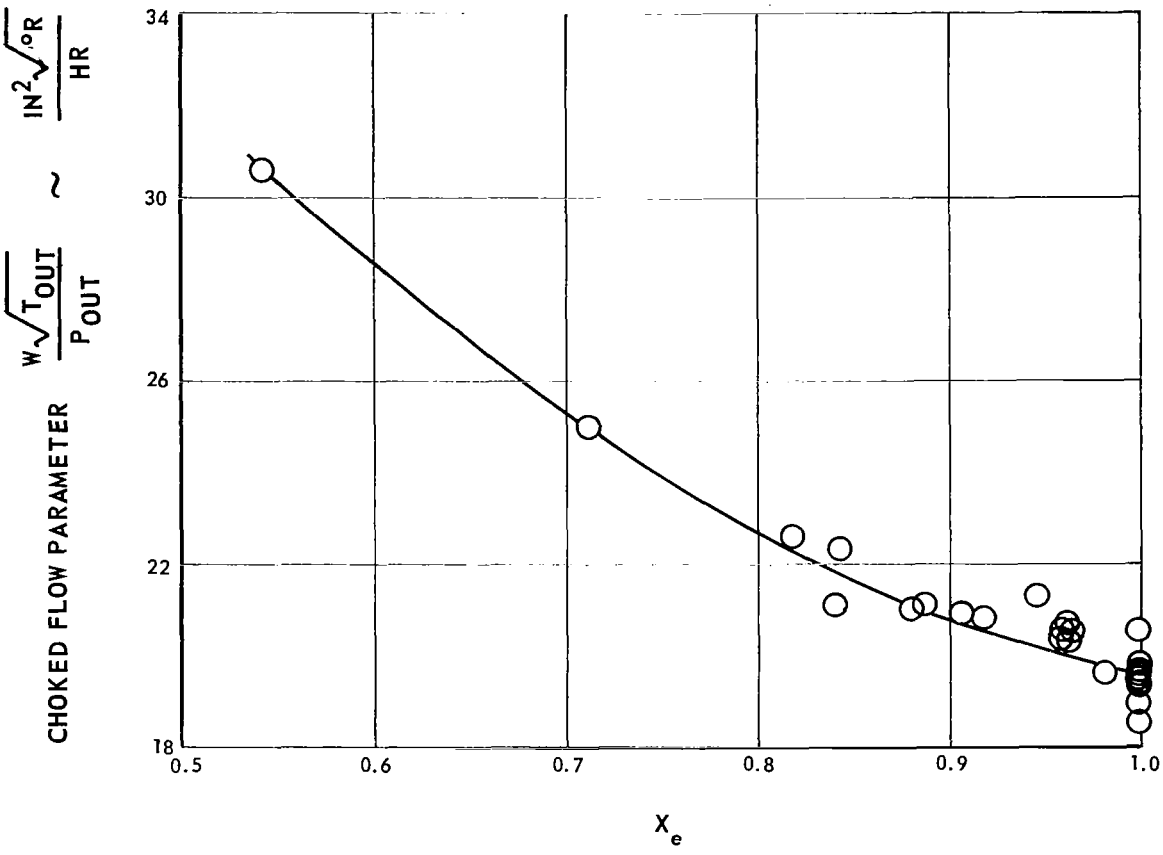


Figure 12 Variation of Choked-Flow Parameter with Boiling-Fluid Exit Quality $X_e$

The variation of the heating-fluid exit temperature $T_{H\ out}$ and the pinch-point temperature difference $\Delta T_p$ with W is shown in Figures 11c and 11d respectively. Both decrease with W until saturated exit conditions are reached at 65 lb/hr. Beyond this point they are relatively insensitive to W. These effects can be explained in the following manner. At flow rates below 65 lb/hr, Figure 10a shows that a portion of the superheat region is replaced by boiling region as the flow rate is increased. Since the heat-transfer coefficient is much higher in the boiling region than in the nonequilibrium-superheat region, the result is an increase in heat transfer over this length. Therefore, additional energy is removed from the heating fluid as the flow rate is increased and $T_{H\ out}$ decreases.

At flow rates above 65 lb/hr, bulk boiling exists as far as the boiler exit. Most of the heat transfer in the boiler occurs in the boiling region. The heat transfer coefficient in this region is relatively insensitive to changes in W. As Figure 10a shows, only small changes occur in the length of the boiling region at flow rates above 65 lb/hr. As a result the heat-transfer area and the heat-transfer coefficient are essentially constant in the boiling region. Under these conditions as the boiling-fluid flow rate is increased above 65 lb/hr, the energy removed from the boiling-fluid remains nearly constant which results in the small observed change of $T_{H\ out}$.

2. Effect of Varying Heating-Fluid Flow Rate

The effects of varying the heating-fluid flow rate $W_H$ are illustrated in Figures 13 and 14. The primary effect of increasing the heating-fluid flow rate is to increase the heat-transfer rate in the boiling and subcooled regions. This is seen by the rapid decrease in the length of the boiling and subcooled regions as shown in Figure 13a.

The rise in the heat-transfer rate as $W_H$ is increased results from increases in both the heat-transfer coefficient and the average heating-fluid temperature. The rise in the average heating-fluid temperature results from a decrease in the difference between $T_{H\ in}$ and $T_{H\ out}$ as $W_H$ is increased, while the total heat transferred remains approximately constant. This is seen in the increased $T_{H\ out}$ shown in Figure 14c. The resulting increase in temperature difference between the heating and boiling fluids at the pinch point is shown by the curve of pinch-point temperature difference, Figure 14d.

As the length of the boiling region diminishes, Figure 13a indicates a corresponding increase in the length of the nonequilibrium-superheat region. This results in a drying out of the vapor and an increase in the superheat. This is shown in Figure 13c where it can be seen that for values of $W_H$ between 400 and 770 lb/hr, the boiling fluid emerges in the nonequilibrium condition with $\Delta T_{SH}$ constantly increasing. Above the nominal value of 770 lb/hr, dry superheated vapor is produced. The lengthening of the nonequilibrium-superheat region is also the primary factor influencing the increase in $\Delta P_B$ shown in Figure 14b.

3. Effect of Varying Heating-Fluid Inlet Temperature

The effects of varying the heating-fluid inlet temperature $T_{H\ in}$ are illustrated

a) Subcooled Length $L_{SC}$ and Boiling Length $L_B$ vs $W_H$

b) Boiling-Fluid Exit Temperature vs $W_H$

c) Boiling-Fluid Superheat $\Delta T_{SH}$ and Exit Quality $X_e$ vs $W_H$

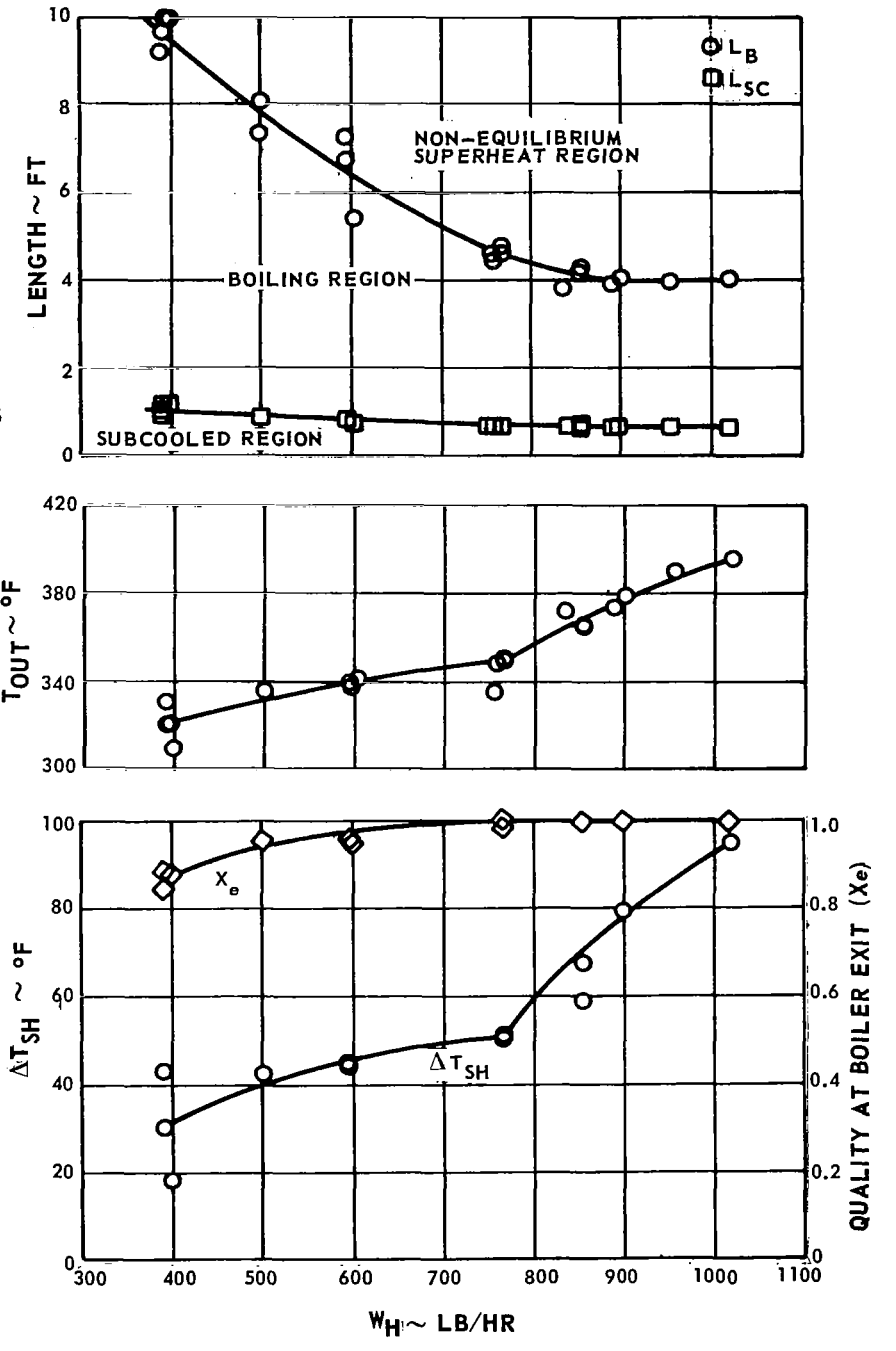


Figure 13 Steady-State Test Results. Variation of Boiler Performance with Heating-Fluid Flow Rate
W =45lb/hr $T_{H\,in}$= 410°F $T_{in}$ = 140°F T.S. valve at nominal setting

a) Boiling-Fluid Exit Pressure vs $W_H$

b) Boiling-Fluid Pressure Drop vs $W_H$

c) Heating-Fluid Exit Temperature vs $W_H$

d) Pinch-Point Temperature Difference vs $W_H$

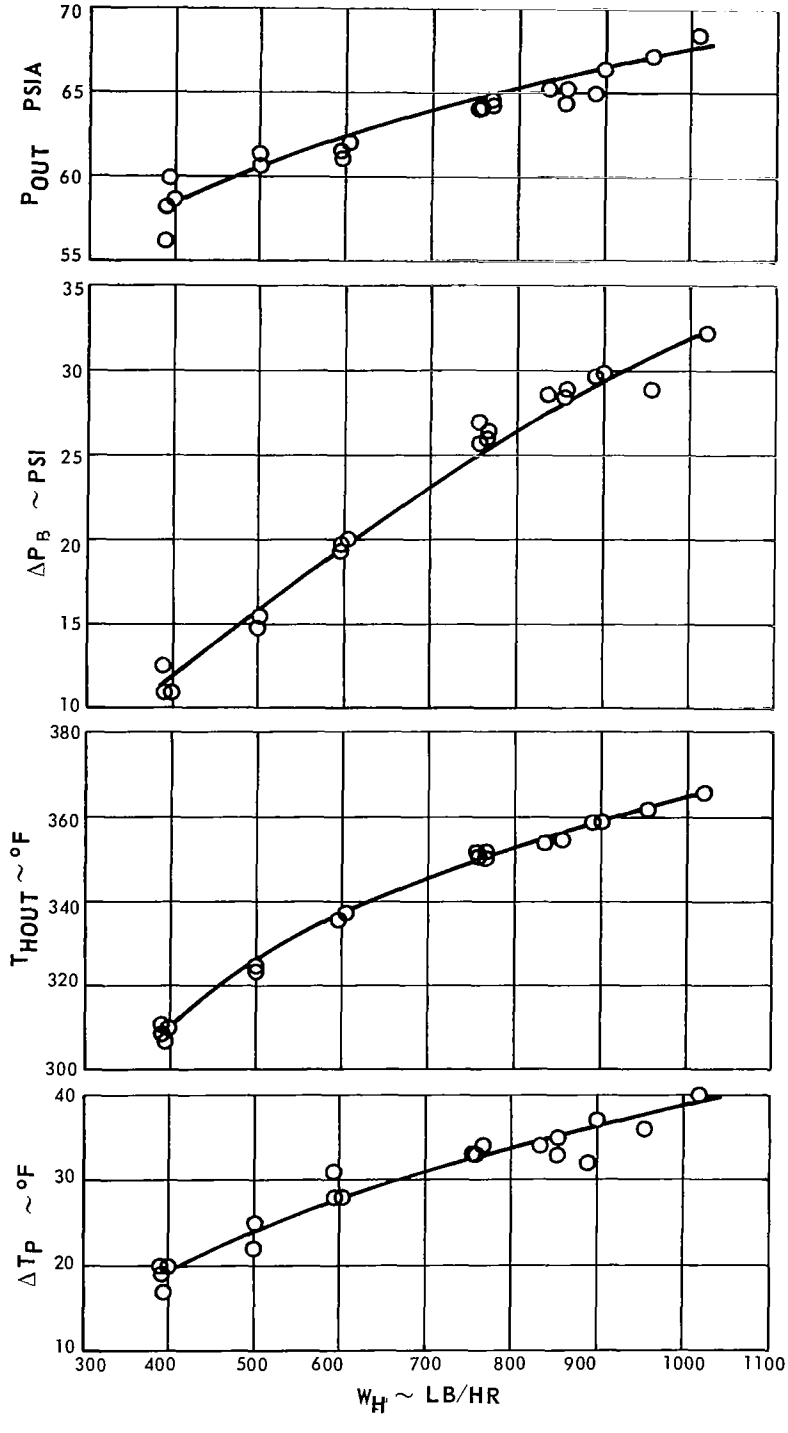


Figure 14 Steady-State Test Results. Variation of Boiler Performance with Heater-Fluid Flow Rate
W = 45 lb/hr $T_{H\,in}$ = 410°F $T_{in}$ = 140°F T.S. valve at nominal setting

in Figures 15 and 16. As can be seen by comparing these figures with Figures 13 and 14, the effect on boiler performance of increasing $T_{H\ in}$ is very similar to that obtained by increasing $W_H$. This is because the primary effect of increasing $T_{H\ in}$ is to increase the temperature difference between the two fluids, thereby increasing the heat transfer rates along the length of the boiler. This is shown by the decrease in the length of the boiling region in Figure 15a and by the increases in $T_{H\ out}$ and $\Delta T_p$ shown in Figures 16c and 16d respectively.

The variation in the exit conditions of the boiling fluid with $T_{H\ in}$ is shown in Figure 15c. For values of $T_{H\ in}$ between 360 and 410°F the vapor is dry. The increases in $X_e$ and $\Delta T_{SH}$ with $T_{H\ in}$ result from the increase in the length of the nonequilibrium-superheat region shown in Figure 15a, as well as the higher heat-transfer rates resulting from the higher temperature differences between the two fluids.

The increase in boiling-fluid pressure drop $\Delta P_B$ with $T_{H\ in}$ shown in Figure 16b is due primarily to the increase in the length of the nonequilibrium-superheat region.

4. Effect of Varying Boiling-Fluid Exit Pressure

The effect of varying the boiling-fluid exit pressure $P_{out}$ is illustrated in Figures 17 and 18. The effect of varying $P_{out}$ is the reverse of the effect of varying $T_{H\ in}$. As $P_{out}$ is increased, the saturation temperature of the boiling-fluid increases, decreasing the temperature difference between the two fluids. This results in reduced heat-transfer rates. The greatest percentage reduction in heat-transfer rates occurs in the vicinity of the pinch point, where the temperature difference between the two fluids is the smallest. These effects can be seen by the increase in length of the boiling region with an increase in $P_{out}$ as shown in Figure 17a, and the decrease in $\Delta T_p$ with an increase in $P_{out}$ shown in Figure 18c.

The variation in the exit conditions of the boiling fluid with $P_{out}$ is shown in Figure 17c. As can be seen for values of $P_{out}$ below the nominal value of 65 psia, the boiling-fluid emerges in a dry superheated condition. Above 65 psia nonequilibrium conditions exist until saturation conditions are approached at

a) Subcooled Length $L_{SC}$ and Boiling Length $L_B$ vs $T_{H\ in}$

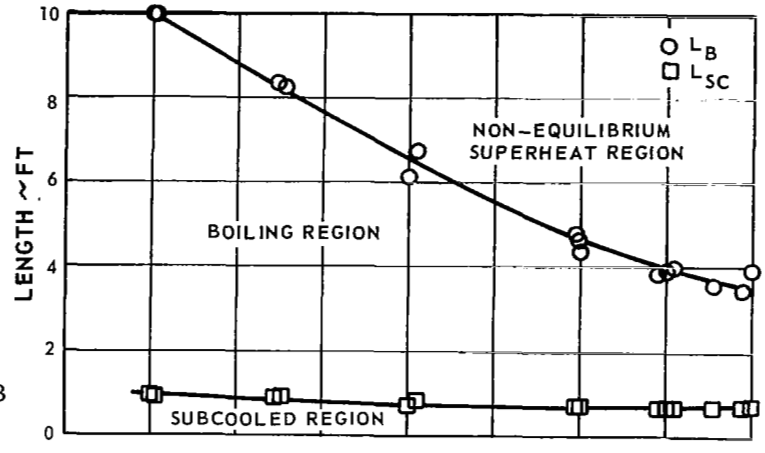


b) Boiling-Fluid Exit Temperature vs $T_{H\ in}$

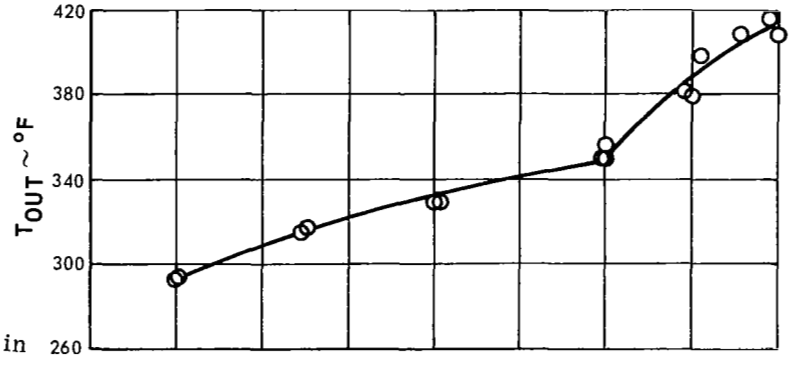


c) Boiling-Fluid Superheat $\Delta T_{SH}$ and Exit Quality $X_e$ vs $T_{H\ in}$

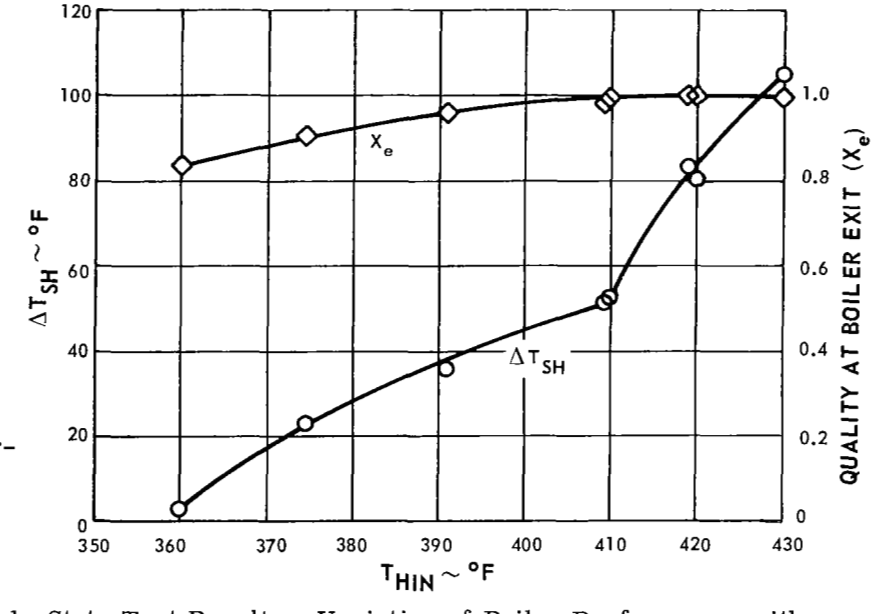


Figure 15 Steady-State Test Results. Variation of Boiler Performance with Heating-Fluid Inlet Temperature
W = 45 lb/hr $W_H$ = 770 lb/hr $T_{in}$ = 140 °F T.S. valve at nominal setting

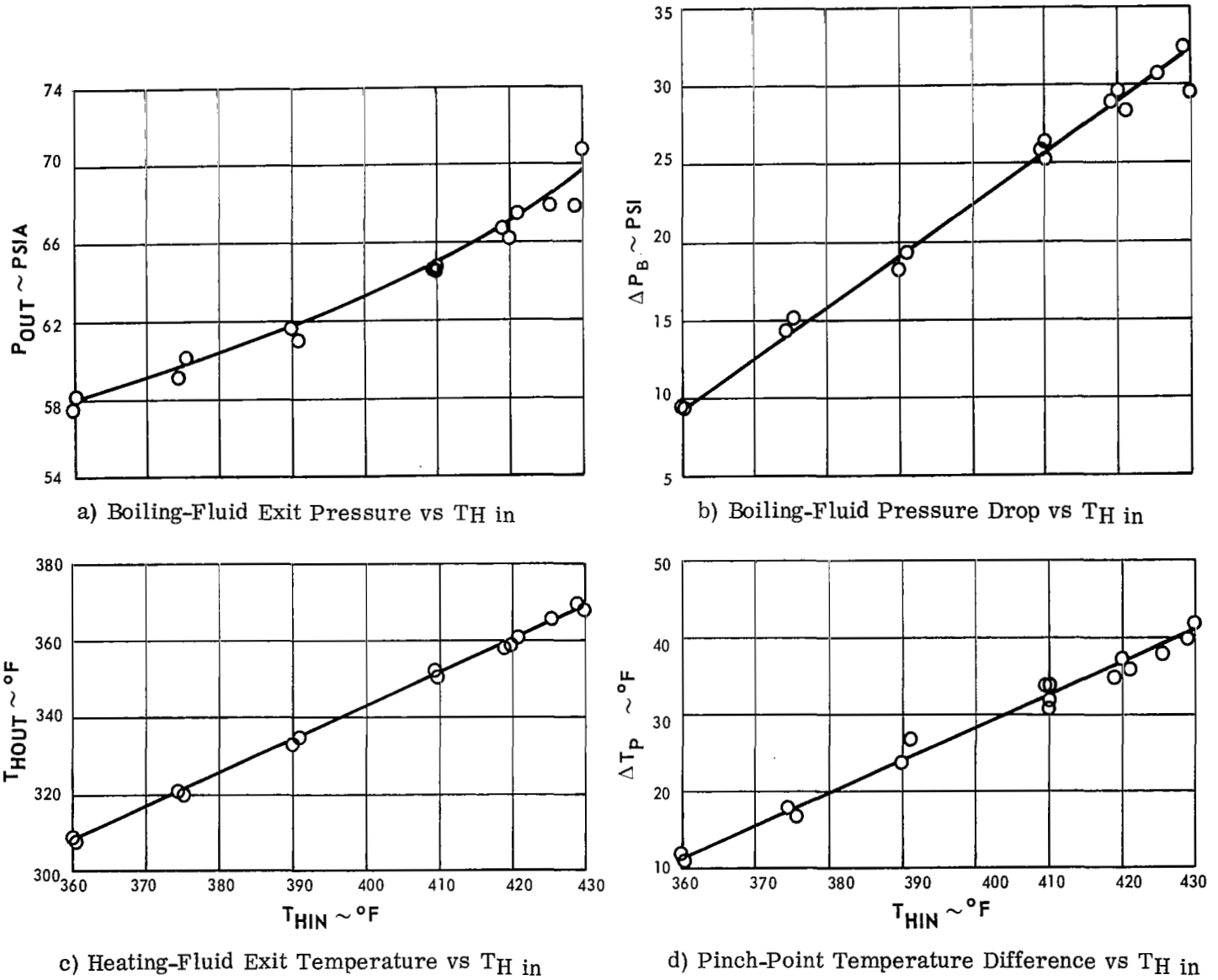


a) Boiling-Fluid Exit Pressure vs $T_H$ in

b) Boiling-Fluid Pressure Drop vs $T_H$ in

c) Heating-Fluid Exit Temperature vs $T_H$ in

d) Pinch-Point Temperature Difference vs $T_H$ in

Figure 16 Steady-State Test Results. Variation of Boiler Performance with Heating-Fluid Inlet Temperature
W = 45 lb/hr $W_H$ = 770 lb/hr $T_{in}$ = 140°F T.S. valve at nominal setting

a) Subcooled Length $L_{SC}$ and Boiling Length $L_B$ vs $P_{out}$

b) Boiling-Fluid Exit Temperature vs $P_{out}$

c) Boiling-Fluid Superheat $\Delta T_{SH}$ and Exit Quality $X_e$ vs $P_{out}$

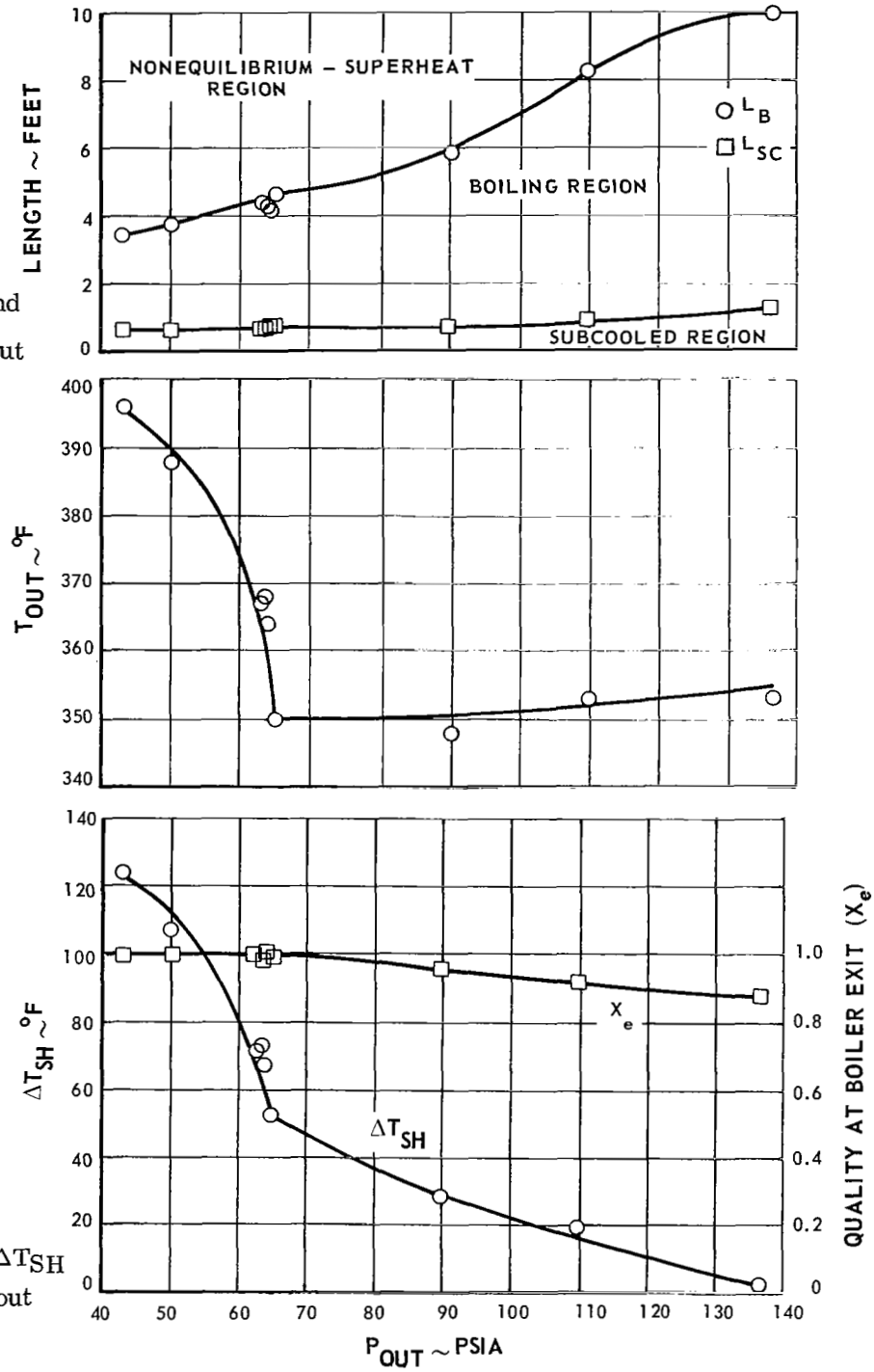


Figure 17 Steady-State Test Results. Variation of Boiler Performance with Boiling-Fluid Exit Pressure W = 45 lb/hr $W_H$ = 770 lb/hr $T_{in}$ = 140°F $T_{H\ in}$ = 410°F

a) Boiling-Fluid Pressure Drop vs $P_{out}$

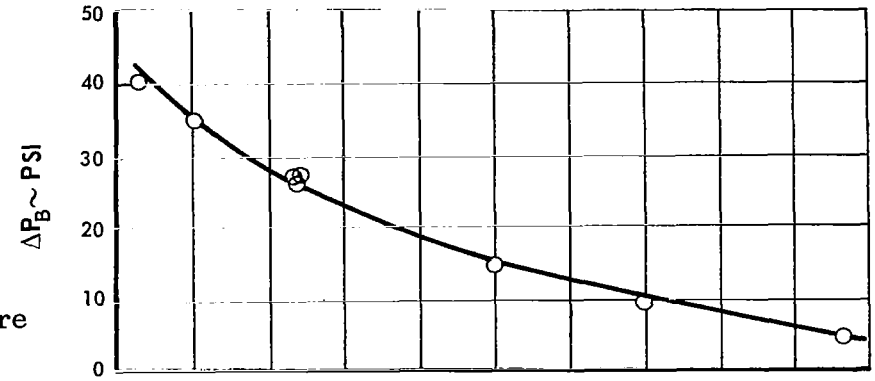


b) Heating-Fluid Exit Temperature vs $P_{out}$

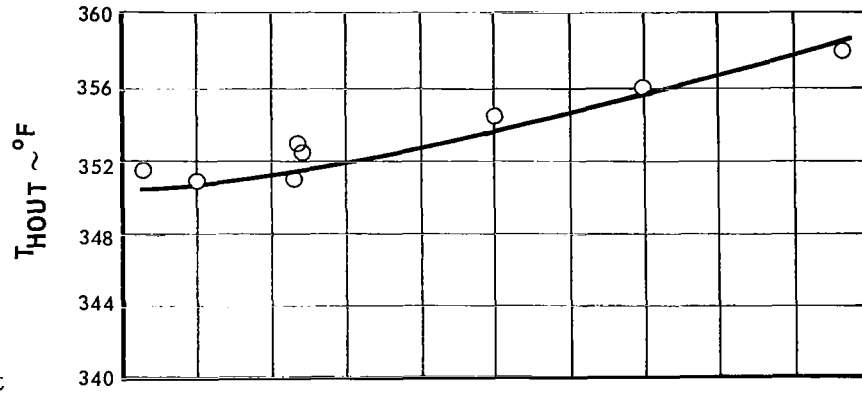


c) Pinch-Point Temperature Difference vs $P_{out}$

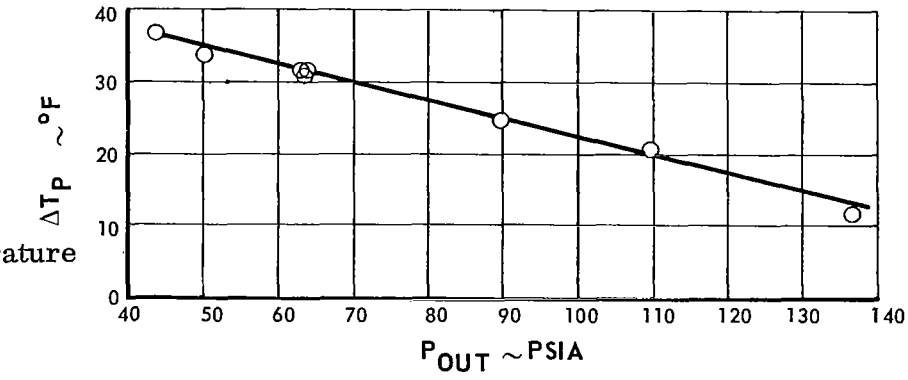


Figure 18 Steady-State Test Results. Variation of Boiler Performance with Boiling-Fluid Exit Pressure
W = 45 lb/hr $W_H$ = 770 lb/hr $T_{in}$ = 140°F $T_{H\,in}$ = 410°F

137 psia. The decrease in $X_e$ and $\Delta T_{SH}$ results from the reduction in the length of the nonequilibrium region shown in Figure 17a, and the reduced heat-transfer rates caused by the reduction in the temperature difference.

The decrease in $\Delta P_B$ with increasing values of $P_{out}$ shown in Figure 17b results primarily from the reduction in the length of the nonequilibrium-superheat region. An increase in the vapor density also contributes.

5. Effect of Varying Boiling-Fluid Inlet Temperature

The effects of varying the boiling-fluid inlet temperature are shown in Figures 19 and 20. Almost all of the performance parameters are relatively independent of $T_{in}$. However, as $T_{in}$ nears 200°F and approaches the saturation temperature of the boiling fluid, some increase in $T_{out}$ and $\Delta T_{SH}$ is observed. This occurs because the principal effect of changing the inlet temperature is to change the subcooled length. Since the subcooled length involves only a relatively small portion of the heat-transfer area in the boiler, the steady-state boiler performance is little affected. However, since a large part of the fluid mass in the boiler resides in the subcooled region, a larger effect on the dynamic characteristics may be produced.

C. Summary of Steady-State Characteristics

The steady-state test results indicate that the principal effect of increasing W on boiler performance is the negative slope observed over a portion of the boiling-pressure-drop curve and the transition in boiling-fluid exit conditions from dry superheated vapor to wet saturated vapor. The principal effect of increasing $W_H$ is an increase in the heat-transfer rate in the boiling region and subcooled region, caused by a higher heat-transfer coefficient and a higher average-temperature-difference between the boiling and heating fluids. Similarly increasing $T_{H\ in}$ raises this temperature difference, increasing the heat-transfer rate in the boiling region and subcooled region. Increasing $P_{out}$ has the reverse effect, since an increase of pressure raises the saturation temperature and decreases this temperature difference. Boiler performance is relatively insensitive to changes in $T_{in}$.

In evaluating this data it should be remembered that these experiments were performed using water, where the heat transfer coefficient of the heating fluid is considerably less than that of the boiling fluid in the boiling region. The heat transfer coefficient of the heating fluid is, therefore, the controlling factor in determining the overall heat transfer coefficient for this region. The sensitivity of boiler performance to changes in the primary variables may be different for typical space power boilers which employ metallic working fluids. In this case the heat transfer coefficients of both boiling and heating fluids in the boiling region are of equal magnitude.

a) Subcooled Length $L_{SC}$ and Boiling Length $L_B$ vs $T_{in}$

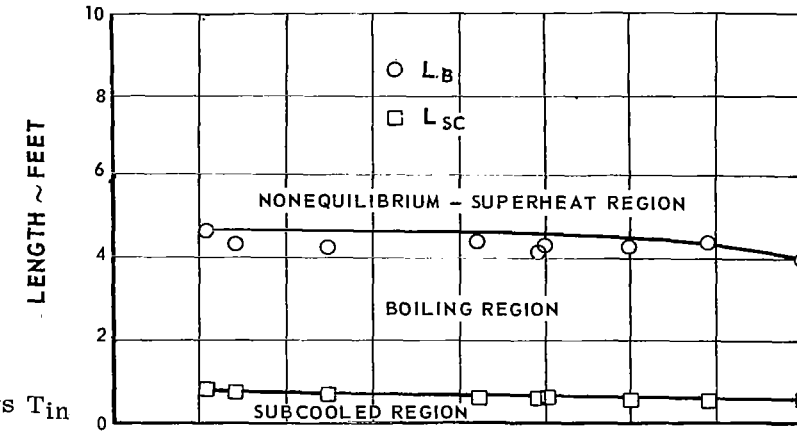


b) Boiling-Fluid Exit Temperature vs $T_{in}$

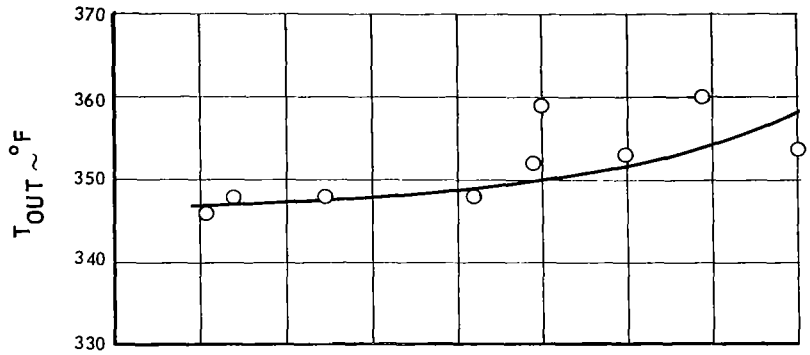


c) Boiling-Fluid Superheat $\Delta T_{SH}$ and Exit Quality $X_e$ vs $T_{in}$

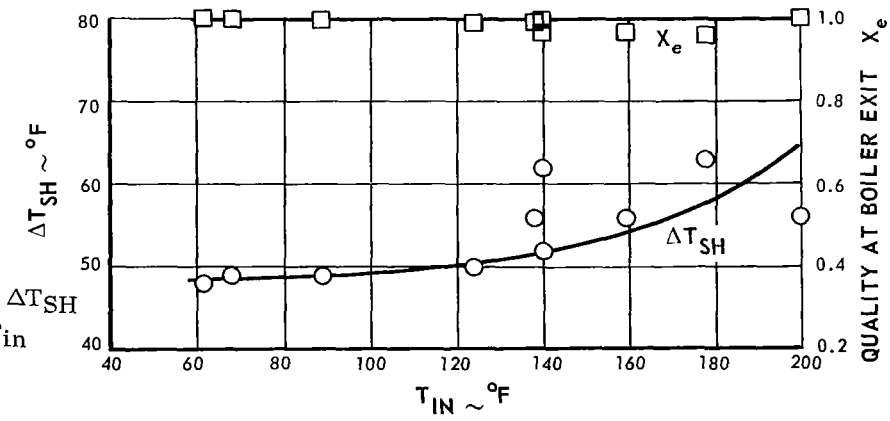


Figure 19 Steady-State Test Results. Variation of Boiler Performance with Boiling-Fluid Inlet Temperature
W = 45 lb/hr $W_H$ = 770 lb/hr T.S. valve at nominal setting $T_{H\,in}$ = 410°F

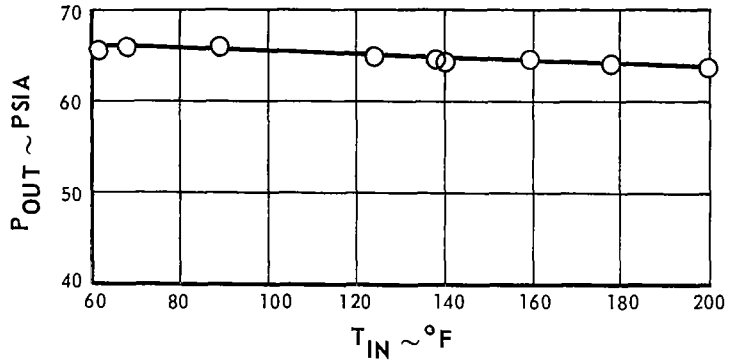


a) Boiling-Fluid Exit Pressure vs $T_{in}$

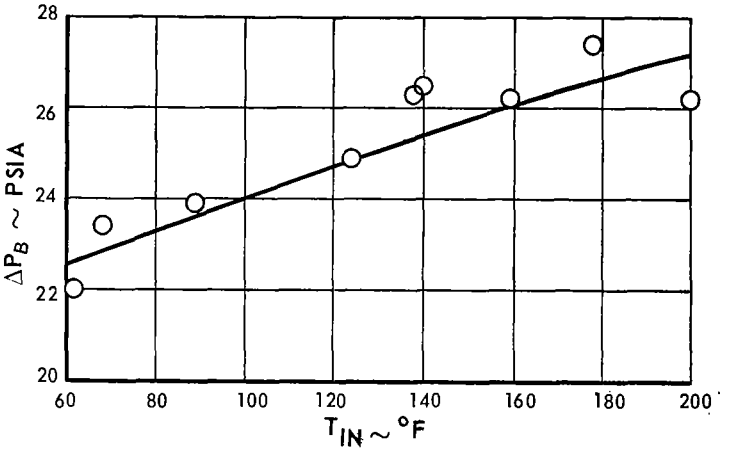


b) Boiling-Fluid Pressure Drop vs $T_{in}$

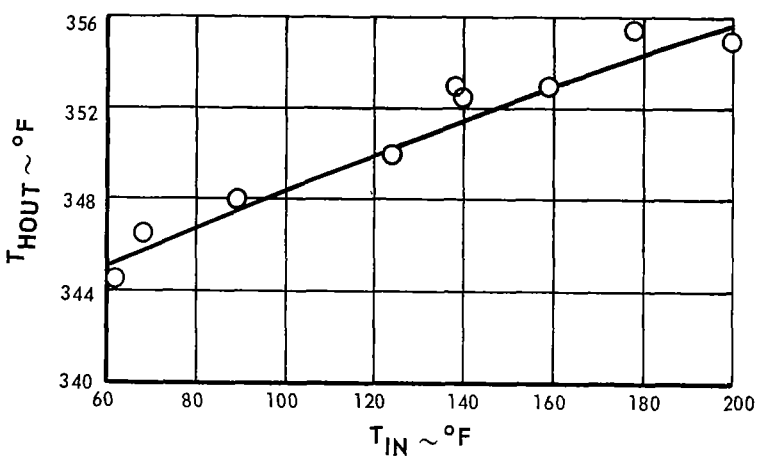


c) Heating-Fluid Exit Temperature vs $T_{in}$

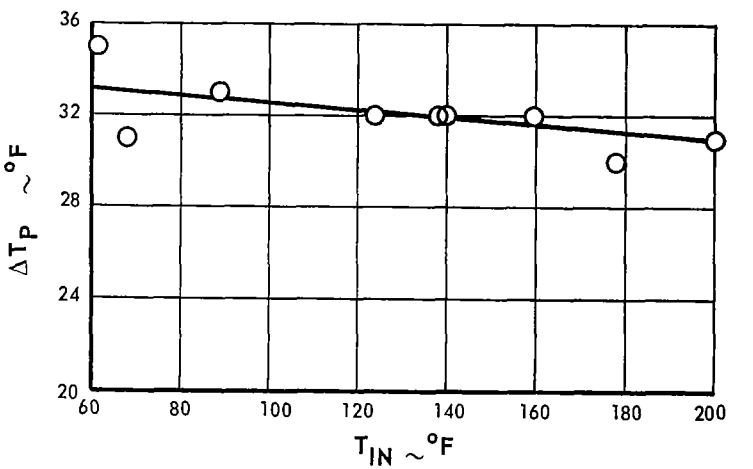


d) Pinch-Point Temperature Difference vs $T_{in}$

Figure 20 Steady-State Test Results. Variation of Boiler Performance with Boiling-Fluid Inlet Temperature $T_{in}$
$\dot{W}$ = 45 lb/hr $W_H$ = 770 lb/hr T.S. valve at nominal setting $T_{Hin}$ = 410°F

# V. DYNAMIC CHARACTERISTICS OF BOILER

Frequency-response and step-response tests were conducted at 21 operating conditions. The purpose of these tests was to determine how the dynamic response characteristics of the boiler are affected by changes in the primary variables. This was done to gain greater insight into the factors involved in the stability of boiler operation for Rankine-cycle space powerplants.

The 21 operating conditions selected for testing are listed in Table 5. Each condition is defined by constant values of the following primary variables.

mean boiling-fluid flow rate W
boiling-fluid inlet temperature $T_{in}$
heating-fluid flow rate $W_H$
heating-fluid inlet temperature $T_{H\ in}$
mean boiling-fluid exit pressure $P_{out}$, or turbine simulator valve setting

These conditions were selected so that each of the primary variables was varied individually about the nominal operating point while the other primary variables were held constant at their nominal values. This section describes the results of the dynamic tests conducted at these conditions.

## A. General Characteristics of the Frequency Response of the Boiler

The frequency-response tests were conducted by perturbing the boiling-fluid flow rate sinusoidally about a mean value as described in Section III above. The purpose of these tests was to determine how the transfer functions of the boiler are affected by the primary variables. In addition the transfer function for the boiling-fluid exit pressure obtained from this data provided an experimental basis for judging the theoretical transfer function presented in Section VII of this report. The frequency-response tests were conducted over a frequency range between 0.003 and 1.0 cycle per second. During the tests the variables listed in Table 4 were recorded as a function of time on film using a CEC Model T5-119 oscillograph recorder.

### 1. Linearity of Boiler Response

The amplitude of the perturbations in the boiling-fluid flow rate was kept small, approximately 6 percent of the mean value, to reduce nonlinear effects. This technique was successful since the variables generally responded in a linear manner. This can be seen in Figure 21a which is a reproduction of one of the

oscillograph recordings. Both the temperature and pressure traces appear as well defined sinusoids in response to the sinusoidal perturbation of boiling-fluid flow rate. The test results shown in Figure 21a were obtained at a heating-fluid flow rate of 840 lb/hr, a condition which produced dry superheated vapor at the boiler exit.

A nonlinear response of the boiling-fluid exit temperature $T_{out}$ did appear as boiling-fluid exit conditions were shifted from those of a dry superheated vapor to the nonequilibrium and wet saturated exit conditions discussed in Section IV above. This type of response can be seen in the nonsinusoidal shape of the $T_{out}$ trace in Figure 21b. The test result shown in Figure 21b was obtained at a boiling exit pressure of 130 psia, a condition which produced a nonequilibrium mixture of superheated vapor and liquid droplets at the boiler exit ($\Delta T_{SH} \approx 5°F$, $X_e \approx 0.88$). The fluctuations in the trace of $T_{out}$ result from the liquid droplets impinging on the thermocouple.

The pressure responses shown in Figure 21b are fairly linear as indicated by their sinusoidal shape. Irregularities superimposed on the sinusoids are probably the result of the passage of the liquid droplets through the choked turbine simulator valve. Nonlinear pressure responses were found only when the boiling fluid emerged in a wet saturated condition. When these nonlinear responses did occur, they were observed only at frequencies below 0.005 cps.

2. Experimental Frequency Responses

Experimental frequency responses to pertubations in boiling-fluid flow rate were determined at each test condition for the following variables.

1) boiling-fluid inlet pressure $P_{in}$
2) boiling-fluid exit pressure $P_{out}$
3) boiling-fluid exit temperature $T_{out}$
4) heating-fluid exit temperature $T_{H\ out}$

For each frequency tested at a given operating condition, the amplitudes and phase lags were determined using data read from the oscillograph recordings. For each operating condition, the amplitudes were normalized by dividing the amplitude read from the oscillograph recordings by the amplitude that resulted when the power-loop flow rate was changed by the same amount at zero frequency (i.e., the steady-state variation).

The normalizing data is presented in Table 11. It was obtained by taking steady-state data at two values of W above and two values below the mean value $\overline{W}$. The resulting values of $P_{in}$, $P_{out}$, $T_{out}$ and $T_{H\ out}$ were plotted

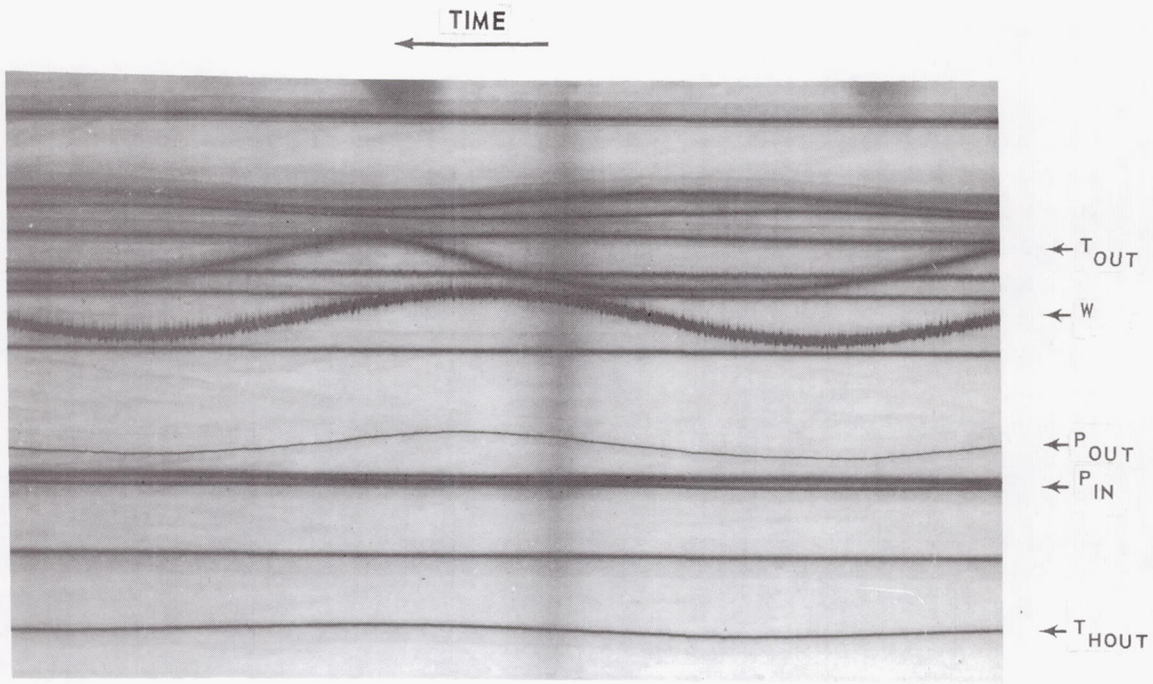


a) Typical Linear Response (obtained at $W_{HL}$ = 840 lb/hr, Frequency = 0.009 cps)

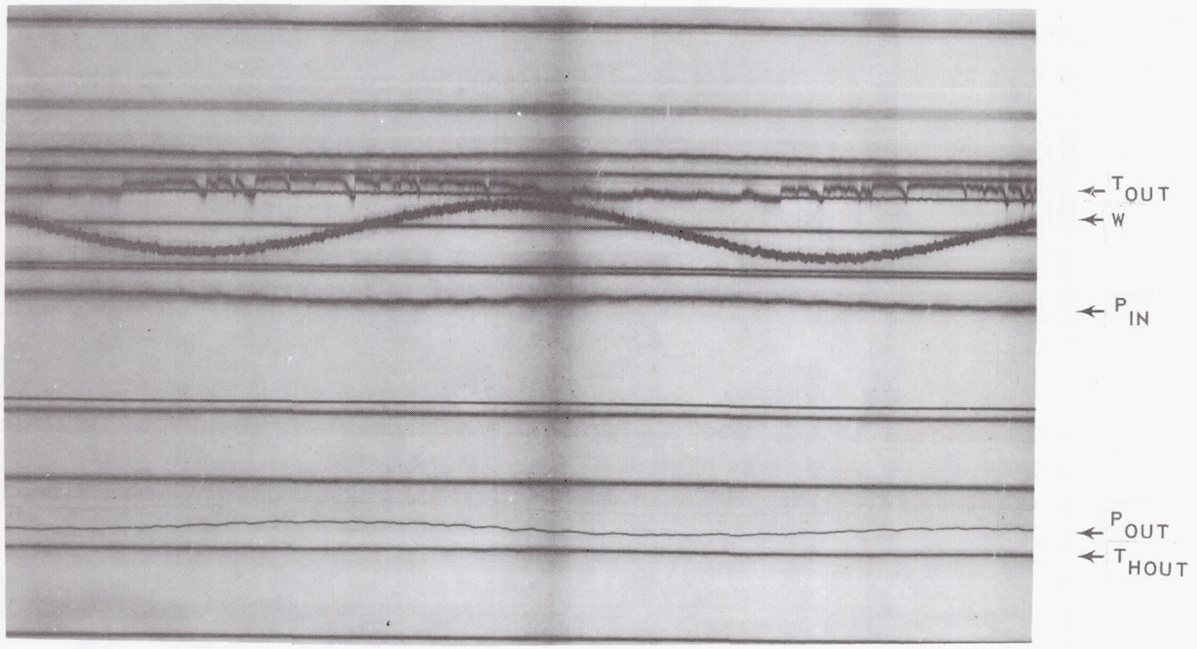


b) Typical Nonlinear Response of $T_{out}$ (obtained at $P_{out}$ = 130 psia, Frequency = 0.01 cps)

Figure 21 Oscillograph Recordings Illustrating the Linearity of the Frequency-Response Tests

as functions of W and a straight line was drawn through the points for each variable. The amplitude at zero frequency was taken as the slope of this straight line.

The experimental frequency responses were plotted in the form of Bode diagrams as shown in Figures 23 through 32. In general the normalized amplitudes presented in these figures are observed to attenuate from values near 1.0 at a frequency of 0.003 cps to extremely low values in the frequency range between 0.1 and 0.3 cps. The normalized amplitude of the heating-fluid exit temperature $T_{Hout}$ frequency response displays a resonance at the higher frequencies. At several test conditions the frequency responses of the boiling-fluid inlet and exit pressures also displayed resonances. However, in no case did any of the resonances display normalized amplitudes greater than 0.6.

Since high amplitude resonances in the frequency responses of the boiling-fluid inlet and exit pressures can have an important influence on hydrodynamic stability, additional scanning type tests were performed at the operating conditions which displayed resonances in these frequency responses. The purpose of these tests was to determine if there were any very high amplitude resonances either between the data points displayed in Figures 23 through 32 or at frequencies higher than those originally tested. These tests were conducted at closely spaced intervals in the frequency range between 0.2 and 2.0 for the conditions indicated on Table 5. In order to permit instant visual determination of a high amplitude resonance, the signals from the inlet and exit pressure transducers were fed directly into an oscilloscope rather than the oscillograph recorder. However, in the course of these tests no very high amplitude resonances were found.

B. Effect of Primary Variables on Boiler Frequency Response

In examining the frequency-response test data, it appears possible to relate the effects of the primary variables on the frequency response to the condition of the boiling fluid at the exit of the boiler. In almost every instance, the normalized amplitude and the phase lag for each frequency response are observed to shift to the left of the Bode diagrams as any of the primary variables is varied, so that the exit conditions change in the direction from dry superheated vapor to wet saturated conditions. In general, this results in a lower amplitude and a greater phase lag at a given frequency. This can be seen by making a side-by-side comparison of the Bode diagrams presented in Figures 23 through 32. This is further illustrated in Figure 22 for the variation of the boiling-fluid flow rate.

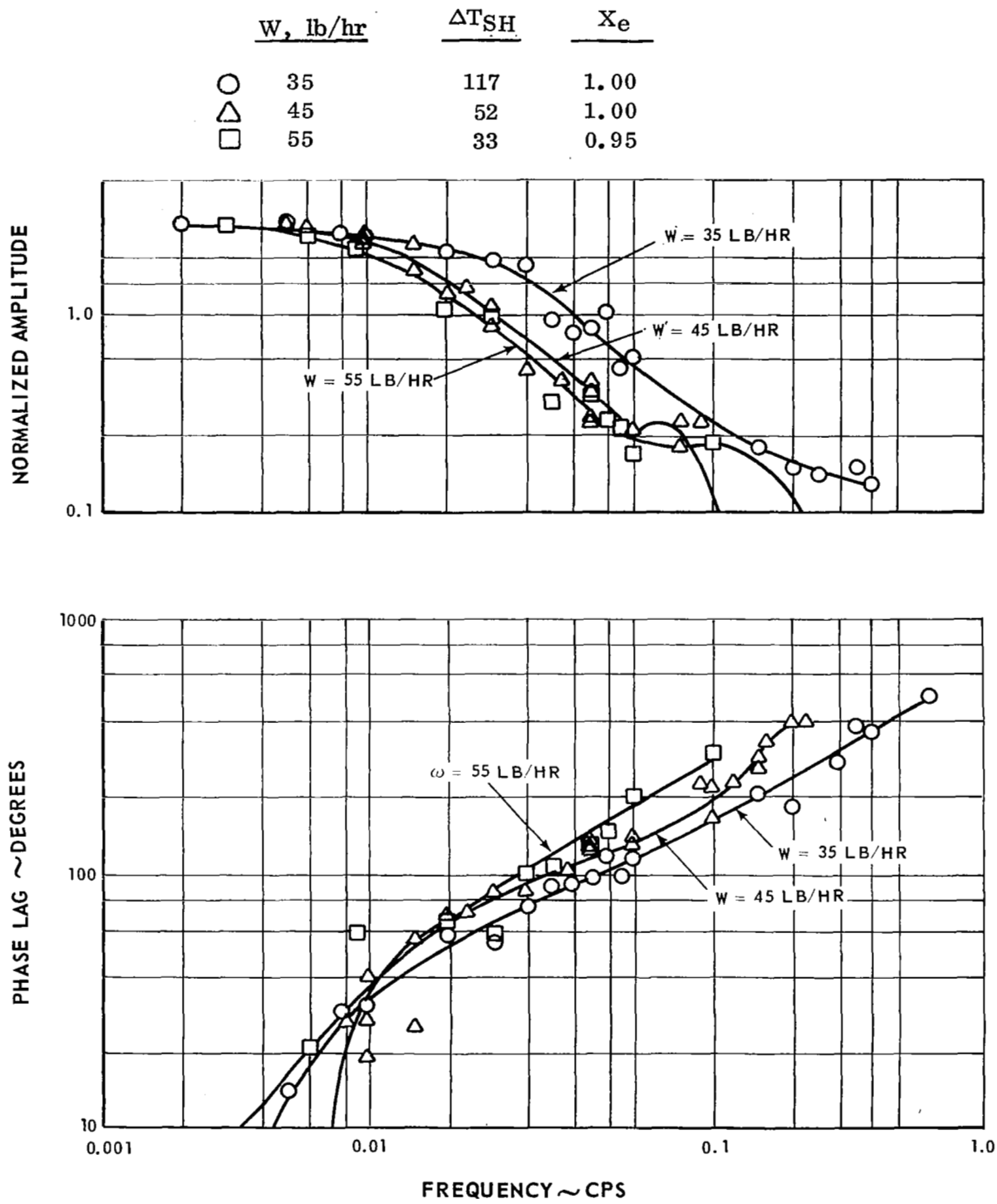


Figure 22 Effect of Boiling-Fluid Flow Rate on $P_{out}$ Frequency Response

The following paragraphs discuss specific characteristics of the experimental frequency-response curves as functions of each primary variable.

1. Effect of Boiling-Fluid Flow Rate

The frequency response for various values of the mean boiling-fluid flow rate, $\overline{W}$ are shown in Figures 23 and 24. The individual graphs are arranged in the order of increasing values of $\overline{W}$ with the 35 lb/hr case representing a dry superheated boiling-fluid exit condition and the 65 lb/hr case representing a wet saturated exit condition.

At a mean boiling-fluid flow rate of 35 lb/hr, Figure 23 shows that the $P_{in}$ frequency response has a normalized amplitude above 3.0 in the middle frequency range. The amplitude then attenuates rapidly to a very low value at 0.25 cps. Two sharp resonances are then found in the frequency range between 0.25 and 1.0 cps. One of these resonances occurs near the frequency of the 180-degree phase lag and may be responsible for the unstable boiler operation observed at flow rates below 30 lb/hr. This is discussed further in Section VI of this report.

As $\overline{W}$ is increased to 45 lb/hr, these sharp resonances are observed to disappear. As $\overline{W}$ is further increased and the boiling-fluid exit conditions become wet (i.e. $X_e < 1.00$), these two resonances reappear at the middle and higher frequencies. In addition, the maximum value of the normalized amplitude curve is observed to decrease towards 1.0 as $\overline{W}$ is increased above 35 lb/hr.

At a mean boiling-fluid flow rate $\overline{W}$ of 35 lb/hr, the normalized amplitude of the $P_{out}$ frequency response does not exhibit the sharp resonances shown by the $P_{in}$ frequency response. As $\overline{W}$ is increased, the normalized amplitude curve of the $P_{out}$ frequency response does not exhibit the sharp resonances shown by the $P_{in}$ frequency response. As $\overline{W}$ is increased, the normalized amplitude curve of the $P_{out}$ frequency response shifts to the left and a slight resonance develops at the

The normalized amplitude of the $T_{H\ out}$ frequency response displays a resonance at all values of $\overline{W}$. As $\overline{W}$ is increased the normalized amplitude curve is observed to shift to the left while the resonance becomes more pronounced.

The normalized amplitude of the $T_{out}$ frequency response is observed to attenuate much more rapidly than the normalized amplitudes of the other frequency responses for values of $\overline{W}$ between 35 and 45 lb/hr. At flow rates above 45 lb/hr, the boiling-fluid exit quality dropped below 1.0 and the response of $T_{out}$ became nonlinear as discussed above. It was not possible to determine a frequency response for $T_{out}$ under these conditions.

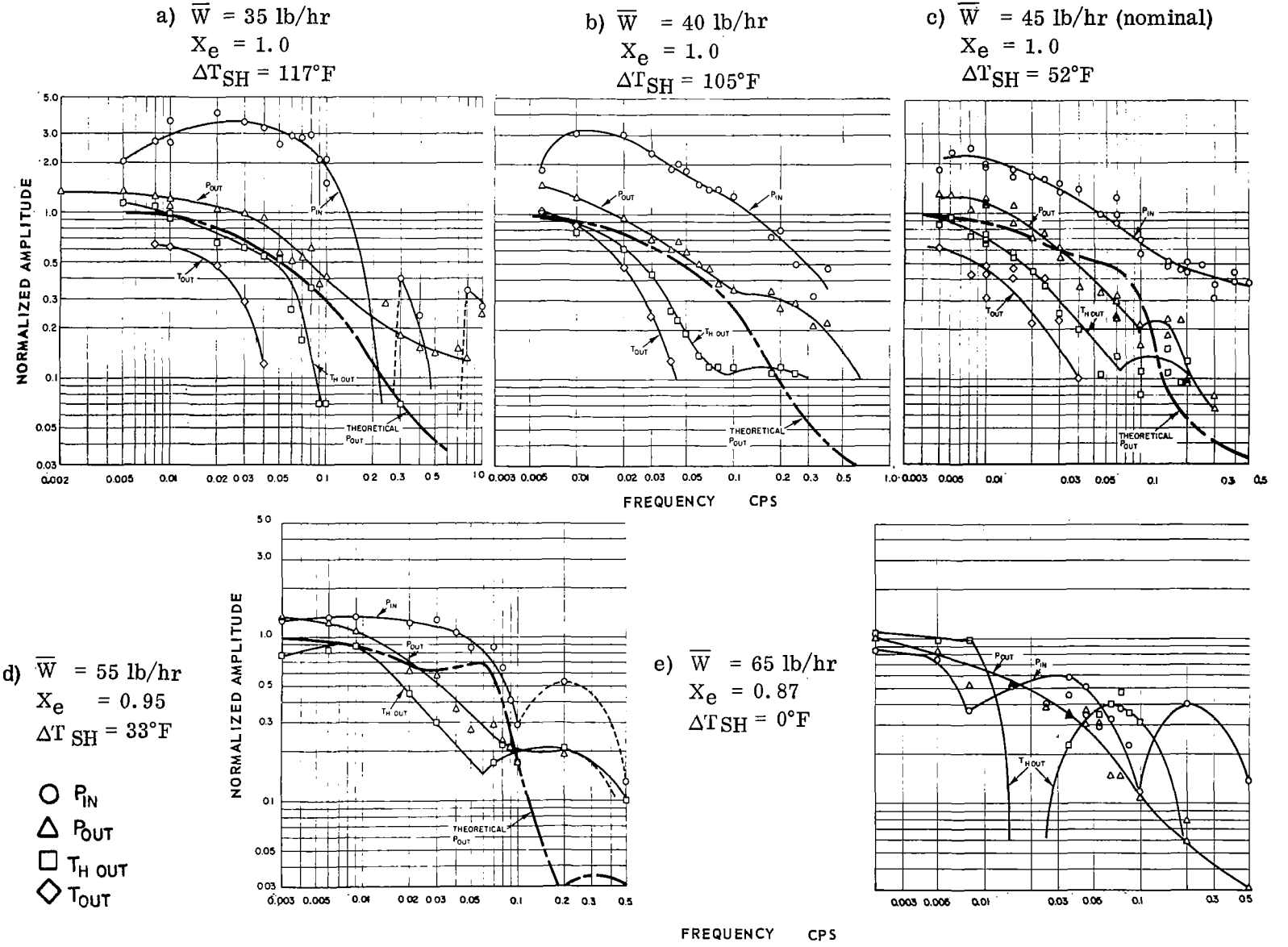


Figure 23 Frequency Response Test Results. Normalized Amplitude vs Frequency at Various Boiling-Fluid Flow Rates. $T_{in}$ = 140°F, $W_H$ = 770 lb/hr, T.S. valve at nominal setting, $T_{H\ in}$ = 410°F

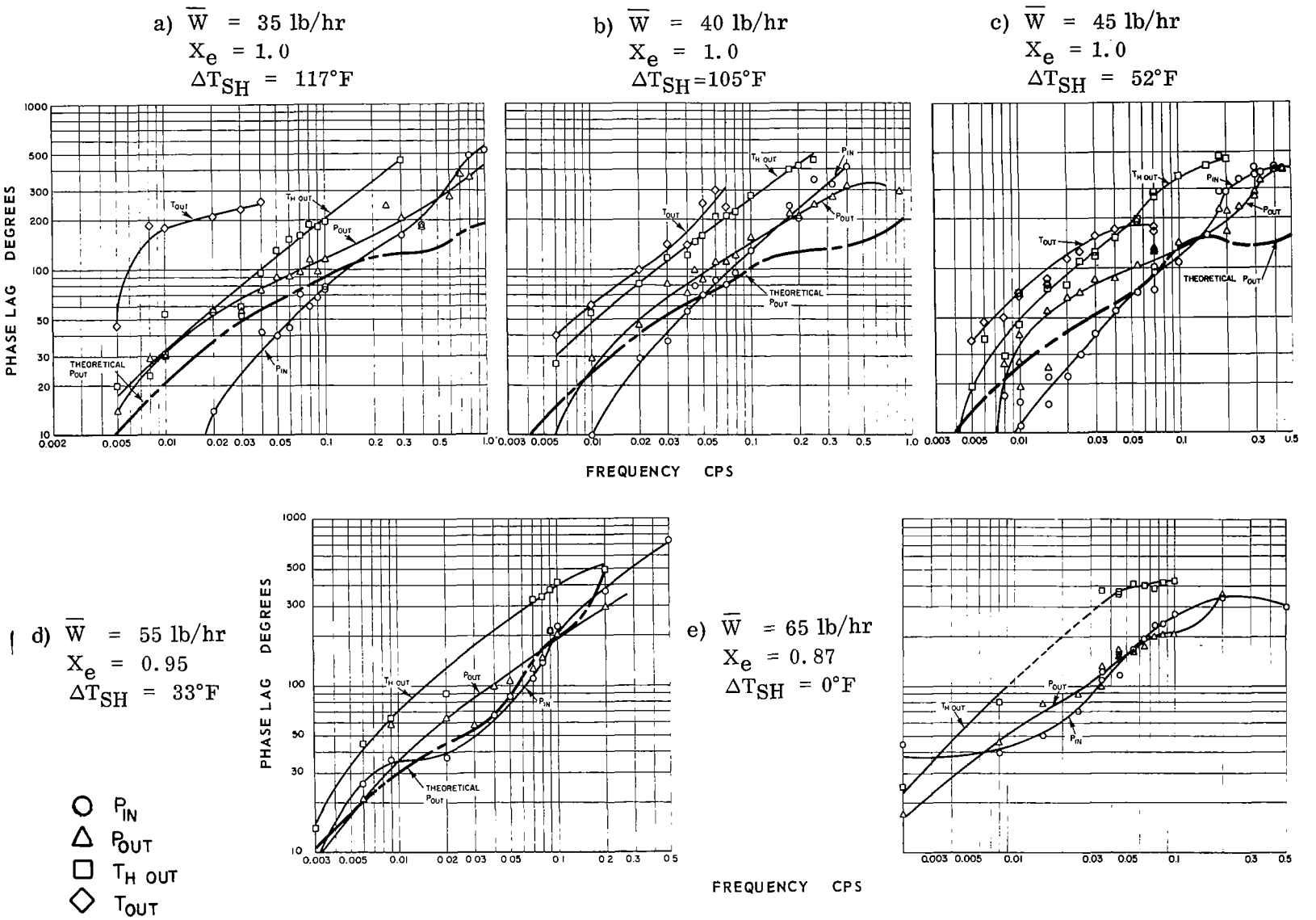


Figure 24 Frequency Response Test Results. Phase Lag vs Frequency at Various Boiling-Fluid Flow Rates. $T_{in}$ = 140°F, $W_H$ = 770 lb/hr, T.S. valve at nominal setting, $T_{H\ in}$ = 410°F

As $\overline{W}$ is increased from 35 lb/hr the phase lag of the $T_{out}$ frequency response shifts to the right as can be seen by comparing Figure 24a to 24 c. This is the principal exception found to the general tendency of both normalized-amplitude and phase-lag curves to shift to the left as boiling-fluid exit conditions change from dry superheated vapor towards wet saturated conditions.

In conducting the frequency-response tests at a mean boiling-fluid flow rate of 35 lb/hr an unusual phenomenon was observed which has not yet been explained. At a single frequency near 3.0 cps the level of the boiling-fluid exit pressure was observed to drop drastically and then remain constant with time. In addition no further fluctuations in exit pressure were observed on the oscillograph recording in response to the sinusoidal perturbations of boiling-fluid flow rate.

2. Effect of Heating-Fluid Flow Rate

The frequency responses for various values of the heating-fluid flow rate $W_H$ are shown in Figures 25 and 26. The individual graphs on these figures are arranged in order of decreasing value of the heating-fluid flow rate, with the 1000 lb/hr case representing a dry superheated boiling-fluid exit condition and the 400 lb/hr case representing a wet nonequilibrium exit condition.

In comparing the frequency responses at the different conditions shown in these figures a general tendency of both normalized-amplitude and phase-lag curves to shift to the left as $W_H$ is decreased can be seen. This corresponds to a change in boiling-fluid exit conditions from dry superheated vapor to wet nonequilibrium conditions.

The normalized amplitude of the $P_{in}$ frequency response exhibits no resonances. The normalized amplitude of the $P_{out}$ frequency response exhibits a slight resonance only in the immediate region of the nominal operating condition of 770 lb/hr. The normalized amplitude of the $T_{Hout}$ frequency response develops a resonance at a heating fluid flow rate of 840 lb/hr. This resonance becomes more pronounced as heating-fluid flow rate is decreased, producing nonequilibrium conditions at the boiling fluid exit.

An interesting phenomenon was observed while testing at the 400 lb/hr condition. When perturbing the boiling-fluid flow rate at a frequency of 0.085 cps, $P_{in}$ and $P_{out}$ responded at a frequency of 0.24 cps, a harmonic of the input frequency, while the other variables responded at the input frequency. This type of response may be related to an area of unstable operation also discovered while testing at the 400 lb/hr condition, which is discussed further in Section VI below.

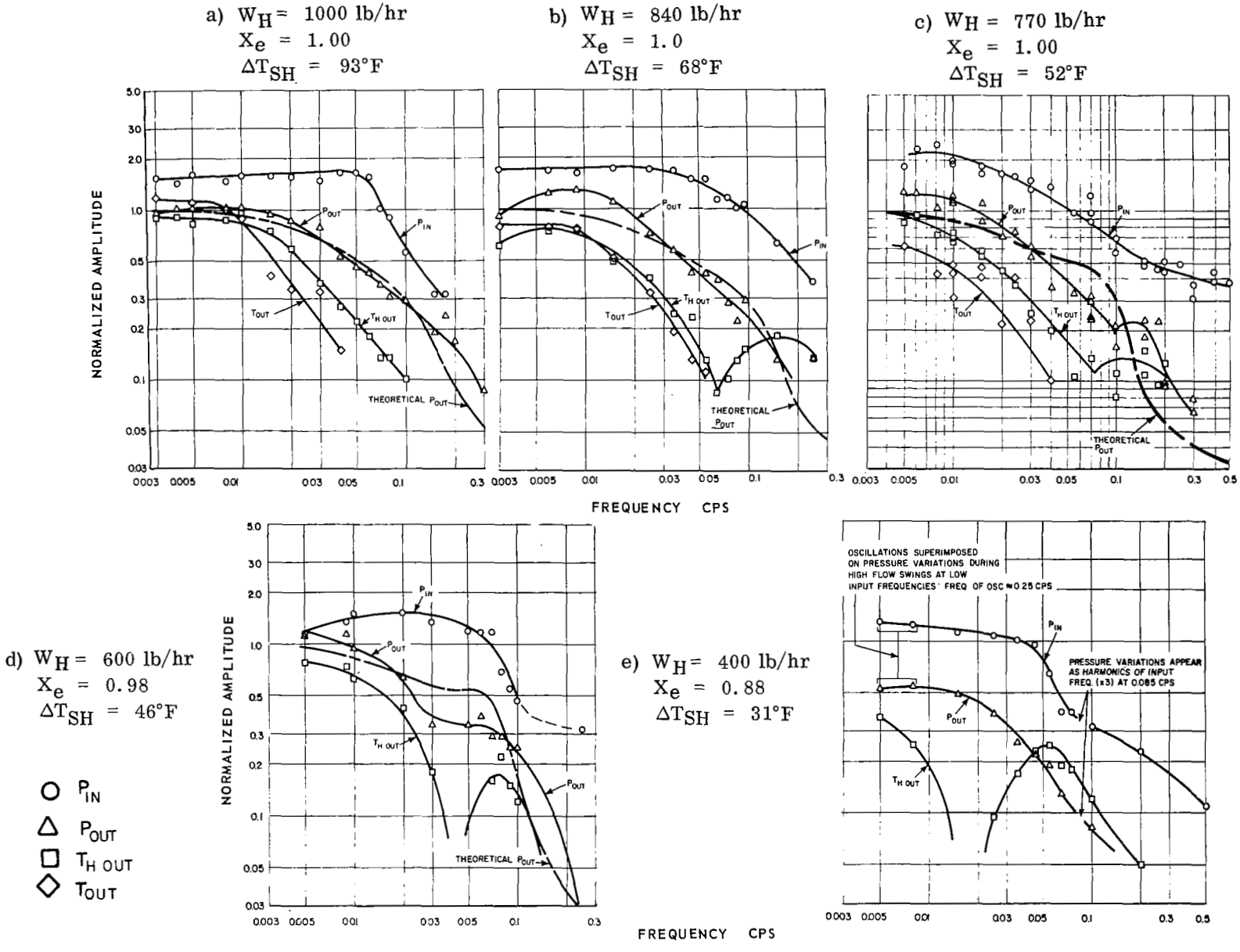


Figure 25 Frequency Response Test Results. Normalized Amplitude vs Frequency at Various Heating-Fluid Flow Rates. W = 45 lb/hr, $T_{H\ in}$ = 410°F, $T_{in}$ = 140°F, T.S. valve at nominal setting

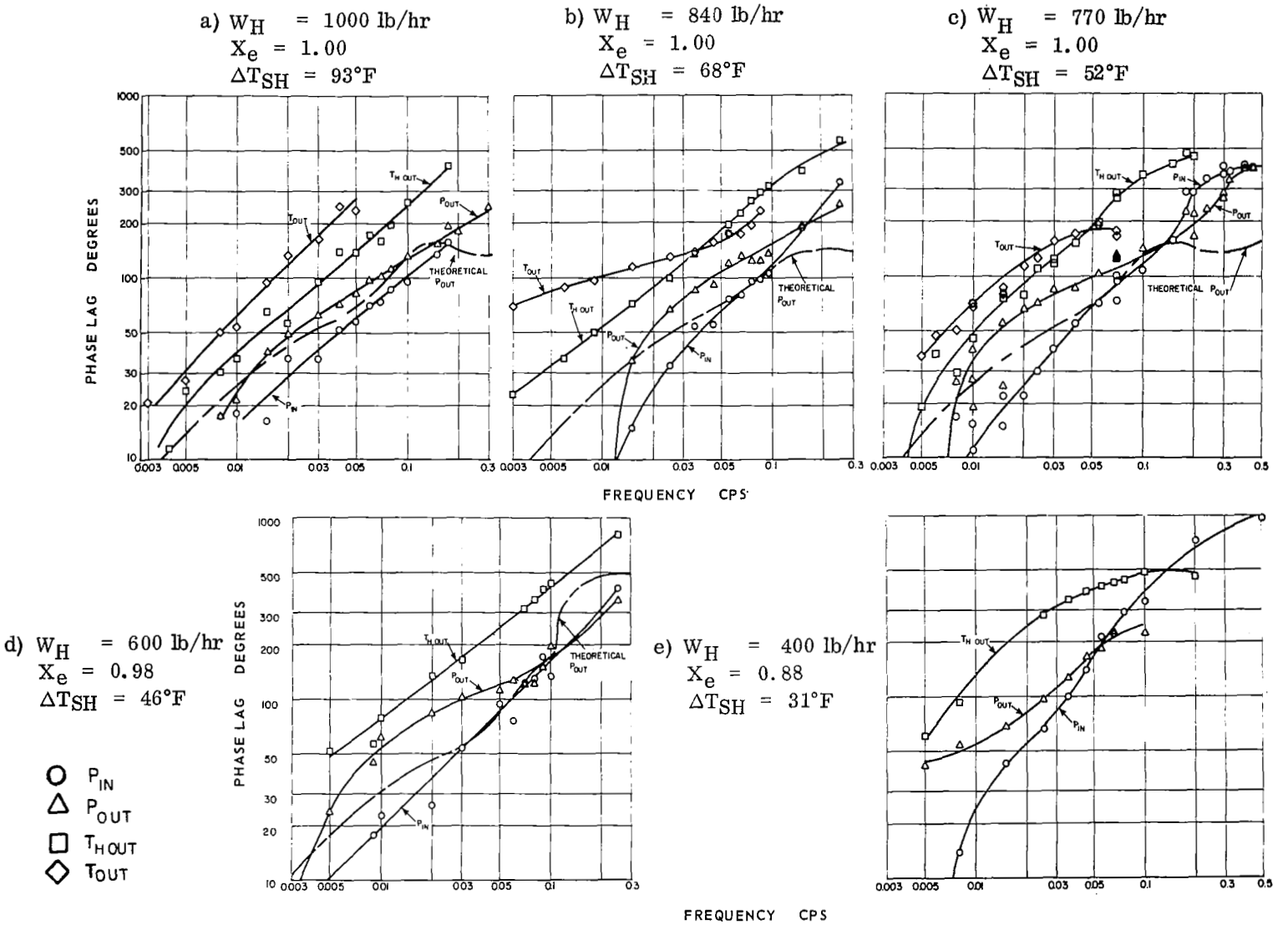


Figure 26 Frequency Response Test Results. Phase Lag vs Frequency at Various Heating-Fluid Flow Rates. W = 45 lb/hr, $T_{H\,in}$ = 410°F, $T_{in}$ = 140°F, T.S. valve at nominal setting

3. Effect of Heating-Fluid Inlet Temperature

The frequency responses for various values of heating-fluid inlet temperature $T_{Hin}$ are shown in Figures 27 and 28. The individual graphs in these figures are arranged in order of decreasing value of heating-fluid inlet temperature with the 430°F case representing a dry superheated boiling fluid exit condition and the 360°F case representing a wet nonequilibrium exit condition.

In comparing the frequency responses at the different test conditions shown in Figures 27 and 28 it can be seen that the normalized-amplitude and phase-lag curves tend to shift to the left as $T_{H\,in}$ is decreased.

The normalized amplitude of the $P_{in}$ frequency response exhibits a resonance at the 360°F condition. The normalized amplitude of the $P_{out}$ frequency response displays a slight resonance for values of $T_{H\,in}$ below 420°F. The normalized amplitude of the $T_{Hout}$ frequency response also develops a resonance at the 420°F condition. This resonance becomes more pronounced as $T_{H\,in}$ is decreased and nonequilibrium exit conditions are achieved.

At the 360°F condition the phase-lag curve of the $T_{Hout}$ frequency response is drawn as a dotted line in the frequency range between 0.01 and 0.03 cps. This was done because the exact shape of the curve in this region is not known. Since there was no readable variation in the amplitude of the $T_{Hout}$ response in this region, it was not possible to determine the phase lag from the oscillograph recording.

4. Effect of Boiling-Fluid Exit Pressure

The frequency responses for various values of the mean boiling-fluid exit pressure $P_{out}$ are shown in Figures 29 and 30. The individual graphs in these figures are arranged in order of increasing value of $P_{out}$, with the 50 psia case representing a dry superheated boiling fluid exit condition and the 130 psia case representing a wet nonequilibrium condition.

In comparing the frequency responses at the different conditions shown in Figures 29 and 30 it can again be seen that all normalized-amplitude and phase-lag curves shift to the left as $P_{out}$ is increased, producing a decrease in boiling-fluid superheat and exit quality. In addition, the maximum value of the normalized amplitude of the $P_{in}$ frequency response is observed to decrease as $P_{out}$ is increased.

The normalized amplitude of the $P_{out}$ frequency response develops a slight resonance near the nominal condition of 65 psia. However, the resonance is not significant at other conditions. The normalized amplitude of the $T_{Hout}$ frequency response exhibts a resonance at all values of $P_{out}$. This resonance is seen to

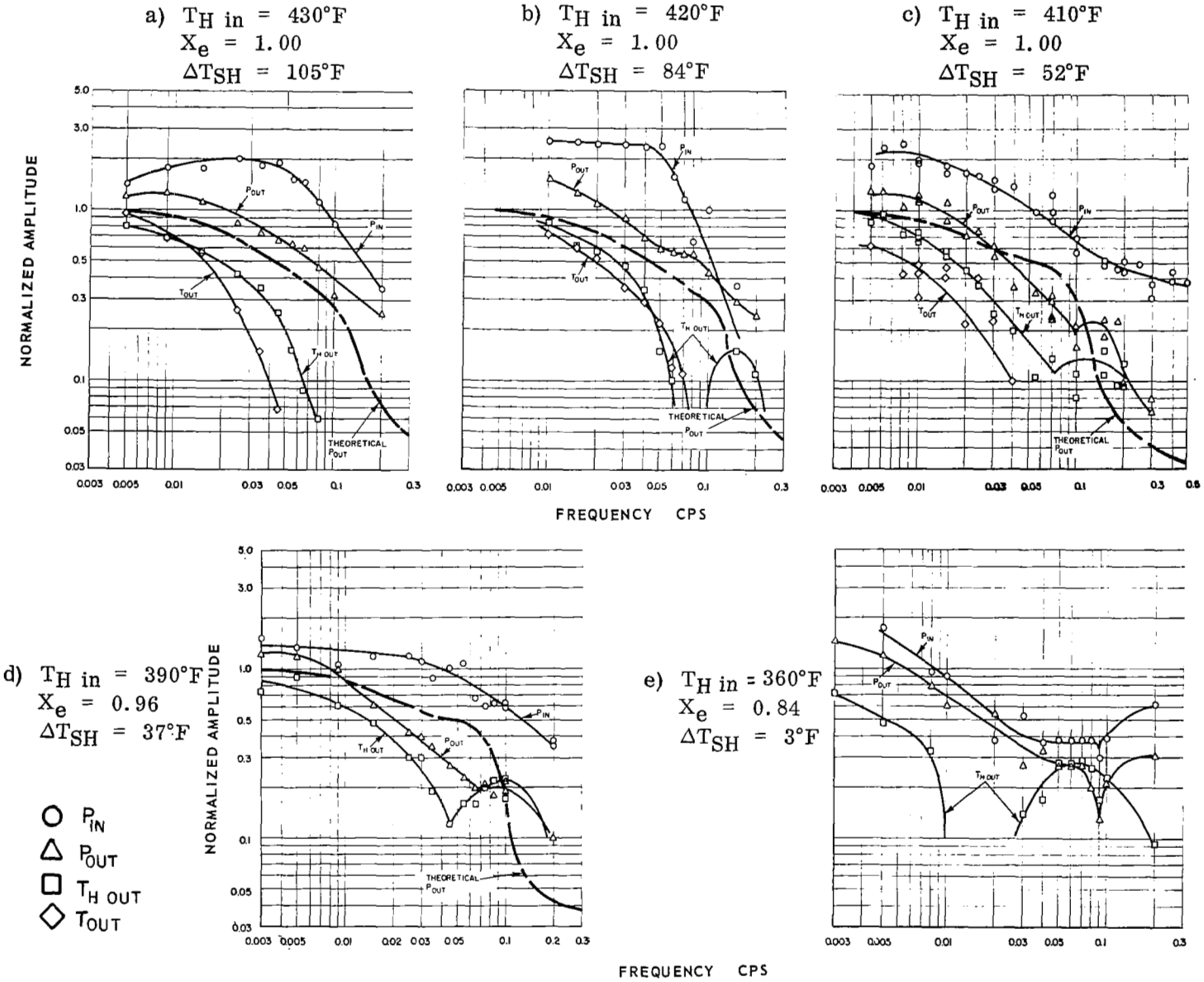


Figure 27 Frequency Response Test Results. Normalized Amplitude vs Frequency at Various Heating-Fluid Inlet Temperatures. W = 45lb/hr, $W_H$ = 770 lb/hr, $T_{in}$ = 140°F, T.S. valve at nominal setting

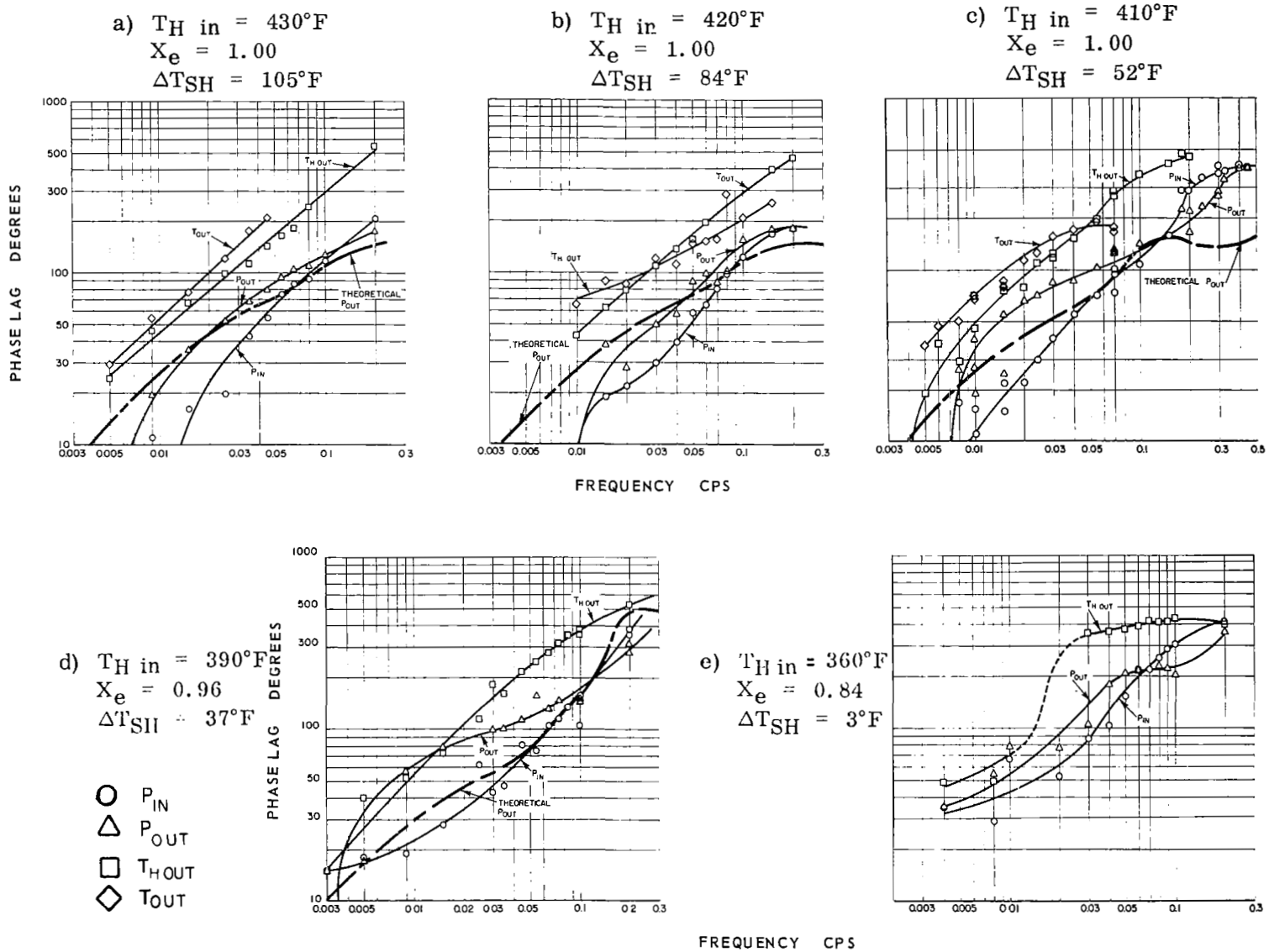


Figure 28 Frequency Response Test Results. Phase Lag vs Frequency at Various Heating-Fluid Inlet Temperatures. W = 45 lb/hr, $W_H$ = 770 lb/hr, $T_{in}$ = 140°F, T.S. valve at nominal setting

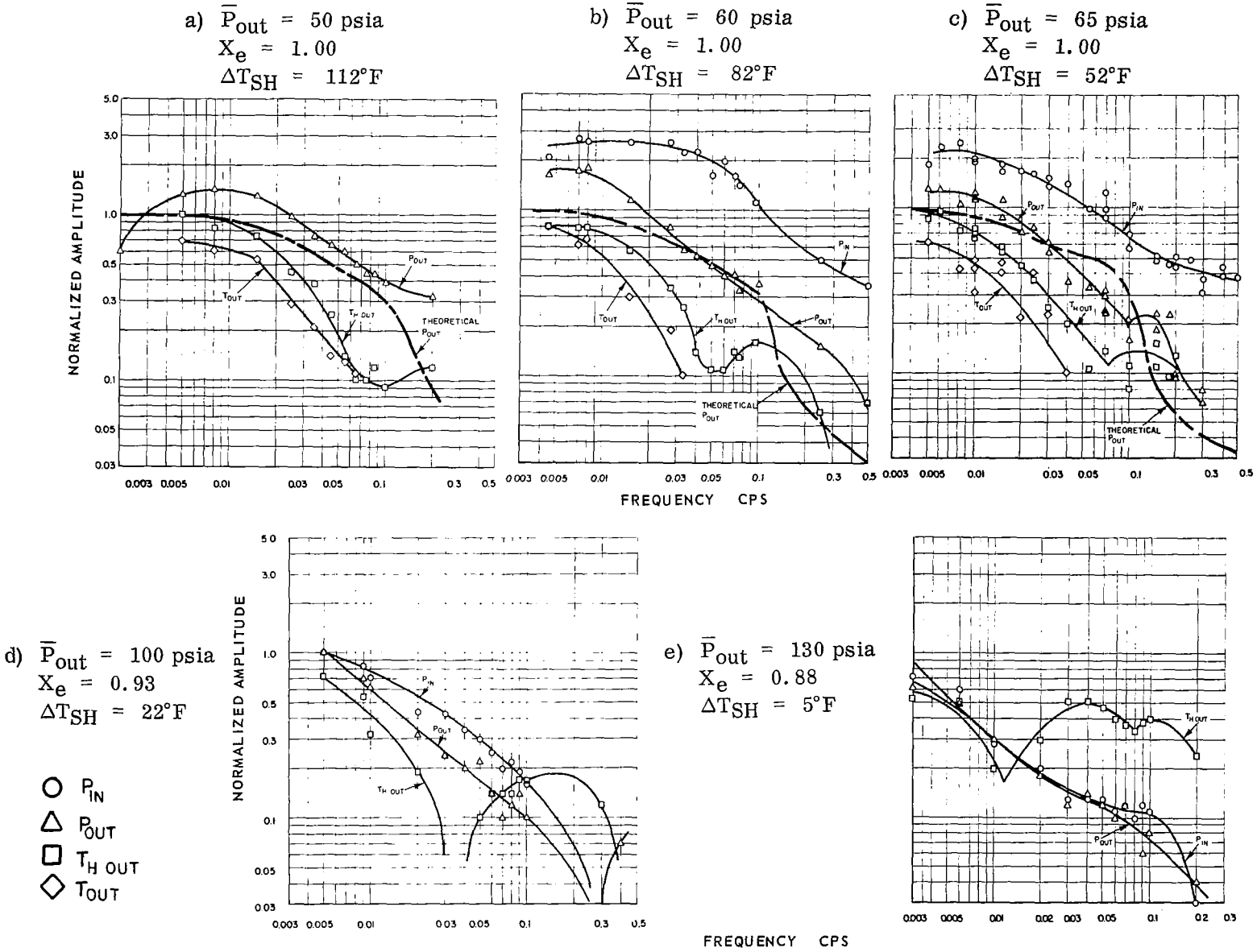


Figure 29 Frequency Response Test Results. Normalized Amplitude vs Frequency at Various Boiling-Boiling-Fluid Exit Pressures. W = 45 lb/hr, $W_H$ = 770 lb/hr, $T_{in}$ = 140°F, $T_{H\ in}$ = 410°F

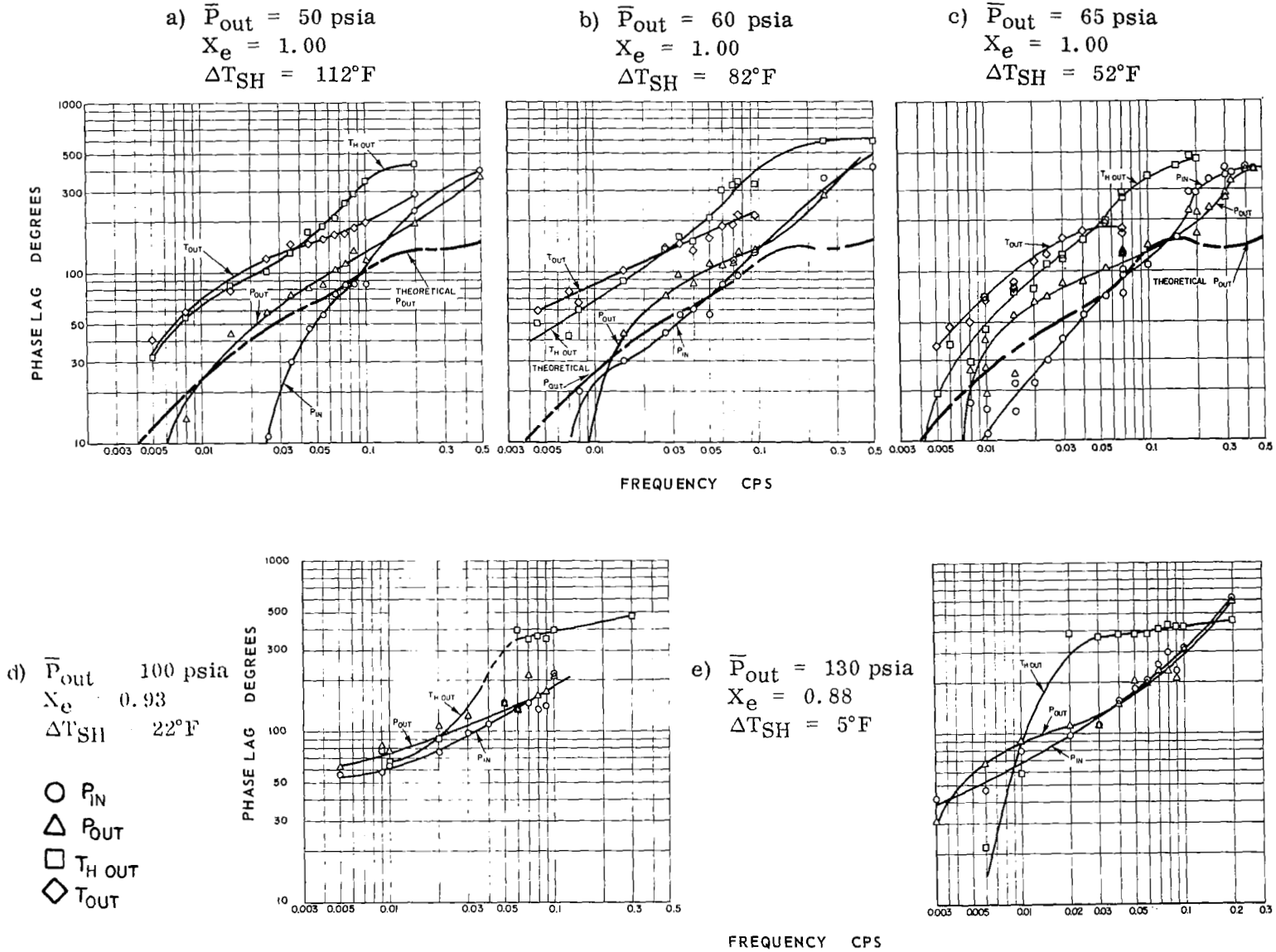


Figure 30 Frequency Response Test Results. Phase Lag vs Frequency at Various Boiling-Fluid Exit Pressures. W = 45 lb/hr, $W_H$ = 770 lb/hr, $T_{in}$ = 140°F, $T_{H\ in}$ = 410°F

become more pronounced and a second resonance is seen to develop as $P_{out}$ is increased, producing nonequilibrium conditions at the boiling-fluid exit.

In Figure 29a it can be seen that no normalized-amplitude curve is plotted for the $P_{in}$ frequency response for the 50 psia case. The reason for this can be seen by examining Figure 33 which is a plot of the steady-state normalizing data, $\Delta P_{in}/\Delta W$ versus $P_{out}$. The normalizing data is seen to approach zero as $P_{out}$ approaches 50 psia. This steady-state behavior results from the fact that the decrease in pressure drop in the boiler with an increase in flow rate nearly equals the increase in pressure upstream of the choked valve with an increase in flow rate. When this data is used to normalize the amplitude of the frequency response for the 50 psia case, values approaching infinity result and the normalized amplitude is no longer a convenient parameter to describe the boiler dynamics.

If the actual amplitude of the frequency response in this region is studied instead of the normalized amplitude, an interesting effect is noticed. Figure 34 shows a plot of actual amplitudes for the $P_{in}$ response at three different exit pressure conditions. The actual amplitudes are almost identical over most of the frequency range for all three conditions. This occurs despite significant differences in the normalized amplitude. This indicates that, although there are advantages in presenting frequency-response data by normalizing variations to their steady-state values, in some cases dynamic similarities may be obscured in the normalizing process.

5. Effect of Boiling-Fluid Inlet Temperature

The frequency response for various values of the boiling-fluid inlet temperature $T_{in}$ are shown in Figures 31 and 32. The individual graphs on these figures are arranged in order of decreasing value of $T_{in}$ which also represents the order of decreasing boiling-fluid superheat.

In comparing the frequency responses at these different conditions, there appears to be very little difference between the frequency responses at each condition. However there is some tendency for the normalized-amplitude and phase-lag curves to shift to the left as $T_{in}$ decreases.

6. Theoretical Transfer Function

Figures 23 through 32 also contain curves representing the theoretical values for the $P_{out}$ transfer function as predicted by the analysis of boiler dynamics presented in Section VII of this report. These curves permit a point-by-point comparison between the theoretical and experimental values for the $P_{out}$ normalized amplitudes and phase lags. Additional comparisons between the theory and the experimental data together with a detailed discussion of these comparisons are presented in Section VII.

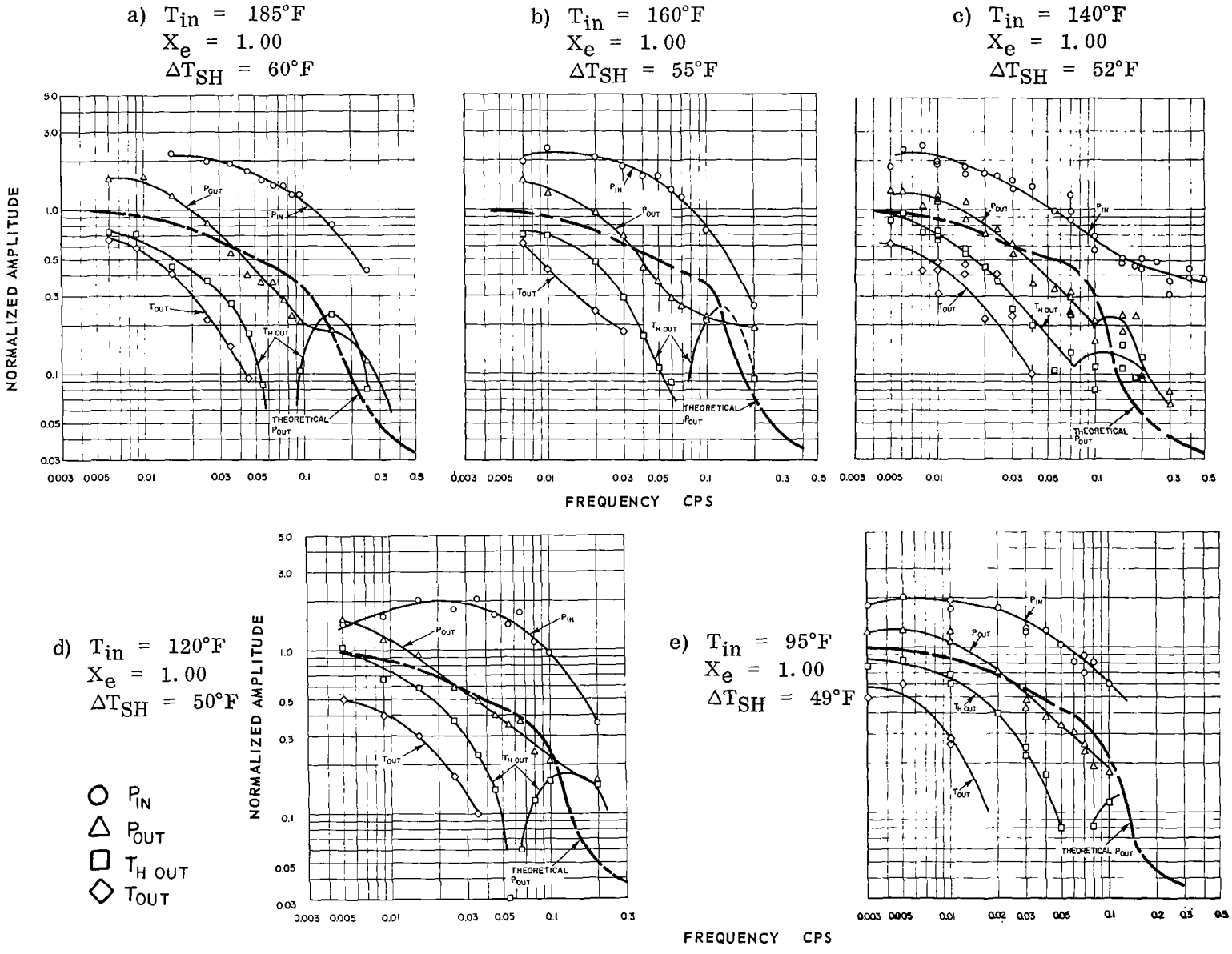


Figure 31 Frequency Response Test Results. Normalized Amplitude vs Frequency at Various Boiling-Fluid Inlet Temperatures. W = 45 lb/hr, $W_H$ = 770 lb/hr, $T_{H\ in}$ = 410°F, T.S. valve at nominal setting

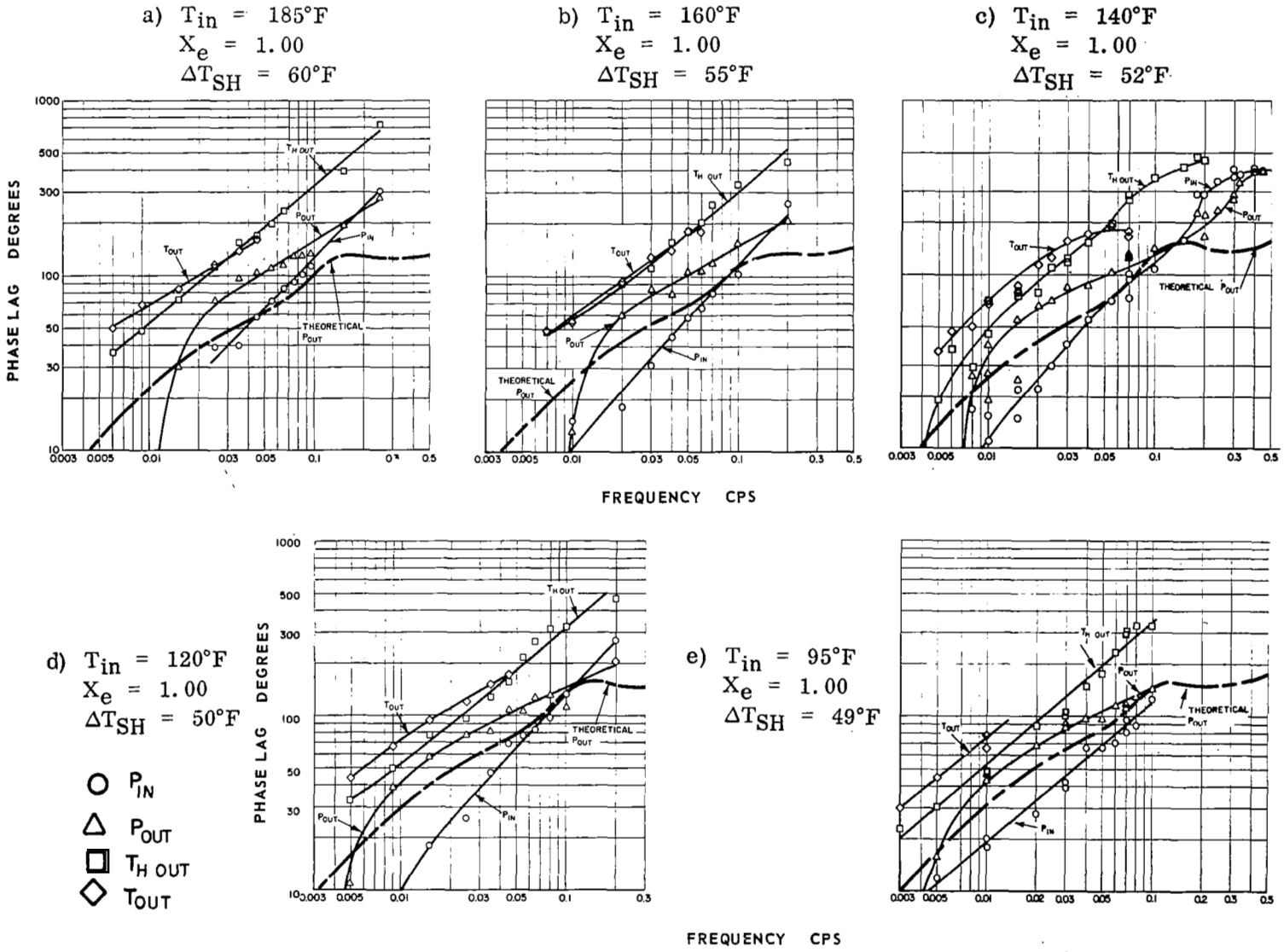


Figure 32 Frequency Response Test Results. Phase Lag vs Frequency at Various Boiling-Fluid Inlet Temperatures. W = 45 lb/hr, $W_H$ = 770 lb/hr, $T_{H\ in}$ = 410°F, T.S. valve at nominal setting

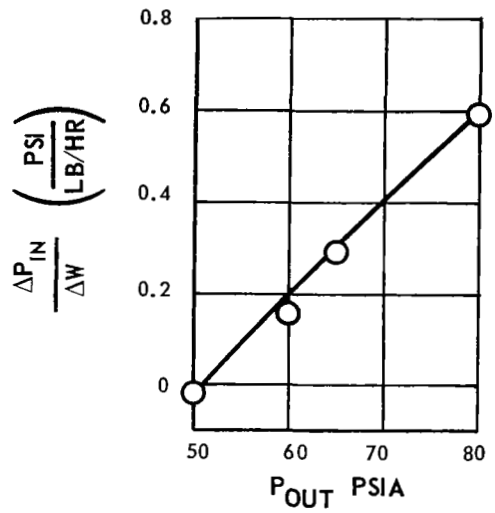


Figure 33 Normalizing Data vs Boiling-Fluid Exit Pressure $P_{out}$

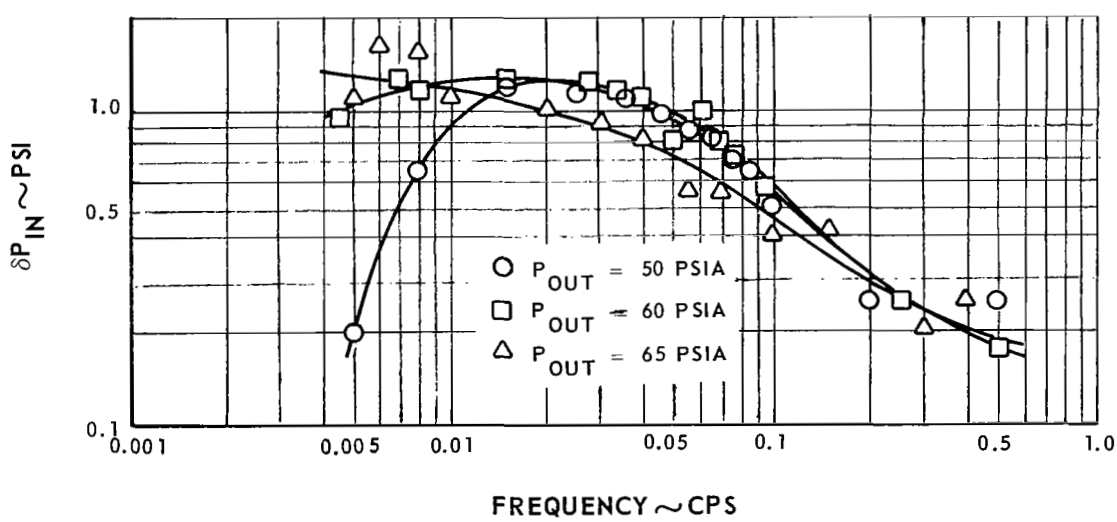


Figure 34 Amplitude of Boiling-Fluid Inlet Pressure Response $\delta P_{in}$ to Sinusoidal Flow Perturbation of ± 3.0 lb/hr

## C. Step-Response Characteristics of Boiler

At each operating condition specified in Table 5 step-response tests were conducted following the procedures described in Section III of this report. The main purpose of the step-response tests was to determine whether resonances were present at higher frequencies than could be obtained in the frequency-response tests. Examination of the oscillograph recordings of the pressure and temperature responses revealed no high-frequency resonances. A photograph of an oscillograph record of the initial portion of one test is presented in Figure 35. In this test a 12 percent step increase in flow rate at the boiler inlet was made starting at a steady-state condition with 60 psia boiler exit pressure. The initial and final positions of the recorded boiler-exit pressure trace are shown with dotted lines in the figure to make the form of the response more apparent. The boiler-exit pressure response is seen to consist of a pure delay of about 2 seconds, followed by an approximately exponential rise with a time constant of about 10 seconds. The responses of the boiler inlet pressure, exit temperature and the heating-fluid exit temperature also tend towards a delay followed by an exponential change, but are less clear-cut. In particular, the boiler inlet pressure underwent readjustments up to 15 minutes after the step change. These readjustments were small in absolute magnitude (less than 1 psi) but relatively large compared to the total change induced by the flow step.

The other steady-state operating conditions at which superheated vapor was produced at the boiler exit showed the same type of responses to a step change in flow rate.

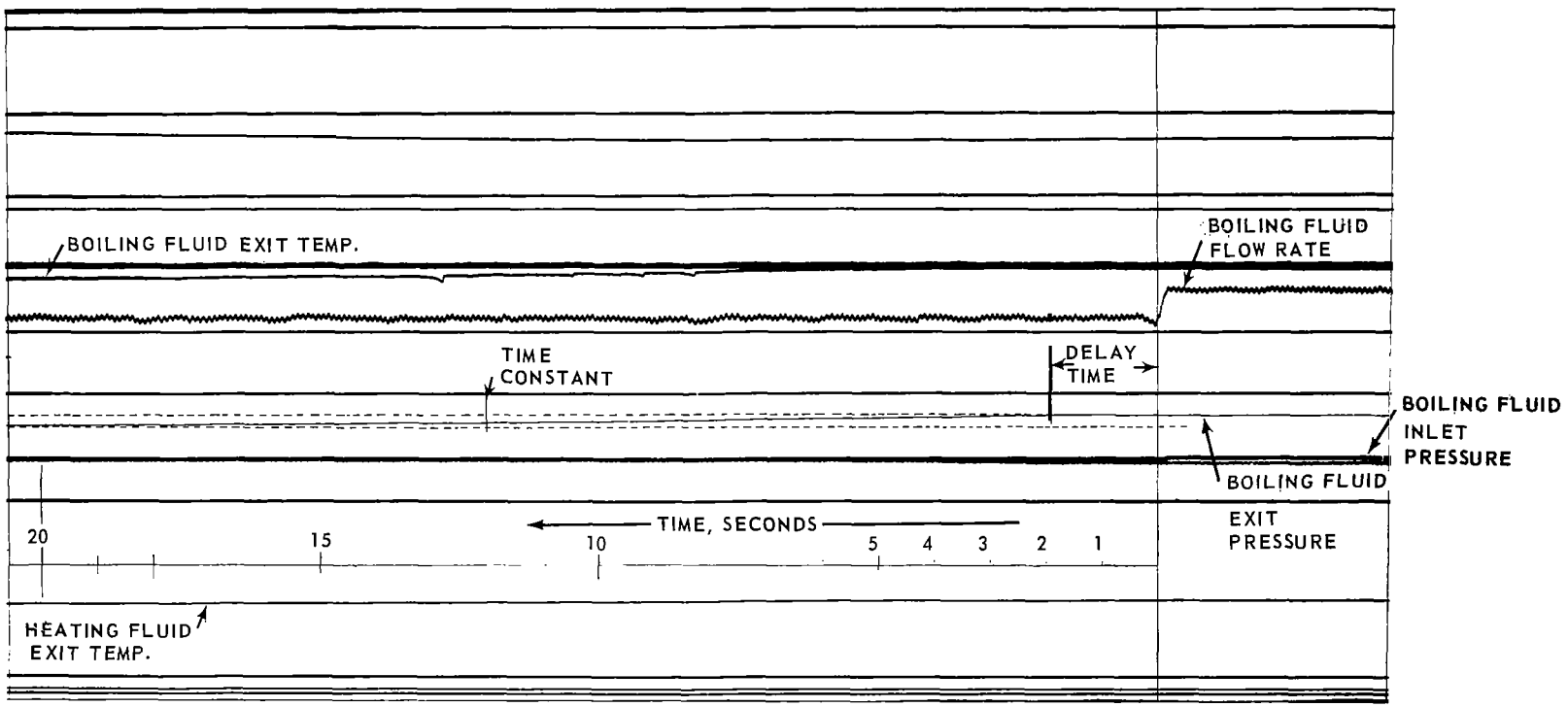


Figure 35 Oscillograph Recording of Response to Step Change in Boiling-Fluid Flow Rate

# VI. BOILER STABILITY

During the course of the testing required under the contract, two areas of unstable boiler operation were observed. These instabilities were characterized by sustained oscillations in boiling fluid pressure. This section discusses the possible causes of these instabilities in terms of the types of instability known to occur in boiling systems.

## A. Types of Boiler Instability

Instability in boiling systems has been observed by a multitude of investigators. The causes for these instabilities are not, as yet, completely understood. They do appear to be closely related to the specific test system configurations employed by each investigator. As a consequence, numerous types of different boiler instability have been cited in the literature. As indicated in Reference 1, the job of classifying and understanding the different types of instability is still in its early stages.

The following paragraphs discuss the types of instability that are pertinent to the boiling system of this study. For purposes of discussion these instabilities will be classified in terms of those that result from interactions between the boiler and the feed system and those that result from dynamic interactions within the boiler itself.

### 1. Feed System-Boiler Instability

The frequency response of the boiler inlet pressure indicates the dynamic head-flow characteristics that are required in the power-loop pump in order to avoid unstable system interactions. A simplified stability criterion for matching the pump and boiler for a typical Rankine-cycle system is presented as follows. The coupling between boiler inlet pressure and pump exit pressure, and between boiler-inlet flow rate and pump-exit flow rate is represented schematically below, using control notation. It will be assumed in the following discussion that the pump exit pressure-versus-flow rate characteristics are linear, that there are no additional impedances between the pump and the boiler, and that there are no time delays between changes in flow rate in the pump and pump exit pressure. This condition is approximated in a powerplant when the pump inlet pressure is held constant, as was done with the test system in this study.

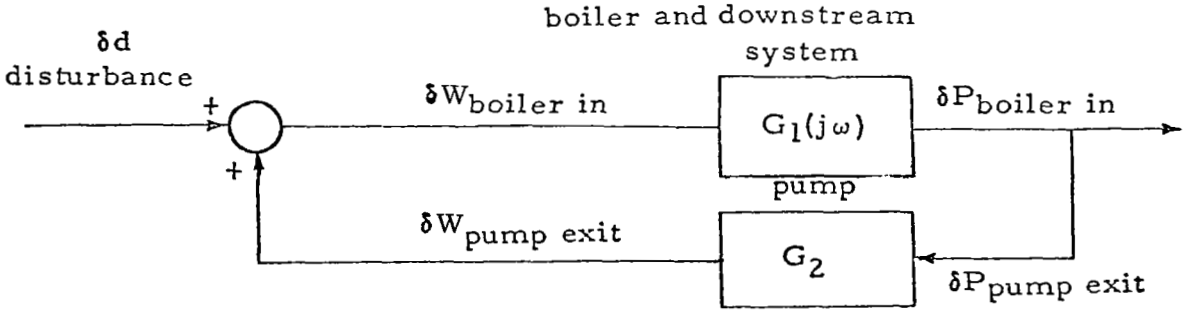

Since the fluid between the pump exit and boiler inlet is in a liquid state and lengths involved are small, the effects of fluid compressibility and momentum are small. The pressure and flow rate are, therefore, approximately equal at the pump exit and boiler inlet. Assuming that a disturbance is introduced into this coupled system, the response of the boiler inlet pressure to the disturbance $\delta d$ may be written

$$\delta P_{\text{boiler in}} = \frac{G_1 (j\omega)}{1 - G_1 (j\omega) G_2} \quad \delta d \tag{2}$$

The terms $G_1 (j\omega)$ and $G_2$ represent the transfer functions of the boiling-fluid inlet pressure, and the pump exit pressure respectively. $G_1 (j\omega)$ is defined by the relation

$$G_1 (j\omega) = \frac{\delta P_{in}}{\delta W_{in}} \quad (j\omega) \tag{3}$$

The experimental values of $G_1 (j\omega)$ obtained from the $P_{in}$ frequency-responses are presented in Figures 23 through 32. Actual amplitudes can be calculated by multiplying the normalized amplitudes presented in these figures by the corresponding values of $\Delta P_{in}/\Delta W$ presented in Table 11.

If it is assumed that the boiler is stable when operated in an open loop, then the closed-loop system diagrammed would be unstable when the following condition is incurred

$$G_1 (j\omega) G_2 \geq 1 \tag{4}$$

From the assumed linear pump characteristics

$$P_{\text{pump exit}} = C_1 - C_2 \, W_{\text{pump exit}} \tag{5}$$

It follows that $$G_2 = \frac{\delta W_{\text{pump exit}}}{\delta P_{\text{pump exit}}} = - \frac{1}{C_2} \tag{6}$$

Consequently this simplified analysis indicates that the system is unstable when

$$\left| G_1 (j\omega) \right| \geq \left| - C_2 \right| \tag{7}$$

According to Equation (7) pump-boiler instabilities will occur under two possible conditions:

a) The amplitude of the boiler transfer function is negative at zero frequency and less than the pump slope, $C_2$, as shown in Equation (8) below:

$$G_1(0) = \left(\frac{\Delta P_{in}}{\Delta W}\right) < -C_2 \qquad (8)$$

b) The amplitude of the boiler transfer function is greater than or equal to $C_2$ at a phase angle of 180 degrees (or an odd multiple of 180 degrees).

The first condition is frequently referred to as a static instability since it results from the static, rather than the dynamic characteristics of the boiler. The static instability results in an unattainable operating point, and system excursions from this point to a stable point. This type of instability is discussed widely in the literature[6].

The pump-boiler combination for the test system of this study is statically stable. This occurs in spite of the negative slope of the curve of boiler pressure loss versus flow rate, and results from the fact that as the boiling-fluid flow rate is increased, the increase in $P_{out}$ resulting from the flow through the choked restriction more than compensates for the reduction in $\Delta P$ due to the negative slope. This is illustrated in Figure 36 where it can be seen that $P_{in}$ increases with flow rate over the range of the conditions tested. The term $(\Delta P_{in}/\Delta W)$ is therefore positive and the system is statically stable.

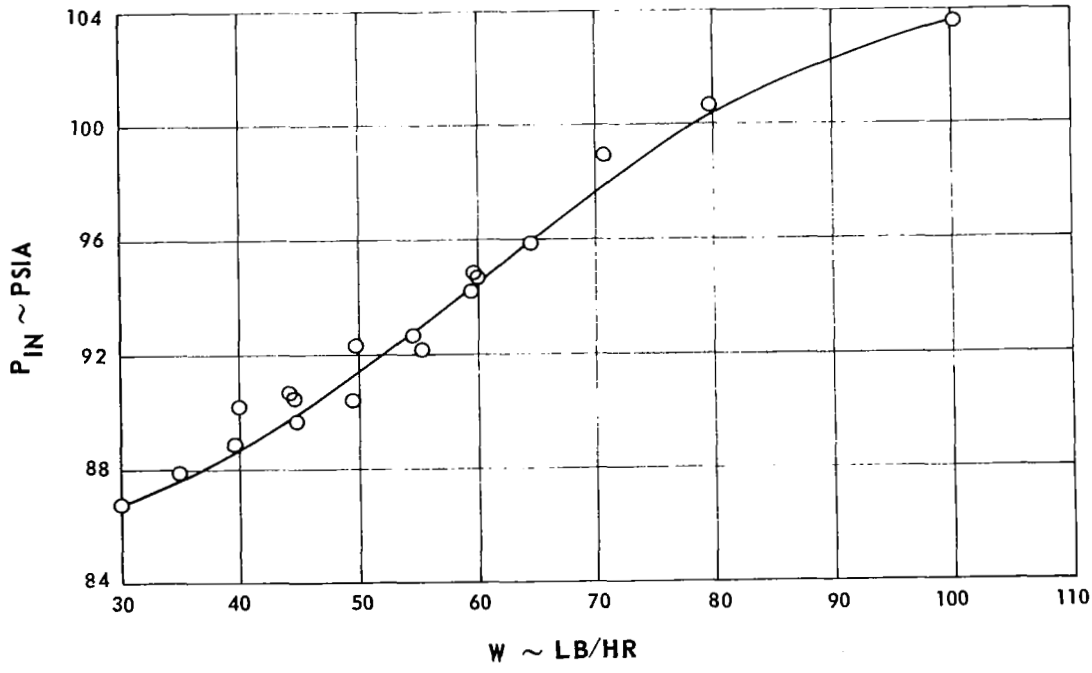


Figure 36 Boiling-Fluid Inlet Pressure vs Boiling-Fluid Flow Rate

The second condition results in an instability which involves the dynamic characteristics of the boiler and the feed system. Under this condition flow rates and pressures are observed to oscillate at the frequency at which the 180-degree phase shift occurs. From examination of Figures 23 through 32, in light of Equation (7), it is evident that dynamic instability is possible in the operation of the test boiler. For many of the conditions tested, the $P_{in}$ transfer function has a relatively large amplitude at the frequency where the 180-degree phase lag occurs. Whether or not such instabilities will occur at a given operating point will then depend upon the pressure-versus-flow characteristics of the feed system.

2. Internal Instability

Internal instabilities arise from the dynamic interactions between the thermal and hydraulic processes occurring within the boiler. The complexity of these interactions can be appreciated by reviewing the analysis of the boiler dynamics discussed in Section VII and Appendix 2.

Several different types of internal instability are possible for the counterflow boiler configuration of the study. One of the more frequently observed internal instabilities results from a transition between different flow regimes. Considering a once-through boiler which produces superheated vapor, the boiling fluid undergoes several transitions between two-phase flow regimes as it passes through the boiler. These regimes include:

1) Bubbly flow
2) Plug-slug flow
3) Annular flow
4) Annular mist transition flow
5) Mist flow

Other transitions are also possible. These include the transition between laminar and turbulent flow and between nucleate and film boiling.

According to Berenson[7], the transitions between: a) bubble, plug, and annular flow; b) laminar and turbulent flow; and c) nucleate and film boiling can all give rise to instabilities. These instabilities include pressure variations, transient pressure drop and recovery, and sustained oscillations.

Closely related to the flow regime transition instabilities is the density wave instability observed by Stenning and Veziroglu[8]. This type of instability involves the dynamic interaction between the flow rate, the two-phase density distribution, and the pressure gradient distribution within the boiler. A detailed discussion of this type of instability is presented in the reference.

A third type of internal instability is possible due to the feed-back characteristics of the counterflow boiler configuration. Temperature fluctuations in the boiling fluid will affect the local heat-transfer rate. This, in turn, will affect both the local rate of vapor generation and the temperature of the heating fluid.

It is possible for a boiling fluid temperature and pressure disturbance originating near the pinch point to propagate down the length of the boiler. This would produce a disturbance in the heating-fluid temperature which would propagate in the opposite direction due to the counter flow of the heating fluid. If this disturbance reached the pinch point 180 degrees out of phase with the initial disturbance, an unstable condition could result. This type of instability would be particularly significant under those conditions where the pinch point temperature difference was relatively small.

B. Areas of Unstable Operation

Oscillatory instabilities were encountered at two operating conditions. The first instability was encountered during steady-state testing when the boiling-fluid flow rate was slightly less than 30 lb/hr with the other primary variables at their nominal values. Neutral or constant-amplitude oscillations occurred with a frequency of approximately 0.9 cps. This unstable condition was first encountered with the electrohydraulic valve at the boiler inlet in the integral flow control mode. An oscillograph recording taken at that time is shown in Figure 37a. The same condition was then set with the electrohydraulic valve in a fixed position, and the oscillograph recording shown in Figure 37b resulted. A comparison of the two records shows that when the valve was put in a fixed position the oscillations had about the same frequency as before, and the amplitude of variation of $P_{in}$, $P_{out}$, $T_{Hout}$, and $T_{out}$ remained about the same. The flow rate trace with a fixed valve position was nearly sinusoidal, while with the valve operating as a flow control, most of the flow variation occurred in about 1/5 of the cycle, and the amplitude of the variation was about 1/3 less. Apparently the flow control system, as set up for these tests, was not sufficiently fast to respond to the frequency of 0.9 cps.

To investigate this instability further, additional tests were made in this unstable region. It was then found that by closing the bypass around the power-loop pump (see Figure 4), the oscillations could be eliminated. Consequently, the cause for this instability was a boiler-feed system coupling. A possible explanation of this phenomenon is presented below.

Using Equation (7), feed system-boiler instabilities can be predicted if the characteristics of the feed system are known and data showing the frequency response of the boiling-fluid inlet pressure to a variation in boiling-fluid flow rate are available up to the threshold of the unstable region. Figures 23a and 24a show that as the boiling-fluid flow rate was reduced towards the threshold of the unstable region (i.e., to 35 lb/hr), the $P_{in}$ frequency response

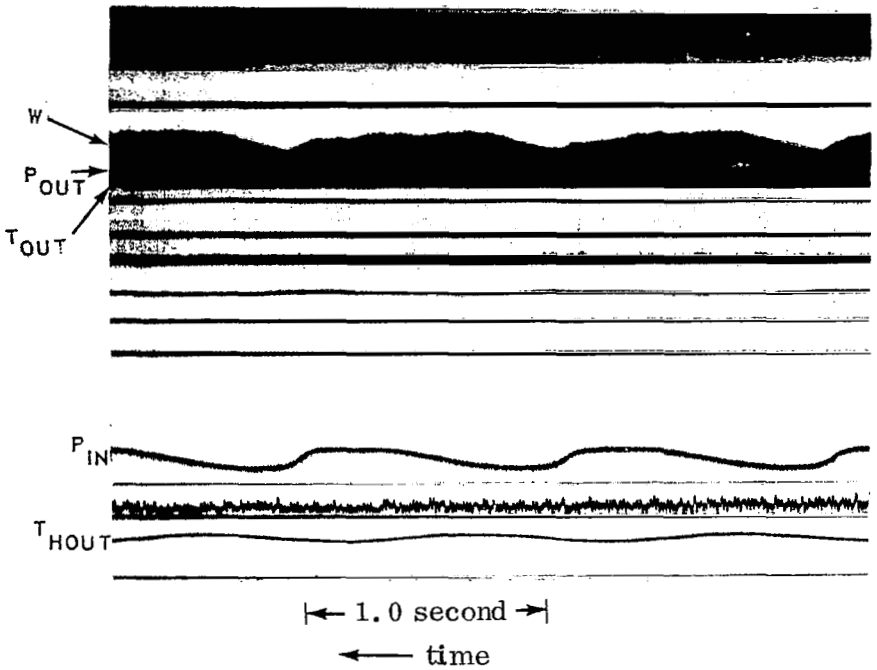


Limits of Variation

W - 25.3 to 26.7 lb/hr
$P_{in}$ - 67.0 to 75.5 psia
$P_{out}$ - 23.0 to 27.5 psi
$T_{out}$ - 410 to 412°F
$T_{H\ out}$ - 376 to 379°F

a) Flow Control Valve in Integral Flow Control Mode

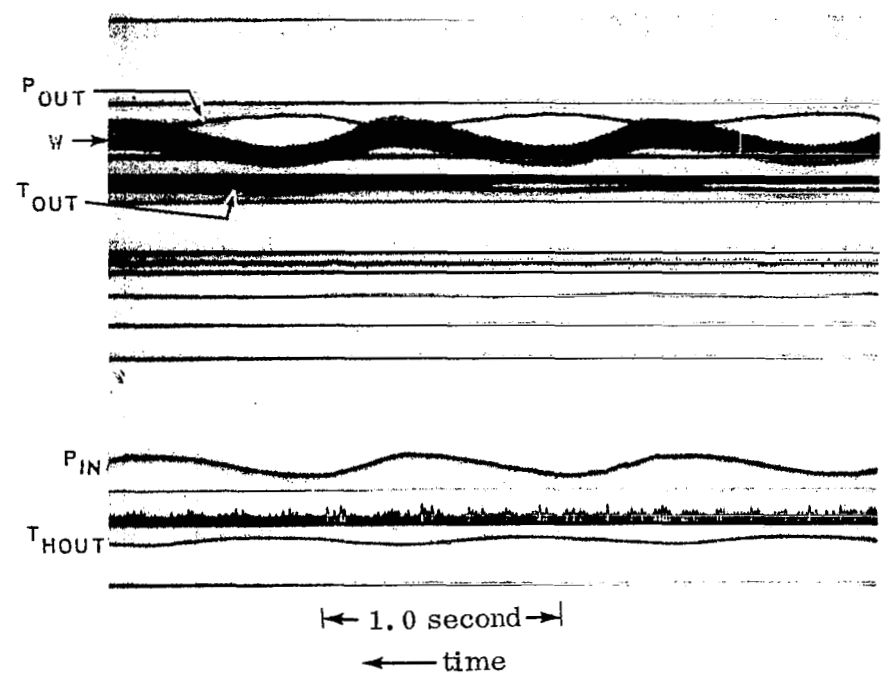


Limits of Variation

W - 25 to 27 lb/hr
$P_{in}$ - 67.0 to 75.5 psia
$P_{out}$ - 23.0 to 27.5 psi
$T_{out}$ - 410 to 412°F
$T_{H\ out}$ - 376 to 379°F

b) Flow Control Valve in Fixed Position

Figure 37 Oscillograph Recording of Instability at Boiling-Fluid Flow Rate of 30 lb/hr

became extremely erratic and displayed several sharp resonances near the frequency at which the 180-degree phase lag occurred.

Figure 38 shows the pressure-versus-flow characteristics of the feed system for the two settings of the bypass valve. The slope of the pressure versus flow curve has a value of -0.1820 psi/lb/hr with the bypass open and a value of -1.40 psi/lb/hr, with the bypass closed.

The observed instability could be explained if the amplitude of the $P_{in}$ frequency response at the 180-degree phase lag point was greater than 0.182 psi/lb/hr, but less than 1.40 psi/lb/hr for flow rates just below 30 lb/hr. The system would then be unstable with the bypass open and stable with the bypass closed. This could happen if one of the resonances shown in Figure 23a increased in amplitude as the boiling-fluid flow rate was reduced from 35 to 30 lb/hr.

If the above explanation were valid, it would be expected that the system would oscillate at the frequency where the 180-degree phase lag occurred. Figure 39 shows this frequency as a function of boiling-fluid flow rate. Extrapolating the data to a flow rate of 30 lb/hr indicates that the 180-degree phase lag could indeed occur near a frequency of 0.9 cps, the frequency at which the system was observed to oscillate.

The second oscillatory instability was observed to occur at a heating-fluid flow rate of 400 lb/hr and at a boiling-fluid flow rate of 47 lb/hr. Since this condition was not set during steady-state testing, the instability was not noted until the frequency response test at $W_H$ = 400 lb/hr was made. In this test low amplitude oscillations with a frequency of approximately 0.24 cps were found on the $P_{in}$ and $P_{out}$ oscillograph traces during the high-flow portion of the inlet flow rate variation cycle. This only occurred when the frequency was low enough (less than 0.01 cps) to allow the oscillations to develop during the high-flow portion of the cycle. Also, at a frequency of 0.085 cps the response of the $P_{in}$ and $P_{out}$ occurred at a frequency of 0.24 cps, a harmonic of the input frequency.

Figure 40 is a photograph of the oscillograph record for the frequency-response test at the 400 lb/hr condition and for a frequency of 0.002 cps. Oscillations occur only in $P_{in}$ and $P_{out}$, and not in the inlet flow rate or any of the other variables. Consequently it seems fairly certain that this instability does not involve coupling with the boiler feed system.

The second instability occurred when the exit quality was less than 90 percent and the subcooled length was relatively long, in contrast to the first instability when the subcooled and boiling lengths were very short and the superheat was near the maximum attainable. In the light of the low-amplitude irregular pressure fluctuations that were often encountered when an appreciable amount of liquid was present at the boiler exit (see Figure 21b), it seems likely that the second instability was a resonant state involving variations in the two-phase flow patterns either at the boiler exit or internally. Since the amplitude of the

oscillations was small, it is questionable whether this kind of oscillation should be considered detrimental to boiler operation.

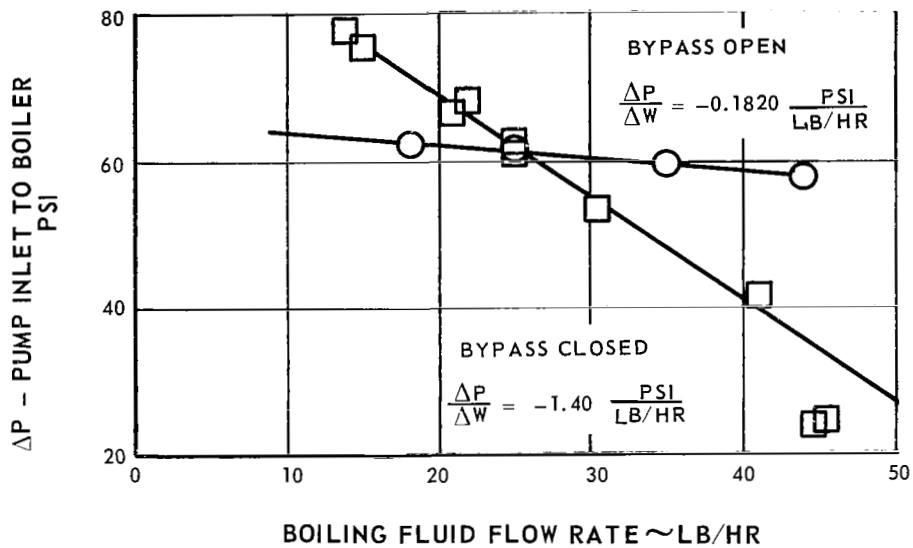


Figure 38 Feed System Pressure vs Flow Characteristics

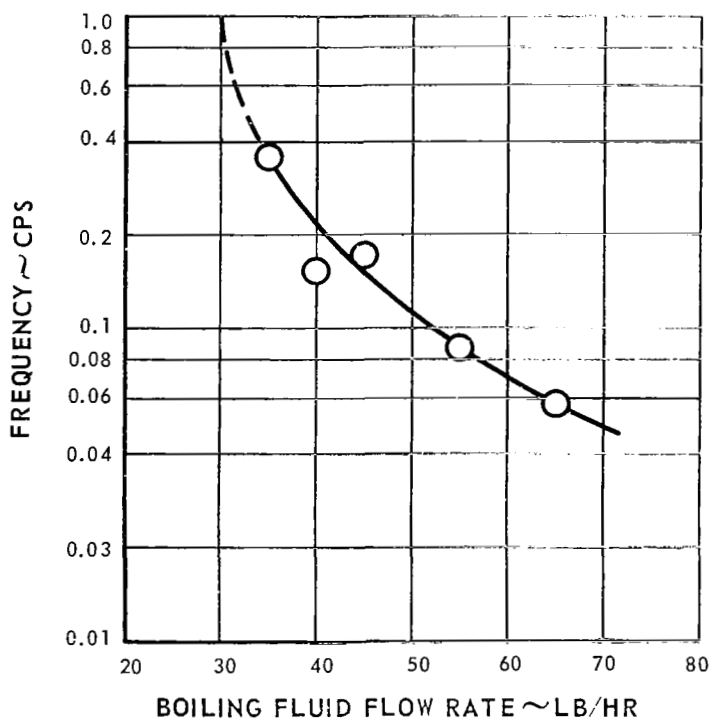


Figure 39 Frequency at which 180 Degrees Phase Lag Occurs for $P_{in}$ Frequency Response

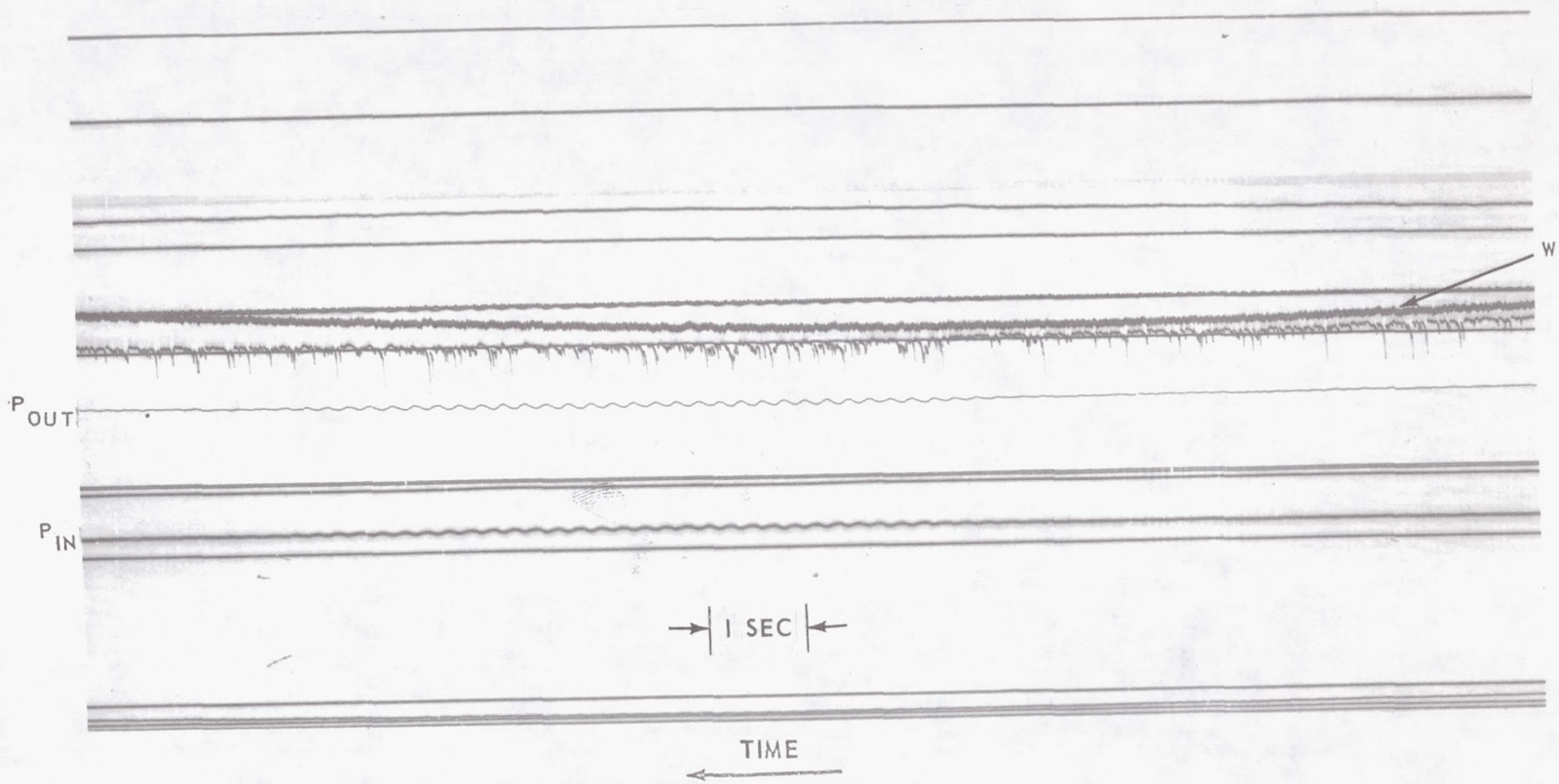


Figure 40 Oscillograph Record of Frequency-Response Test at $W_H$ = 400 lb/hr and $\omega$ = 0.002 cps Showing Pressure Oscillations

# VII. THEORETICAL ANALYSIS OF BOILER DYNAMICS

An analysis of the boiler dynamics was performed to derive a theoretical relation for predicting the $P_{out}$ transfer function. The purpose of this analysis was to determine whether a theoretical transfer function could be formulated that showed sufficiently good agreement with the experimental data of this study so that it could be employed in predicting the dynamic performance of boilers in Rankine-cycle space powerplants.

This analysis employed linearized relationships and a simplified model of the boiler. The distributed-parameters approach was employed wherever possible in analyzing components of the boiler. The resulting equation for the transfer function was a complicated relationship between 22 parameters.

A comparison was made between the theoretical transfer function obtained from this analysis and the experimental transfer function obtained from the frequency-response data. In calculating the theoretical transfer function, values for the 22 parameters were determined from the experimental data obtained from the steady-state tests.

This section contains a brief description of the derivation of the expression for the theoretical transfer function and a discussion of the comparison between the theoretical and experimental transfer functions. A detailed description of the derivation is presented in Appendix 2.

## A. Description of Derivation

The geometry of the boiler considered for the analysis is described in Section III above. The boiler can be classified as a single-tube counterflow heat exchanger designed to produce superheated vapor and having a choked restriction downstream of the boiling fluid exit. Provision was made in the analysis to account for the effects of the spiralled plug inserted in the boiler tube.

The boiler was divided into three regions: subcooled, boiling, and superheated, each of which was analyzed separately. These regions correspond to the regions observed in the steady-state data described in Section IV above. For simplicity however, it was assumed that the evaporation process was completed in the boiling region so that the boiling fluid entered the superheat region as a dry saturated vapor. This assumption is justified by the lack of specific knowledge of the rate of droplet evaporation in the nonequilibrium-superheat region

of the actual boiler. Dynamic equations were derived for these three regions and for the boiler as a whole. The equations include:

Overall Equations

continuity equation of the boiling fluid
pressure-drop equation for the boiling fluid
choked valve equation

Subcooled Region

energy equation of the boiling fluid
energy equation of the plug wall

Boiling Region

energy equation of heating fluid
energy equation of shell wall
energy equation of the boiling fluid

Superheated Region

energy equation of the boiling fluid

The basic approach followed in the derivation was to linearize these equations for small perturbations around a steady-state point and take the Laplace transforms of the perturbed variables.

Simplifications were introduced into the analysis, where required, in an effort to keep the analysis reasonably manageable. The principal simplifying concept was made in the derivation of the continuity and pressure drop equations where it was assumed that the density change of the boiling fluid occurred at one discrete location in the boiler. The fluid density and flow rate were, therefore, considered to be independent of axial position and equal to the inlet values everywhere upstream of this location. Similarly, the fluid density and flow rate are considered to be independent of axial position and equal to the exit values everywhere downstream of this location. The location at which the density change was assumed to occur is the point at which a liquid-vapor interface would be present if all the liquid in the boiler at any instant, filled the flow passage starting from the inlet (see Figure 41). It was further assumed that the movement of this point is simply related by a proportionality constant to the movement of the pinch point. This was done to provide a common reference point for the continuity, pressure drop and energy equations.

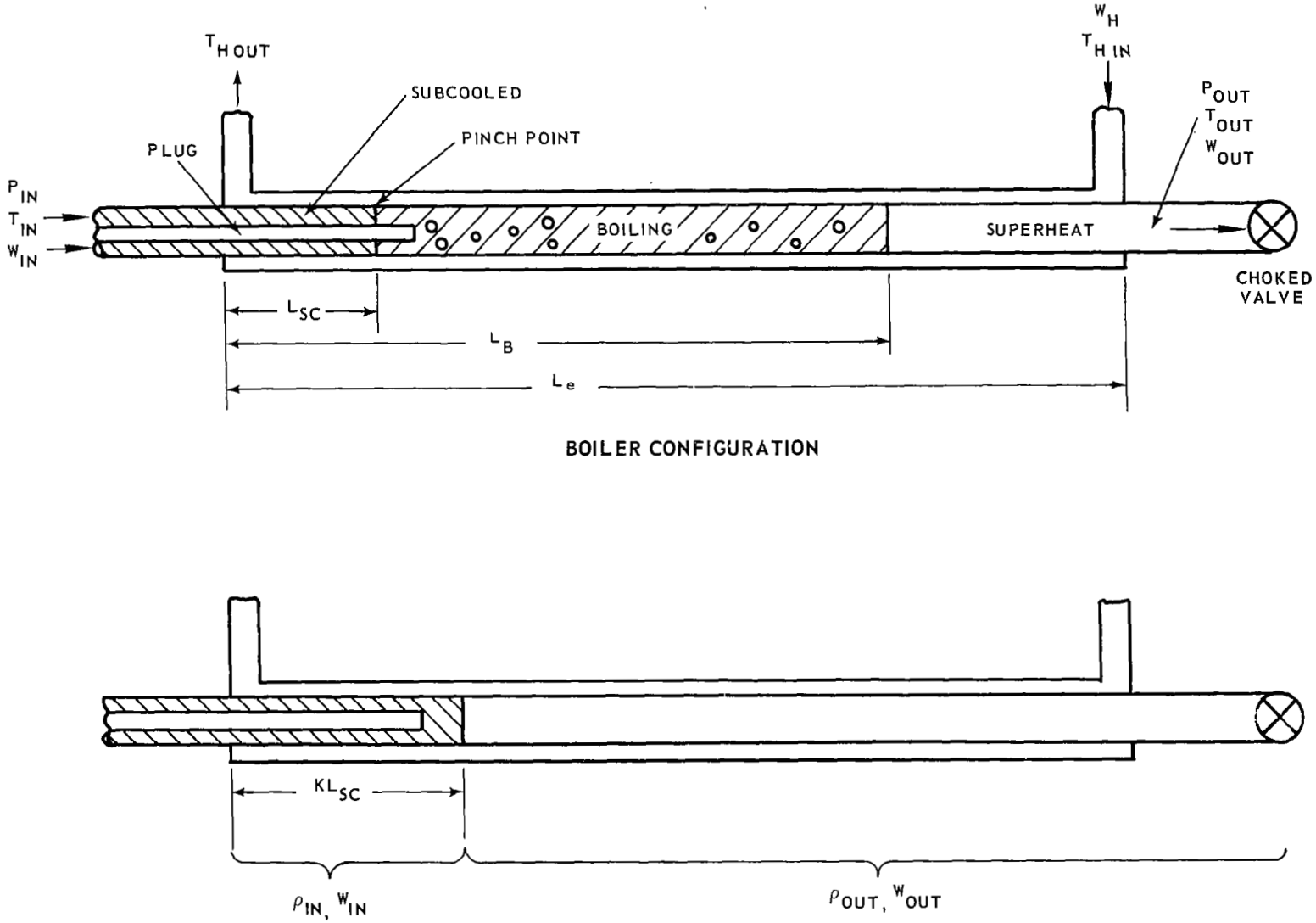


Figure 41 Lumped Density Change Model

In the derivation of the energy equations the distributed-parameters concept was employed wherever practical. This was possible in the derivation of five of the six individual energy equations where partial differential equations were derived with time and axial distance as the independent variables. These equations were then linearized, transformed and solved for the variation in the axial direction.

The solution to the partial differential equation for the boiling fluid in the boiling region, however, proved to be too complicated for the purposes of this analysis. In its place a quasidynamic equation was written with coefficients evaluated by means of steady-state relationships, and with transport time lags superimposed. The transport times appear in the equation in the form they would take in an approximate solution to a single-phase partial differential energy equation. The transport times in the boiling region are referred to the time it takes a liquid particle to travel the length of the boiling region.

In deriving these individual energy equations a fixed frame of reference was used, although the locations of the boundaries of both the subcooled and boiling regions fluctuate with time. The energy equations of the three regions were connected in a fixed reference frame by employing linearized perturbations about the steady-state boundaries in the boundary conditions of the equations.

The energy equations for the boiling and subcooled regions were combined into a single equation. The resulting five basic equations are tabulated below*.

Choked valve

$$\frac{\hat{P}_{out}}{P_{out,o}} = \frac{\hat{W}_{out}}{W_o} + \frac{\hat{T}_{out}}{2T_{out,o}} \tag{9}$$

Pressure drop

$$\frac{\hat{P}_P}{P_{P,o}} = \frac{\hat{P}_{out}}{P_{out,o}} + \left(\frac{\partial\,(\Delta P_B / P_{P,o})}{\partial\,(L_{SC} / L_{SC,o})}\right)\left(\frac{\hat{L}_{SC}}{L_{SC,o}}\right) \tag{10}$$

Continuity

$$\frac{\hat{W}_{in}}{W_o} - \frac{\hat{W}_{out}}{W_o} = K\tau_{SC}s\,\frac{\hat{L}_{SC}}{L_{SC,o}} + \tau_{VS}\,\frac{\hat{P}_{out}}{P_{out,o}} \tag{11}$$

*Symbols are defined in the nomenclature, in Figure 41, and in Appendix 2

Combined energy equation

$$\frac{\hat{L}_{SC}}{L_{SC,o}} = \textcircled{A}\frac{\hat{W}_{in}}{W_o} + \textcircled{B}\frac{\hat{P}_P}{P_{P,o}} + \textcircled{C}\frac{\hat{W}_{out}}{W_o} \tag{12}$$

Energy equation of superheated region

$$\frac{\hat{T}_{out}}{2T_{out,o}} = \textcircled{D}\frac{\hat{P}_P}{P_{P,o}} + \textcircled{E}\frac{\hat{W}_{out}}{W_o} + \textcircled{F}\frac{\hat{P}_{out}}{P_{out,o}} + \textcircled{G}\frac{\hat{L}_{SC}}{L_{SC,o}} \tag{13}$$

Equations (9) through (12) were combined into a single expression for the transfer function between boiling-fluid exit pressure and boiling-fluid inlet flow rate.

$$\frac{\hat{P}_{out}/P_{out,o}}{\hat{W}_{in}/W_o} = \frac{\left[1-\beta_3\textcircled{B}\right]\left[1+\dfrac{\hat{T}_{out}/2T_{out,o}}{\hat{W}_{in}/W_o}\right] - SK\tau_{SC}\left[\textcircled{A}-\textcircled{C}\dfrac{\hat{T}_{out}/2T_{out,o}}{\hat{W}_{in}/W_o}\right]}{\left[1+\tau_V S\right]\left[1-\beta_3\textcircled{B}\right] + SK\tau_{SC}\left[\textcircled{B}+\textcircled{C}\right]} \tag{14}$$

Where S is the complex operator and where the term $\dfrac{\hat{T}_{out}/2T_{out,o}}{\hat{W}_{in}/W_o}$

is obtained from the following expression which results from the combination of Equations (9) through (13).

$$\frac{\hat{T}_{out}/2T_{out,o}}{\hat{W}_{in}/W_o} = \frac{-\gamma_{22} + \dfrac{\gamma_{21}\left[\left[1-\beta_3\textcircled{B}\right] - SK\tau_{SC}\textcircled{A}\right]}{\left[1+\tau_V S\right]\left[1-\beta_3\textcircled{B}\right] + SK\tau_{SC}\left[\textcircled{B}+\textcircled{C}\right]}}{1 - \dfrac{\gamma_{21}\left[1-\beta_3\textcircled{B} + SK\tau_{SC}\textcircled{C}\right]}{\left[1+\tau_V S\right]\left[1-\beta_3\textcircled{B}\right] + SK\tau_{SC}\left[\textcircled{B}+\textcircled{C}\right]}} \tag{15}$$

Normalizing at zero frequency (i.e., at S = 0) the result is

$$\left(\frac{\hat{P}_{out}}{\hat{W}_{in}}\right)_{normalized} = \frac{\left(\dfrac{\hat{P}_{out}}{\hat{W}_{in}}\right)_{(s)}}{\left(\dfrac{\hat{P}_{out}}{\hat{W}_{in}}\right)_{(s=0)}} = \frac{(\hat{P}_{out}/\hat{W}_{in})}{\dfrac{P_{out,o}}{W_o}\left[1+\left(\dfrac{\hat{T}_{out}/2T_{out,o}}{\hat{W}_{in}/W_o}\right)_{(s=0)}\right]} \tag{16}$$

Combining Equations (14) and (16) the normalized transfer function becomes

$$\left(\frac{\hat{P}_{out}}{\hat{W}_{in}}\right)_{normalized} = \frac{\left[1-\beta_3\textcircled{B}\right]\left[1+\dfrac{\hat{T}_{out}/2T_{out,o}}{\hat{W}_{in}/W_o}\right] - SK\tau_{SC}\left[\textcircled{A}-\textcircled{C}\dfrac{\hat{T}_{out}/2T_{out,o}}{\hat{W}_{in}/W_o}\right]}{\left[1+\left(\dfrac{\hat{T}_{out}/2T_{out,o}}{\hat{W}_{in}/W_o}\right)_{(s=0)}\right]\left[\left[1+\tau_V S\right]\left[1-\beta_3\textcircled{B}\right] + SK\tau_{SC}\left[\textcircled{B}+\textcircled{C}\right]\right]} \tag{17}$$

The equation for the theoretical transfer function is a very large complicated expression employing complex variables. At the initiation of this study it was desired to obtain a relatively simple expression for the transfer function. It was hoped that such an expression might indicate, by cursory inspection, the important parameters which affect the boiler dynamics and give insight into the manner in which they interact to produce the effects observed. However, due to the complexity of the boiler geometry and the multitude of different regions and processes affecting the boiler dynamics, no simple relation was possible. In fact, Equation (17) itself is highly simplified over the relation that would have resulted if the approximations discussed above and in Appendix 2 had not been made.

The details of the complete analysis are presented in Appendix 2.

## B. Comparison between Theoretical and Experimental Data

The theoretical transfer function predicted by the analysis of the boiler dynamics was evaluated as a function of frequency for the boiler operating conditions at which the frequency-response tests were conducted. The theoretical normalized amplitudes and phase lags were compared with their corresponding experimental values. The following paragraphs contain a brief discussion of the calculation of the theoretical transfer function and a discussion of the comparison between the theoretical and experimental results.

### 1. Calculation of Theoretical Transfer Function

To calculate the theoretical transfer function it was first necessary to evaluate the 22 parameters required by Equation (17). This was done using the results of the steady-state tests described in Section IV of this report. The methods used to evaluate these parameters from the steady-state test data are discussed in Appendix 3. This appendix also contains a set of curves showing these parameters as functions of the primary variables. The complexity of these parameter curves, as demonstrated by the sharp breaks displayed as boiler exit conditions change, indicates the need for thoroughly understanding the steady-state performance of the boiler in order to predict its dynamic performance.

The normalized amplitude and phase lag were calculated as a function of frequency using Equation (17) and the parameter curves of Appendix 3. This was done for the boiler operating conditions at which frequency-response tests had been conducted. Since Equation (17) was derived for the boiler operating conditions where a superheat region existed, the theoretical transfer function was not calculated for those test conditions which did not exhibit a nonequilibrium-superheat region at the exit of the boiler.

## 2. Description of Comparison between Theoretical and Experimental Data

The results of the above calculations were plotted on the same Bode diagrams as the corresponding experimental values for the $P_{out}$ transfer function. These plots are shown in Figures 23 through 32 in Section IV and in Figures 42 through 46 in this section. Figures 23 through 32 permit a direct point-by-point comparison between the theoretical and experimental transfer functions at each boiler operating condition. Figures 42 through 46 show the manner in which both theoretical and experimental transfer functions are affected by the primary variables.

In examining these figures, it can be seen that the theory predicts the same general trends for the $P_{out}$ transfer function as shown in the experimental data. For example, the normalized amplitudes predicted by the theory attenuate in the same manner as those of the experimental data. In addition, Figures 42 through 46 show that the experimental data tends to bracket the theoretical normalized amplitudes. The phase lags predicted by the theory also tend to increase with frequency in the same manner as those of the experimental data. This agreement is an indication of the validity of the basic approach taken in the linearized analysis of the boiler dynamics.

However, while the theory and the experimental data show similar trends, the magnitudes of the normalized amplitude and phase lag predicted by the theory are not always in close agreement with the experimental data over the full range of frequencies. For example, it can be seen in Figures 42a through 46a that at the lower frequencies the theory does not predict normalized amplitudes greater than 1.0 as observed in the experimental data. Figures 42b through 46b also show that the phase lags of the experimental data tend to be somewhat higher than predicted by the theory, particularly in the middle frequency range.

Figures 42 through 46 also indicate that closer agreement between the theory and the data is achieved under those conditions where the boiling fluid emerges as a dry superheated vapor. For example, Figure 43 shows excellent agreement for a heating-fluid flow rate of 1000 lb/hr, where the boiling fluid is superheated by 93°F, as opposed to the poorer agreement shown for the 600 lb/hr case where the boiling fluid emerges in a nonequilibrium condition. This is probably a result of the fact that the assumptions concerning the superheating of the boiling fluid made in the analysis of the boiler dynamics become less valid as nonequilibrium conditions become pronounced.

a)

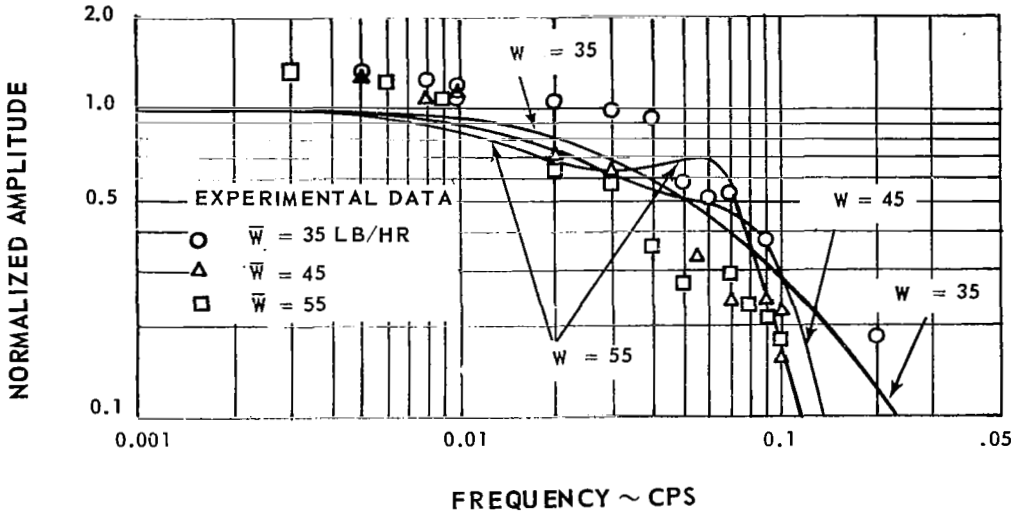


b)

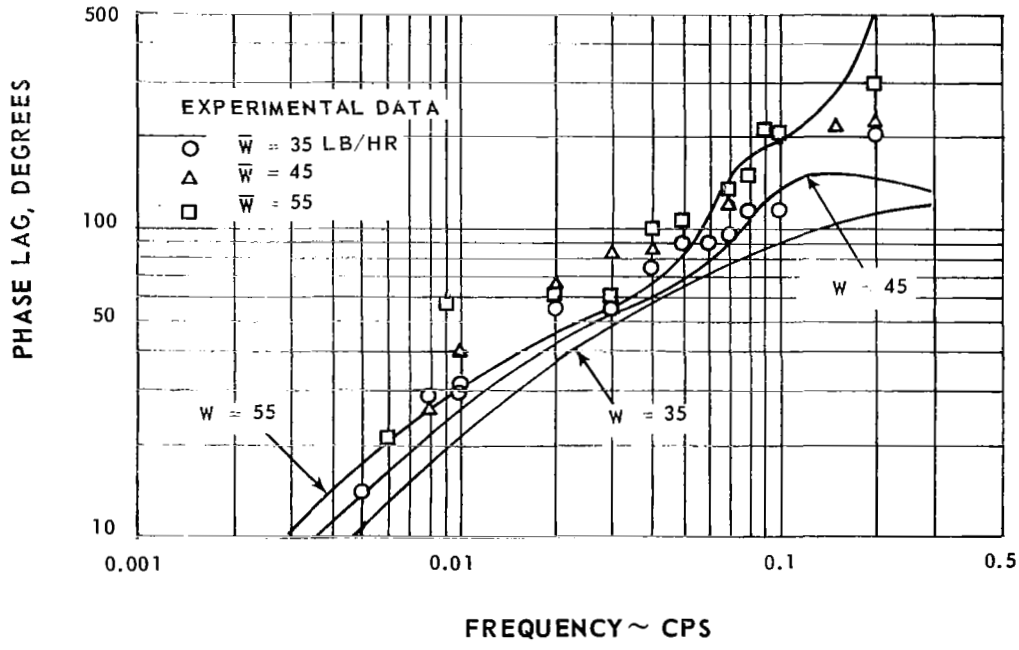


Figure 42 Comparison between Theoretical Transfer Function and Experimental Values of $P_{out}$ Frequency Response for Various Values of Boiling-Fluid Flow Rate

a)

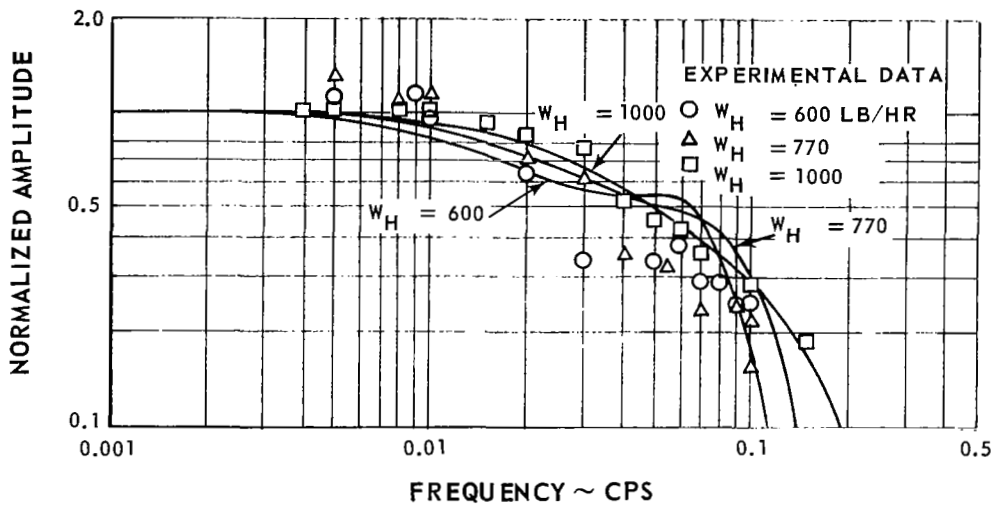


b)

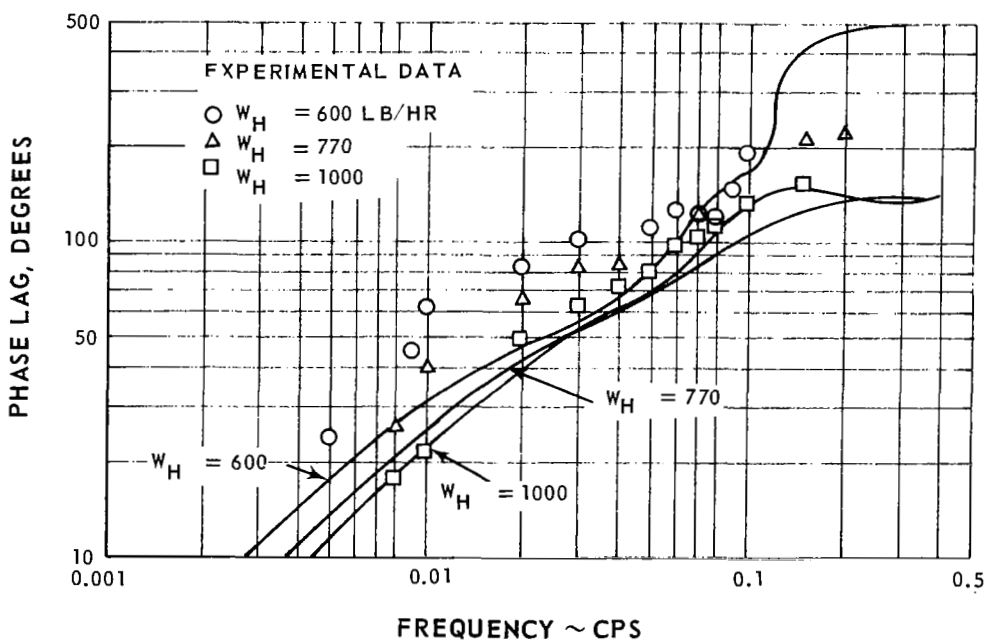


Figure 43 Comparison between Theoretical Transfer Function and Experimental Values of $P_{out}$ Frequency Response for Various Values of Heating-Fluid Flow Rate

a)

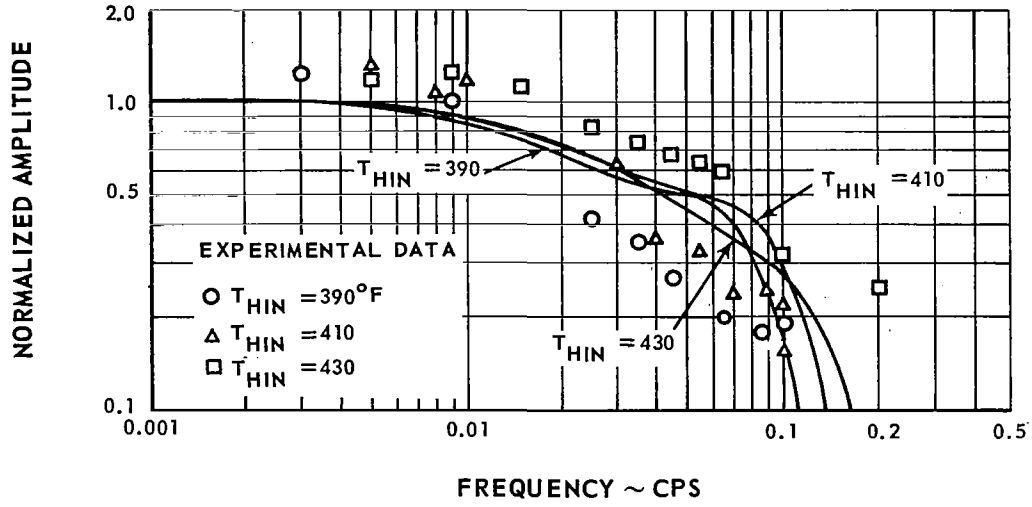


b)

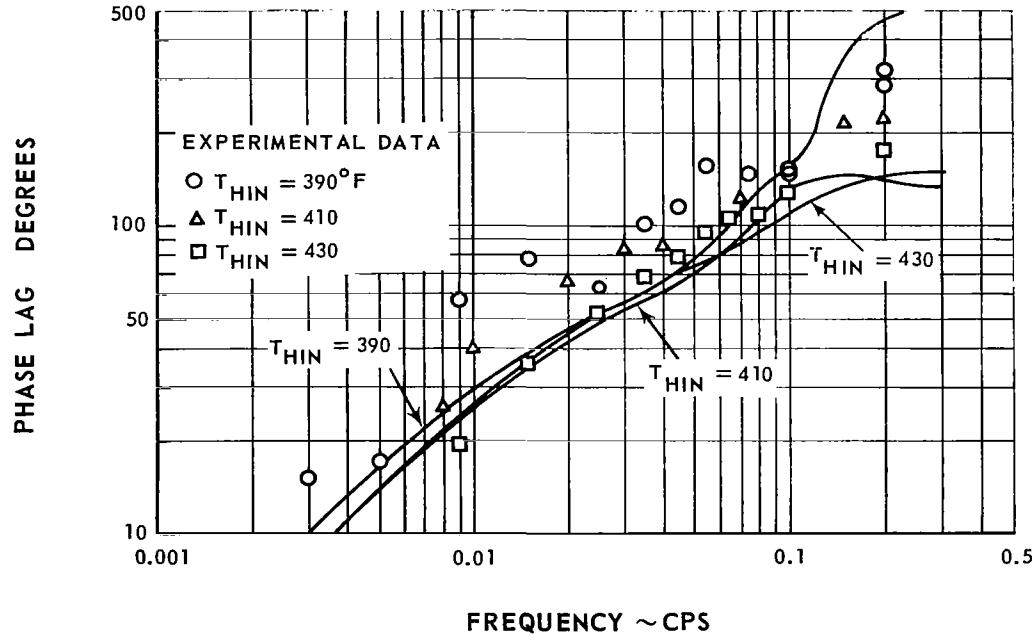


Figure 44 Comparison between Theoretical Transfer Function and Experimental Values of $P_{out}$ Frequency Response for Various Values of Heating-Fluid Inlet Temperature

a)

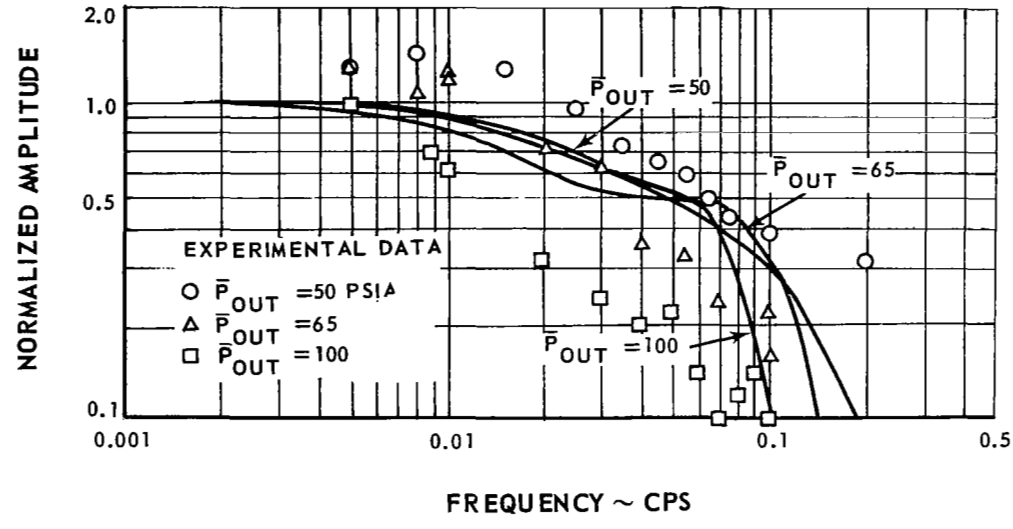


b)

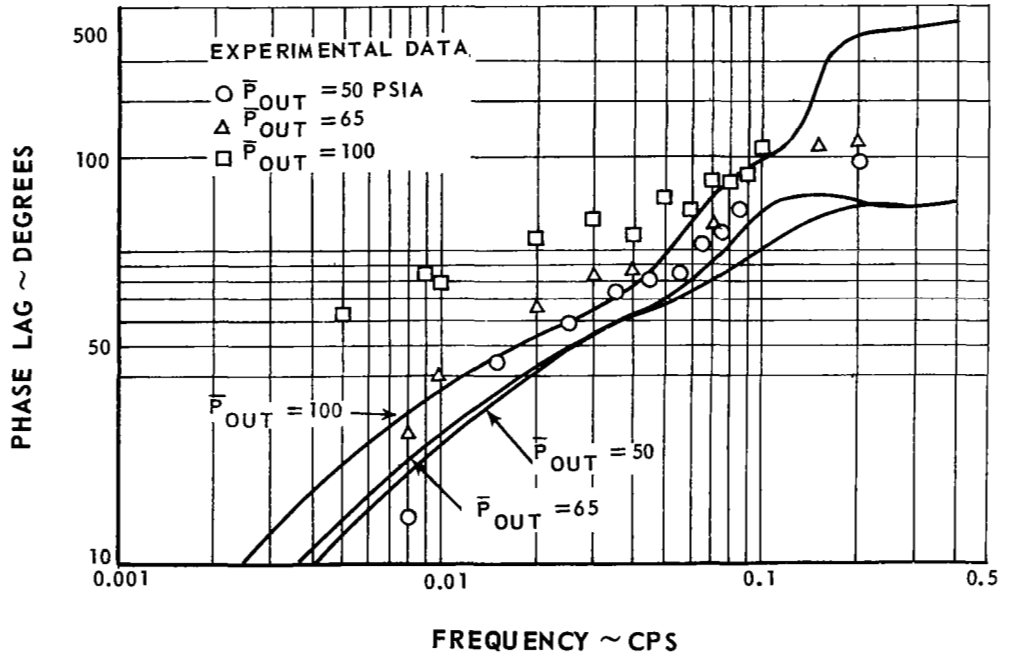


Figure 45 Comparison between Theoretical Transfer Function and Experimental Values of $P_{out}$ Frequency Response for Various Values of Boiling-Fluid Exit Pressure

a)

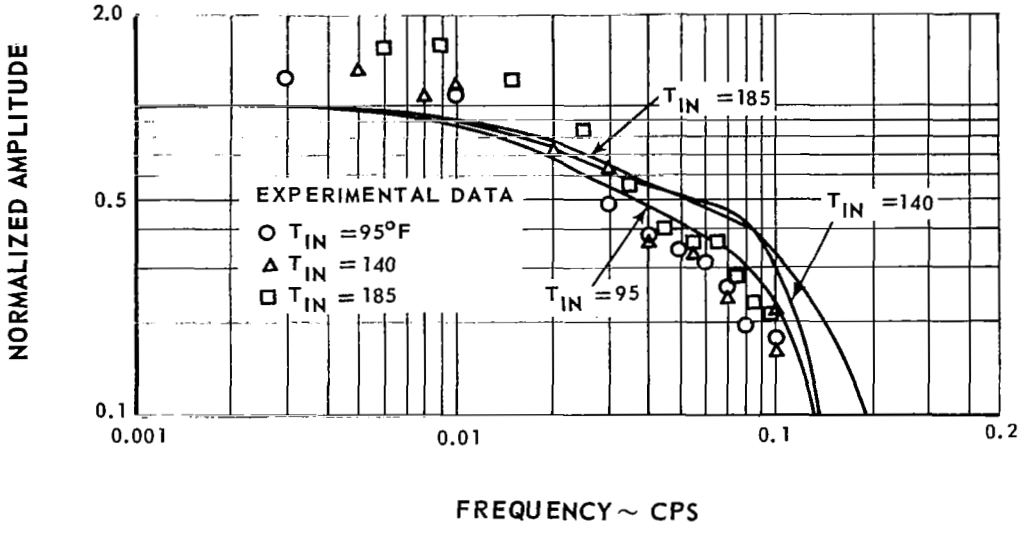


b)

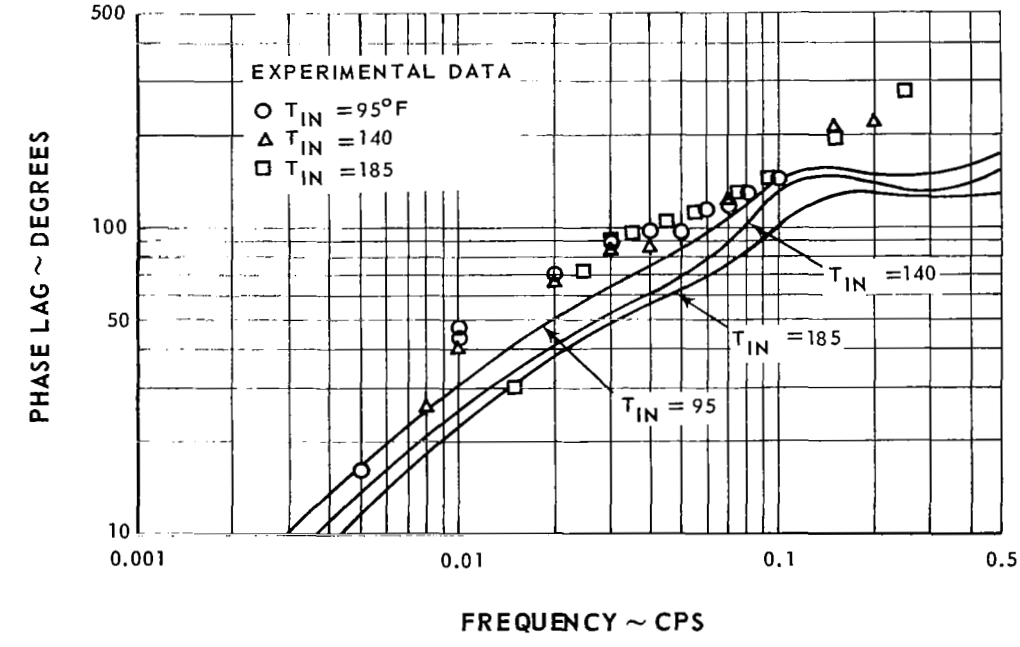


Figure 46 Comparison between Theoretical Transfer Function and Experimental Values of $P_{out}$ Frequency Response for Various Values of Boiling-Fluid Inlet Temperature

Close scrutiny of Figures 23 through 32 indicates that the best agreement between the theory and the experimental data occurs in the middle frequency range, usually between 0.01 and 0.1 cps. Below these frequencies the normalized amplitudes of the experimental data tend to be greater than the value of 1.0 predicted by the theory. Above these frequencies there is little agreement between the phase lags of the theory and those of the experimental data.

In studying the stability of the interactions between the boiler and the feed system of a Rankine-cycle space powerplant, the amplitude of the transfer function of the boiler at a phase lag of 180 degrees is a very important consideration. Since, in most of the cases considered, the phase lag of 180 degrees occurs at frequencies above 0.10 cps, caution should be exercised in applying Equation (17) to predict the stability of the interactions between the feed system and the boiler.

### 3. Evaluation of Comparison Between Theoretical and Experimental Data

In evaluating the results of this comparison, it should be remembered that the analysis presented in this section represents an initial effort to analyze the dynamics of an extremely complex nonlinear device. The degree of agreement that was achieved between the theory and the data is an indication of the validity of the basic approach of performing a separate linearized analysis for each section of the boiler. However, in order to develop a more useful tool for predicting boiler stability, modifications to this analysis are required in order to achieve closer agreement between the theory and the data at the higher frequencies. This can probably be accomplished by refining the analysis to remove several of the simplifying assumptions. The following modifications to the analysis are recommended:

1) A more exact description of the distribution of the boiling fluid mass within the boiler and the manner in which this mass responds to perturbations in the flow rate.

2) Replacement of the quasi-dynamic relation employed as the energy equation of the boiling fluid in the boiling region, with a relation based on the distributed-parameters approach.

3) Inclusion of the effects of the heat capacities of the tube, the shell, and spiralled plug insert in all sections of the boiler.

## VIII. CONCLUSIONS

The following conclusions have been reached on the basis of the results presented in this report.

1. The condition of the boiling fluid at the exit of the boiler is a significant characteristic in describing the steady-state and dynamic behavior of the boiler. This is seen in the sharp breaks, rather than smooth transitions, displayed by many of the steady-state performance and boiler parameter curves as the boiler exit conditions change from a dry superheated vapor to a nonequilibrium mist and from a nonequilibrium mist to a wet saturated condition. This is also seen in the general shift of the experimental frequency-response curves as the boiler exit conditions vary in the direction from dry superheated vapor to wet saturated conditions.

2. For small perturbations of the boiling-fluid flow rate, the boiler can be treated as a linear element over much of the operating range investigated. This is shown by the linear responses observed in the oscillograph traces for the boiling-fluid inlet and exit pressures and the heating-fluid exit temperature over virtually the entire range of conditions tested. In studying the response of the boiling-fluid exit temperature, the linear approximation is valid only for dry boiling-fluid exit conditions.

3. The boiling system of this study is statically stable in spite of the negative slope of the curve of boiling-fluid pressure drop versus flow. This is shown by the positive slope of the curve of boiling-fluid inlet pressure versus flow which results from the effects of the choked restriction downstream of the boiler exit.

4. The boiling system of this study can undergo dynamic instabilities. The possibility of dynamic instabilities arising from the dynamic interactions between the feed system and the boiler is indicated by the experimental frequency-response curves. In these curves it can be seen that the $P_{in}$ transfer function has a relatively large amplitude at the 180-degree phase lag point for many of the cases studied. This type of instability was experienced at one point in the test program. A second type of instability which can probably be attributed to dynamic interactions within the boiler itself was also observed during testing.

5. The basic linearized approach taken in the analysis of the boiler dynamics appears to be valid in view of the agreement found between the trends of the experimental and theoretical values for the $P_{out}$ transfer function. Further work in this area appears desirable in order to develop a more useful analytical tool for predicting the stability of the dynamic interactions between the boiler and the feed system.

## NOMENCLATURE

| | |
|---|---|
| $A$ | cross-sectional area, $ft^2$ |
| Ⓐ | defined by Equation (98), dimensionless |
| Ⓑ | defined by Equation (99), dimensionless |
| $C_p$ | specific heat at constant pressure, $Btu/lb_m - °F$ |
| $C$ | arbitrary constant |
| Ⓒ | defined by Equation (100), dimensionless |
| Ⓓ | defined by Equation (121), dimensionless |
| $d_h$ | hydraulic diameter, ft |
| $d_i$ | tube inside diameter, ft |
| $d_m$ | tube mean diameter, ft |
| $d_o$ | tube outside diameter, ft |
| Ⓔ | defined by Equation (122), dimensionless |
| $e$ | base of natural logarithms |
| Ⓕ | defined by Equation (123), dimensionless |
| $f$ | friction factor, dimensionless |
| Ⓖ | defined by Equation (124), dimensionless |
| $g$ | acceleration due to gravity, $ft/hr^2$ |
| $G$ | mass flux, $lb_m/hr-ft^2$ |
| $G_1$ | transfer function defined in Section VI |
| $G_2$ | transfer function defined in Section VI |
| $G_3$ | mass flux after expansion, $lb_m/hr-ft^2$ |
| $h$ | convective heat transfer coefficient, $Btu/hr-ft^2-°F$ |
| $H_{fg}$ | heat of vaporization, $Btu/lb_m$ |
| $j$ | $\sqrt{-1}$ |
| $k$ | thermal conductivity, $Btu/hr-ft-°F$ |
| $K$ | defined by Equation (34), dimensionless |
| $l$ | axial distance, ft |
| $L$ | axial distance from boiler inlet, ft |
| $M$ | fluid mass, $lb_m$ |
| $N$ | number of 90-degree bends |
| $n$ | defined by $U \propto V^n$, dimensionless |
| $p$ | heat transfer perimeter, ft |
| $P$ | pressure, psia |
| $Pr$ | Prandtl number |
| $q$ | heat flux, $Btu/hr-ft^2$ |
| $Q$ | heat transferred, Btu/hr |
| $R$ | gas constant, $ft-lb_f/lb_m-°R$ |
| $R_b$ | flow resistance due to bends, dimensionless |
| $R_g$ | vapor fraction of two-phase flow, dimensionless |
| $R_l$ | flow resistance due to length, dimensionless |
| $R_L$ | liquid fraction of two-phase flow, dimensionless |

| | |
|---|---|
| $R_t$ | total flow resistance, dimensionless |
| Re | Reynolds number |
| S | complex operator, $hr^{-1}$ |
| t | time, hr |
| $t_h$ | tube thickness, ft |
| T | temperature, °F |
| U | overall heat transfer coefficient, Btu/hr-$ft^2$-°F |
| v | specification volume, $ft^3/lb_m$ |
| V | fluid velocity, ft/hr |
| Vol | volume, $ft^3$ |
| W | mass flow rate, $lb_m$/hr |
| x | axial distance, ft |
| X | quality |
| $(L/D)_{eq}$ | equivalent length-to-diameter ratio |
| $\Delta P_B$ | pressure drop of boiling fluid across boiler, psi |
| $\Delta T_{LM}$ | logarithmic mean temperature difference, °F |
| $\Delta T_M$ | arithmetic mean temperature difference, °F |
| $\Delta T_P$ | difference between heating and boiling fluid temperatures at pinch point, °F |
| $\Delta T_{SH}$ | superheat at boiling fluid exit, °F |
| $\Delta P_{in}/\Delta W$ | amplitude of $P_{in}$ frequency response at zero frequency, psi-hr/$lb_m$ |
| $\Delta P_{out}/\Delta W$ | amplitude of $P_{out}$ frequency response at zero frequency, psi-hr/$lb_m$ |
| $\Delta T_{H\,out}/\Delta W$ | amplitude of $T_{Hout}$ frequency response at zero frequency, °F hr/$lb_m$ |
| $\Delta T_{out}/\Delta W$ | amplitude of $T_{out}$ frequency response at zero frequency, °F hr/$lb_m$ |

| | |
|---|---|
| $\alpha$ | defined in Appendix 3, dimensionless |
| $\beta 1$ | defined by Equation(57), dimensionless |
| $\beta 2$ | defined by Equation (116), dimensionless |
| $\beta 3$ | defined by Equation (126), dimensionless |
| $\gamma$ | ratio of specific heats $C_p/C_v$, dimensionless |
| $\gamma_1$ | defined by Equation (59), dimensionless |
| $\gamma_2$ | defined by Equation (60), dimensionless |
| $\gamma_3$ | defined by Equation (61), dimensionless |
| $\gamma_4$ | defined by Equation (83), dimensionless |
| $\gamma_5$ | defined by Equation (84), dimensionless |
| $\gamma_{11}$ | defined by Equation (132), dimensionless |
| $\gamma_{12}$ | defined by Equation (133), dimensionless |
| $\gamma_{13}$ | defined by Equation (134), dimensionless |
| $\gamma_{21}$ | defined by Equation (137), dimensionless |
| $\gamma_{22}$ | defined by Equation (138), dimensionless |
| $\theta$ | defined by Equation (38), $hr^{-1}$ |

| | |
|---|---|
| $\theta_1$ | defined by Equation (38), $hr^{-1}$ |
| $\theta_2$ | defined by Equation (42), $hr^{-1}$ |
| $\theta_B$ | defined by Equation (63), $hr^{-1}$ |
| $\theta_{B1}$ | defined by Equation (64), $hr^{-1}$ |
| $\theta_{B2}$ | defined by Equation (69), $hr^{-1}$ |
| $\theta_{SH}$ | defined by Equation (102), $hr^{-1}$ |
| $\rho$ | density, $lb_m/ft^3$ |
| $\sigma$ | ratio of initial to expanded flow area, dimensionless |
| $\tau$ | transport time of fluid in subscripted region, hr |
| $\phi_1$ | defined by Equation (56), dimensionless |
| $\phi_2$ | defined by Equation (78), dimensionless |
| $\phi_3$ | defined by Equation (92), dimensionless |
| $\phi_4$ | defined by Equation (114), dimensionless |
| $\phi_5$ | defined by Equation (117), dimensionless |
| $\omega$ | frequency of disturbance, cps |

## Subscripts

| | |
|---|---|
| B | boiling region of boiler |
| e | boiling fluid exit |
| H | heating fluid |
| Hin | heating fluid entering boiler |
| Hout | heating fluid leaving boiler |
| HP | heating fluid at pinch point |
| in | boiling fluid entering boiler |
| L | liquid |
| o | steady-state condition |
| out | boiling fluid leaving boiler |
| P | boiling fluid at pinch point |
| PM | plug metal |
| SAT | boiling-fluid saturation condition at pinch point |
| SAT OUT | boiling-fluid saturation condition at boiler exit pressure |
| SC | subcooled region of boiler |
| SF | swirl flow |
| SH | superheat region of boiler |
| SM | shell metal |
| SV | dry saturated vapor |
| T | tube |
| TPF | two-phase flow |
| V | vapor |

Note: Non-subscripted variables refer to boiling fluid

## Superscripts

| | |
|---|---|
| $(\hat{\ })$ | Laplace transform of linearized variable |
| $(\bar{\ })$ | mean value |

## REFERENCES


1. "Two-Phase Gas-Liquid Flow Oscillations: Preliminary Survey", by S.W. Gouse, Jr., Report DSR 8734-5, Massachusetts Institute of Technology, July 1964

2. "Frequency Response of Forced-Flow Single Tube Boiler", by E.A. Krejsa, J.H. Goodykoontz, and G.H. Stevens, NASA TN D-4039, June 1967

3. "Frequency Response of a Forced-Flow Single-Tube Boiler", by R.G. Dorsch, NASA TM X-52306, 1967

4. "Steady-State and Dynamic Operating Characteristics of a Simulated Three-Loop Space Rankine-Cycle Powerplant" by J.R. Hooper, NASA CR-625, November 1966

5. "Analysis of Pressure Drop Function in Rankine Space Power Boilers with Discussion of Flow Maldistribution Implications", by A. A. Schoenberg and D. R. Packe, NASA TN-D-4498, April 1968

6. "Analysis and Measurement of Flow Oscillations", by E.R. Quandt, Chemical Engineering Progress Symposium Series, No. 32, Vol. 57, pp 111-126, 1961

7. "Flow Stability in Multitube Forced-Convection Vaporizers", by P.J. Berenson, Technical Documentary Report No. APL TDR 64-117, Air Force Aero Propulsion Laboratory, Wright Patterson Air Force Base, Ohio 1964

8. "Flow Oscillation Modes in Forced-Convection Boiling", by A.H. Stenning and T.N. Veziroglu, Proceedings of the 1965 Heat Transfer and Fluid Mechanics Institute, Stanford University Press, 1965

9. "Heat Transmission, Second Edition", by H.W. McAdams, p. 168, McGraw-Hill, New York, 1942

10. "Heat Transfer and Pressure-Drop Characteristics of Wire-Coil Type Turbulence Promoters", by Eldor W. Sams, Lewis Flight Propulsion Laboratory, NACA Cleveland, Ohio. Presented at the Reactor Heat Transfer Conference, Nov. 1, 1956, Hotel Statler, New York City

11. "Flow of Fluids", Crane Technical Paper No. 410, Crane Corp., Chicago. pps. 2-12, A-27, (Primary ref. - K. H. Beij, Pressure Losses for fluids in 90° pipe Bends, J. of Res. of NBS, Vol. 21, July 1938)

12. "Prediction of Pressure Drop during Forced-Circulation Boiling of Water", by R. C. Martinelli and D. B. Nelson, Trans. ASME, Aug 1948, pps 695-702

13. "Two-Phase Pressure Loss across Abrupt Contractions and Expansions, Steam-Water at 600 to 1400 psi", by E. Janssen, Proceedings of the Third International Heat Transfer conference, Aug. 7-12, 1966, Chicago, Vol. IV, pp. 12-23

# APPENDIX 1

## Boiler Design Calculation

The boiler design is described in detail in Section III. This appendix contains a brief description of the thermal and hydraulic analyses which served as the basis for this design. Since the actual computations are long and complex, this appendix will be limited to a description of the basic relations and assumptions employed in the analyses and a comparison between the predicted and the measured performance of the boiler.

In analyzing the thermal and hydraulic performance, it was necessary to divide the boiler into six different sections which were analyzed spparately. These sections, designated by the station numbers illustrated in Figure 47, are classified by the state of the boiling fluid flow as shown below:

| Section | Station Numbers |
|---|---|
| 1) Subcooled flow through the plug | 0 - 1 |
| 2) Boiling flow through the plug | 1 - 2 |
| 3) Sudden expansion at the end of the plug | 2 - 3 |
| 4) Boiling flow from end of plug to 80.9% quality | 3 - 4 |
| 5) Boiling flow from 80.9% quality to 100% quality | 4 - 5 |
| 6) Superheating of the vapor flow | 5 - 6 |

The boiling fluid was maintained in a swirl-flow pattern throughout the length of the boiler to enhance its heat-transfer coefficient. In Sections 1 and 2 of the boiler, the swirl-flow pattern was induced using a spiral-flow channel formed between the machined plug and the tube wall. In the remaining sections of the boiler the swirl-flow pattern was maintained by means of a wire coil brazed to the tube wall. The effects of these swirl-inducing devices were included in the analysis. During the course of the analysis a number of assumptions were made. These were particularly necessary since little is known about heat transfer and fluid friction for the types of swirl flow encountered in this boiler design. These assumptions are stated in the discussion that follows wherever they are applied.

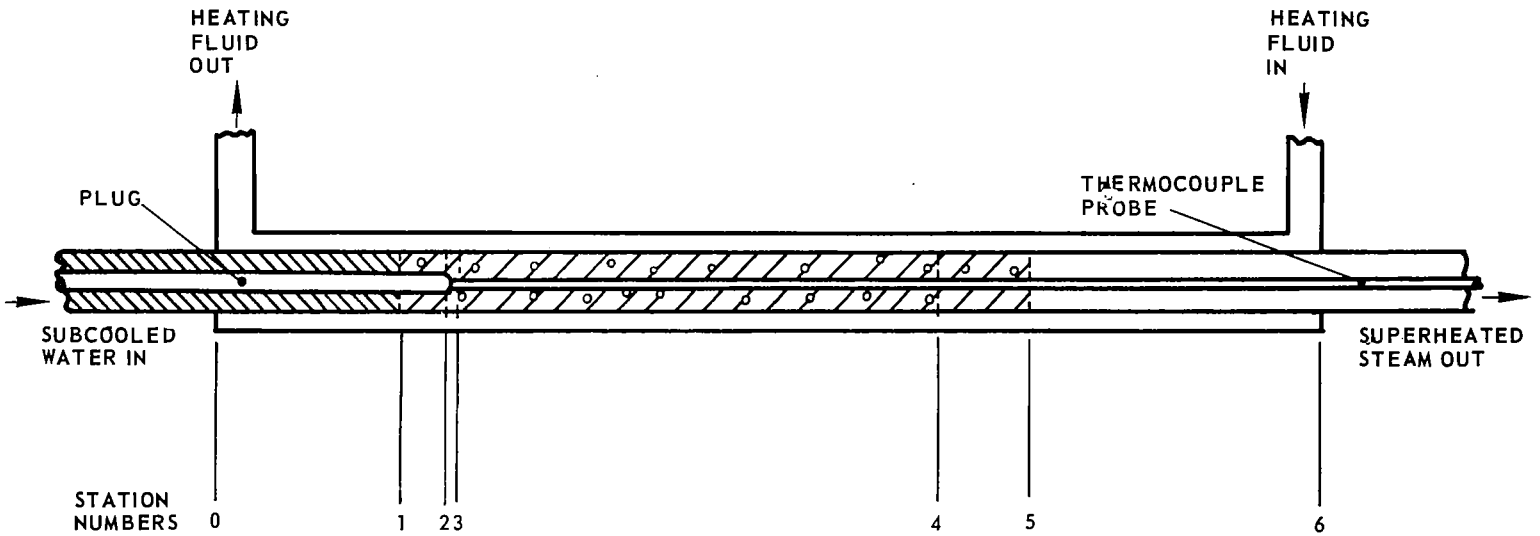


Figure 47 Boiler Configuration Showing Sections

The relations used to calculate the heat-transfer coefficients in the different sections of the boiler are discussed below. The heat-transfer coefficient of the heating fluid in all sections of the boiler was predicted using the relation

$$h = 0.023 \frac{k}{d_H} (Re)^{0.8} (Pr)^{0.4} \tag{18}$$

This is the familiar McAdams relation[9] for predicting the heat-transfer coefficient for the turbulent flow of a single-phase fluid through a channel.

The heat-transfer coefficient for the boiling fluid in Sections 1 and 6 of the boiler where single-phase flow occurred was predicted using the relation

$$h = 0.023 \frac{k}{d_H} (Re)^{0.8} (Pr)^{0.4} \left( \frac{h_{SF}}{h_{SC}} \right) \tag{19}$$

Equation (19) is the McAdams equation multiplied by the factor ( $h_{SF}/ h_{SC}$) to account for the increase in heat-transfer coefficient resulting from the swirl flow of the fluid. In determining this factor, it was assumed that the swirl-flow data of Sams[10] could be applied to the cases at hand. This data was taken for the swirl flow of air induced by a wire coil inside of a tube.

Since the swirl flow of superheated vapor through Section 6 of the boiler closely resembled the flow configuration of Reference 10, the factor ( $h_{SF}/ h_{SC}$) was determined directly from Figure 10 of the reference.

In Section 1 of the boiler, however, the swirl-flow pattern was induced using a spiral-flow channel rather than a coil inside of a tube. Since no heat transfer data could be found for this type of flow configuration, it was assumed that the relationship between heat-transfer coefficient and friction factor in the data of Reference 10 could be applied to the spiral flow case. To relate the heat-transfer coefficient and the friction factor, the following approximate relation was fitted to the data taken at a coil pitch-to-wire diameter ratio of 10.

$$\left( \frac{h_{SF}}{h_{SC}} \right) = \left( \frac{f_{SF}}{f_{SC}} \right)^{0.28} \tag{20}$$

In evaluating the ratio of the friction factors, the following relationship was assumed to apply

$$\frac{f_{SF}}{f_{SC}} = \frac{\Delta P_{SF}}{\Delta P_{SC}} \tag{21}$$

where $\Delta P_{SF}$ is the pressure loss for the flow through the spiral channel calculated using Equations (23) and (24) below, and $\Delta P_{SC}$ is the pressure loss for an equivalent straight channel having the same flow rate and linear and cross-sectional dimensions as the spiral channel.

Due to the lack of adequate boiling heat transfer data for the swirl-flow configurations of this boiler, it is necessary to assume values for the boiling heat transfer coefficient. For Sections 2 and 4 of the boiler the bulk boiling coefficient was assumed to be constant at a value of 6,000 Btu/hr - $ft^2$ - °F. For Section 5, where film boiling was assumed to take place, the heat transfer was assumed to vary linearly with boiling fluid quality from the bulk boiling coefficient to the vapor coefficient. This is shown in the following equation.

$$h = 6000 - \left(\frac{6000 - h_{SV}}{0.191}\right) (X - 0.809) \tag{22}$$

The term $h_{SV}$ in Equation (22) represents the heat transfer coefficient of the dry saturated vapor at Station 5. Equation (19) was used to calculate $h_{SV}$.

The relations used to calculate the boiling fluid pressure losses are discussed below. The momentum pressure drop of the boiling fluid from the inlet to the exit was estimated to be only 0.2 psi. As a consequence, only frictional losses were considered.

Pressure losses for the single-phase flow of the boiling fluid were calculated using two different methods depending upon the location in the boiler. For Section 1 of the boiler, where the fluid flows in a spiral path, the following equations were used to calculate the pressure loss

$$\Delta P = 4f\left(\frac{L}{D}\right)_{eq} \frac{G^2}{2g\rho} \tag{23}$$

where

$$\left(\frac{L}{D}\right)_{eq} = R_t + (N-1)\left(R_1 + \frac{R_b}{2}\right) \tag{24}$$

These equations are based on the method presented in Reference 11 for flow through a spiral tube. Values for $R_t$, $R_1$, and $R_b$ can be obtained from Figure 48.

Data Source Reference 11

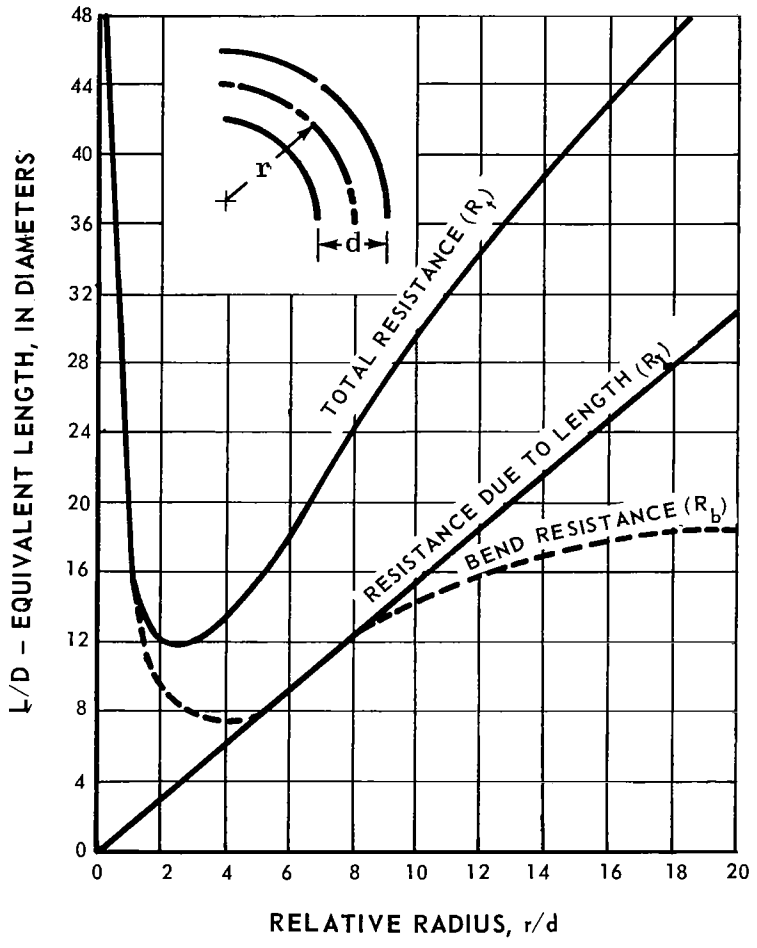


Figure 48 Equivalent Resistances for Flow Through Pipe Bends

For Section 6 of the boiler where the swirl flow is maintained by a wire coil brazed inside the tube, the pressure loss calculations were based on the method presented by Sams [10].

$$\Delta P = 4f \frac{1}{d_H} \left(\frac{f_{SF}}{f_{SC}}\right) \frac{G^2}{2g\rho} \tag{25}$$

The term ( $f_{SF}/ f_{SC}$) was determined by an extrapolation of the data of Reference 10.

For Sections 2, 4, and 5 of the boiler, where two-phase flow occurred, the method of Martinelli and Nelson [12] was employed for calculating pressure losses.

$$\frac{dP}{dl} = \frac{\left(\frac{dP}{dl}\right)_{TPF}}{\left(\frac{dP}{dl}\right)_L} \left(\frac{dP}{dl}\right)_L \tag{26}$$

The parameter $(dP/dl)_{TPF}/(dP/dl)_L$ can be obtained from Figure 3 of Reference 12 as a function of boiling-fluid quality and pressure. The term $(dP/dl)_L$ in Equation (26) is the frictional pressure gradient that would exist if the flow were entirely liquid. This term was calculated for the different sections of the boiler using the following relations:

Section 2

$$-\left(\frac{dP}{dl}\right)_L = 4f \frac{\left(\frac{L}{D}\right)_{eq}}{l_{actual}} \frac{G^2}{2g\rho} \tag{27}$$

Sections 4 and 5

$$-\left(\frac{dP}{dl}\right)_L = \frac{4f}{d_h} \left(\frac{f_{SF}}{f_{SC}}\right) \frac{G^2}{2g\rho} \tag{28}$$

Equations (27) and (28) represent differentiated forms of Equations (23) and (25) respectively.

The pressure drop for the two-phase sudden expansion that takes place in Section 3 of the boiler was calculated using the following equation which was presented by Jansen [13]

$$\Delta P = \frac{G_3^2 v_L}{g\sigma} \left[ \frac{v_V}{v_L} \frac{X^2}{Rg} (1-\sigma) \right] \tag{29}$$

The vapor fraction $R_g$ was determined using the correlation found in Figure 5 of Reference 12.

The thermodynamic performance of Sections 1 and 6 of the boiler was calculated using the log mean temperature difference method

$$Q = U A \Delta T_{LM} \tag{30}$$

where

$$U = \frac{1}{\frac{d_o}{h d_i} + \frac{t_H d_o}{k d_m} + \frac{1}{h_H}}$$

These sections are the subcooled and superheated regions where no change of phase is assumed to occur. In these sections, the rate at which the boiling fluid temperature increases with length is directly dependent upon the local rate of heat transfer. For these conditions Equation (30) provides a reasonable description of heat-exchanger performance. In Sections 2, 4 and 5 where boiling occurred, the boiling fluid was assumed to be saturated. Under these conditions, boiling fluid temperature becomes directly dependent upon the boiling-fluid pressure, rather than the local rate of heat transfer. As a consequence, the following differential equations were derived to describe the heat exchange process in Sections 2, 4 and 5 of the boiler.

$$\frac{dX}{dl} = \frac{q \pi d_o}{W h_{fg}} \tag{31}$$

where $q = U \Delta T$

$$\frac{d(\Delta T)}{dl} = \left[ \frac{W H_{fg}}{W_H C_{PH}} \frac{dX}{dl} - \left(\frac{dT}{dP_{sat}}\right)\left(\frac{dP}{dl}\right) \right] \tag{32}$$

Equation (31) relates the rate of change in boiling fluid quality to the local heat flux q which in turn is dependent upon the local temperature difference between the two fluids $\Delta T$. The first term on the right hand side of Equation (32) relates the rate of change of the heating-fluid temperature to the rate of change in the boiling-fluid quality, while the second term relates the rate of change of the boiling-fluid temperature to the boiling-fluid pressure gradient.

For each of the boiler sections under consideration, Equations (30) through (32) were combined with the appropriate relations for heat-transfer coefficients and pressure gradient, and solved using numerical integration.

The design calculations were based on the following set of conditions as specified in Task I of the contract.

1) Boiling-fluid flow rate W — 50 lb/hr

2) Heating-fluid flow rate $W_H$ — 650 lb/hr

3) Boiling-fluid inlet temperature $T_{in}$ — 140°F

4) Heating-fluid inlet temperature $T_{H\ in}$ — 402°F

5) Boiling-fluid inlet pressure $P_{out}$ — 85 psia

The values calculated for the important thermodynamic variables at each station shown in Figure 47 are tabulated below:

| Station No. | Axial Length L, ft | Boiling Fluid Pressure P, psia | Boiling Fluid Quality X | Boiling Fluid Temperature T, °F | Heating Fluid Temperature $T_H$ °F |
|---|---|---|---|---|---|
| 0 | 0 | 85.0 | Subcooled | 140 | 323 |
| 1 | 1.25 | 83.8 | 0 | 316 | 336 |
| 2 | 2.15 | 76.0 | 0.068 | 308 | 339 |
| 3 | 2.15 | 76.0 | 0.068 | 308 | 339 |
| 4 | 6.65 | 72.2 | 0.809 | 305 | 387 |
| 5 | 7.55 | 70.6 | 1.00 | 304 | 400 |
| 6 | 10.00 | 67.7 | Superheated | 377 | 402 |

In addition, a comparison between the calculated performance of the boiler and that which was experimentally determined by running the boiler at the design conditions is presented below:

| | Calculated | Measured |
|---|---|---|
| Total heat transferred Q | 54,000 Btu/hr | 51,000 Btu/hr |
| Pinch point temperature difference $\Delta T_p$ | 20°F | 19°F |
| Boiling- fluid pressure drop $\Delta P$ | 17.3 psi | 16.2 psi |
| Boiling-fluid exit temperature $T_{out}$ | 377°F | 338°F |
| Boiling-fluid superheat $\Delta T_{SH}$ | 76°F | 37°F |

| | Calculated | Measured |
|---|---|---|
| Boiling-fluid exit quality $X_e$ | 1.00 | 0.949 |
| Heating-fluid exit temperature $T_{H\ out}$ | 323°F | 330°F |

This analysis was able to predict the total heat transferred within 6 percent, the pinch-point temperature difference within 1°F, and the pressure drop of the boiling fluid within 1.1 psi. However, since the dynamics of the two-phase flow was not considered, the analysis was not able to predict the nonequilibrium exit conditions observed for the boiling fluid. Instead of emerging as a dry vapor superheated by 76°F as predicted by the analysis, the boiling fluid emerged as a mist containing, by weight, 94.9 percent vapor superheated by 37°F and 5.1 percent droplets of saturated liquid.

In order to eliminate liquid at the boiler exit during testing, the nominal design operating conditions were changed to those presented in Section III.

# APPENDIX 2

## Derivation of Theoretical Transfer Function

The details of a derivation of a transfer function between boiler exit pressure and boiler inlet flow rate are presented in this appendix. The configuration considered is a single-tube counterflow boiler using a liquid heating fluid, designed to produce superheated vapor and having a choked restriction at its exit. A complete description of this boiler is presented in Section III of this report. Provisions was made in the analysis to account for the effects of the swirl-inducing plug inserted in the boiling fluid stream at the inlet end of the boiler.

In the analysis, the boiler was divided into three regions: subcooled, boiling, and superheated, each of which was analyzed separately. These regions correspond to those observed in the steady-state data which are described in Section IV of this report. For simplicity however, it was assumed that the evaporation process was completed in the boiling region so that the boiling fluid entered the superheat region as a dry saturated vapor. This assumption is justified by the lack of specific knowledge of the rate of droplet evaporation in the nonequilibrium-superheat region of the actual boiler.

Dynamic equations were derived for these three regions and for the boiler as a whole. These equations include:

### Overall Equations

Continuity equation of the boiling fluid
Pressure-drop equation for the boiling fluid
Choked valve equation

### Subcooled Region

Energy equation of the boiling fluid
Energy equation of the plug wall

### Boiling Region

Energy equation of heater-loop fluid
Energy equation of shell wall
Energy equation of the boiling fluid

### Superheated Region

Energy equation of the boiling fluid

The basic approach followed in the derivation was to linearize these equations for small perturbations around a steady-state point and take the Laplace transforms of the perturbed variables.

Simplifications have been introduced into the analysis, where required, in an effort to keep the transfer function reasonably manageable. The principal simplifying concept is that in the derivation of the continuity and pressure-drop equations, the density change of the boiling fluid is assumed to occur at one discrete location in the boiler. The fluid density and flow rate are, therefore, considered to be independent of axial position and equal to the inlet values everywhere upstream of this location. Similarly, the fluid density and flow rate are considered to be independent of axial position and equal to the exit values everywhere downstream of this location. The location at which the density change is assumed to occur is the point at which a liquid-vapor interface would be present if all the liquid in the boiler at any instant filled the flow passage starting from the inlet (see Figure 41).

The boiler-fluid inlet temperature, the heating-fluid inlet temperature, the heating-fluid flow rate and the size of the choked restriction are assumed constant in this analysis. Additional assumptions are stated whenever they are used in the derivation.

Overall Equations

For flow through a choked restriction the total pressure of the flow entering the restriction is proportional to the mass flow rate and the square root of the total temperature.

$$P_{out} \propto W_{out} \sqrt{T_{out}}$$

Linearizing this expression for small perturbations about a steady-state point and transforming the variables, the result is

$$\frac{\hat{P}_{out}}{P_{out,\,o}} = \frac{\hat{W}_{out}}{W_o} + \frac{\hat{T}_{out}}{2T_{out,\,o}} \tag{33}$$

The continuity equation was written to account for changes in the location of the point where density change is assumed to occur and changes in the vapor density due to changes in exit pressure. The distance from the boiler inlet to the density change point is assumed to be proportional to the length of the subcooled region. This simplification avoids the necessity of describing analytically the dynamic two-phase flow mechanisms. It is a reasonable approximation to the

extent that most of the mass of the boiler fluid resides in the subcooled and very low quality regions. The resulting differential equation is presented below.

$$W_{in} - W_{out} = K(\rho_L - \rho_V) A_{SC} \left(\frac{dL_{SC}}{dt}\right) + \left(\frac{Vol_V}{RT_{out}}\right)\left(\frac{dP_{out}}{dt}\right)$$

The proportionality constant K is defined by the relation

$$K = \frac{\partial \left[\int_o^{L_e} \rho A dx\right]}{\partial \left[\rho_L A_{SC} L_{SC}\right]} \tag{34}$$

and can be evaluated from the steady-state experimental test data in which W was varied.

Linearizing the equation for small perturbations about a steady-state point and transforming the variables the result is

$$\frac{\hat{W}_{in}}{W_o} - \frac{\hat{W}_{out}}{W_o} = K\tau_{SC}S \frac{\hat{L}_{SC}}{L_{SC,o}} + \tau_V S \frac{\hat{P}_{out}}{P_{out,o}} \tag{35}$$

where

$$\tau_{SC} = \frac{(\rho_L - \rho_V) A_{SC} L_{SC}}{W_o}$$

$$\tau_V = \frac{P_{out} Vol_V}{W_o}$$

In keeping with the concept of a sudden density change at a discrete point, the pressure drop between the end of the subcooled region and the boiler exit is expressed in the form of a single-phase pressure drop, i.e., proportional to length and to flow rate squared, and inversely proprotional to density.

$$(P_{out} - P_P) \propto \frac{W_{out}^2 \quad length}{\rho_{out}} \tag{36}$$

Since most of the pressure drop in the boiler is due to the vapor phase, the boiler exit density and flow rate are used. When the pressure-drop equation is written in this form, the length cannot be taken as a literal length because of flow-area changes caused by inserts inside the boiler tube. Consequently, changes in the fictitious length are approximately related to changes in the subcooled length by means of the empirical coefficient

$$\beta_3 = \frac{\partial (\Delta P_B / P_{P,o})}{\partial (L_{SC}/L_{SC,o}}$$

Combining Equations (33) and (36) with the perfect gas law, the result is

$$(P_{out} - P_P) \propto (P_{out})(\text{length})$$

Linearizing, transforming, and relating a perturbation in the fictitious length to a perturbation in subcooled length, the result is

$$\frac{\hat{P}_P}{P_{P,o}} = \frac{\hat{P}_{out}}{P_{out,o}} + \left(\frac{\partial (\Delta P_B/P_{P,o})}{\partial (L_{SC}/L_{SC,o})}\right)\left(\frac{\hat{L}_{SC}}{L_{SC,o}}\right) \qquad (37)$$

The combined energy equation incorporates the five individual energy equations written for different portions of the subcooled and boiling regions into a single relation. This combined equation describes perturbations in the length of the subcooled region as a function of the perturbations of the inlet flow rate, exit flow rate and exit pressure of the boiling fluid.

Four of the five energy equations were derived using the distributed-parameter approach whereby a partial differential equation was derived with time and axial distance as the independent variables. The solution to the partial differential equation for the boiling fluid in the boiling region, however, proved to be too complicated for the purposes of this analysis. In its place a quasi-dynamic equation was written with coefficients evaluated by means of steady-state relationships, and with transport time lags superimposed. The transport times appear in the equation in the form they would take in an approximate solution to a single-phase partial differential energy equation. The transport times in the boiling region are referred to the time it takes a liquid particle to travel the length of the boiling region.

In deriving these energy equations a fixed frame of reference was used, although the locations of the boundaries of both the subcooled and boiling regions fluctutate with time. The energy equations of the two regions were connected in a fixed reference frame by employing linearized perturbations about the steady-state boundaries in the boundary conditions of the equations.

Subcooled Region

In deriving the energy equation in the subcooled region the following basic assumptions were made:

1) No change in heating-fluid temperature takes place due to heat transfer in the subcooled region. Consequently, the only heating-fluid temperature changes are those which are transported into the subcooled region due to changes with time at the pinch point.

2) Heat storage occurs in the plug metal but not in the tube metal or shell metal. Infinite thermal conductivity of the plug metal in the radial direction and zero conductivity in the axial direction are assumed in calculating heat transfer from plug metal to boiling fluid.

3) The overall heat-transfer coefficient between heating fluid and boiler fluid changes (for small perturbations about a point) with boiling fluid velocity to the $n_{SC}$ power. The boiling-fluid heat-transfer coefficient is considered constant for the purpose of calculating heat transfer from plug metal to boiling fluid.

4) Average properties in the region are used for both fluids.

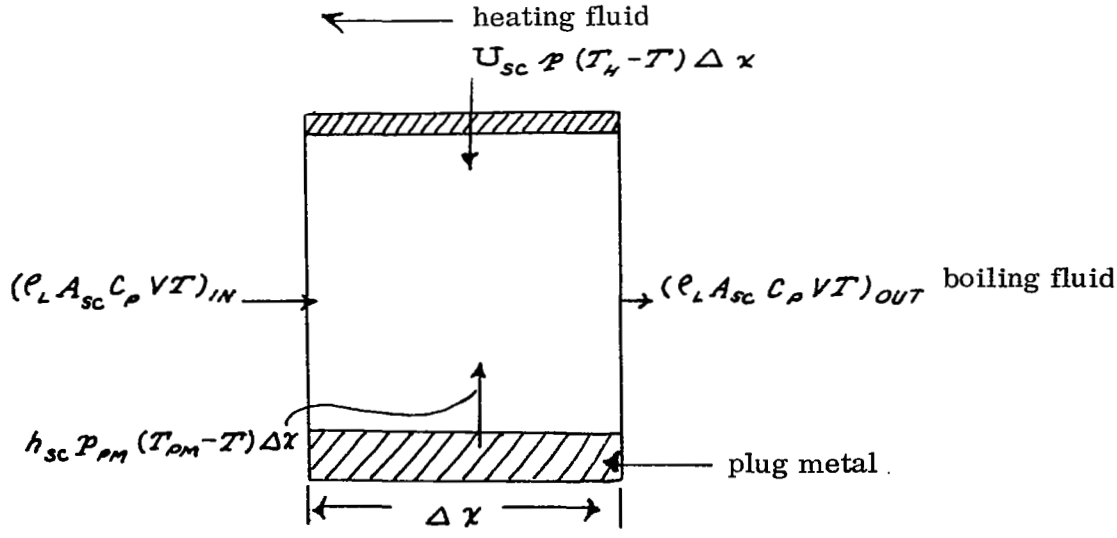

Taking an energy balance on a differential element of the boiling fluid

energy in = energy out + energy stored

$$(\rho_L A_{sc} C_p V T)_{IN} + U_{sc} \mathcal{P}_T (T_H - T) \Delta x + h_{sc} \mathcal{P}_{PM} (T_{PM} - T) \Delta x = (\rho_L A_{sc} C_p V T)_{OUT} + \rho_L A_{sc} C_p \frac{\partial T}{\partial t}$$

$$\rho_L A_{sc} C_p V \left[ T - \frac{\partial T}{\partial x} \frac{\Delta x}{2} \right] + U_{sc} p (T_H - T) \Delta x + h_{sc} \mathcal{P}_{PM} (T_{PM} - T) \Delta x =$$

$$\rho_L A_{sc} C_p V \left[ T + \frac{\partial T}{\partial x} \frac{\Delta x}{2} \right] + \rho_L A_{sc} C_p \frac{\partial T}{\partial t}$$

$$\frac{\partial T}{\partial t} + V \frac{\partial T}{\partial x} = \Theta (T_H - T) + \Theta_1 (T_{PM} - T) \tag{38}$$

where $\Theta = \dfrac{U_{sc} \mathcal{P}_T}{\rho_L A_{sc} C_p}$ ( $U_{SC}$ is assumed variable)

$\Theta_1 = \dfrac{h_{sc} \mathcal{P}_{PM}}{\rho_L A_{sc} C_p}$ ( $h_{SC}$ is assumed constant)

Linearizing for small perturbations about a steady point and transforming the variables the result is:

$$s\hat{T} + V_o \frac{d\hat{T}}{dx} + \hat{V} \frac{\partial T_o}{\partial x} = \hat{\Theta} (T_{Ho} - T_o) + \Theta_o (\hat{T}_H - \hat{T}) + \Theta_1 (\hat{T}_{PM} - \hat{T}) \tag{39}$$

Steady-State Equation

$$V_o \frac{\partial T_o}{\partial x} = \Theta (T_{Ho} - T_o)$$

Steady-State Solution

$$T_o = T_{Ho} - (T_{Ho} - T_{IN}) e^{-\frac{\Theta_o}{V_o} x} \tag{40}$$

$$\frac{\partial T_o}{\partial x} = \frac{\Theta_o}{V_o} (T_{Ho} - T_{IN}) e^{-\frac{\Theta_o}{V_o} x} \tag{41}$$

Energy Equation of Plug Metal in Subcooled Region

Taking a heat balance on a differential element of the plug metal

energy in = energy stored

$$-h_{sc}\, \mathcal{P}_{PM}\,(T_{PM}-T)\,\Delta x = \rho_{PM} A_{PM} C_{P_{PM}} \Delta x \frac{\partial T_{PM}}{\partial t}$$

$$\frac{\partial T_{PM}}{\partial t} = -\Theta_2\,(T_{PM}-T) \tag{42}$$

where $\Theta_2 = \dfrac{h_{sc}\, \mathcal{P}_{PM}}{\rho_{PM} A_{PM} C_{P_{PM}}}$

Linearizing and transforming the variables the result is

$$s\hat{T}_{PM} = -\Theta_2\,(\hat{T}_{PM} - \hat{T}) \tag{43}$$

Solution of Differential Equations

On the basis of the first basic assumption

$$T_{H_2O} = T_{H_2O} \;,\quad \therefore \frac{\partial T_H}{\partial x} = 0 \tag{44}$$

$$\hat{T}_H = \hat{T}_{HP}\; e^{-\frac{s(L_{sc,o}-x)}{V_H}} \tag{45}$$

On the basis of the third basic assumption

$$\Theta = C V^{n_{sc}},\quad \therefore \hat{\Theta} = \frac{\Theta_o}{V_o} n_{sc} \hat{V} \tag{46}$$

Combining Equations (39), (40), (41), (43), (44), (45), and (46) the result is

$$\frac{d\hat{T}}{d\chi} + \left[\frac{s+\Theta_o-\Theta_1\left(\frac{\Theta_2}{s+\Theta_2}-1\right)}{V_o}\right]\hat{T} = -\frac{\Theta_o}{V_o^2}(1-n_{sc})(T_{HPO}-T_{IN})\,e^{-\frac{\Theta_o}{V_o}\chi}\,\hat{V} + \frac{\Theta_o}{V_o}\,e^{-\frac{s(L_{sc,o}-\chi)}{V_H}}\,\hat{T}_{HP} \tag{47}$$

The general solution to Equation (47) is

$$\hat{T} = e^{-[\quad]\chi}\left[\int\left(-\frac{\Theta_o}{V_o^2}(1-n_{sc})(T_{HPO}-T_{IN})e^{-\frac{\Theta_o}{V_o}\chi}\hat{V} + \frac{\Theta_o}{V_o}e^{-s\left(\frac{L_{sc,o}-\chi}{V_H}\right)}\hat{T}_{HP}\right)e^{+[\quad]\chi}\,d\chi + c\right]$$

which upon integration becomes

$$\hat{T} = -\frac{\frac{\Theta_o}{V_o}(1-n_{sc})(T_{HPO}-T_{IN})}{s-\Theta_1\left(\frac{\Theta_2}{s+\Theta_2}-1\right)}\,e^{-\frac{\Theta_o}{V_o}\chi}\,\hat{V} + \frac{\frac{\Theta_o}{V_o}e^{-s\tau_{HSC}}e^{\frac{s\chi}{V_H}}}{\left\{\frac{s+\Theta_o-\Theta_1\left(\frac{\Theta_2}{s+\Theta_2}-1\right)}{V_o}+\frac{s}{V_H}\right\}}\,\hat{T}_{HP} + c\,e^{-\left[\frac{s+\Theta_o-\Theta_1\left(\frac{\Theta_2}{s+\Theta_2}-1\right)}{V_o}\right]\chi} \tag{48}$$

Applying the boundary condition $\hat{T} = 0$ at $x = 0$ the result is

$$\hat{T} = -\frac{\frac{\Theta_o}{V_o}(1-\eta_{SC})\,(T_{HPO}-T_{IN})}{s-\Theta_1\left(\frac{\Theta_2}{s+\Theta_2}-1\right)}\left[e^{-\frac{\Theta_o}{V_o}x}-e^{-\left\{\frac{s+\Theta_o-\Theta_1\left(\frac{\Theta_2}{s+\Theta_2}-1\right)}{V_o}\right\}x}\right]\hat{V}$$

$$+\frac{\frac{\Theta_o}{V_o}e^{-s\tau_{HSC}}}{\left\{\frac{s+\Theta_o-\Theta_1\left(\frac{\Theta_2}{s+\Theta_2}-1\right)}{V_o}+\frac{s}{V_H}\right\}}\left[e^{\frac{sx}{V_H}}-e^{-\left\{\frac{s+\Theta_o-\Theta_1\left(\frac{\Theta_2}{s+\Theta_2}-1\right)}{V_o}\right\}x}\right]\hat{T}_{HP} \qquad (49)$$

at $x = L_{SCO}$; $\hat{T} = \hat{T}_p$ and

$$\hat{T}_p = -(1-\eta_{SC})\left[\frac{\Theta_o}{V_o}(T_{HPO}-T_{IN})\,e^{-\Theta_o\tau_{SC}}\right]\left[\frac{1-e^{-\left\{s-\Theta_1\left(\frac{\Theta_2}{s+\Theta_2}-1\right)\right\}\tau_{SC}}}{s-\Theta_1\left(\frac{\Theta_2}{s+\Theta_2}-1\right)}\right]\frac{\hat{W}_{IN}}{\rho_L A_{SC}}$$

$$+\frac{\frac{\Theta_o}{V_o}}{\left\{\frac{s+\Theta_o-\Theta_1\left(\frac{\Theta_2}{s+\Theta_2}-1\right)}{V_o}+\frac{s}{V_H}\right\}}\left[1-e^{-\left\{s+\Theta_o-\Theta_1\left(\frac{\Theta_2}{s+\Theta_2}-1\right)\right\}\tau_{SC}-s\tau_{HSC}}\right]T_{HP} \qquad (50)$$

where $$\frac{L_{SC,O}}{V_o} = \tau_{SC} \qquad (51)$$

$$\frac{L_{SC,O}}{V_H} = \tau_{HSC} \qquad (52)$$

$$V = \frac{W_{IN}}{\rho_L A_{SC}} \;;\; \therefore \hat{V} = \frac{\hat{W}_{IN}}{\rho_L A_{SC}} \qquad (53)$$

Boundary Condition at Pinch Point

Defining the subcooled length as the distance from the boiler inlet required for the boiling fluid to reach the saturation temperature, small perturbations of the subcooled length around steady-state value can be expressed by the following equation

$$\hat{L}_{sc} = \frac{\hat{T}_p - \hat{T}_{SAT}}{-\left(\frac{\partial T_o}{\partial x}\right)_{x=L_{sc,o}}} \tag{54}$$

And Equation (50) becomes

$$\hat{L}_{sc} = (1-n_{sc})\left(\frac{1-e^{-\left[s-\theta_1\left(\frac{\theta_2}{s+\theta_2}-1\right)\right]\tau_{sc}}}{s-\theta_1\left(\frac{\theta_2}{s+\theta_2}-1\right)}\right)\hat{W}_{IN}\left(\frac{L_{po}}{W_o\,\tau_{sc}}\right)$$

$$-\left(\frac{L_{sc,o}}{(T_{HP,o}-T_{IN})\,e^{-\theta_o\tau_{sc}}}\right)\left(\frac{1-e^{-\left[s+\theta_o-\theta_1\left(\frac{\theta_2}{s+\theta_2}-1\right)\right]\tau_{sc}-s\tau_{HSC}}}{\left[s+\theta_o-\theta_1\left(\frac{\theta_2}{s+\theta_2}-1\right)\right]\tau_{sc}+s\tau_{HSC}}\right)\hat{T}_{HP}$$

$$+\frac{\hat{T}_{SAT}}{\frac{\theta_o}{V_o}\left[T_{HPo}-T_{IN}\right]e^{-\theta_o\tau_{sc}}} \tag{55}$$

For $x = L_{SC,0}$ Equation (40) becomes

$$e^{\theta_o\tau_{sc}} = \frac{T_{HP,o}-T_{IN}}{\Delta T_{p,o}} \equiv \phi_1 \tag{56}$$

For small perturbations

$$\frac{\hat{T}_{SAT}}{\Delta T_{po}} = \left[ \frac{\partial \left( T_{SAT} / \Delta T_{po} \right)}{\partial \left( P / P_{po} \right)} \right]_{L_{sc,o}} \frac{\hat{P}_p}{P_{po}} = \beta_1 \frac{\hat{P}_p}{P_{po}} \qquad (57)$$

Combining equations (55), (56) and (57) and noting that

$$\left[ \frac{\Theta_2}{s + \Theta_2} - 1 \right] = \frac{s\Theta_2}{s^2 - \Theta_2^2} - \frac{s^2}{s^2 - \Theta_2^2}$$

The result is:

$$\frac{\hat{L}_{sc}}{L_{sc,o}} = \frac{\gamma_1}{s\tau_{sc}} \frac{\hat{W}_{IN}}{W_o} - \gamma_2 \frac{\hat{T}_{HP}}{\Delta T_{po}} + \gamma_3 \frac{\hat{P}_p}{P_{po}} \qquad (58)$$

where

$$\gamma_1 = \left[ \frac{1 - \left[ e^{-\left( \frac{\Theta_1 s^2}{s^2 - \Theta_2^2} \right) \tau_{sc}} \right] e^{-s\left( 1 - \frac{\Theta_1 \Theta_2}{s^2 - \Theta_2^2} \right) \tau_{sc}}}{1 - \frac{\Theta_1 \Theta_2}{s^2 - \Theta_2^2} + s\left[ \frac{\Theta_1}{s^2 - \Theta_2^2} \right]} \right] (1 - \eta_{sc}) \qquad (59)$$

$$\gamma_2 = \frac{1 - \left[ \left( \frac{1}{\phi_1} \right) e^{-\left( \frac{\Theta_1 s^2}{s^2 - \Theta_2^2} \right) \tau_{sc}} \right] e^{-s\left[ \left( 1 - \frac{\Theta_1 \Theta_2}{s^2 - \Theta_2^2} \right) \tau_{sc} + \tau_{Hsc} \right]}}{\left[ \ln \phi_1 + \left( \frac{\Theta_1 s^2}{s^2 - \Theta_2^2} \right) \tau_{sc} \right] + s\left[ \left( 1 - \frac{\Theta_1 \Theta_2}{s^2 - \Theta_2^2} \right) \tau_{sc} + \tau_{Hsc} \right]} \qquad (60)$$

$$\gamma_3 = \frac{\beta_1}{\ln \phi_1} \qquad (61)$$

## Boiling Region

In deriving the energy equations in the boiling region the following basic assumptions were made:

1) Heat storage occurs in the shell metal but not in the tube metal or probe metal. Infinite thermal conductivity of the shell metal in the radial direction and zero conductivity in the axial direction are assumed.

2) All heat-transfer coefficients are constant and independent of the boiling-fluid flow rate.

3) The saturation temperature is independent of axial distance and equal to the value determined by the pinch-point pressure.

4) The transport time of a liquid particle in the boiling region is the principal dynamic element in the boiling-fluid energy relationships.

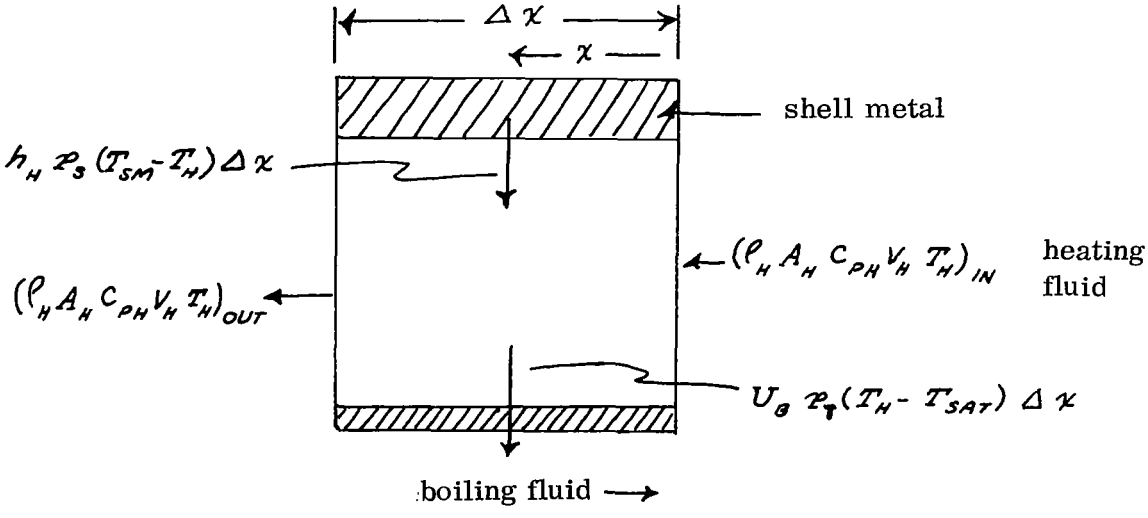


Taking x in the direction of the heating fluid flow, an energy balance on a differential element of the heater loop fluid becomes

energy in = energy out + energy stored

$$(\rho_H A_H C_{PH} V_H T_H)_{IN} + h_H \mathcal{P}_{SM} (T_{SM} - T_H) \Delta x = U_B \mathcal{P}_T (T_H - T_{SAT}) \Delta x +$$

$$(\rho_H A_H C_{PH} V_H T_H)_{OUT} + \rho_H A_H C_{PH} \frac{\partial T_H}{\partial t} \Delta x$$

$$\rho_H A_H C_{PH} \frac{\partial T_H}{\partial t} \Delta x + \rho_H A_H C_{PH} V_H \left[ T_H + \frac{\partial T_H}{\partial x} \frac{\Delta x}{2} \right] = \rho_H A_H C_{PH} V_H \left[ T_H - \frac{\partial T_H}{\partial x} \frac{\Delta x}{2} \right]$$

$$+ U_B \mathcal{P}_T (T_{SAT} - T_H) + h_H \mathcal{P}_{SM} (T_{SM} - T_H)$$

$$\frac{\partial T_H}{\partial t} + V_H \frac{\partial T_H}{\partial x} = \Theta_B (T_{SAT} - T_H) + \Theta_{B_1} (T_{SM} - T_H) \qquad (62)$$

where

$$\Theta_B = \frac{U_B \mathcal{P}_T}{\rho_H A_H C_{PH}} \qquad (63)$$

$$\Theta_{B_1} = \frac{h_H \mathcal{P}_{SM}}{\rho_H A_H C_{PH}} \qquad (64)$$

Linearizing for small perturbations about a steady point and taking the Laplace transforms of the perturbed variables the result is

$$\frac{d \hat{T}_H}{d x} + \frac{s}{V_H} \hat{T}_H = \frac{\Theta_B}{V_H} (\hat{T}_{SAT} - \hat{T}_H) + \frac{\Theta_{B_1}}{V_H} (\hat{T}_{SM} - \hat{T}_H) \qquad (65)$$

Steady-State Equation

$$V_H \frac{\partial T_{H,O}}{\partial x} = - \Theta_B (T_{H,O} - T_{SAT,O})$$

Steady-State Solution

$$T_{H,O} = T_{SAT,O} + (T_{H\,IN} - T_{SAT,O}) e^{- \frac{\Theta_B}{V_H} x} \qquad (66)$$

$$\frac{\partial T_{H,O}}{\partial x} = - \frac{\Theta_B}{V_H} (T_{H\,IN} - T_{SAT,O}) e^{- \frac{\Theta_B}{V_H} x} \qquad (67)$$

Energy Equation of the Shell Metal in the Boiling Region

Assuming no heat loss to the surroundings the heat balance for a differential element of the shell metal becomes

energy in = energy stored

$$h_H \mathcal{P}_{SM} (T_H - T_{SM}) \Delta x = \rho_{SM} C_{P SM} A_{SM} \frac{\partial T_{SM}}{\partial t} \Delta x$$

or

$$\frac{\partial T_{SM}}{\partial t} = - \Theta_{B_2} (T_{SM} - T_H) \tag{68}$$

where

$$\Theta_{B_2} = \frac{h_H \mathcal{P}_{SM}}{\rho_{SM} C_{P SM} A_{SM}} \tag{69}$$

Linearizing and transforming the variables the result is

$$s \hat{T}_{SM} = - \Theta_{B_2} (\hat{T}_{SM} - \hat{T}_H) \tag{70}$$

Solution of the Differential Equations

Combining Equations (65) and (70) the result is

$$\frac{d\hat{T}_H}{dx} + \left[\frac{s + \theta_B - \theta_{B_1}\left(\frac{\theta_{B_2}}{s+\theta_{B_2}} - 1\right)}{V_H}\right] \hat{T}_H = \frac{\theta_B}{V_H} \hat{T}_{SAT} \qquad (71)$$

On the basis of the third basic assumption

$$\hat{T}_{SAT} = \hat{T}_{SAT,\rho} \neq f(x)$$

The general solution to Equation (71) is then

$$\hat{T}_H = e^{-[\ ]x}\left[\int \frac{\theta_B}{V_H} \hat{T}_{SAT}\, e^{[\ ]x}\, dx + C\right] \qquad (72)$$

which upon integration becomes

$$\hat{T}_H = \frac{\theta_B}{s + \theta_B - \theta_{B_1}\left(\frac{\theta_{B_2}}{s+\theta_{B_2}} - 1\right)} \hat{T}_{SAT} + C e^{-\left[\frac{s+\theta_B-\theta_{B_1}\left(\frac{\theta_{B_2}}{s+\theta_{B_2}}-1\right)}{V_H}\right]x} \qquad (73)$$

Applying the boundary condition

$$\hat{T}_H = \left(\frac{\partial T_{Ho}}{\partial x}\right)_{x=0^+} \hat{L}_B \qquad (74)$$

AT $x = 0^+$

which relates small perturbations in the heating-fluid temperature to small perturbations in the location of the end of the boiling region. The result is

$$\hat{T}_H = \left[ \frac{1 - e^{-\left[\frac{s + \Theta_B - \Theta_{B_1}\left(\frac{\Theta_{B_2}}{s+\Theta_{B_2}} - 1\right)}{V_H}\right]\chi}}{s + \Theta_B - \Theta_{B_1}\left(\frac{\Theta_{B_2}}{s+\Theta_{B_2}} - 1\right)} \right] \Theta_B \hat{T}_{SAT} +$$

$$- \left[ \frac{s + \Theta_B - \Theta_{B_1}\left(\frac{\Theta_{B_2}}{s+\Theta_{B_2}} - 1\right)}{V_H} \right] \chi$$

$$\left(\frac{\partial T_{H,0}}{\partial \chi}\right)_{\chi=0} \hat{L}_B \, e \qquad (75)$$

At the pinch point $x = (L_{B',O} - L_{sc,d})$ , $\hat{T}_H = \hat{T}_{HP}$ and Equation (75) becomes

$$\hat{T}_{HP} = \left[ \frac{1 - e^{-\left[s + \Theta_B - \Theta_{B_1}\left(\frac{\Theta_{B_2}}{s+\Theta_{B_2}} - 1\right)\right]\tau_{HB}}}{s + \Theta_B - \Theta_{B_1}\left(\frac{\Theta_{B_2}}{s+\Theta_{B_2}} - 1\right)} \right] \Theta_B \hat{T}_{SAT} +$$

$$- \left[ s + \Theta_B - \Theta_{B_1}\left(\frac{\Theta_{B_2}}{s+\Theta_{B_2}} - 1\right) \right] \tau_{HB}$$

$$\left(\frac{\partial T_{H,0}}{\partial \chi}\right)_{\chi=0} \hat{L}_B \, e \qquad (76)$$

where

$$\tau_{HB} = \frac{L_{B,O} - L_{SC,O}}{V_H} \tag{77}$$

At the pinch point Equation (66) becomes

$$e^{\theta_B \tau_{HB}} = \frac{T_{H\,IN} - T_{SAT,O}}{\Delta T_{PO}} \equiv \phi_2 \tag{78}$$

while at x = 0 Equation (67) becomes

$$\left(\frac{\partial T_{H,O}}{\partial x}\right)_{x=0} = - \frac{\theta_B}{V_H} \left(T_{H\,IN} - T_{SAT,O}\right) \tag{79}$$

Combining Equations (77), (78), and (79) the result is

$$\left(\frac{\partial T_{H,O}}{\partial x}\right)_{x=0} = - \frac{\ln \phi_2 \; \Delta T_{PO}}{(L_{B,O} - L_{SC,O})} e^{\theta_B \tau_{HB}} \tag{80}$$

Combining Equations (76), (78), and (80)

$$\frac{\hat{T}_{HP}}{\Delta T_{PO}} = \ln \phi_2 \left[ \frac{1 - \left(\frac{1}{\phi_2}\right) e^{-\left[s - \theta_{B_1}\left(\frac{\theta_{B_2}}{s+\theta_{B_2}} - 1\right)\right]\tau_{HB}}}{\ln \phi_2 + \left[s - \theta_{B_1}\left(\frac{\theta_{B_2}}{s+\theta_{B_2}} - 1\right)\right]\tau_{HB}} \right] \frac{\hat{T}_{SAT}}{\Delta T_{PO}} -$$

$$(\ln \phi_2)\, e^{-\left[s - \theta_{B_1}\left(\frac{\theta_{B_2}}{s+\theta_{B_2}} - 1\right)\right]\tau_{HB}} \frac{\hat{L}_B}{(L_{B,O} - L_{SC,O})} \tag{81}$$

Combining Equations (57) and (81) and noting that

$$\left[\frac{\theta_{B2}}{S+\theta_{B2}} - 1\right] = \frac{S\theta_{B2}}{S^2-\theta_{B2}^2} - \frac{S^2}{S^2-\theta_{B2}^2}$$

the result is

$$\frac{\hat{T}_{HP}}{\Delta T_{Po}} = \gamma_4 \frac{\hat{P}_P}{P_{Po}} - \gamma_5 \frac{\hat{L}_B}{(L_{B,O} - L_{SC,O})} \tag{82}$$

where

$$\gamma_4 = \beta_1 \ln \phi_2 \left[ \frac{1 - \left(\frac{1}{\phi_2}\right) e^{-\left[\frac{\theta_{B1} S^2}{S^2-\theta_{B2}^2}\right] T_{HB}} e^{-S\left[1 - \frac{\theta_{B1}\theta_{B2}}{S^2-\theta_{B2}^2}\right] T_{HB}}}{\left[\ln \phi_2 + \frac{\theta_{B1} S^2 T_{HB}}{S^2-\theta_{B2}^2}\right] + S\left[1 - \frac{\theta_{B1}\theta_{B2}}{S^2-\theta_{B2}^2}\right] T_{HB}} \right] \tag{83}$$

$$\gamma_5 = \left[ (\ln \phi_2)\, e^{-\left[\frac{\theta_{B1} S^2}{S^2-\theta_{B2}^2}\right] T_{HB}} \right] e^{-S\left[1 - \frac{\theta_{B1}\theta_{B2}}{S^2-\theta_{B2}^2}\right] T_{HB}} \tag{84}$$

Energy Equation of the Boiling Fluid in the Boiling Region

Assuming that changes in $L_B$ can be described using a chain rule type of equation where the independent variables are subject to time lags, the result is

$$\frac{d L_B}{d t} = \left(\frac{\partial L_B}{\partial W_{OUT}}\right) \frac{d[W_{OUT}(t - \tau_B/2)]}{d t} + \left(\frac{\partial L_B}{\partial L_{SC}}\right) \frac{d[L_{SC}(t - \tau_B)]}{d t} +$$

$$\left(\frac{\partial L_B}{\partial P_p}\right) \frac{d[P_p(t - \tau_B)]}{d t} + \left(\frac{\partial L_B}{\partial T_{HP}}\right) \frac{d[T_{HP}(t - \tau_B)]}{d t} \tag{85}$$

where $\tau_B$ is the time required for a liquid particle to travel the length of the boiling region.

Linearizing about a steady point and transforming the variables the result is

$$\hat{L}_B = \left(\frac{\partial L_B}{\partial W_{OUT}}\right)_0 \hat{W}_{OUT}\, e^{-\frac{s\tau_B}{2}} + \left(\frac{\partial L_B}{\partial L_{SC}}\right)_0 \hat{L}_{SC}\, e^{-s\tau_B} +$$

$$\left(\frac{\partial L_B}{\partial P_p}\right)_0 \hat{P}_p\, e^{-s\tau_B} + \left(\frac{\partial L_B}{\partial T_{HP}}\right)_0 \hat{T}_{HP}\, e^{-s\tau_B} \tag{86}$$

Taking a steady-state energy balance over the entire boiling region the result is

$$Q_B = W_o H_{fg} = W_H C_{PH} (T_{HIN} - T_{HP}) \quad (87)$$

Assuming that the heat transferred in the boiling region can be described using an arithmetic mean temperature difference, the result is

$$Q_B = U_B P_T (L_B - L_{SC}) \Delta T_M \quad (88)$$

where $$\Delta T_M = \frac{(T_{HIN} - T_{SAT}) + (T_{HP} - T_{SAT})}{2}$$

$$= \left( \frac{T_{HIN} + T_{HP}}{2} \right) - T_{SAT}$$

Combining Equations (87) and (88) the result is

$$L_B = \frac{W_o H_{fg}}{U_B P_T \Delta T_M} + L_{SC} \quad (89)$$

Differentiating Equation (89) the result is

$$\frac{\partial L_B}{\partial W_{OUT}} = \frac{H_{fg}}{U_B P_T \Delta T_M} = \frac{L_{B,o} - L_{SC,o}}{W_o} \quad (90)$$

$$\frac{\partial L_B}{\partial L_{sc}} = 1 = \frac{T_{HSC}}{T_{HB}} \cdot \left( \frac{L_{B,o} - L_{sc,o}}{L_{sc,o}} \right) \tag{91}$$

$$\frac{\partial L_B}{\partial P_p} = \left( \frac{\partial L_B}{\partial \Delta T_M} \right) \left( \frac{\partial \Delta T_M}{\partial T_{SAT}} \right) \left( \frac{\partial T_{SAT}}{\partial P_p} \right)$$

$$= - \left( \frac{W_o H_{fg}}{U_B P_T \Delta T_M^2} \right) (-1) \left( \frac{\partial T_{SAT}}{\partial P_p} \right)$$

Combining the above equation with Equation (89) and the definition of $\beta_1$ the result is

$$\frac{\partial L_B}{\partial P_p} = \frac{L_{B,o} - L_{sc,o}}{\Delta T_M} \quad \frac{\Delta T_{po}}{P_{po}} \quad \beta_1$$

or

$$\frac{\partial L_B}{\partial P_p} = \frac{(L_{B,o} - L_{sc,o})}{P_{po}} \phi_3 \beta_1 \tag{92}$$

where

$$\phi_3 = \frac{\Delta T_{po}}{\Delta T_M}$$

$$\frac{\partial L_B}{\partial T_{HP}} = \left( \frac{\partial L_B}{\partial \Delta T_M} \right) \left( \frac{\partial \Delta T_M}{\partial T_{H,P}} \right)$$

$$= \left( - \frac{W_o H_{fg}}{U_B P_T \Delta T_M^2} \right) \left( \frac{1}{2} \right)$$

Combining with Equation (89)

$$\frac{\partial L_B}{\partial T_{HP}} = - \frac{(L_{B,o} - L_{sc,o})}{2 \Delta T_M} \tag{93}$$

Combining Equations (86), (90), (91), (92), and (93) the result is

$$\frac{\hat{L}_B}{L_{B,o} - L_{sc,o}} = \frac{\hat{W}_{OUT}}{W_o} e^{-\frac{s\tau_B}{2}} + \left(\frac{T_{HSC}}{T_{HB}}\right) \frac{\hat{L}_{sc}}{L_{sc,o}} e^{-s\tau_B}$$

$$+ \phi_3 \beta_1 \frac{\hat{P}_P}{P_{Po}} e^{-s\tau_B} - \frac{\phi_3}{2} \frac{\hat{T}_{HP}}{\Delta T_{PO}} e^{-s\tau_B} \tag{94}$$

Combined Energy Equation

Combining Equations (58) and (82) the result is

$$\frac{\hat{L}_{sc}}{L_{sc,o}} = \frac{\gamma_1}{s\tau_{sc}} \frac{\hat{W}_{IN}}{W_o} + \left[\gamma_3 - \gamma_2 \gamma_4\right] \frac{\hat{P}_P}{P_{P,o}} + \gamma_2 \gamma_5 \frac{\hat{L}_B}{L_{B,o} - L_{sc,o}} \tag{95}$$

Combining Equations (82) and (94) the result is

$$\left[1 - \frac{\gamma_5 \phi_3}{2} e^{-s\tau_B}\right] \frac{\hat{L}_B}{L_{B,o} - L_{sc,o}} = e^{-\frac{s\tau_B}{2}} \frac{\hat{W}_{OUT}}{W_o}$$

$$+ \frac{T_{HSC}}{T_{HB}} e^{-s\tau_B} \frac{\hat{L}_{sc}}{L_{sc,o}} - \phi_3 \left[\frac{\gamma_4}{2} - \beta_1\right] e^{-s\tau_B} \frac{\hat{P}_P}{P_{P,o}} \tag{96}$$

Combining Equations (95) and (96) the result is

$$\frac{\hat{L}_{sc}}{L_{sc,o}} = \textcircled{A}\,\frac{\hat{W}_{IN}}{W_o} + \textcircled{B}\,\frac{\hat{P}_p}{P_{p,o}} + \textcircled{C}\,\frac{\hat{W}_{OUT}}{W_o} \tag{97}$$

where

$$\textcircled{A} = \left[\frac{\gamma_1 / s\tau_{sc}}{1 - \dfrac{\gamma_2\gamma_5\left(\frac{\tau_{HSC}}{\tau_{HB}}\right)e^{-s\tau_B}}{\left\{1 - \frac{\gamma_5\phi_3}{2}e^{-s\tau_B}\right\}}}\right] \tag{98}$$

$$\textcircled{B} = \left[\frac{\gamma_3 - \gamma_2\gamma_4 - \dfrac{\gamma_2\gamma_5\phi_3\left(\frac{\gamma_4}{2} - \beta_1\right)e^{-s\tau_B}}{1 - \frac{\gamma_5\phi_3}{2}e^{-s\tau_B}}}{1 - \dfrac{\gamma_2\gamma_5\left(\frac{\tau_{HSC}}{\tau_{HB}}\right)e^{-s\tau_B}}{\left\{1 - \frac{\gamma_5\phi_3}{2}e^{-s\tau_B}\right\}}}\right] \tag{99}$$

$$\textcircled{C} = \left[\frac{\dfrac{\gamma_2\gamma_5 e^{-s\frac{\tau_B}{2}}}{1 - \frac{\gamma_5\phi_3}{2}e^{-s\tau_B}}}{1 - \dfrac{\gamma_2\gamma_5\left(\frac{\tau_{HSC}}{\tau_{HB}}\right)e^{-s\tau_B}}{\left\{1 - \frac{\gamma_5\phi_3}{2}e^{-s\tau_B}\right\}}}\right] \tag{100}$$

Energy Equation in the Superheated Region

The energy equation for the superheated region is written to account for the perturbations in the boiling-fluid outlet temperature resulting from perturbations in the boiling-fluid outlet flow rate and pressure as well as perturbations in the boiling length $L_B$. The equation is based on the solution of the partial differential energy equation of the boiling fluid, subject to the following assumptions:

1) No change in heating-fluid temperature takes place due to heat transfer in the superheat region. Consequently, the temperature is constant at the value of the heating-fluid inlet temperature.

2) Negligible heat storage occurs in all metal volumes.

3) The overall heat transfer coefficient between heating fluid and boiling fluid varies (for small perturbations around a point), with boiling fluid velocity to the $n_{SH}$ power.

4) The density of the superheated vapor is considered constant at its value at the boiler exit.

5) The steady-state value of the boiling-fluid temperature entering the superheated region is equal to the saturation temperature determined by the steady-state value of the outlet pressure $P_{out,o}$.

## Energy Equation of the Boiling Fluid in the Superheated Region

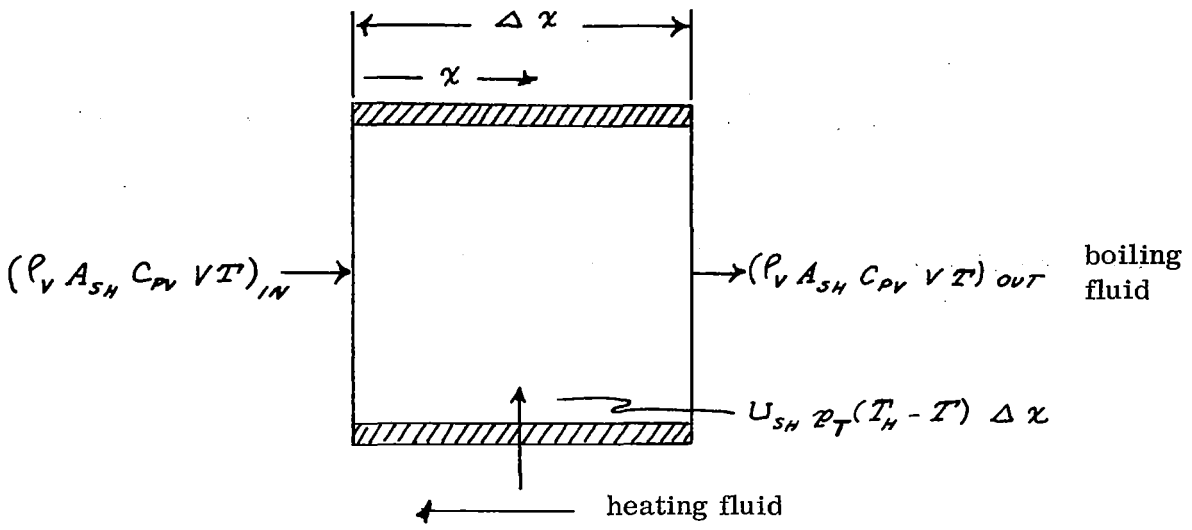


Taking an energy balance on a differential element of the boiling fluid the result is

energy in = energy out + energy stored

$$(\rho_v A_{SH} C_{pv} V_v T)_{IN} + U_{SH} \mathcal{P}_T (T_{H\,IN} - T) \Delta x = (\rho_v A_{SH} C_{pv} V_v T)_{OUT} + \rho_v C_{pv} A_{SH} \Delta x \frac{\partial T}{\partial t}$$

$$\rho_v C_{p,v} A_{SH} \Delta x \frac{\partial T}{\partial x} + \rho_v A_{SH} C_{pv} V_v \left[ T + \frac{\partial T}{\partial x} \frac{\Delta x}{2} \right] = \rho_v A_{SH} C_{pv} V_v \left[ T - \frac{\partial T}{\partial x} \frac{\Delta x}{2} \right] + U_{SH} \mathcal{P}_T [T_{H\,IN} - T] \Delta x$$

$$\frac{\partial T}{\partial t} + V_v \frac{\partial T}{\partial x} = \theta_{SH} (T_{HIN} - T) \tag{101}$$

where

$$\theta_{SH} = \frac{U_{SH} \mathcal{P}_T}{\rho_v C_{pv} A_{SH}} \quad (U_{SH} \text{ is a variable}) \tag{102}$$

Linearizing for small perturbations around a steady point and transforming the perturbed variables, the result is

$$s\hat{T} + V_{v,0} \frac{\partial \hat{T}}{\partial x} + \hat{V}_v \frac{\partial T_0}{\partial x} = \hat{\theta}_{SH} (T_{HIN} - T_0) - \theta_{SH,0} \hat{T} \tag{103}$$

Steady-State Equation

$$V_{v,0} \frac{\partial T_0}{\partial x} = \theta_{SH,0} (T_{HIN} - T_0)$$

Steady-State Solution

$$T_0 = T_{HIN} - (T_{HIN} - T_{SAT,0}) e^{-\frac{\theta_{SH,0}}{V_{v,0}} x} \tag{104}$$

$$\frac{\partial T_0}{\partial x} = \frac{\theta_{SH,0}}{V_{v,0}} (T_{HIN} - T_{SAT,0}) e^{-\frac{\theta_{SH,0}}{V_{v,0}} x} \tag{105}$$

On the basis of the third basic assumption

$$\theta_{SH} = c V_v^{n_{SH}}$$

or

$$\hat{\theta}_{SH} = \frac{\theta_{SH,0}}{V_{v,0}} n_{SH} \hat{V}_v \tag{106}$$

Combining Equations (103) and (106) and rearranging the result is

$$\frac{\partial \hat{T}}{\partial x} + \frac{(s + \theta_{SH,0})}{V_{v,0}} \hat{T} = -(1 - n_{SH}) \frac{\theta_{SH,0}}{V_{v,0}^2} (T_{HIN} - T_{SAT,0}) e^{-\frac{\theta_{SH,0}}{V_{v,0}} x} (\hat{V}_v) \tag{107}$$

The general solution to Equation (107) is

$$\hat{T} = e^{-\left(\frac{s + \theta_{SH,0}}{V_{v,0}}\right)x} \left[ \int -(1-n_{SH}) \frac{\theta_{SH,0}}{V_{v,0}^2} (T_{HIN} - T_{SAT,0}) e^{\frac{s}{V_{v,0}} x} \hat{V}_v \, dx + c \right]$$

which upon integration becomes

$$\hat{T} = e^{-\left(\frac{s + \theta_{SH,0}}{V_{v,0}}\right)x} \left[ -(1-n_{SH}) \frac{\theta_{SH,0}}{s V_{v,0}} (T_{HIN} - T_{SAT,0}) e^{\frac{s}{V_{v,0}} x} \hat{V}_v + c \right] \tag{108}$$

Applying the boundary condition which accounts for perturbations of saturation temperature and the boiling length

$$\hat{T} = \left(\frac{\partial T_{SAT}}{\partial P}\right) \hat{P}_{OUT} - \left(\frac{\partial T_0}{\partial x}\right)_{x=0} \hat{L} \tag{109}$$

at $x = 0$

and introducing Equation (105), Equation (108) becomes

$$\hat{T} = -(1-\eta_{SH})\,\Theta_{SH,0}\,(T_{HIN}-T_{SAT,0})\,e^{-\frac{\Theta_{SH,0}}{V_{V,0}}x}\,\frac{\left(1-e^{-\frac{s}{V_{V,0}}x}\right)}{s}\,\frac{\hat{V}_V}{V_{V,0}} +$$

$$\left(\frac{\partial T_{SAT}}{\partial P}\right)e^{-\left(\frac{s+\Theta_{SH,0}}{V_{V,0}}\right)x}\hat{P}_{OUT} - \frac{\Theta_{SH,0}}{V_{V,0}}(T_{HIN}-T_{SAT,0})\,e^{-\left(\frac{s+\Theta_{SH,0}}{V_{V,0}}\right)x}\hat{L}_B \qquad (110)$$

let $$\tau_{SH} = \frac{(L_{SH,0}-L_{B,0})}{V_{V,0}} \qquad (111)$$

From continuity considerations

$$\frac{\hat{V}_V}{V_{V,0}} = \frac{\hat{W}_{OUT}}{W_0} \qquad (112)$$

At the boiler exit x = ($L_{SH,0}$ - $L_{B,0}$). Introducing Equations (111) and (112) and evaluating Equation (110) at the boiler exit the result is

$$\hat{T}_{OUT} = -(1-\eta_{SH})(\Theta_{SH,0}\,\tau_{SH})(T_{HIN}-T_{SAT,0})\,e^{-\Theta_{SH,0}\tau_{SH}}\,\frac{(1-e^{-s\tau_{SH}})}{s\,\tau_{SH}}\,\frac{\hat{W}_{OUT}}{W_0}$$

$$+\left(\frac{\partial T_{SAT}}{\partial P}\right)e^{-(s+\Theta_{SH,0})\tau_{SH}}\hat{P}_{OUT} - \Theta_{SH,0}\tau_{SH}\,(T_{HIN}-T_{SAT,0})\,e^{-(s+\Theta_{SH,0})\tau_{SH}}\,\frac{\hat{L}_B}{L_{SH,0}-L_{B,0}} \qquad (113)$$

Evaluating Equation (104) at $x = (L_{SH,0} - L_{B,0})$ the result is

$$e^{-\Theta_{SH,0}\,\tau_{SH}} = \frac{\Delta T_{OUT}}{T_{HIN} - T_{SAT,0_{OUT}}} \equiv \phi_4 \tag{114}$$

where $$\Delta T_{OUT} = T_{HIN} - T_{OUT,0} \tag{115}$$

defining

$$\beta_2 \equiv \frac{\partial\left(\frac{T_{SAT}}{\Delta T_{OUT}}\right)}{\partial\left(\frac{P}{P_{OUT,0}}\right)} \tag{116}$$

$$\phi_5 \equiv \frac{\Delta T_{OUT}}{2\,T_{OUT,0}} \tag{117}$$

Combining Equations (113), (114), (116) and (117)

$$\frac{\hat{T}_{OUT}}{2T_{OUT,0}} = (1-\eta_{SH})\,\phi_5 \ln\phi_4 \left(\frac{1-e^{-s\tau_{SH}}}{s\tau_{SH}}\right) \frac{\hat{W}_{OUT}}{W_0} +$$

$$\beta_2\,\phi_4\,\phi_5\,e^{-s\tau_{SH}}\,\frac{\hat{P}_{OUT}}{P_{OUT,0}} + \phi_5 \ln\phi_4\, e^{-s\tau_{SH}}\,\frac{\hat{L}_B}{L_{SH,0} - L_{B,0}} \tag{118}$$

Combining Equations (82) and (94) the result is

$$\left[1 - \frac{\gamma_5 \phi_3}{2} e^{-s\tau_B}\right] \frac{\hat{L}_B}{(L_{B,0} - L_{SC,0})} = \frac{\hat{W}_{OUT}}{W_0} e^{-\frac{s\tau_B}{2}} + \left(\frac{\tau_{HSC}}{\tau_{HB}}\right) e^{-s\tau_B} \frac{\hat{L}_{SC}}{L_{SC,0}}$$

$$+ \phi_3 \left[\beta_1 - \frac{\gamma_4}{2}\right] e^{-s\tau_B} \frac{\hat{P}_P}{P_{P,0}} \qquad (119)$$

Combining Equations (118) and (119) and noting that

$$\left[\frac{L_{B,0} - L_{SC,0}}{L_{SH,0} - L_{B,0}}\right] = \frac{\tau_{HB}}{\tau_{HSH}}$$

the result is

$$\frac{\hat{T}_{OUT}}{2T_{OUT,0}} = (D) \frac{\hat{P}_P}{P_{P,0}} + (E) \frac{\hat{W}_{OUT}}{W_0} + (F) \frac{\hat{P}_{OUT}}{P_{OUT,0}} + (G) \frac{\hat{L}_{SC}}{L_{SC,0}} \qquad (120)$$

where

$$(D) = \frac{\phi_3 \phi_5 \ln \phi_4 \left(\frac{\tau_{HB}}{\tau_{HSH}}\right)\left[\beta_1 - \frac{\gamma_4}{2}\right] e^{-s(\tau_{SH} + \tau_B)}}{\left[1 - \frac{\gamma_5 \phi_3}{2} e^{-s\tau_B}\right]} \qquad (121)$$

$$\textcircled{E} = \phi_5 \ln \phi_4 \left[ (1 - m_{SH}) \left( \frac{1 - e^{-s\tau_{SH}}}{s\tau_{SH}} \right) + \frac{\left( \frac{\tau_{HB}}{\tau_{HSH}} \right) e^{-s\left( \tau_{SH} + \frac{\tau_B}{2} \right)}}{\left( 1 - \frac{\gamma_5 \phi_3}{2} e^{-s\tau_B} \right)} \right] \tag{122}$$

$$\textcircled{F} = \beta_2 \phi_4 \phi_5 e^{-s\tilde{\tau}_{SH}} \tag{123}$$

$$\textcircled{G} = \frac{\phi_5 \ln \phi_4 \left( \frac{\tilde{\tau}_{HSC}}{\tilde{\tau}_{HSH}} \right) e^{-s(\tilde{\tau}_{SH} + \tilde{\tau}_B)}}{\left[ 1 - \frac{\gamma_5 \phi_3}{2} e^{-s\tilde{\tau}_B} \right]} \tag{124}$$

Transfer Function Between Boiling-Fluid Exit Pressure and Boiling-Fluid Inlet Flow Rate

Equations (33), (35), (37) and (97) are now combined to obtain a normalized transfer function between boiler exit pressure and boiler-inlet flow rate in terms including the transfer function between boiler exit temperature and boiler-inlet flow rate. Consequently, this latter transfer function may be eliminated when it is not significant or it may be evaluated from experimental data or an analytical expression derived below when it is significant.

Combining Equations (33), (37) and (97)

$$\left[1-\textcircled{B}\beta_3\right]\frac{\hat{L}_{sc}}{L_{sc,o}} = \textcircled{A}\frac{\hat{W}_{IN}}{W_o} + \left[\textcircled{B}+\textcircled{C}\right]\frac{\hat{P}_{OUT}}{P_{OUT,o}} - \textcircled{C}\frac{\hat{T}_{OUT}}{2T_{OUT,o}} \tag{125}$$

where

$$\beta_3 \equiv \left[\frac{\partial\left(\Delta P_B/P_{B,o}\right)}{\partial\left(L_{sc}/L_{sc,o}\right)}\right] \tag{126}$$

Combining Equations (33) and (35) the result is

$$\frac{\hat{L}_{sc}}{L_{sc,o}} = \frac{\frac{\hat{W}_{IN}}{W_o} - (1-\tau_v S)\frac{\hat{P}_{OUT}}{P_{OUT,o}} + \frac{\hat{T}_{OUT}}{2T_{OUT,o}}}{K\tau_{sc}S} \tag{127}$$

Combining Equations (125) and (127) the result is

$$\frac{\hat{P}_{OUT}/P_{OUT,o}}{\hat{W}_{IN}/W_o} = \frac{\left[1-\beta_3\textcircled{B}\right]\left[1+\frac{\hat{T}_{OUT}/2T_{OUT,o}}{\hat{W}_{IN}/W_o}\right] - SK\tau_{sc}\left[\textcircled{A}-\textcircled{C}\frac{\hat{T}_{OUT}/2T_{OUT,o}}{\hat{W}_{IN}/W_o}\right]}{\left[1+\tau_v S\right]\left[1-\beta_3\textcircled{B}\right]+SK\tau_{sc}\left[\textcircled{B}+\textcircled{C}\right]} \tag{128}$$

Normalizing at zero frequency (i.e., at S = 0)

$$\left(\frac{\hat{P}_{OUT}}{\hat{W}_{IN}}\right)_{NORMALIZED} = \frac{\left(\frac{\hat{P}_{OUT}}{\hat{W}_{IN}}\right)(S)}{\left(\frac{\hat{P}_{OUT}}{W_{IN}}\right)_{(S=0)}} = \frac{\left(\hat{P}_{OUT}/\hat{W}_{IN}\right)}{\frac{P_{OUT,0}}{W_0}\left[1+\left(\frac{\hat{T}_{OUT}/2T_{OUT,0}}{\hat{W}_{IN}/W_0}\right)_{S=0}\right]} \tag{129}$$

Combining Equations (128) and (129) the result is

$$\left(\frac{\hat{P}_{OUT}}{\hat{W}_{IN}}\right)_{NORMALIZED} = \frac{\left[1-\beta_3\,(B)\right]\left[1+\frac{\hat{T}_{OUT}/2T_{OUT,0}}{\hat{W}_{IN}/W_0}\right]-SK\tau_{sc}\left[(A)-(C)\frac{\hat{T}_{OUT}/2T_{OUT,0}}{\hat{W}_{IN}/W_0}\right]}{\left[1+\left(\frac{\hat{T}_{OUT}/2T_{OUT,0}}{\hat{W}_{IN}/W_0}\right)_{S=0}\right]\left[\left(1+\tau_v S\right)\left(1-\beta_3\,(B)+SK\tau_{sc}\left((B)+(C)\right)\right)\right]} \tag{130}$$

Transfer Function Between Boiling-Fluid Outlet Temperature and Boiling-Fluid Inlet Flow Rate

In this section Equations (33), (35), (37), (120) and (128) are combined to obtain a theoretical expression for the transfer function between the boiling-fluid outlet temperature and the boiling-fluid inlet flow rate for use with Equation (130).

Combining Equations (37) and (120) the result is

$$\frac{\hat{T}_{OUT}}{2\,T_{OUT,0}} = \gamma_{11}\,\frac{\hat{W}_{OUT}}{W_0} + \gamma_{12}\,\frac{\hat{P}_{OUT}}{P_{OUT,0}} + \gamma_{13}\,\frac{\hat{L}_{sc}}{L_{sc,0}} \qquad (131)$$

where

$$\gamma_{11} \equiv \textcircled{E} \qquad (132)$$

$$\gamma_{12} \equiv \left[\textcircled{D} + \textcircled{F}\right] \qquad (133)$$

$$\gamma_{13} \equiv \left[\beta_3 \textcircled{D} + \textcircled{G}\right] \qquad (134)$$

Combining Equations (131) and (35) the result is

$$\frac{\hat{T}_{OUT}}{2\,T_{OUT,0}} = \left[\gamma_{12} - \frac{\tau_v S}{K\,\tau_{sc} S}\,\gamma_{13}\right]\frac{\hat{P}_{OUT}}{P_{OUT,0}} + \frac{\gamma_{13}}{K\,\tau_{sc} S}\,\frac{\hat{W}_{IN}}{W_0} + \left[\gamma_{11} - \frac{\gamma_{13}}{K\,\tau_{sc} S}\right]\frac{\hat{W}_{OUT}}{W_0} \qquad (135)$$

Combining Equations (135) and (33) the result is

$$\frac{\hat{T}_{OUT}}{2T_{OUT,0}} = \gamma_{21}\frac{\hat{P}_{OUT}}{P_{OUT,0}} - \gamma_{22}\frac{\hat{W}_{IN}}{W_{OUT}} \tag{136}$$

where

$$\gamma_{21} \equiv \frac{\gamma_{13}(1+\tau_v s) - sk\tau_{sc}(\gamma_{11}+\gamma_{12})}{\gamma_{13} - sk\tau_{sc}(1+\gamma_{11})} \tag{137}$$

$$\gamma_{22} \equiv \frac{\gamma_{13}}{\gamma_{13} - sk\tau_{sc}(1+\gamma_{11})} \tag{138}$$

Combining Equations (128) and (136) the result is

$$\frac{\left(\hat{T}_{OUT}/2T_{OUT,0}\right)}{\left(\hat{W}_{IN}/W_0\right)} = \frac{-\gamma_{22} + \dfrac{\gamma_{21}\left[\left(1-\beta_3\textcircled{B}\right) - sk\tau_{sc}\textcircled{A}\right]}{\left[\left(1+\tau_v s\right)\left(1-\beta_3\textcircled{B}\right) + sk\tau_{sc}\left(\textcircled{B}+\textcircled{C}\right)\right]}}{1 - \dfrac{\gamma_{21}\left[\left(1-\beta_3\textcircled{B}\right) + sk\tau_{sc}\textcircled{C}\right]}{\left[\left(1+\tau_v s\right)\left(1-\beta_3\textcircled{B}\right) + sk\tau_{sc}\left(\textcircled{B}+\textcircled{C}\right)\right]}} \tag{139}$$

## APPENDIX 3

### Boiler Parameters

In order to calculate values for the theoretical transfer function derived in Appendix 2, it was necessary to evaluate the 22 parameters listed in Table 12. These parameters were calculated using the steady-state test data described in Section IV of this report. The method of calculating most of the parameters in Table 12 is obvious from their definition. However, the definitions of several of these parameters are not sufficiently explicit that the exact methods of calculating them from the experimental data are apparent without further explanation. This appendix contains two parts. The first part describes the methods of calculating those parameters which require further explanation while the second part presents curves of the parameters as a function of the primary variables.

#### Calculation of Boiler Parameters

In the derivation of the theoretical transfer function the boiler was divided into several sections which were analyzed separately. Inherent in this division is the assumption that a clearly-defined boundary existed between the boiling and superheat regions. Examination of the steady-state test data, described in Section IV of this report, indicated that there was no abrupt transition between saturated boiling conditions and superheating of the vapor. Instead, an intermediate condition existed in which superheating of the vapor and evaporation of the liquid took place simultaneously. The boiling fluid during this transition consisted of a mist containing superheated vapor and droplets of saturated liquid. Therefore it was not possible to discern a clearly-defined boundary between the region where only boiling took place and the region where the fluid was superheated as a dry vapor. For the purposes of calculating the boiler parameters, it was therefore necessary to define an artificial boundary.

The most obvious criterion for defining this boundary would have been to select the point at which the temperature of the boiling fluid departed from the saturation conditions. However, there were not sufficient temperature measurements within the boiler to establish this point with any accuracy. As a consequence, the following procedure was adopted.

Using the internal temperature measurements and local heat balances within the boiler, an estimate was made of the boiling-fluid quality distribution along the length of the boiler. The results were plotted as shown in Figure 49. A straight line was then drawn from the point of zero quality, the pinch point, to the point of 80 percent quality. This line was then extended to 100 percent quality. The point where the straight line reached 100 percent quality was taken

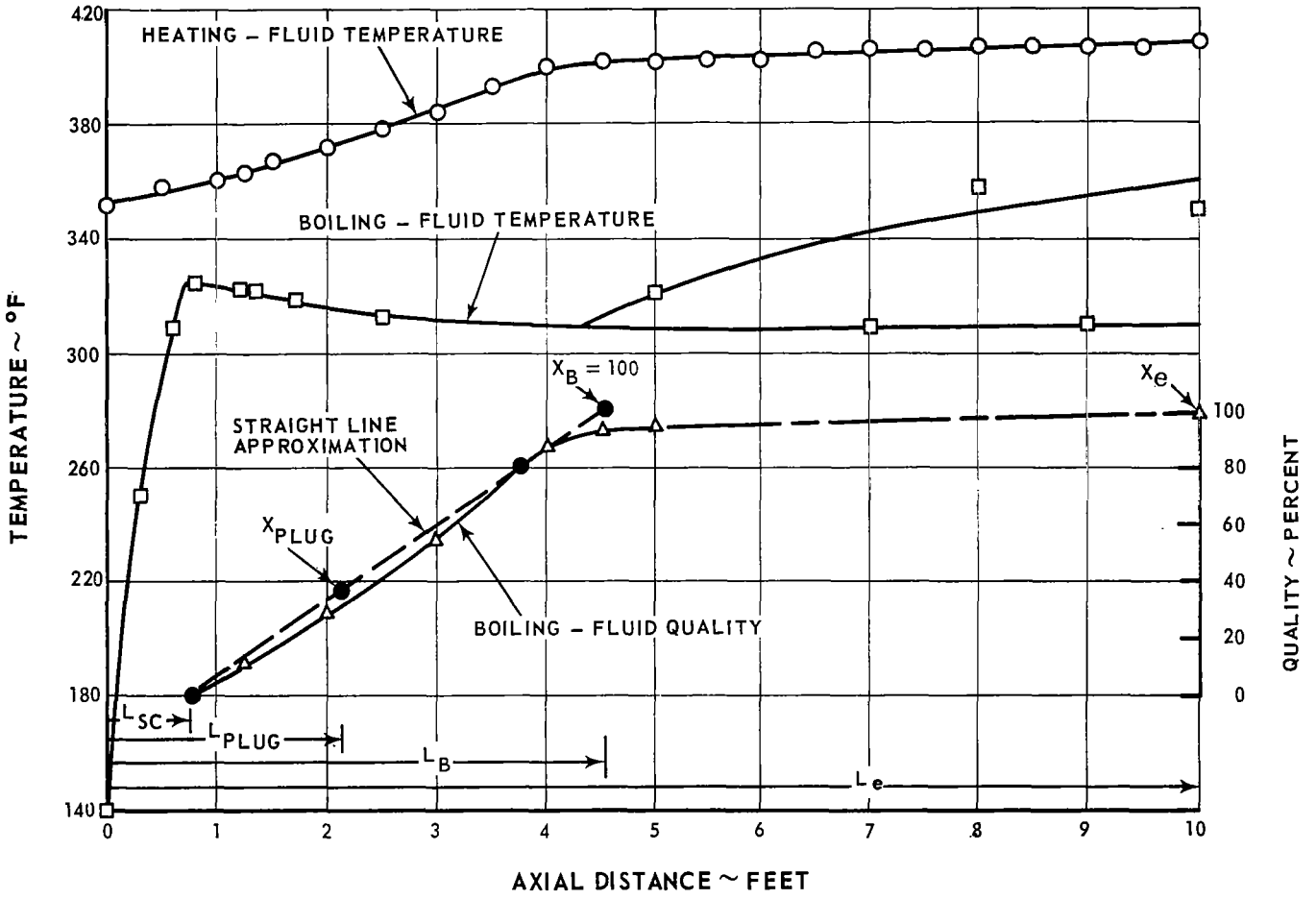


Figure 49 Straight Line Approximation of Boiling-Fluid Quality Distribution at Nominal Operating Conditions

as the boundary between the two regions as shown in Figure 49. The axial distance between the boiling fluid inlet and this point was defined as the boiling length $L_B$. For those cases where the straight line did not reach 100 percent quality before the end of the boiler, no appreciable superheating of the vapor was observed and $L_B$ was taken as equal to the length of the boiler.

Calculation of K

The parameter K is defined by the relation

$$K = \frac{\partial\left(\int_0^{L_e} \rho A \, d\ell\right)}{\partial\left(\rho_L A_{SC} L_{SC}\right)} = \frac{\partial M_{total}}{\partial M_{SC}} \tag{140}$$

which relates the total mass of the boiling fluid in the boiler $M_{total}$ to the mass of boiling fluid in the subcooled region $M_{SC}$.

In evaluating the total mass of the boiling fluid, it was assumed that the mass of the vapor in the boiler was negligible compared to the mass of the liquid. As a consequence, only the subcooled and boiling regions needed to be considered in the integral, and the density of the fluid in the boiling region could be approximated by the relation

$$\rho = R_L \rho_L \tag{141}$$

The term $R_L$ in Equation (141) is the liquid fraction of the two-phase flow. Incorporating the above assumption in the integral to calculate $M_{total}$ the result is

(142)

$$M_{total} = \int_0^{L_e} \rho A \, d\ell = \int_0^{L_{sc}} \rho_L A_{plug} \, d\ell + \int_{L_{sc}}^{L_{plug}} \rho_L R_L A_{plug} \, d\ell + \int_{L_{plug}}^{L_b} \rho_L R_L A_{probe} \, d\ell$$

The terms $A_{plug}$ and $A_{probe}$ refer to the cross-sectional areas of the flow passages on a plane perpendicular to the boiler axis.

In evaluating the second term on the right-hand side of Equation (142) it was assumed that boiling-fluid quality varied linearly with length according to the relation

$$X = \frac{X_B}{L_B - L_{SC}} \left(\ell - L_{SC}\right) \tag{143}$$

Equation (143) describes the straight-line relationship used to define $L_B$. As can be seen in Figure 49 this relation gives a reasonable approximation to the quality variation.

Differentiating Equation (143) and rearranging the result is

$$d\ell = \left(\frac{L_B - L_{SC}}{X_B}\right) dX \tag{144}$$

The liquid fraction $R_L$ was determined using the following relationship which was fitted as an approximation of the liquid fraction data of Martinelli and Nelson, Reference 12.

$$R_L = e^{\alpha X^{1/3}} - e^{\alpha} \tag{145}$$

The parameter $\alpha$ is a function of pressure and is tabulated below

| P, psia | $\alpha$ |
|---|---|
| 14.7 | - 4.78 |
| 60.0 | - 4.21 |
| 200.0 | - 3.51 |

Equations (142), (144) and (145) were combined with the result

$$M_{total} = \int_0^{L_{sc}} \rho_L A_{plug}\, d\ell + \int_{x=0}^{x=x_{plug}} A_{plug}\rho_L \frac{\left(L_B - L_{SC}\right)}{X_B} \left[e^{\alpha X^{1/3}} - e^{\alpha}\right] dX$$

$$+ \int_{x=x_{plug}}^{x=x_B} A_{probe}\rho_L \frac{\left(L_B - L_{SC}\right)}{X_B} \left[e^{\alpha X^{1/3}} - e^{\alpha}\right] dX \qquad (146)$$

The term $X_{plug}$ in the limits of integration is the quality at the end of the plug as determined by the linear approximation (see Figure 49).

Equation (146) was integrated numerically using values of $L_{SC}$, $L_B$, $X_{plug}$ and $X_B$ determined from the steady-state test data. The results were plotted as a function of the mass of the boiling fluid in the subcooled region $M_{SC} = \rho_L A_{plug} L_{SC}$. A single line was drawn through the data as shown in Figure 50. The parameter K was then determined as a function of $M_{SC}$ by taking slopes of the curve in Figure 50. The results are shown in Figure 51. K was then evaluated by determining $M_{SC}$ for each steady-state test point and then reading the value from Figure 51.

## Calculation of $\tau_B$

$\tau_B$ is defined as the time required for a liquid particle to travel the length of the boiling region. It was calculated by means of the integral

$$\tau_b = \int_{L=L_{SC}}^{L=L_B} \frac{d\ell}{V_L} \qquad (147)$$

where $V_L$ is the axial component of the velocity of the liquid phase.

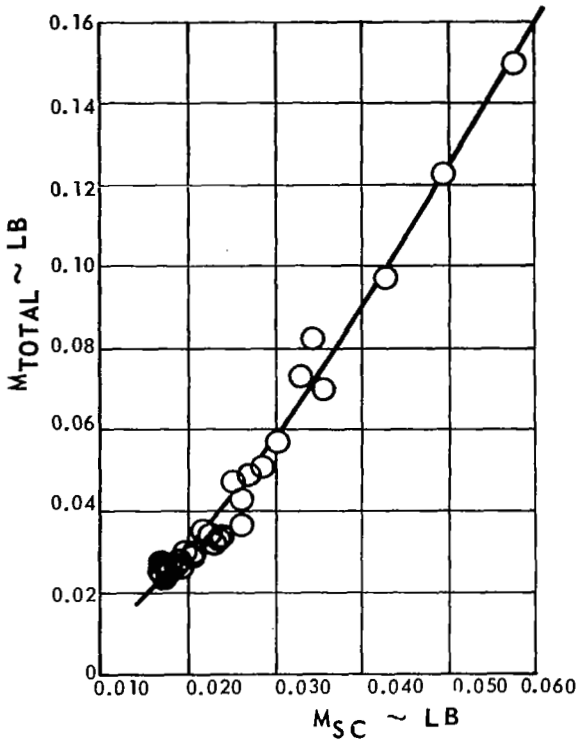


Figure 50 Total Mass of Boiling Fluid $M_{total}$ vs Mass of Boiling Fluid in Subcooled Region $M_{SC}$

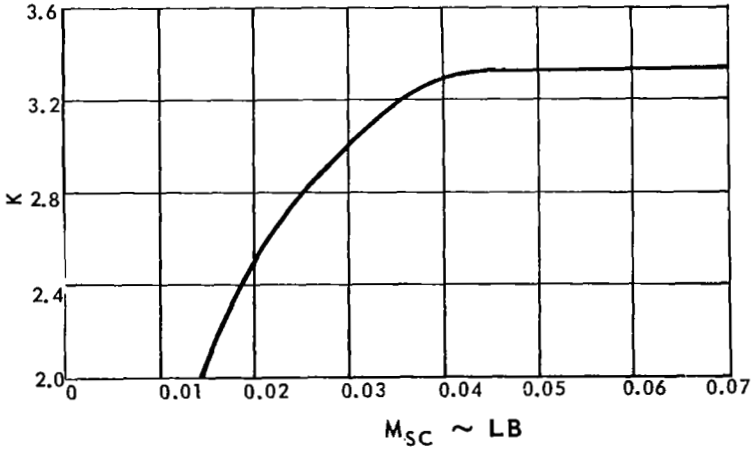


Figure 51 K vs Mass of Boiling Fluid in Subcooled Region $M_{SC}$

From continuity considerations

$$V_L = \frac{W_L}{\rho_L A_L} \tag{148}$$

Introducing the boiling fluid quality $X = (W - W_L)/W$ and the liquid fraction $R_L$ Equation (148) becomes

$$V_L = \frac{\left(1-X\right)W}{\rho_L R_L A} \tag{149}$$

where $A = A_{plug}$; $0 \leq X \leq X_{plug}$

$A = A_{probe}$; $X_{plug} < X \leq X_B$

Combining Equations (144) for the quality distribution and Equation (145) for liquid fraction with Equations (147) and (149), the result is

$$\tau_b = \int_{x=0}^{x=x_{plug}} \frac{\rho_L A_{plug} (L_B - L_{SC})}{W} \frac{}{X_B} \left[\frac{e^{\alpha X^{1/3}} - e^{\alpha}}{1-X}\right] dX$$

$$+ \int_{x=x_{plug}}^{x=x_B} \frac{\rho_L A_{probe} (L_B - L_{SC})}{W} \frac{}{X_B} \left[\frac{e^{\alpha X^{1/3}} - e^{\alpha}}{1-X}\right] dX \tag{150}$$

Equation (150) was integrated numerically using values of $L_{SC}$, $L_B$, $X_{plug}$ and $X_B$ obtained from the steady-state test data.

Calculation of $\beta_3$

The parameter $\beta_3$ is defined by the following equation which relates the change in boiling fluid pressure drop to the change in subcooled length that results when the boiling-fluid flow rate is perturbed

$$\beta_3 = \frac{\partial\left(\frac{\Delta P_B}{P_{P,o}}\right)}{\partial\left(\frac{L_{SC}}{L_{SC,o}}\right)} = \left(\frac{\partial \Delta P_B}{\partial L_{SC}}\right)\left(\frac{L_{SC,o}}{P_{P,o}}\right) \tag{151}$$

In calculating the derivative in Equation (151) $\Delta P_B$ was plotted as a function of $L_{SC}$ for the steady-state test conditions where boiling-fluid flow rate was varied. A single curve was drawn through the data as shown in Figure 52. The derivative was then determined by taking the slope of this curve at various values of $L_{SC}$. The results are shown in Figure 53.

In calculating $\beta_3$ from Equation (151), it was assumed that the boiling fluid pressure at the pinch point $P_{P,o}$ was equal to the boiling-fluid inlet pressure obtained from the steady-state data. The subcooled length $L_{SC}$ was also obtained from the steady-state data while the derivative was obtained as a function of $L_{SC}$ from Figure 53.

Calculation of $n_{SC}$ and $n_{SH}$

The exponent $n_{SC}$ was defined by the equation

$$U_{SC} = cV_{SC}^{n_{SC}} \tag{152}$$

which relates the boiling-fluid velocity in the subcooled region $V_{SC}$ to the overall heat-transfer coefficient of that region $U_{SC}$. From continuity considerations, $V_{SC}$ is proportional to the boiling-fluid flow rate W, with the result that Equation (152) can be re-expressed in the form

$$U_{SC} = C_3 W^{n_{SC}} \tag{153}$$

Taking logarithms of both sides of Equation (153) and rearranging the result is

$$n_{SC} = \frac{\ln U_{SC} - \ln C_3}{\ln W} \tag{154}$$

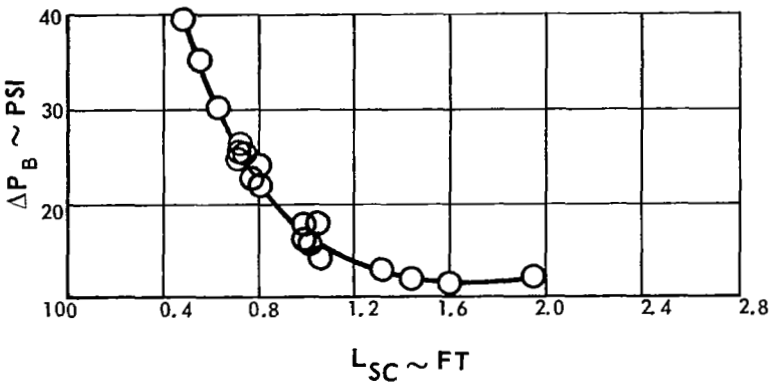


Figure 52 Boiling-Fluid Pressure Drop $\Delta P_B$ vs Subcooled Length $L_{SC}$

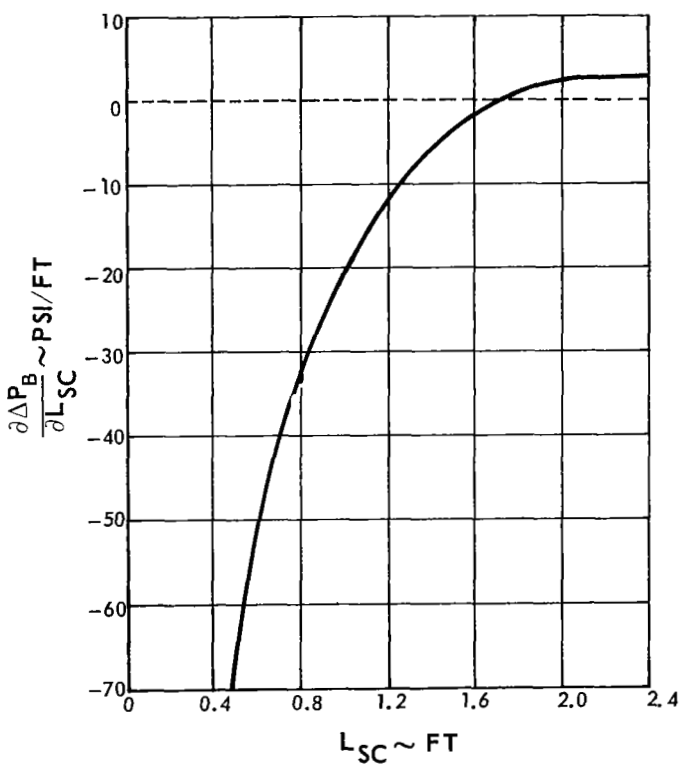


Figure 53 $\frac{\partial \Delta P_B}{\partial L_{SC}}$ vs Subcooled Length $L_{SC}$

which in differential form becomes

$$n_{SC} = \frac{d\,(\ln U_{SC})}{d\,(\ln W)} \tag{155}$$

The overall heat-transfer coefficient was calculated using the equation

$$U_{SC} = \frac{1}{\frac{d_o}{h_{SC}\,d_i} + \frac{t_h\,d_o}{k\,d_m} + \frac{1}{h_{H\,SC}}} \tag{156}$$

where the heat-transfer coefficients of the two fluids were determined using the methods described in Appendix 1.

The heat-transfer coefficient of the boiling fluid $h_{SC}$ was calculated as a function of W using Equations (19), (20) and (21) while the heat-transfer coefficient of the heating fluid $h_{SC}$ was calculated using Equation (18). These values were then employed to calculate $U_{SC}$ from Equation (156). The results were plotted on log-log graph paper as shown in Figure 54. The exponent $n_{SC}$ was then determined on the basis of Equation (155) by taking the slopes of the curves of constant $W_H$ plotted in Figure 54. The results are shown as a function of W and $W_H$ in Figure 55.

The exponent $n_{SH}$ was defined by the relation

$$U_{SH} = cV_{SH}^{n_{SH}} \tag{157}$$

which relates the boiling-fluid velocity in the superheat region to the overall heat-transfer coefficient of that region. The exponent was calculated using the same methods described above for determining $n_{SC}$ except that the data of Reference 10 was employed in place of Equations (20) and (21). The results indicated that for the conditions under study, $n_{SC}$ was independent of W and $W_H$ and equal to a constant value of 0.751.

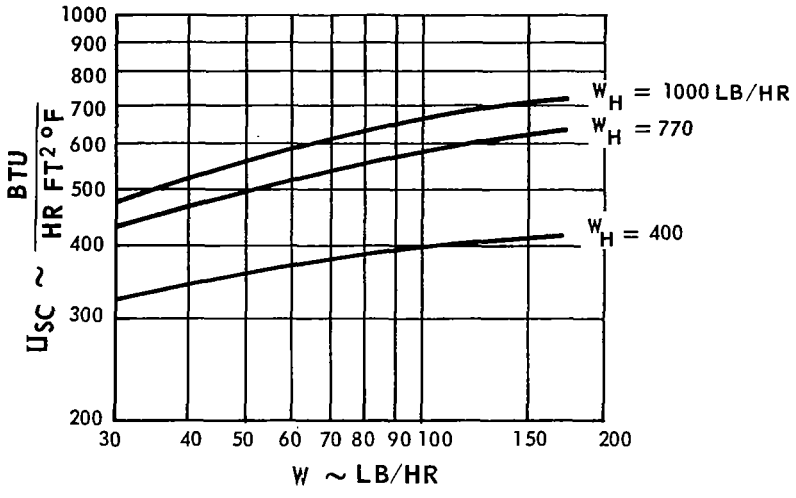


Figure 54 Variation of Overall Heat Transfer Coefficient $U_{SC}$ with Boiling-Fluid Flow Rate and Heating-Fluid Flow Rate

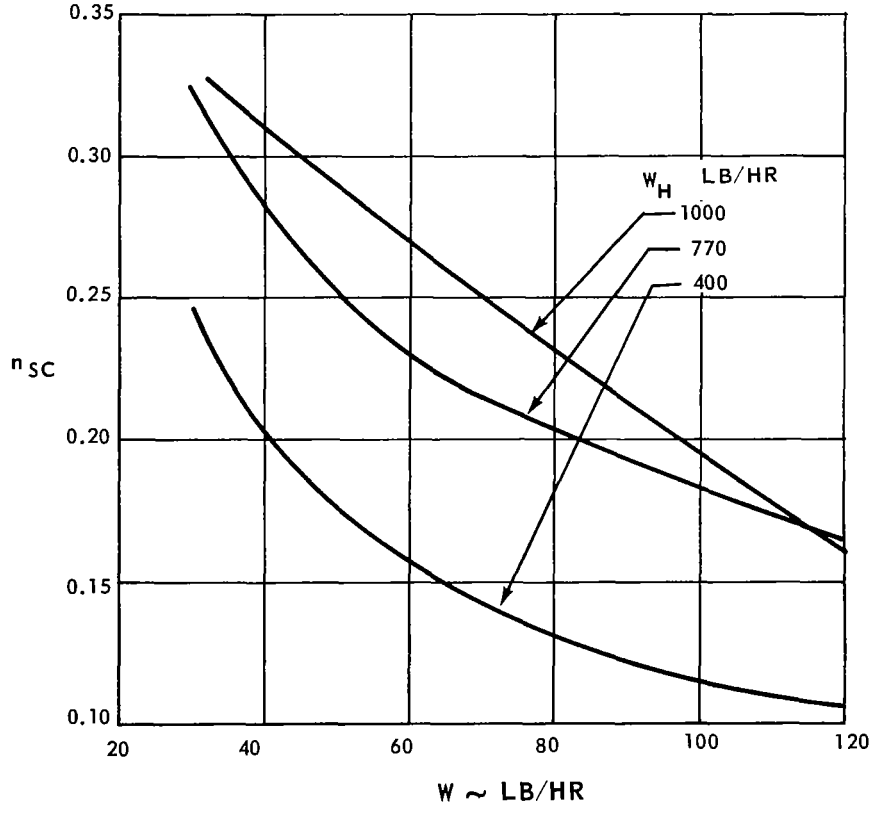


Figure 55 Variation of $n_{SC}$ with Boiling-Fluid Flow Rate and Heating-Fluid Flow Rate

## Curves of the Boiler Parameters

The following pages present curves of the boiler parameters as functions of the primary variables. These parameters were calculated on the basis of the steady-state test results described in Section IV of this report. These curves were employed in the calculation of the theoretical transfer function described in Section VII of the report.

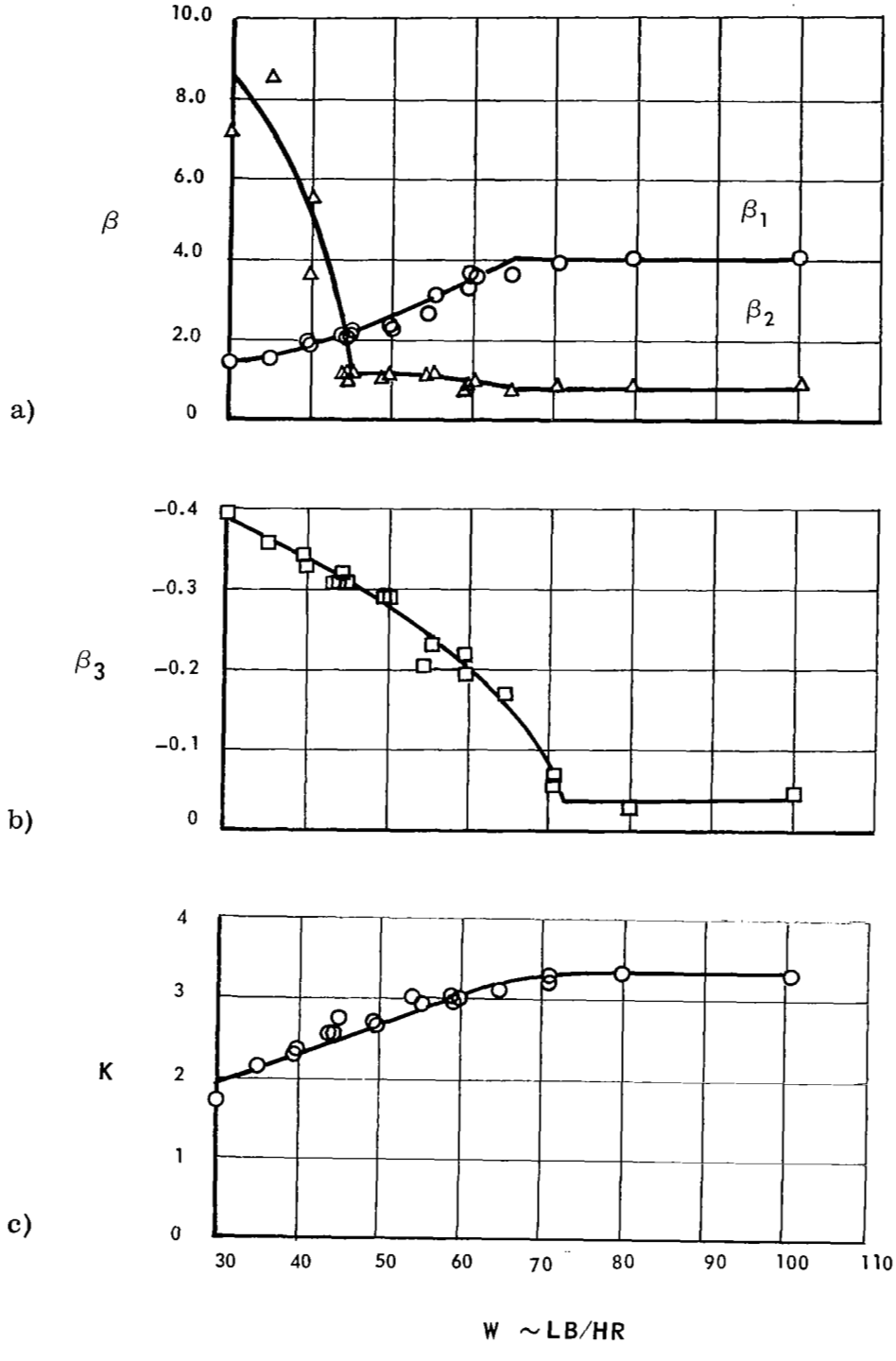


Figure 56 Variation of Boiler Parameters with Boiling-Fluid Flow Rate
$T_{in}$ = 140°F T.S. valve at nominal setting $W_H$ = 770 lb/hr $T_{H\,in}$ = 410°F

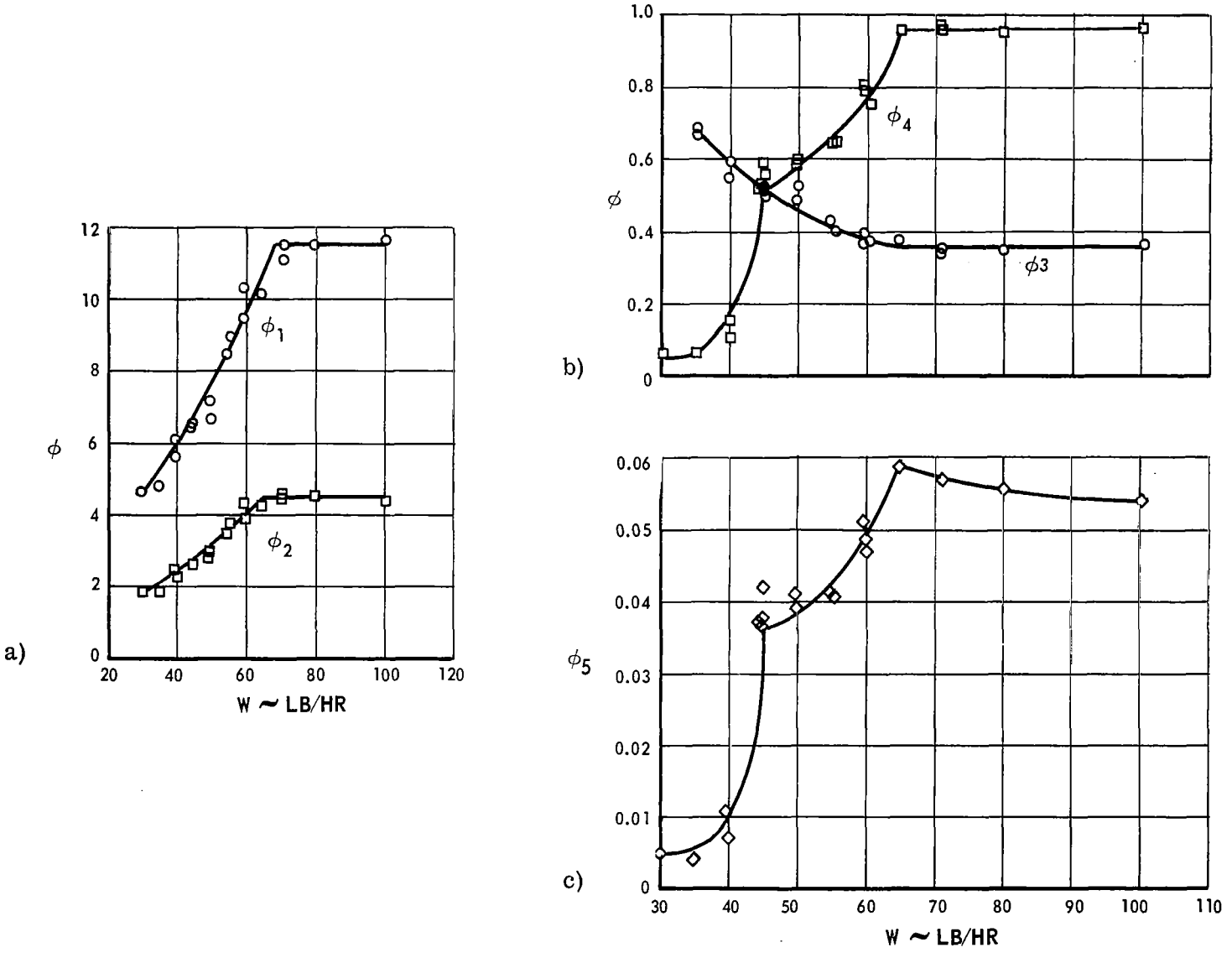


Figure 57 Variation of Boiler Parameters with Boiling-Fluid Flow Rate
$T_{in}$ = 140°F T.S. valve at nominal setting $W_H$ = 770 lb/hr $T_{H\ in}$ = 410°F

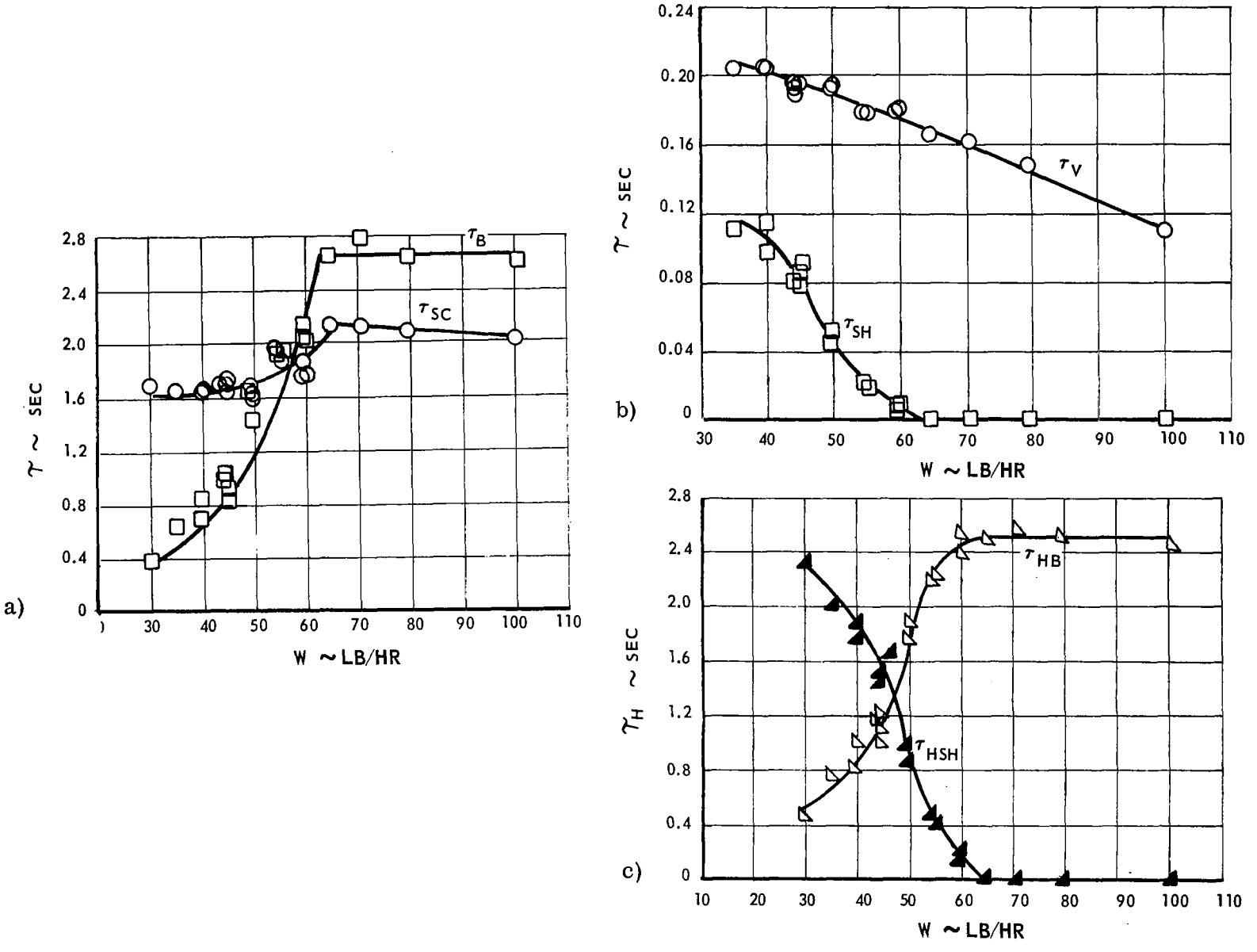


Figure 58 Variation of Boiler Parameters with Boiling-Fluid Flow Rate
$T_{in}$ = 140°F T.S. valve at nominal setting $W_H$ = 770 lb/hr $T_{H\,in}$ = 410°F

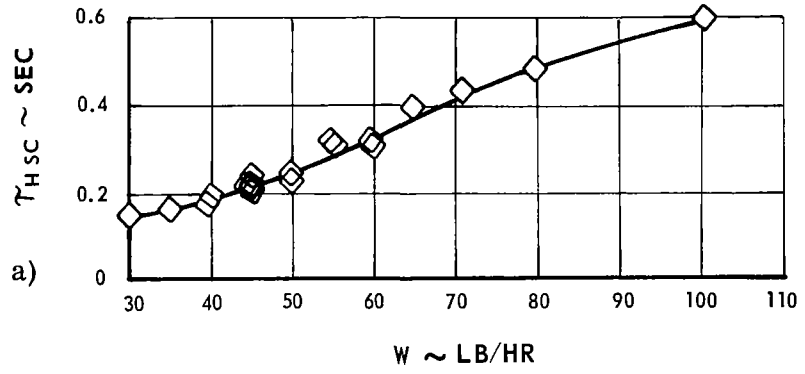


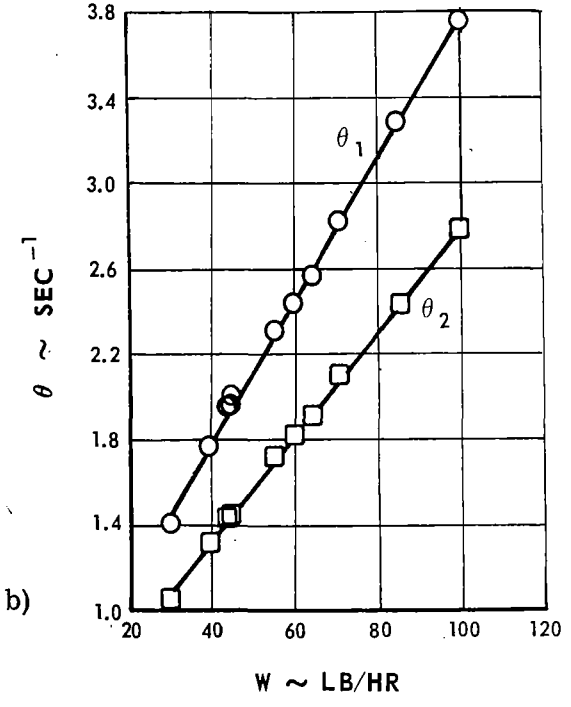


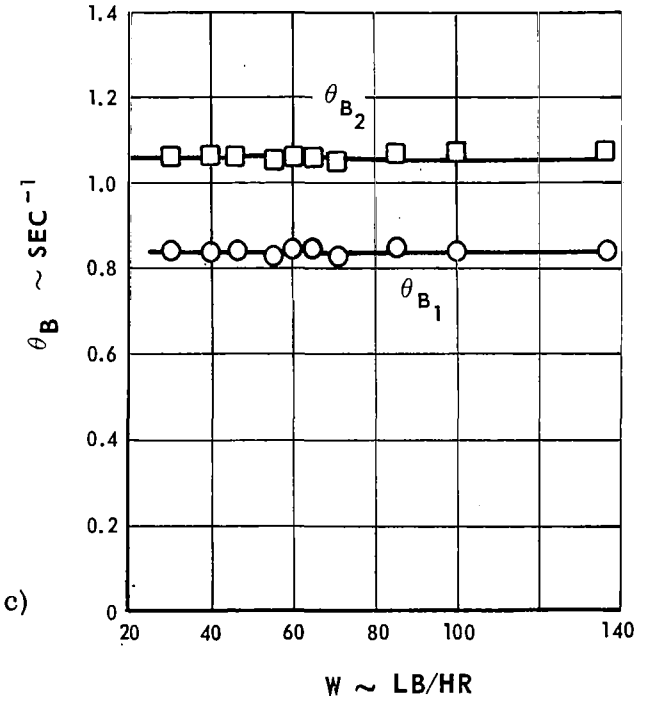


Figure 59 Variation of Boiler Parameters with Boiling-Fluid Flow Rate
$T_{in}$ = 140°F T.S. valve at nominal setting $W_H$ = 770 lb/hr $T_{H\,in}$ = 410°F

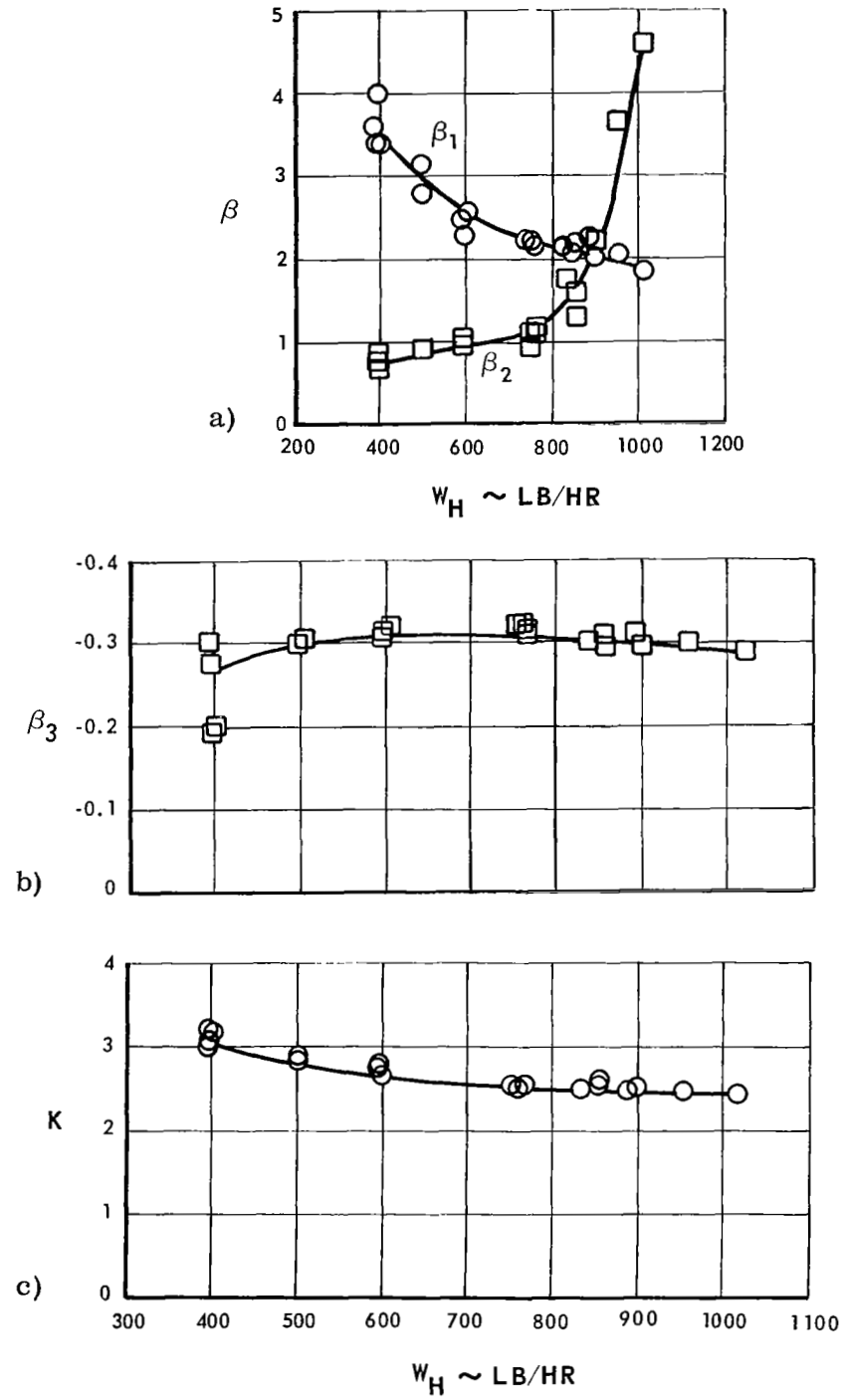


Figure 60 Variation of Boiler Parameters with Heating-Fluid Flow Rate
W = 45 lb/hr $T_{H\,in}$ = 410°F $T_{in}$ = 140°F T.S. valve at nominal setting

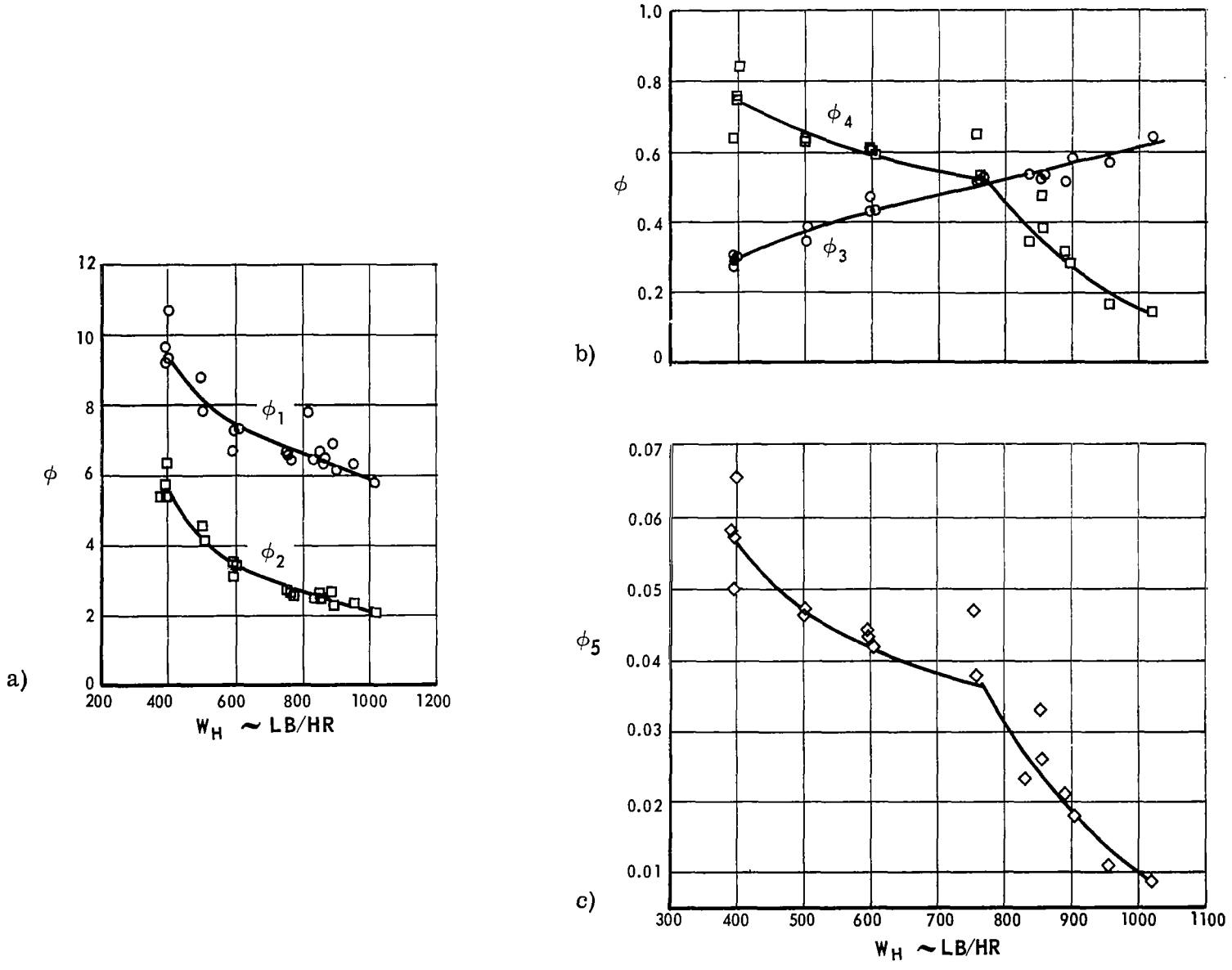


Figure 61 Variation of Boiler Parameters with Heating-Fluid Flow Rate
W = 45lb/hr $T_{H\,in}$ = 410°F $T_{in}$ = 140°F T.S. valve at nominal setting

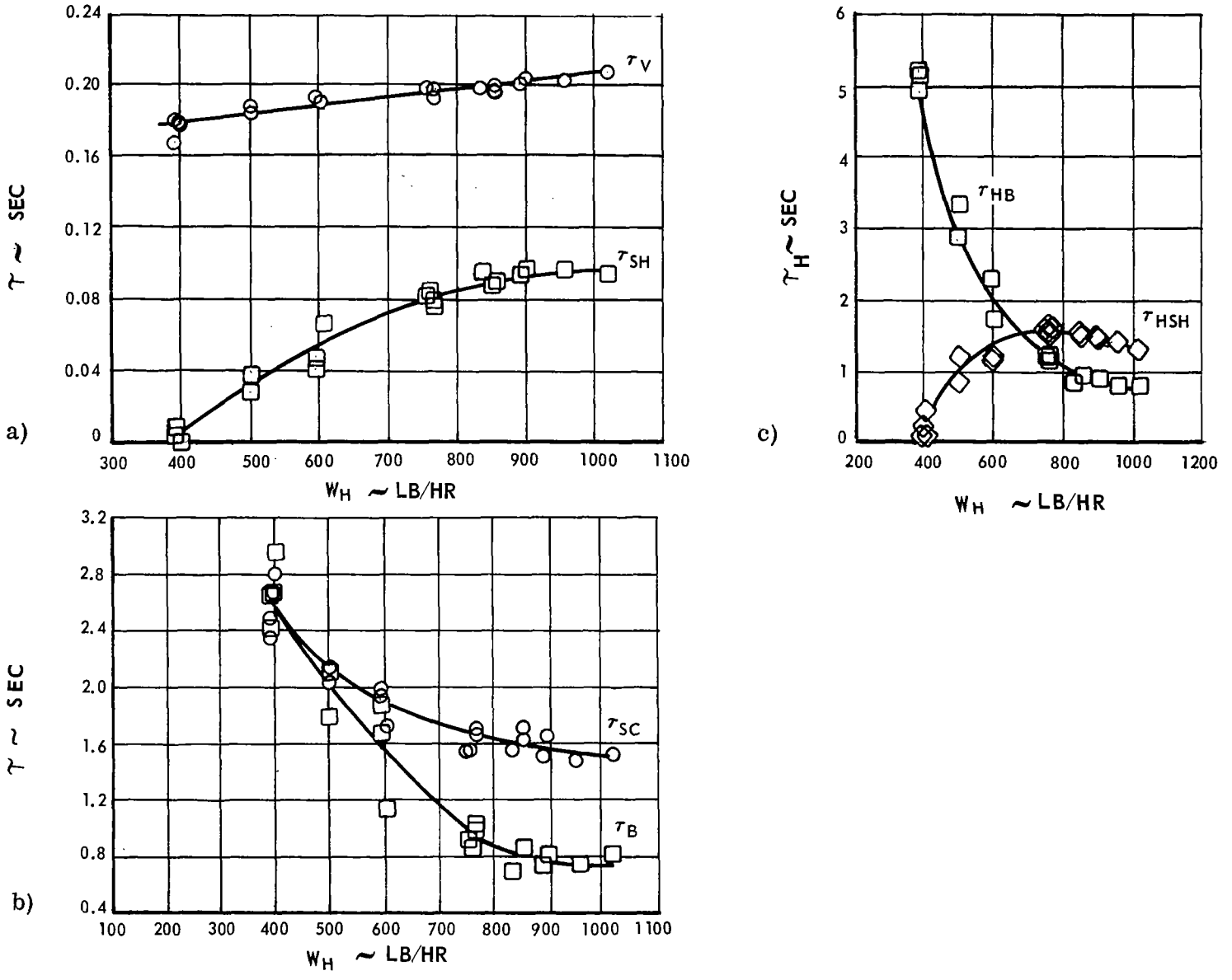


Figure 62 Variation of Boiler Parameters with Heating-Fluid Flow Rate
W = 45 lb/hr $T_{H\,in}$ = 410°F $T_{in}$ = 140°F T.S. valve at nominal setting

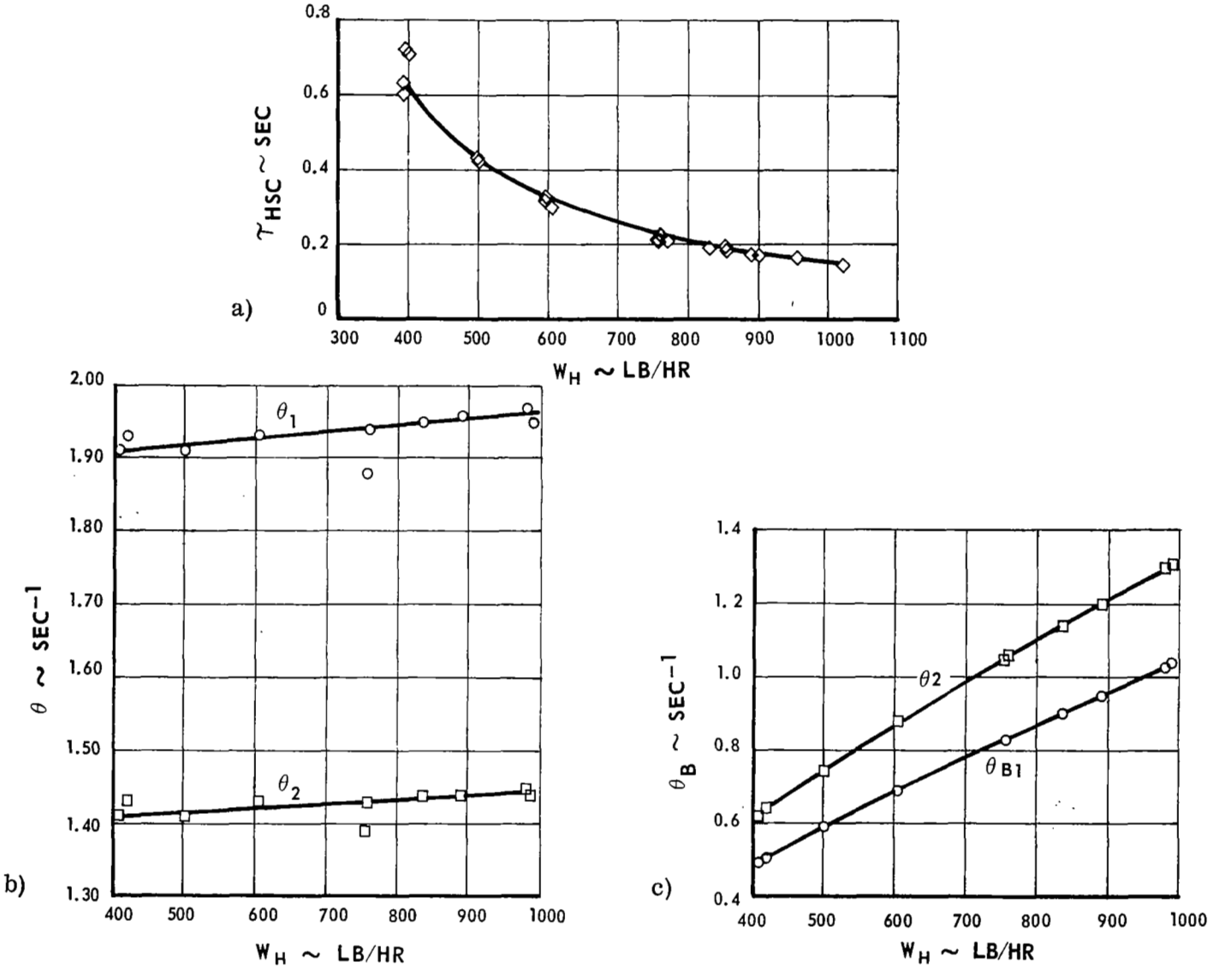


Figure 63 Variation of Boiler Parameters with Heating-Fluid Flow Rate
W = 45 lb/hr $T_{H\,in}$ = 410°F $T_{in}$ = 140°F T.S. valve at nominal setting

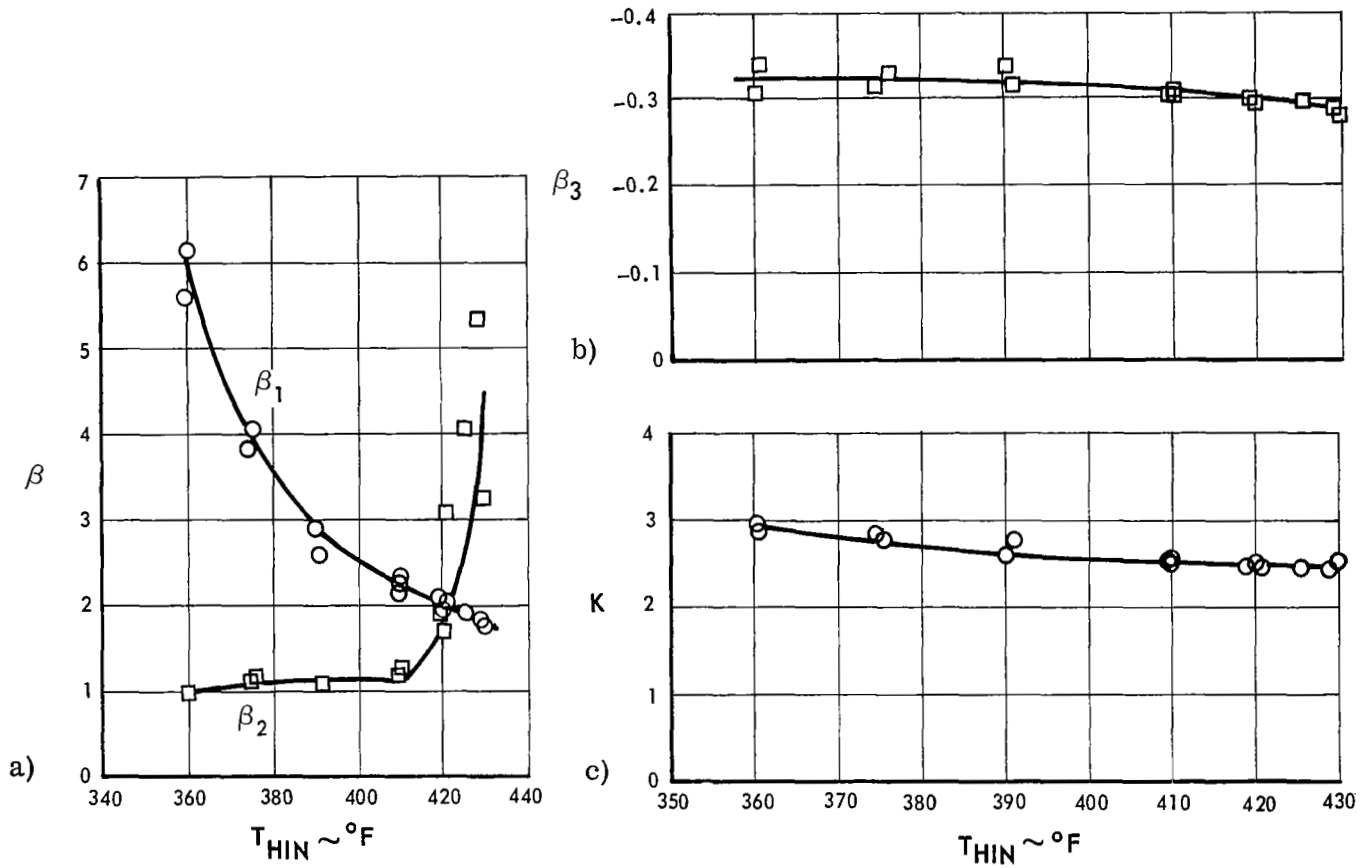


Figure 64 Variation of Boiler Parameters with Heating-Fluid Inlet Temperature
$W_{.}$ = 45 lb/hr $T_{in}$ = 140°F $W_H$ = 770 lb/hr T.S. valve at nominal setting

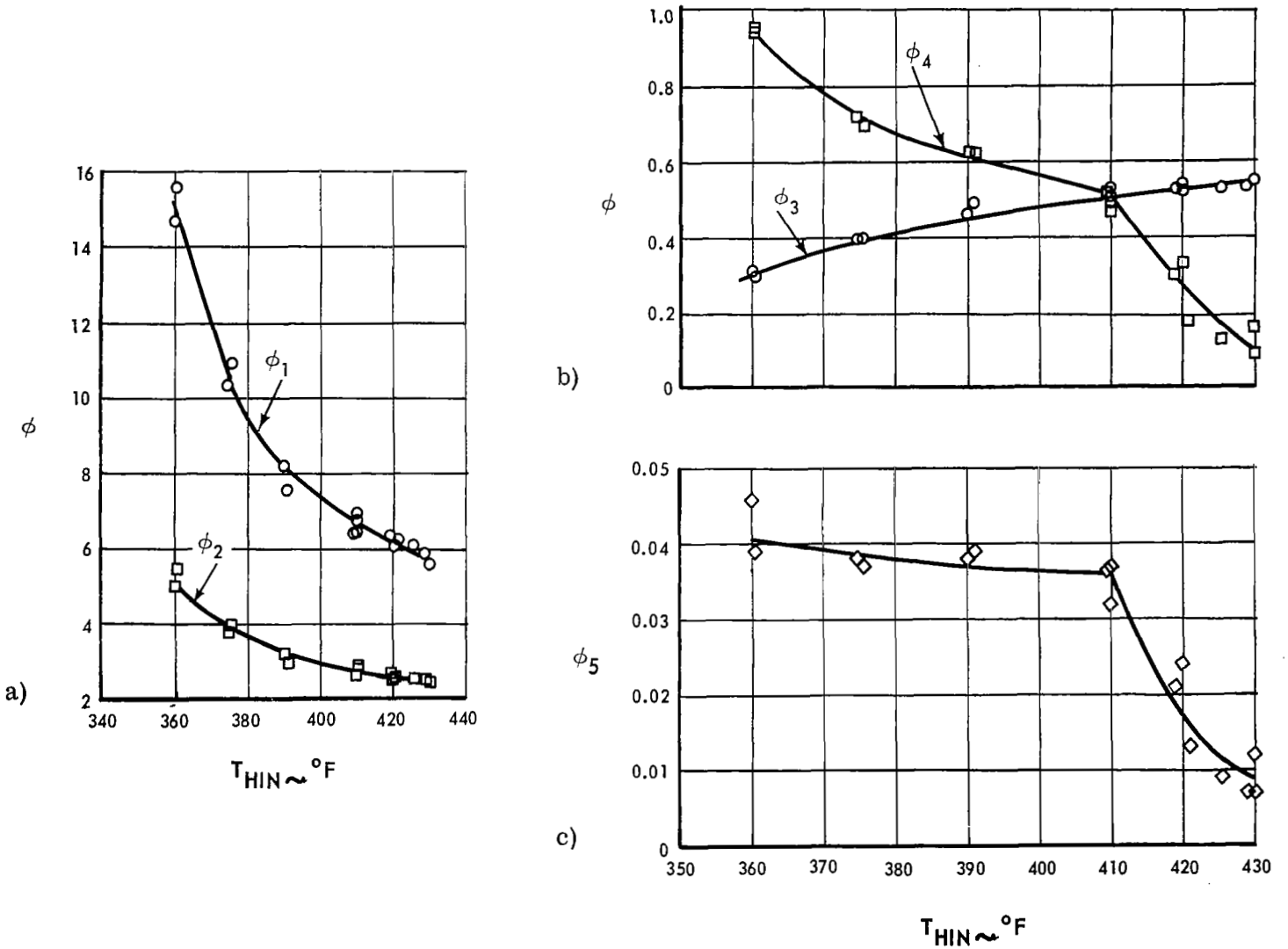


Figure 65 Variation of Boiler Parameters with Heating-Fluid Inlet Temperature
W = 45 lb/hr $T_{in}$ = 140°F $W_H$ = 770 lb/hr T.S. valve at nominal setting.

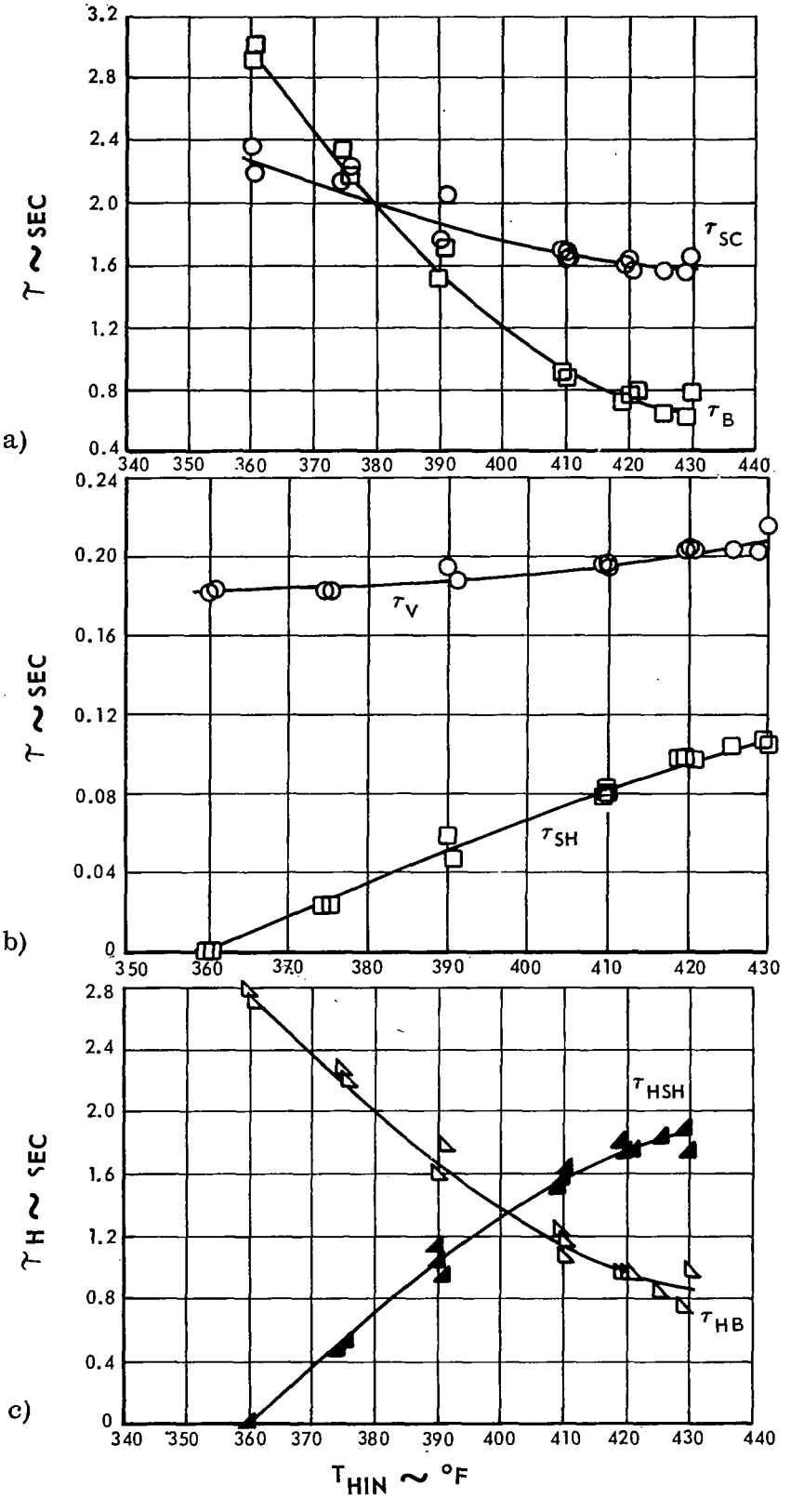


Figure 66 Variation of Boiler Parameters with Heating-Fluid Inlet Temperature
W = 45 lb/hr $T_{in}$ = 140°F $W_H$ = 770 lb/hr T.S. valve at nominal setting

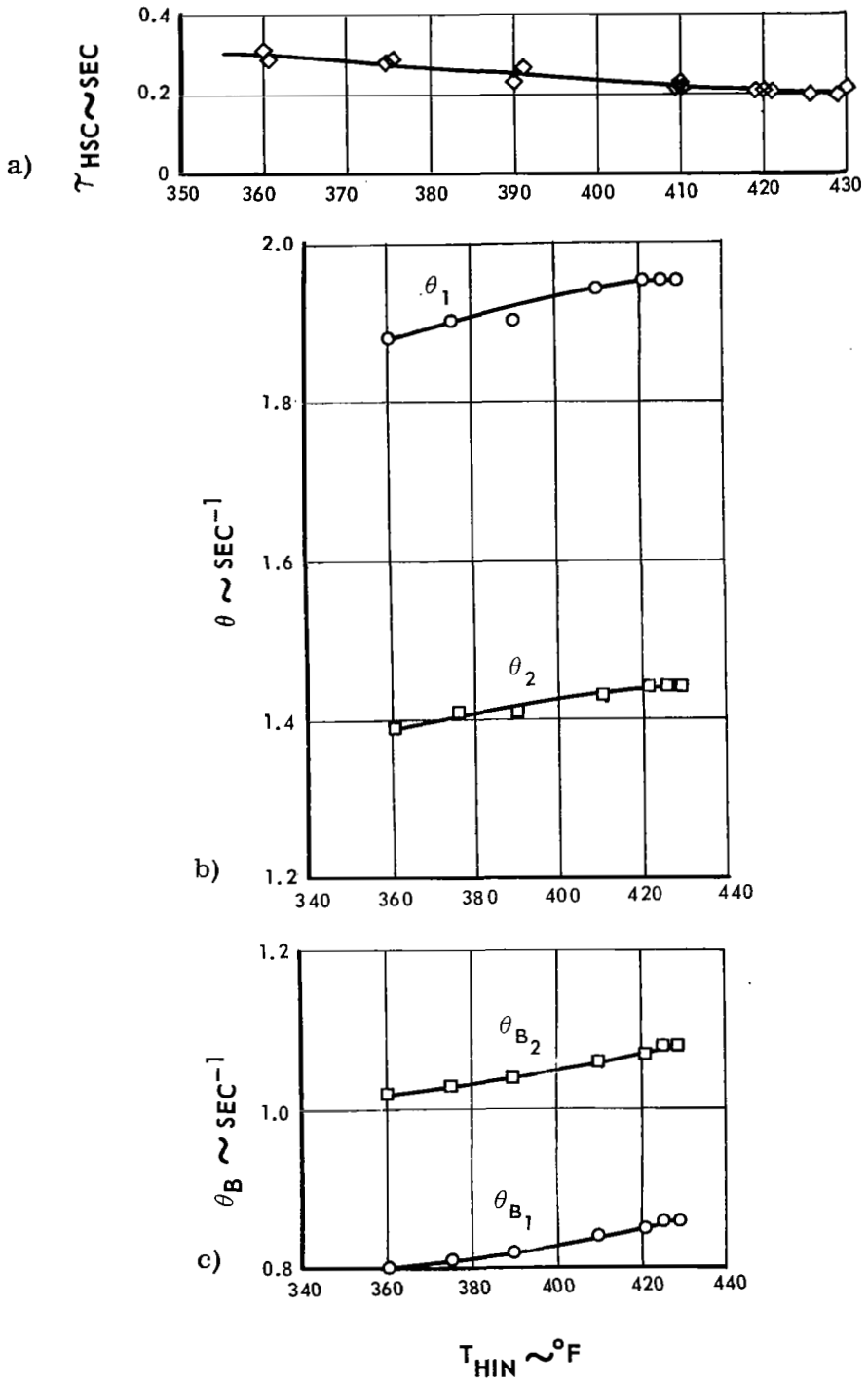


Figure 67 Variation of Boiler Parameters with Heating-Fluid Inlet Temperature
W = 45 lb/hr $T_{in}$ = 140°F $W_H$ = 770 lb/hr T.S. valve at nominal setting

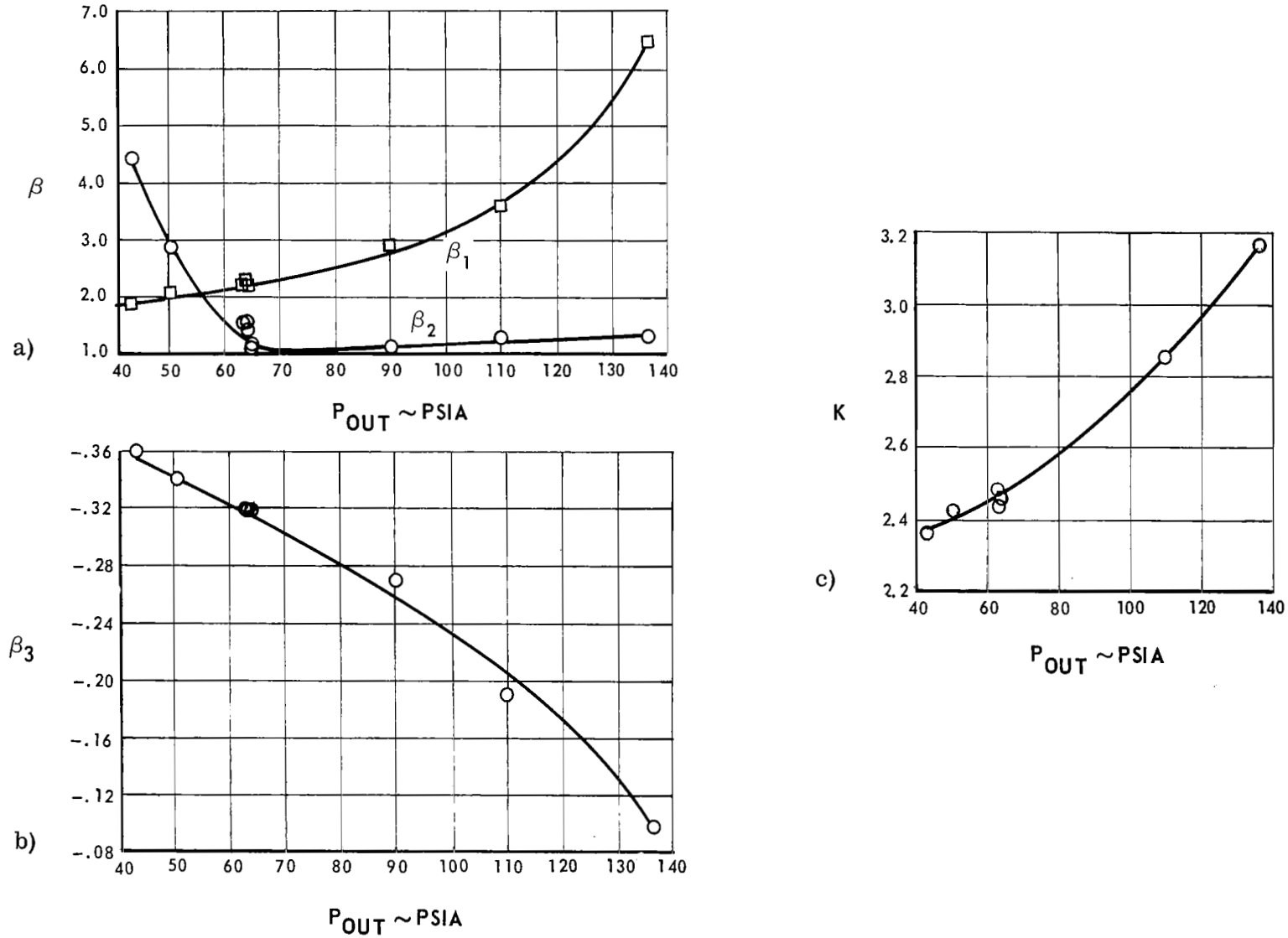


Figure 68 Variation of Boiler Parameters with Boiling-Fluid Exit Pressure
W = 45 lb/hr $T_{in}$ = 140°F $W_H$ = 770 lb/hr $T_{H\,in}$ = 410°F

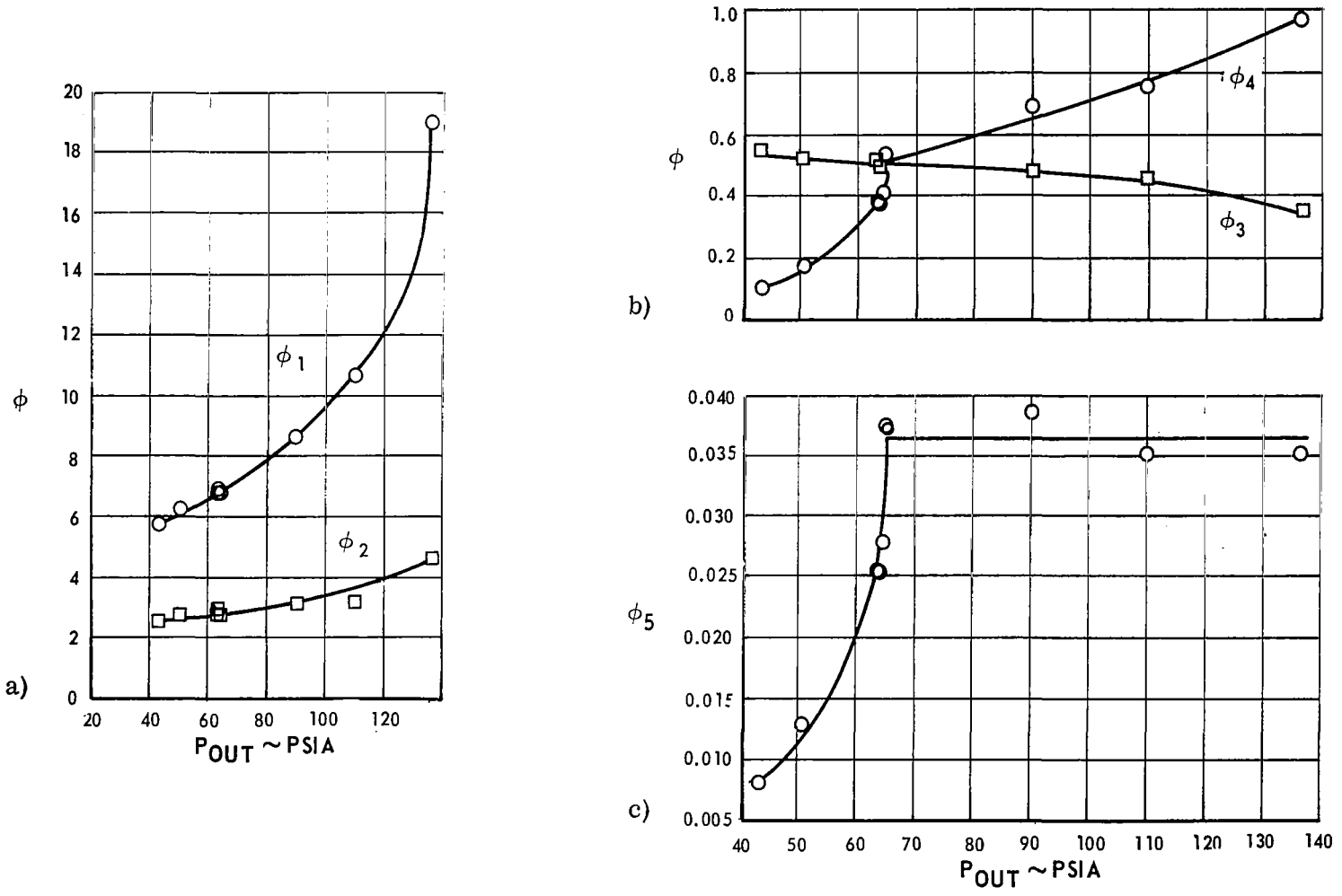


Figure 69 Variation of Boiler Parameters with Boiling-Fluid Exit Pressure
W = 45 lb/hr $T_{in}$ = 140°F $W_H$ = 770 lb/hr $T_{H\,in}$ = 410°F

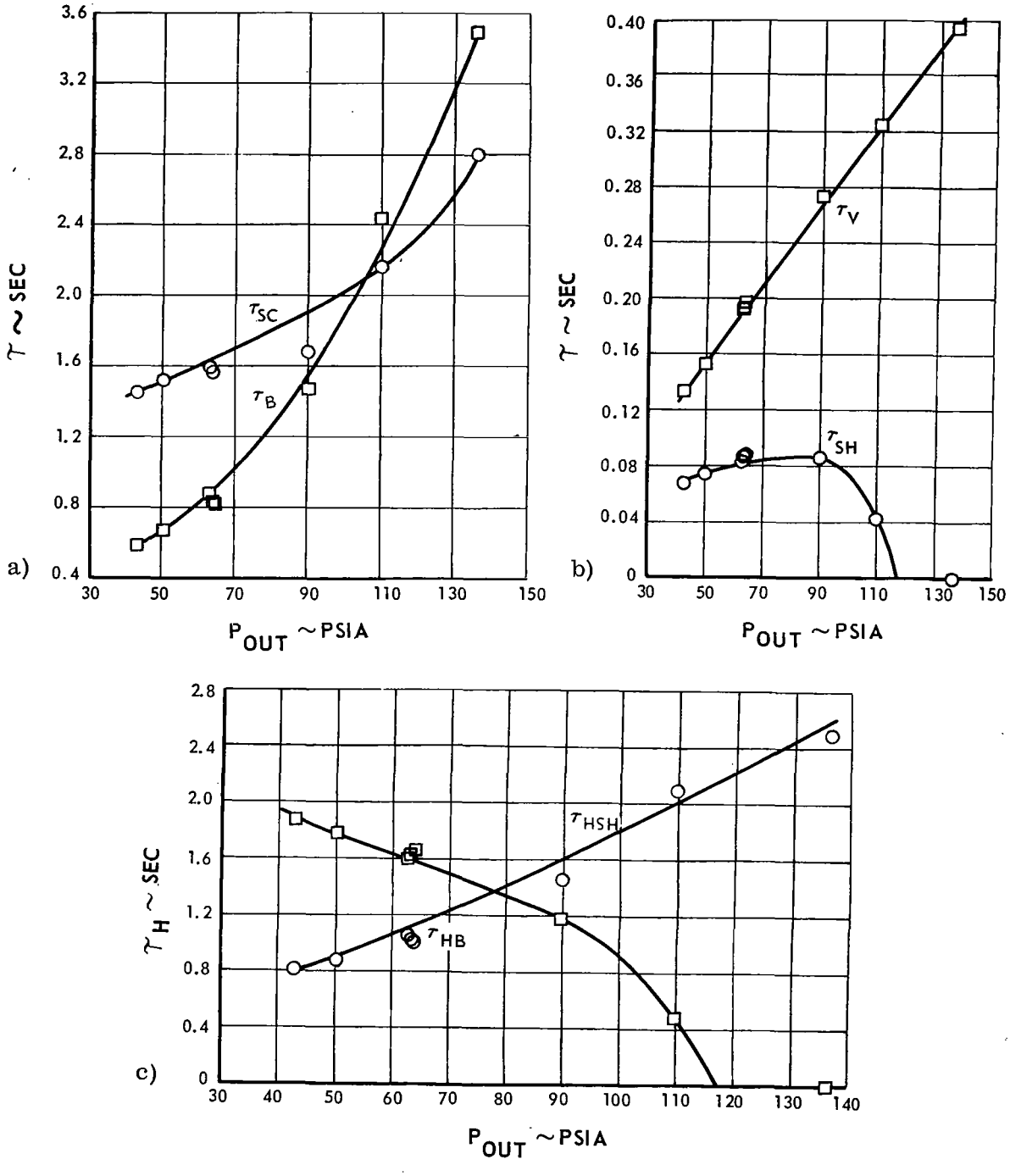


Figure 70 Variation of Boiler Parameters with Boiling-Fluid Exit Pressure
W = 45 lb/hr $T_{in}$ = 140°F $W_H$ =770 lb/hr $T_{H\,in}$= 410°F

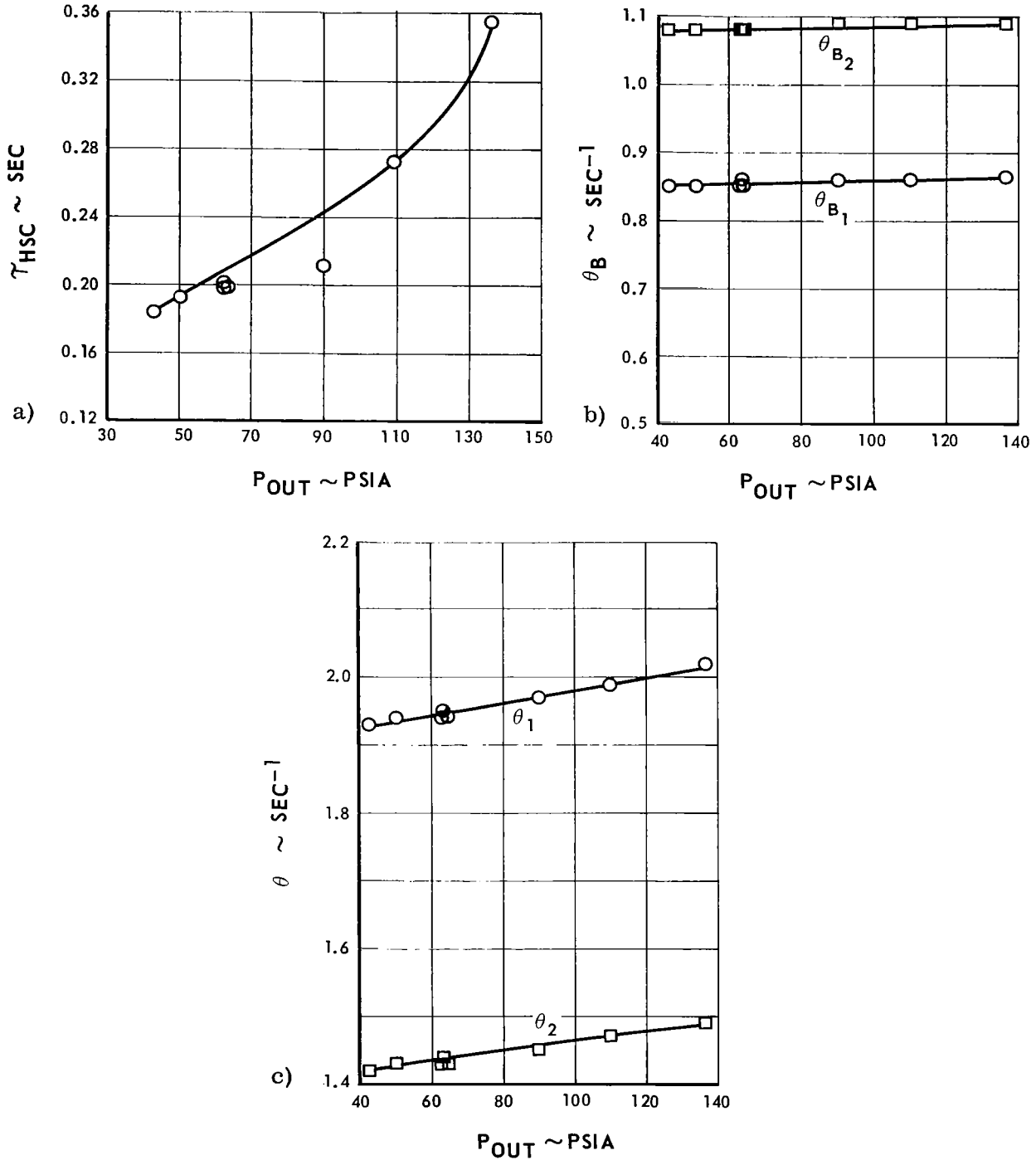


Figure 71 Variation of Boiler Parameters with Boiling-Fluid Exit Pressure
W = 45 lb/hr $T_{in}$ = 140 °F $W_H$ = 770 lb/hr $T_{H\,in}$ = 410°F

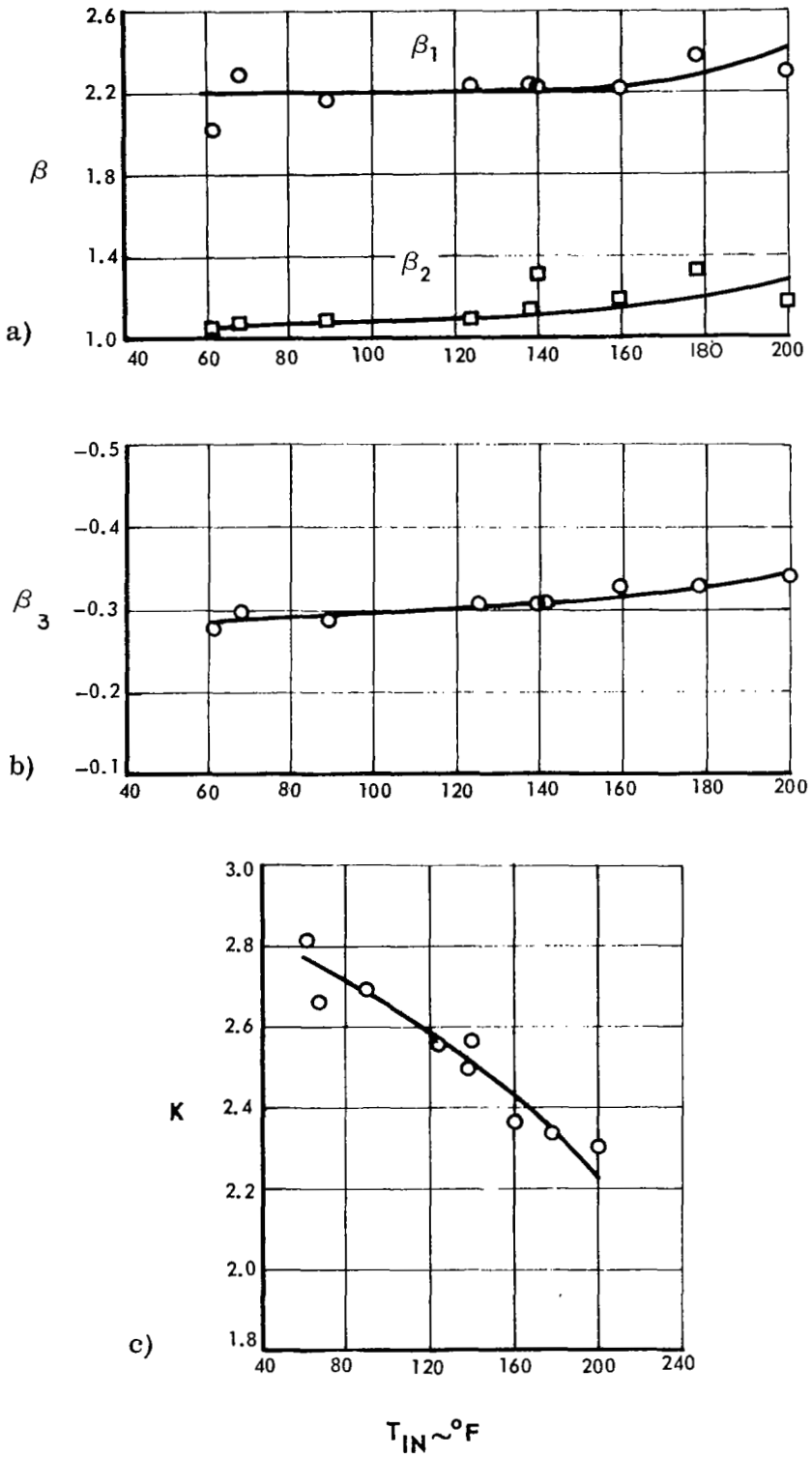


Figure 72 Variation of Boiler Parameters with Boiling-Fluid Inlet Temperature
W = 45 lb/hr $W_H$ = 770 lb/hr T.S. valve at nominal setting $T_{H\,in}$= 410°F

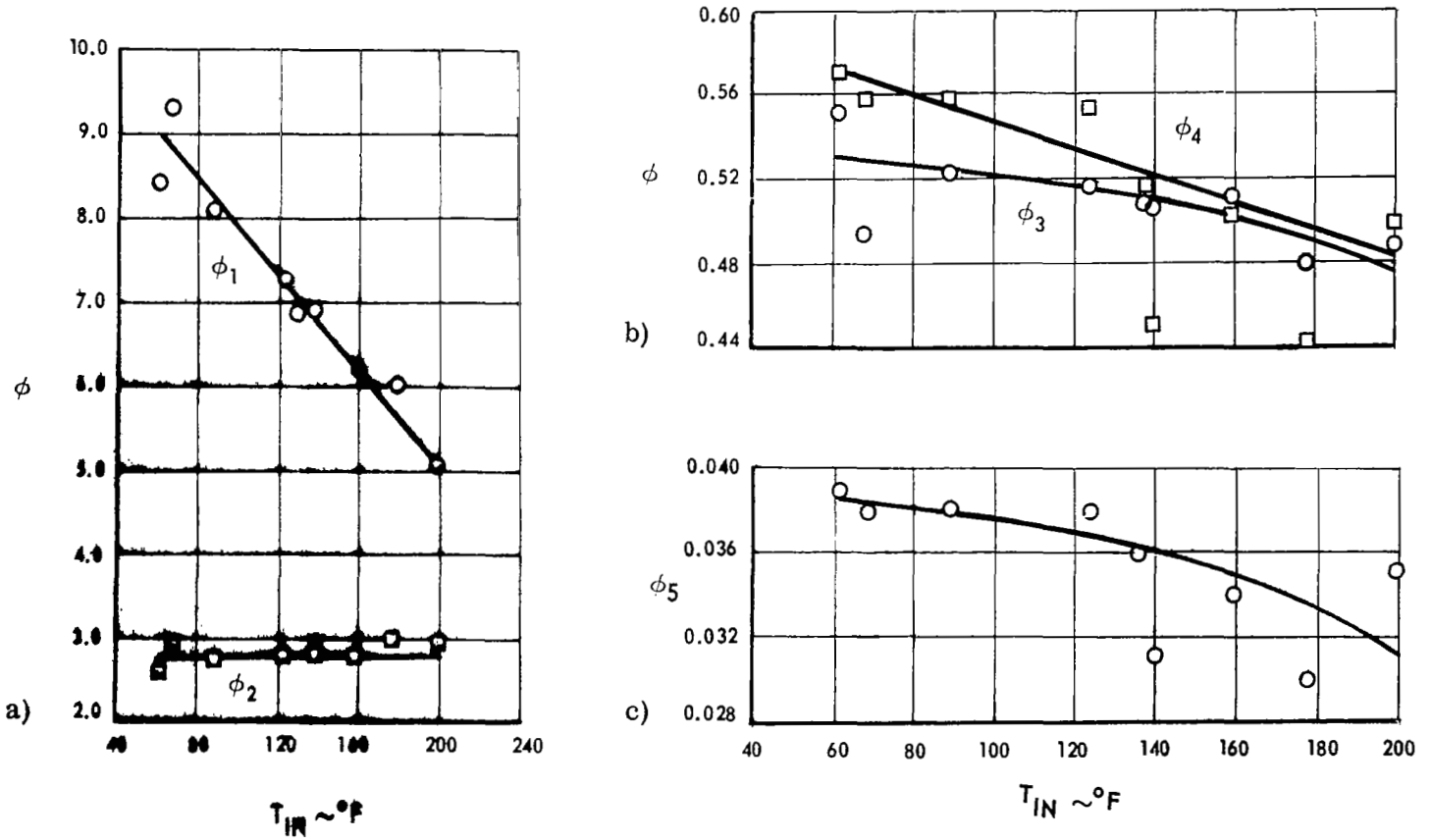


**Figure 73 Variation** of Boiler Parameters with Boiling-Fluid Inlet Temperature
$W$ = 45 lb/hr $W_H$ = 770 lb/hr T.S. valve at nominal setting $T_{H\ in}$ = 410°F

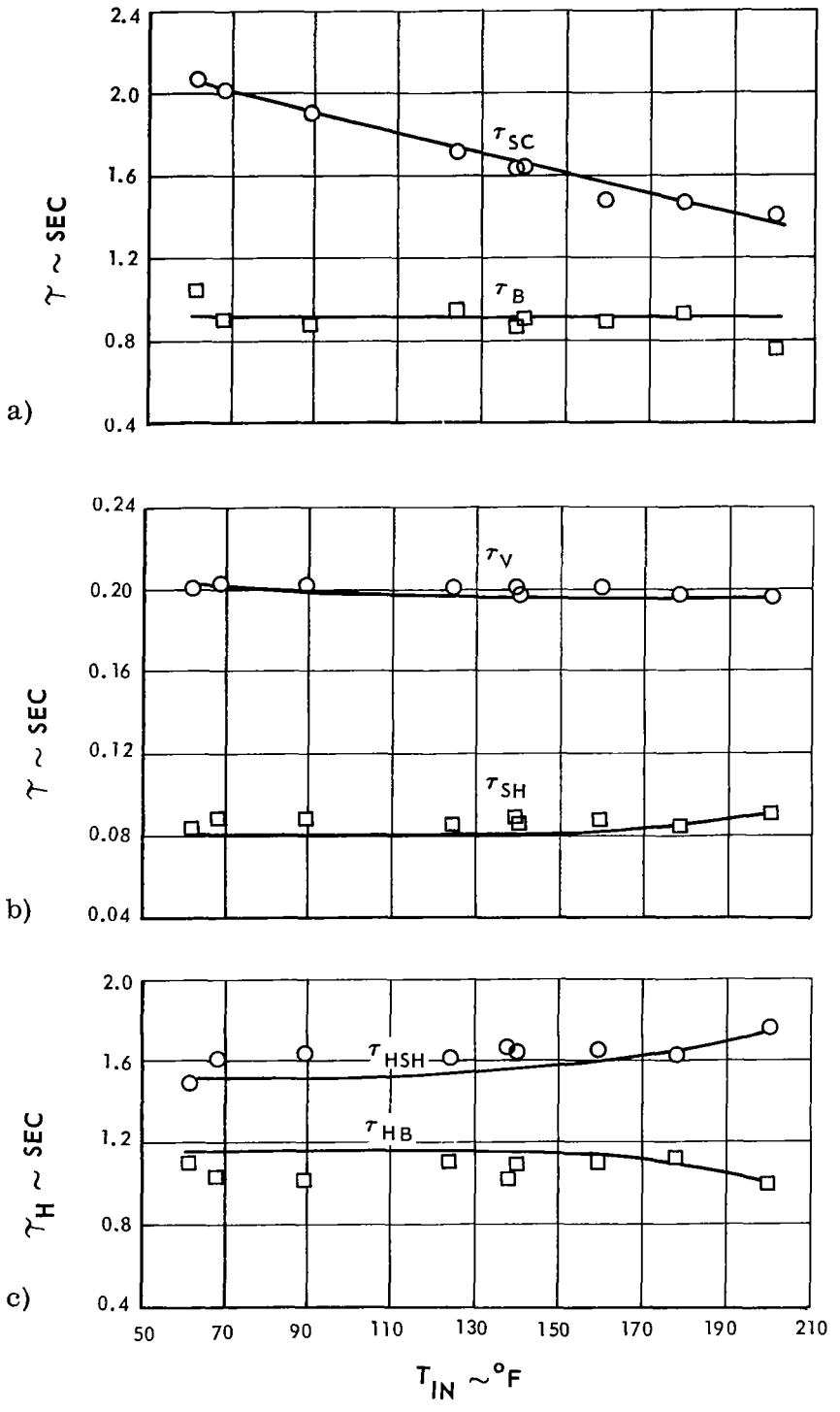


Figure 74 Variation of Boiler Parameters with Boiling-Fluid Inlet Temperature
W = 45 lb/hr $W_H$ = 770 lb/hr T.S. valve at nominal setting $T_{H\ in}$ = 410°F

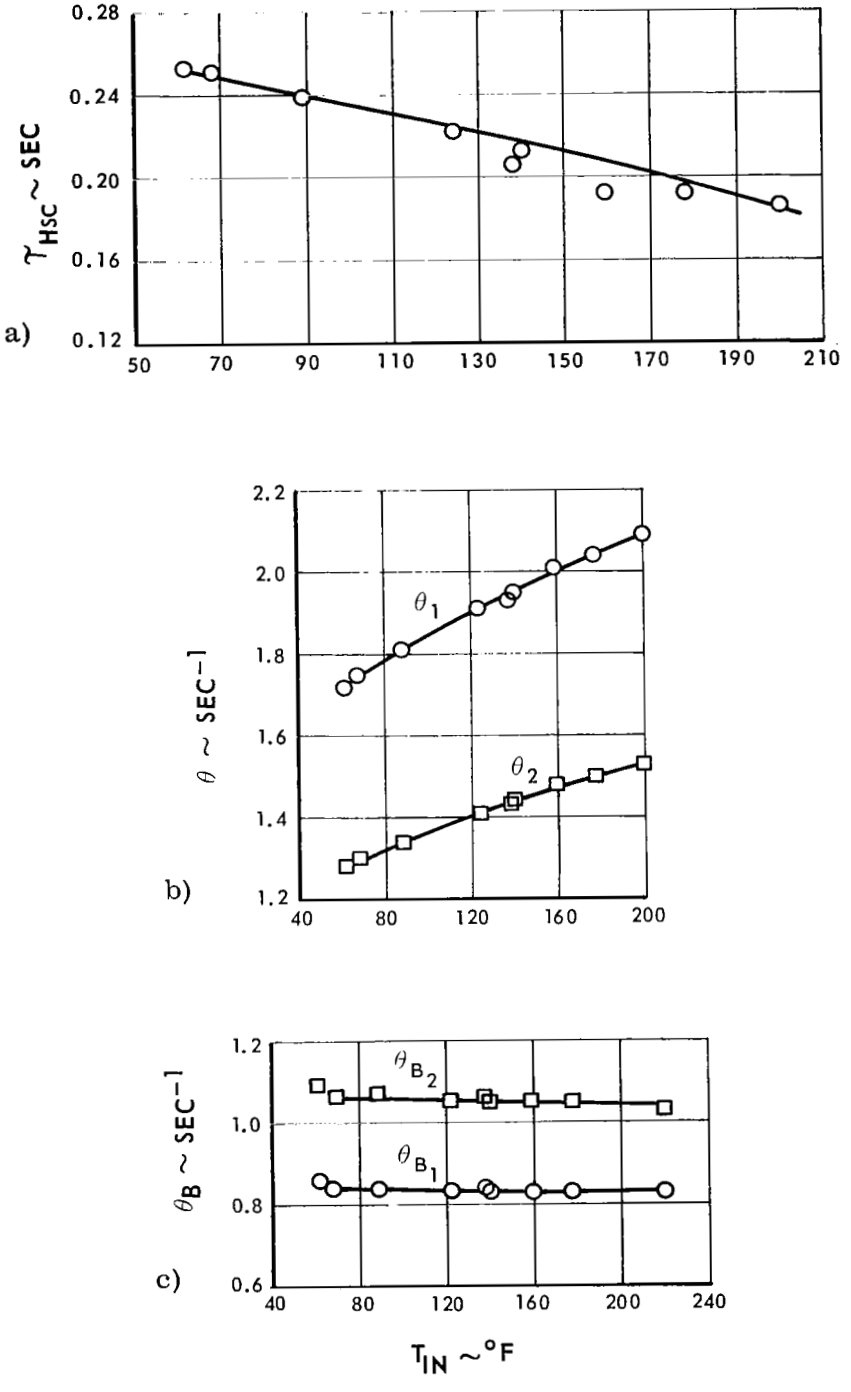


Figure 75 Variation of Boiler Parameters with Boiling-Fluid Inlet Temperature
W = 45 lb/hr $W_H$ = 770 lb/hr T.S. valve at nominal setting $T_{H\,in}$ = 410°F

# APPENDIX 4

## Tables

### TABLE 1

### Boiler Thermocouple Locations

#### Boiler Shell

| Thermocouple Number | *Distance, Inches | Thermocouple Number | Distance, Inches |
|---|---|---|---|
| 1 | 6 | 11 | 60 |
| 2 | 12 | 12 | 66 |
| 3 | 15 | 13 | 72 |
| 4 | 18 | 14 | 78 |
| 5 | 24 | 15 | 84 |
| 6 | 30 | 16 | 90 |
| 7 | 36 | 17 | 96 |
| 8 | 42 | 18 | 102 |
| 9 | 48 | 19 | 108 |
| 10 | 54 | 20 | 114 |

#### Boiler Plug Insert

| | | | |
|---|---|---|---|
| 1 | 3.6 | 5 | 14.4 |
| 2 | 7.2 | 6 | 16.3 |
| 3 | 9.6 | 7 | 20.4 |
| 4 | 12.0 | 8 | 22.8 |

#### Thermocouple Probe

| | |
|---|---|
| 1 | 30 |
| 2 | 60 |
| 3 | 84 |
| 4 | 96 |
| 5 | 108 |

*Axial distances from base of spiralled plug insert

# TABLE 2

## Test System Instrumentation

| | Location | Type | Make and Model | Range | Estimated Accuracy | Estimated Time Constant |
|---|---|---|---|---|---|---|
| Temperatures | (See Figure 4) $T_6$, $T_7$, $T_8$, $T_9$, $T_{10}$, $T_{11}$, $T_{12}$, $T_{13}$, T14 | thermocouple | 1/16" chromel-alumel sheathed sealed junction | - | ±1.5°F | 100 millisec. |
| | $T_2$ $T_4$ | thermocouple | 0.020" chromel-alumel sheathed exposed junction | - | ±1.5°F | 40 millisec. |
| | $T_3$ | thermocouple | 0.20" chromel-alumel sheathed sealed junction | - | ±1.5°F | 200 millisec. |
| | $T_1$ $T_5$ | thermocouple | 1/32" chromel-alumel sheathed sealed junction | - | ±1.5°F | 75 millisec. |
| Pressures<br>A. Transients | $P_{t1}$ | strain gage transducer | CEC Model 4-316-0001 | 0-150 psig | ±1.3% F.R. | 1 millisec. |
| | $P_{t2}$ | strain gage transducer | CEC Model 4-316-0001 | 0-150 psig | ±1.0% F.R. | 1 millisec. |
| | $P_{t3}$ | strain gage transducer | CEC Model 4-326-0003 | 0-40 psig | ±1.5% F.R. | 1 millisec. |
| | $P_{t4}$ | strain gage transducer | CEC Model 4-312-0001 | ±25 psid | ±1.0% F.R. | - |
| B. Steady State | $P_1$ | Bourdon-tube gage | Heise 16" with Auto Thermal Compensator | 0-200 psig | ±0.1% F.R. | - |
| | $P_2$ | Bourdon-tube gage | Heise 16" with Auto Thermal Compensator | 0-150 psig | ±0.1% F.R. | - |
| | $P_3$, $P_4$ | Bourdon-tube gage | Helicoid Type 410 4-1/2" | -30"-30 psig | ±1.5% F.R. | - |
| | $P_5$ | Bourdon-tube gage | Helicoid Type 410 4-1/2" | 0-200 psig | ±1.5% F.R. | - |
| | $P_6$, $P_8$ | Bourdon-tube gage | Barton Instrument 5-1/2" | 0-15 psid | ±1.5% F.R. | - |
| | $P_7$ | Bourdon-tube gage | Barton Instrument 3" | 0-70 psid | ±2.0% F.R. | - |
| | $P_9$, $P_{10}$ | Bourdon-tube gage | Helicoid Type 410 4-1/2" | 0-1000 psig | ±1.5% F.R. | - |
| | $P_{11}$ | Bourdon-tube gage | Helicoid Type 410 4-1/2" | 0-200 psig | ±1.5% F.R. | - |
| Flows | $F_1$, $F_2$ | turbine flowmeter | Potter, Model 60-4115 Micro Flowmeter | 20-200 pph | ±0.25% repeatability<br>±1.0% F.R. linearity | 5 millisec. |
| | $F_3$, $F_4$ | turbine flowmeter | Fischer & Porter, Model 10C 1505, 1/2 - 4 | 100-5000 pph | ±1.5% F.R. | |
| | $O_1$ | orifice | P & WA | 45 lb/hr at 0.5 psi | | |
| | $O_2$ | orifice | P & WA | 1100 lb/hr at 15 psi | | |
| | $O_3$ | orifice | P & WA | 400 lb/hr at 60 psi | | |
| Auxiliary Equip. | 1 | flowmeter frequency translator | P&WA Model 1158-004 | 0-200 & 0-1000 pph | ±1.0% F.R. | 20-25 millisec. |
| | | thermocouple translator | P&WA Model 851-1 | 150°F ref. | ±2.0% F.R. | |
| | | pressure pickup power supply | P&WA Model 840-20 | 0-12 vdc | | |
| | | frequency generator | Wavetek Model 112 | 0.0015 Hz-10 $KH_z$ | 0.5% F.R. | |
| | | recording oscillo-graph | CEC., 50 Channel Model T5-119 | | 3.0% absolute<br>1.0% variation | |
| | | T.C. readout potentiometer | Brown Model 156 Vertical Scale | 0-600°F | ±0.2% F.R. | |

TABLE 3

Operating Conditions for Steady-State Tests

| Heating-Fluid Inlet Temperature, °F | Heating-Fluid Flow Rate, lb/hr | Boiling-Fluid Flow Rate, lb/hr | Boiling-Fluid Inlet Temperature, °F | Boiling-Fluid Exit Pressure, psia |
|---|---|---|---|---|
| 360 | 770 | 45 | 140 | * |
| 375 | 770 | 45 | 140 | * |
| 390 | 770 | 45 | 140 | * |
| 420 | 770 | 45 | 140 | * |
| 425 | 770 | 45 | 140 | * |
| 430 | 770 | 45 | 140 | * |
| 410 | 400 | 45 | 140 | * |
| 410 | 500 | 45 | 140 | * |
| 410 | 600 | 45 | 140 | * |
| 410 | 840 | 45 | 140 | * |
| 410 | 910 | 45 | 140 | * |
| 410 | 1000 | 45 | 140 | * |
| 410+ | 770+ | 25+ | 140+ | *+ |
| 410 | 770 | 30 | 140 | * |
| 410 | 770 | 40 | 140 | * |
| 410** | 770** | 45** | 140** | 65** |
| 410 | 770 | 55 | 140 | * |
| 410 | 770 | 60 | 140 | * |
| 410 | 770 | 65 | 140 | * |
| 410 | 770 | 70 | 140 | * |
| 410 | 770 | 80 | 140 | * |
| 410 | 770 | 100 | 140 | * |

TABLE 3 (CONTINUED)

Operating Conditions for Steady-State Tests

| Heating-Fluid Inlet Temperature, °F | Heating-Fluid Flow Rate, lb/hr | Boiling-Fluid Flow Rate, lb/hr | Boiling-Fluid Inlet Temperature, °F | Boiling-Fluid Exit Pressure, psia |
|---|---|---|---|---|
| 410 | 770 | 45 | 60 | * |
| 410 | 770 | 45 | 90 | * |
| 410 | 770 | 45 | 120 | * |
| 410 | 770 | 45 | 160 | * |
| 410 | 770 | 45 | 180 | * |
| 410 | 770 | 45 | 200 | * |
| 410 | 770 | 45 | 140 | 40 |
| 410 | 770 | 45 | 140 | 50 |
| 410 | 770 | 45 | 140 | 60 |
| 410 | 770 | 45 | 140 | 90 |
| 410 | 770 | 45 | 140 | 110 |
| 410 | 770 | 45 | 140 | 130 |

*Value determined by setting of turbine simulator valve at nominal operating conditions
**Nominal operating conditions
+Unstable operating region (see Section VI of report)

TABLE 4

Variables Recorded by Oscillograph

| Variable | Range |
|---|---|
| boiling-fluid flow rate W | 13-72 lb/hr |
| boiling-fluid inlet pressure $P_{in}$ | 0-120 psig |
| boiling-fluid exit pressure $P_{out}$ | 0-150 psig |
| boiling-fluid inlet temperature $T_{in}$ | 60-220°F |
| boiling-fluid exit temperature $T_{out}$ | 320-430°F |
| electrohydraulic valve position | 0-100% of full stroke |
| power-loop orifice pressure drop | 0-10 psid |
| heating-fluid flow rate $W_H$ | 240-1000 lb/hr |
| heating-fluid inlet temperature $T_{H\,in}$ | 320-430°F |
| heating-fluid exit temperature $T_{H\,out}$ | 320-430°F |
| boiling-fluid condenser inlet temperature | 250-400°F |
| boiling-fluid condenser exit temperature | 65-200°F |
| boiling-fluid condenser inlet pressure | 0-40 psig |
| condenser coolant flow rate | 120-800 lb/hr |
| condenser coolant inlet temperature | 30-75°F |
| condenser coolant exit temperature | 80-200°F |

TABLE 5

Operating Conditions for Dynamic Tests

| Heating-Fluid Inlet Temperature, °F | Heating-Fluid Flow Rate, lb/hr | Boiling-Fluid Flow Rate (mean), lb/hr | Boiling-Fluid Inlet Temperature, °F | Boiling-Fluid Exit Pressure (mean), psia | Screening Test Runs |
|---|---|---|---|---|---|
| 360 | 770 | 45 | 140 | * | no |
| 390 | 770 | 45 | 140 | * | no |
| 420 | 770 | 45 | 140 | * | no |
| 430 | 770 | 45 | 140 | * | no |
| 410 | 400 | 45 | 140 | * | yes |
| 410 | 600 | 45 | 140 | * | yes |
| 410 | 840 | 45 | 140 | * | no |
| 410 | 1000 | 45 | 140 | * | no |
| 410 | 770 | 35 | 140 | * | yes |
| 410 | 770 | 40 | 140 | * | yes |
| 410 | 770 | 55 | 140 | * | yes |
| 410 | 770 | 65 | 140 | * | yes |
| 410 | 770 | 45 | 95 | * | no |
| 410 | 770 | 45 | 120 | * | no |
| 410 | 770 | 45 | 160 | * | no |
| 410 | 770 | 45 | 185 | * | no |
| 410 | 770 | 45 | 140 | 50 | yes |
| 410 | 770 | 45 | 140 | 60 | yes |
| 410** | 770** | 45** | 140** | 65** | yes |
| 410 | 770 | 45 | 140 | 100 | yes |
| 410 | 770 | 45 | 140 | 130 | yes |

*Value determined by setting of turbine simulator valve at nominal operating conditions
**Nominal operating conditions

TABLE 6

Steady-State Test Results - Variation of Boiling-Fluid Flow Rate

| Point No. | Boiling-Fluid Flow Rate, lb/hr W | Heating-Fluid Flow Rate, lb/hr $W_H$ | Boiling-Fluid Inlet Temp., °F $T_{in}$ | Heating-Fluid Inlet Temp., °F $T_{H\,in}$ | Boiling-Fluid Exit Pressure, psia $P_{out}$ | Boiling-Fluid Pressure Drop, psi $\Delta P_B$ | Boiling-Fluid Exit Temp., °F $T_{out}$ | Heating-Fluid Exit Temp., °F $T_{H\,out}$ | Pinch-Point Temp. Difference, °F $\Delta T_P$ | Boiling-Fluid Superheat, °F $\Delta T_{SH}$ | Boiling-Fluid Exit Quality $X_e$ | Heat Balance Btu/hr × $10^{-3}$ | | Length of Subcooled Region, ft $L_{SC}$ | Distance to End of Boiling Region, ft $L_B$ |
|---|---|---|---|---|---|---|---|---|---|---|---|---|---|---|---|
| | | | | | | | | | | | | Q Boiler Shell | Q Cond Shell | | |
| 1 | 30 | 762 | 140 | 410 | 47.4 | 39.4 | 401.5 | 369.5 | 50 | 124 | 1.000 | 33.1 | 32.7 | 0.48 | 2.08 |
| 2 | 35 | 767 | 140 | 409.5 | 52.7 | 35.2 | 402 | 364 | 48 | 117 | 1.000 | 37.6 | 38.0 | 0.55 | 3.07 |
| 3 | 39.7 | 765 | 140 | 410 | 60 | 28.9 | 392 | 356 | 36 | 99 | 1.000 | 44.2 | 43.3 | 0.62 | 3.46 |
| 4 | 40 | 764.8 | 140 | 410 | 60.1 | 30.1 | 398 | 357 | 40 | 105 | 1.000 | 43.4 | 44.2 | 0.63 | 3.96 |
| 5 | 44.1 | 767.5 | 139 | 410 | 64.5 | 26.2 | 350.5 | 351 | 34 | 53 | 1.000 | 48.7 | 49.6 | 0.72 | 4.65 |
| 6 | 44.5 | 767 | 139 | 409.5 | 64.7 | 25.8 | 350 | 352.5 | 34 | 52 | 0.982 | 47.0 | 47.0 | 0.72 | 4.80 |
| 7 | 44.6 | 765 | 140 | 411 | 64.5 | 24.8 | 343 | 351.5 | 34 | 46 | 1.000 | 48.7 | 47.3 | 0.71 | 4.62 |
| 8 | 44.8 | 765 | 140 | 411 | 64.4 | 25.3 | 350 | 352 | 33 | 53 | 1.000 | 48.3 | 47.4 | 0.74 | 4.26 |
| 9 | 44.8 | 765 | 140 | 410 | 64.9 | 24.1 | 347 | 350 | 32 | 50 | 1.000 | 49.1 | 48.5 | 0.80 | 4.62 |
| 10 | 49.6 | 760.8 | 140 | 410 | 68.4 | 22 | 344 | 344 | 30 | 43 | 1.000 | 53.4 | 52.4 | 0.80 | 7.00 |
| 11 | 49.8 | 770.8 | 140 | 410 | 69.7 | 22.6 | 347 | 347 | 32 | 44 | 0.963 | 51.8 | 53.8 | 0.77 | 6.60 |
| 12 | 54.5 | 760 | 140 | 409.5 | 74.7 | 18 | 343 | 340 | 25 | 35.4 | 0.965 | 56.8 | 58.5 | 1.05 | 8.43 |
| 13 | 55.3 | 762 | 142 | 409 | 74.5 | 17.7 | 343 | 339 | 23 | 36 | 0.951 | 56.8 | 57.3 | 0.99 | 8.63 |
| 14 | 59.4 | 767.8 | 140 | 410 | 78.4 | 15.8 | 330 | 335 | 20 | 20 | 0.948 | 61.0 | 60.4 | 1.00 | 9.43 |
| 15 | 59.6 | 770.8 | 140 | 410 | 80.8 | 14.1 | 333 | 337 | 22 | 20 | 0.920 | 59.8 | 61.5 | 1.06 | 9.50 |
| 16 | 60 | 765 | 141.5 | 410 | 79 | 15.7 | 335 | 335 | 20 | 24 | 0.932 | 60.7 | 59.9 | 1.01 | 9.34 |
| 17 | 64.6 | 765 | 142 | 409.5 | 83 | 12.9 | 318 | 332 | 20 | 3.5 | 0.892 | 63.1 | 61.9 | 1.32 | 10.00 |
| 18 | 70.7 | 767.5 | 141 | 410 | 87.1 | 11.9 | 320.5 | 331 | 18.5 | 2.5 | 0.819 | 64.6 | 65.9 | 1.44 | 10.00 |
| 19 | 79.7 | 770.8 | 141 | 410 | 89.3 | 11.4 | 323 | 330.5 | 18 | 4 | 0.712 | 65.3 | 66.3 | 1.60 | 10.00 |
| 20 | 100.2 | 760.8 | 140 | 410 | 91.6 | 12 | 325 | 327.5 | 18 | 3.0 | 0.542 | 67.1 | 66.9 | 1.95 | 10.00 |

TABLE 7

Steady-State Test Results - Variation Of Heating-Fluid Flow Rate

| Point No. | Boiling-Fluid Flow Rate, lb/hr W | Heating-Fluid Flow Rate, lb/hr $W_H$ | Boiling-Fluid Inlet Temp., °F $T_{in}$ | Heating-Fluid Inlet Temp., °F $T_{H\,in}$ | Boiling-Fluid Exit Pressure, psia $P_{out}$ | Boiling-Fluid Pressure Drop, psi $\Delta P_B$ | Boiling-Fluid Exit Temp., °F $T_{out}$ | Heating-Fluid Exit Temp., °F $T_{H\,out}$ | Pinch-Point Temp. Difference, °F $\Delta T_P$ | Boiling-Fluid Superheat, °F $\Delta T_{SH}$ | Boiling-Fluid Exit Quality $X_e$ | Heat Balance $Btu/hr \times 10^{-3}$ | | Length of Subcooled Region, ft $L_{SC}$ | Distance to End of Boiling Region, ft $L_B$ |
|---|---|---|---|---|---|---|---|---|---|---|---|---|---|---|---|
| | | | | | | | | | | | | Q Boiler Shell | Q Cond Shell | | |
| 21 | 44.5 | 391.4 | 140 | 410 | 56.2 | 12.6 | 331 | 311 | 20 | 43 | 0.843 | 41.2 | 44.2 | 1.00 | 9.25 |
| 22 | 44.0 | 391.8 | 139 | 411 | 58.2 | 11.0 | 321 | 308.5 | 19 | 30.3 | 0.888 | 42.6 | 45.9 | 1.05 | 9.70 |
| 23 | 44.7 | 395 | 140 | 410 | 60 | 9.5 | 321 | 307 | 17 | 28.3 | 0.914 | 44.3 | 45.1 | 1.20 | 10.0 |
| 24 | 44.5 | 400 | 139 | 411 | 58.7 | 11.0 | 310 | 310 | 20 | 18.4 | 0.880 | 42.8 | 44.7 | 1.20 | 10.0 |
| 25 | 44.5 | 500 | 140.5 | 409 | 61.4 | 14.8 | 336 | 324 | 22 | 42 | 0.941 | 45.2 | 46.2 | 0 91 | 7.36 |
| 26 | 44.5 | 501 | 140 | 411.5 | 60.7 | 15.6 | 336 | 325 | 25 | 42.5 | 0.962 | 46.1 | 47.6 | 0.91 | 8.10 |
| 27 | 44.5 | 594 | 140 | 409 | 61.6 | 19.4 | 340 | 336 | 31 | 45.0 | 0.962 | 46.2 | 46.7 | 0.82 | 7.28 |
| 28 | 44.5 | 596 | 141.5 | 409 | 61.2 | 19.7 | 338 | 336 | 28 | 44.2 | 0.958 | 45.9 | 48.4 | 0.85 | 6.78 |
| 29 | 44.6 | 604 | 141 | 410 | 62.1 | 20.1 | 342 | 337.5 | 28 | 47 | 0.976 | 46.7 | 46.7 | 0.78 | 5.43 |
| 30 | 44.6 | 755 | 138 | 410.5 | 64.1 | 27.0 | 336 | 352 | 33 | 36 | 0.991 | 47.5 | 47.8 | 0.70 | 4.65 |
| 31 | 44.5 | 758 | 140 | 409.5 | 64.2 | 25.8 | 349 | 351 | 33 | 50 | 0.994 | 47.4 | 47.7 | 0.70 | 4.49 |
| 32 | 44.5 | 835 | 141.5 | 411 | 65.3 | 28.6 | 372 | 358 | 34 | 74 | 0.975 | 46.6 | 48.0 | 0.69 | 3.84 |
| 33 | 44.5 | 853.9 | 139.5 | 410 | 64.4 | 28.4 | 356.5 | 355 | 33 | 59.5 | 1.000 | 50.6 | 47.8 | 0.69 | 4.20 |
| 34 | 44.5 | 856 | 140 | 409 | 65.3 | 28.9 | 366 | 355 | 35 | 67.7 | 1.000 | 49.6 | 48.5 | 0.73 | 4.30 |
| 35 | 44.4 | 890 | 142 | 409.5 | 65 | 29.7 | 374 | 359 | 32 | 76 | 1.000 | 48.2 | 48.4 | 0.67 | 3.95 |
| 36 | 44.3 | 899.9 | 139.5 | 410 | 66.4 | 29.9 | 379 | 359 | 37 | 79.6 | 1.000 | 49.7 | 49.2 | 0.70 | 4.08 |
| 37 | 44.7 | 955 | 139 | 409 | 67.2 | 29.0 | 390.5 | 362 | 36 | 90.3 | 1.000 | 49.9 | 48.5 | 0.67 | 4.00 |
| 38 | 44.3 | 1019 | 139 | 411 | 68.4 | 32.3 | 396 | 366 | 40 | 95 | 1.000 | 49.1 | 49.0 | 0.65 | 4.05 |

TABLE 8

Steady-State Test Results - Variation of Heating-Fluid Inlet Temperature

| Point No. | Boiling-Fluid Flow Rate, lb/hr W | Heating-Fluid Flow Rate, lb/hr $W_H$ | Boiling-Fluid Inlet Temp., °F $T_{in}$ | Heating-Fluid Inlet Temp., °F $T_{H\,in}$ | Boiling-Fluid Exit Pressure, psia $P_{out}$ | Boiling-Fluid Pressure Drop, psi $\Delta P_B$ | Boiling-Fluid Exit Temp., °F $T_{out}$ | Heating-Fluid Exit Temp., °F $T_{H\,out}$ | Pinch-Point Temp. Difference, °F $\Delta T_P$ | Boiling-Fluid Superheat, °F $\Delta T_{SH}$ | Boiling-Fluid Exit Quality $X_e$ | Heat Balance Btu/hr × $10^{-3}$ Q Boiler Shell | Heat Balance Btu/hr × $10^{-3}$ Q Cond Shell | Length of Subcooled Region, ft $L_{SC}$ | Distance to End of Boiling Region, ft $L_B$ |
|---|---|---|---|---|---|---|---|---|---|---|---|---|---|---|---|
| 39 | 44.3 | 768.3 | 139.5 | 360 | 57.5 | 9.5 | 293 | 309 | 12 | 3 | 0.841 | 41.0 | 43.2 | 1.0 | 10 |
| 40 | 44.6 | 774 | 141.5 | 360.5 | 58.2 | 9.4 | 294 | 308 | 11 | 23.2 | 0.875 | 42.5 | 42.2 | 0.93 | 10 |
| 41 | 44.5 | 776 | 141 | 374.5 | 59.2 | 14.4 | 315 | 321 | 18 | 23.2 | 0.908 | 43.8 | 45.6 | 0.91 | 8.37 |
| 42 | 44.3 | 766 | 140 | 375.5 | 60.2 | 15.2 | 318 | 320 | 17 | 25 | 0.932 | 44.7 | 44.2 | 0.92 | 8.27 |
| 43 | 44.4 | 767 | 140.5 | 390 | 61.7 | 18.3 | 330 | 333 | 24 | 36 | 0.971 | 46.3 | 45.6 | 0.75 | 6.14 |
| 44 | 44.3 | 773 | 138 | 391 | 61.1 | 19.4 | 330 | 335 | 27 | 36.1 | 0.959 | 45.8 | 46.5 | 0.87 | 6.77 |
| 45 | 44.6 | 765 | 139.5 | 410 | 64.6 | 25.3 | 350 | 351 | 32 | 53 | 1.000 | 48.3 | 47.1 | 0.71 | 4.39 |
| 46 | 44.6 | 762 | 141 | 410 | 64.8 | 25.4 | 357 | 350.5 | 31 | 50 | 1.000 | 48.5 | 48.2 | 0.71 | 4.38 |
| 47 | 44.5 | 759 | 140 | 419 | 66.7 | 29.0 | 383 | 358 | 35 | 83.3 | 1.000 | 49.1 | 48.5 | 0.68 | 3.84 |
| 48 | 44.5 | 776.9 | 141 | 420 | 66.2 | 29.7 | 379.5 | 359 | 37.5 | 80.5 | 1.000 | 51.3 | 48.6 | 0.70 | 3.93 |
| 49 | 44.8 | 759 | 140 | 421 | 67.5 | 28.4 | 399 | 361 | 36 | 99 | 1.000 | 49.1 | 49.1 | 0.67 | 4.00 |
| 50 | 44.5 | 768 | 139.5 | 425.5 | 67.9 | 30.8 | 409 | 365.5 | 38 | 108 | 1.000 | 49.8 | 48.9 | 0.66 | 3.57 |
| 51 | 44.4 | 768 | 141 | 429 | 67.9 | 32.5 | 416.5 | 369.5 | 40 | 116 | 1.000 | 49.5 | 48.9 | 0.66 | 3.44 |
| 52 | 44.3 | 759.3 | 139 | 430 | 70.8 | 29.6 | 409 | 368 | 42 | 105 | 1.000 | 50.9 | 49.6 | 0.70 | 3.93 |

TABLE 9

Steady-State Test Results - Variation of Boiling-Fluid Inlet Temperature

| Point No. | Boiling-Fluid Flow Rate, lb/hr W | Heating-Fluid Flow Rate, lb/hr $W_H$ | Boiling-Fluid Inlet Temp., °F $T_{in}$ | Heating-Fluid Inlet Temp., °F $T_{H\,in}$ | Boiling-Fluid Exit Pressure, psia $P_{out}$ | Boiling-Fluid Pressure, Drop, psi $\Delta P_B$ | Boiling-Fluid Exit Temp., °F $T_{out}$ | Heating-Fluid Exit Temp., °F $T_{H\,out}$ | Pinch-Point Temp Difference, °F $\Delta T_P$ | Boiling-Fluid Superheat, °F $\Delta T_{SH}$ | Boiling-Fluid Exit Quality $X_e$ | Heat Balance $Btu/hr \times 10^{-3}$ Q Boiler Shell | Heat Balance $Btu/hr \times 10^{-3}$ Q Cond Shell | Length of Subcooled Region, ft $L_{SC}$ | Distance to End of Boiling Region, ft $L_B$ |
|---|---|---|---|---|---|---|---|---|---|---|---|---|---|---|---|
| 53 | 44.3 | 784 | 61.5 | 409 | 65.7 | 22.0 | 346 | 344.5 | 35 | 48 | 1.000 | 54.0 | 53.9 | 0.86 | 4.74 |
| 54 | 44.2 | 767 | 68 | 409.5 | 66.0 | 23.4 | 348 | 346.5 | 31 | 49 | 1.000 | 51.7 | 51.5 | 0.84 | 4.42 |
| 55 | 44.5 | 769 | 89 | 409.5 | 66.0 | 23.9 | 348 | 348 | 33 | 49 | 1.000 | 50.6 | 49.7 | 0.80 | 4.34 |
| 56 | 44.6 | 761 | 124 | 409 | 65.3 | 24.9 | 348 | 350 | 32 | 50 | 0.990 | 48.1 | 49.2 | 0.73 | 4.50 |
| 57 | 44.2 | 767 | 138 | 410 | 64.7 | 26.3 | 352 | 353 | 32 | 56 | 0.985 | 46.8 | 48.1 | 0.69 | 4.23 |
| 58 | 44.6 | 761 | 140 | 409.5 | 64.4 | 26.5 | 359 | 352.5 | 32 | 62 | 0.966 | 46.4 | 46.8 | 0.70 | 4.41 |
| 59 | 44.5 | 758 | 159.5 | 409 | 64.7 | 26.2 | 353 | 353 | 32 | 56 | 0.967 | 45.5 | 45.7 | 0.63 | 4.36 |
| 60 | 44.5 | 758 | 178 | 410 | 64.0 | 27.4 | 360 | 355.5 | 30 | 63 | 0.959 | 44.3 | 45.5 | 0.63 | 4.45 |
| 61 | 44.8 | 761 | 200 | 410 | 64.6 | 26.2 | 353.5 | 355 | 31 | 56 | 0.998 | 45.2 | 43.4 | 0.61 | 4.00 |

TABLE 10

Steady-State Test Results - Variation Of Boiling-Fluid Exit Pressure

| Point No. | W | $W_H$ | $T_{in}$ | $T_{H\,in}$ | $P_{out}$ | $\Delta P$ | $T_{out}$ | $T_{H\,out}$ | $\Delta T_P$ | $\Delta T_{SH}$ | $X_e$ | Q Boiler Shell | Q Cond Shell | $L_{SC}$ | $L_B$ |
|---|---|---|---|---|---|---|---|---|---|---|---|---|---|---|---|
| 62 | 44.7 | 779 | 141 | 410 | 43.1 | 40.2 | 396 | 351.5 | 37 | 124 | 1.000 | 48.8 | 49.2 | 0.62 | 3.46 |
| 63 | 44.8 | 779 | 139 | 410 | 50.3 | 35.0 | 388 | 351 | 34 | 107 | 1.000 | 49.2 | 49.6 | 0.65 | 3.75 |
| 64 | 44.7 | 779 | 140 | 409 | 63.0 | 27.1 | 367 | 351 | 32 | 71 | 1.000 | 48.4 | 49.0 | 0.68 | 4.38 |
| 65 | 45.0 | 782 | 140 | 410 | 63.7 | 26.2 | 368 | 353 | 31 | 73 | 0.988 | 47.7 | 48.6 | 0.67 | 4.26 |
| 66 | 44.7 | 779 | 139 | 410 | 64.1 | 27.3 | 364 | 352.5 | 32 | 67 | 1.000 | 47.9 | 49.0 | 0.67 | 4.19 |
| 67 | 44.7 | 782 | 141 | 410 | 89.9 | 15.0 | 348 | 354.5 | 25 | 28 | 0.959 | 46.5 | 46.0 | 0.72 | 5.86 |
| 68 | 44.8 | 782 | 140 | 410 | 109.8 | 9.9 | 353 | 356 | 21 | 19 | 0.919 | 45.2 | 45.5 | 0.93 | 8.30 |
| 69 | 44.8 | 782 | 140 | 410 | 136.5 | 5.0 | 353 | 358 | 12 | 2 | 0.872 | 43.6 | 43.2 | 1.21 | 10.0 |

TABLE 11

Normalizing Data (Amplitudes at Zero Frequency)

| Variable | $\Delta P_{in}/\Delta W$ psi/lb/hr | $\Delta P_{out}/\Delta W$ psi/lb/hr | $\Delta T_{H\ out}/\Delta W$ °F/lb/hr | $\Delta T_{out}/\Delta W$ °F/lb/hr |
|---|---|---|---|---|
| W, lb/hr | | | | |
| 35 | 0.190 | 1.30 | 1.30 | 1.0 |
| 40 | 0.230 | 1.15 | 1.28 | 3.7 |
| 45 | 0.200 | 1.05 | 1.14 | 5.3 |
| 55 | 0.306 | 0.93 | 0.83 | --- |
| 65 | 0.385 | 0.80 | 0.45 | --- |
| $W_H$, lb/hr | | | | |
| 400 | 0.212 | 0.915 | 1.35 | --- |
| 600 | 0.258 | 1.08 | 1.42 | --- |
| 770 | 0.200 | 1.05 | 1.15 | 5.3 |
| 840 | 0.224 | 1.12 | 1.12 | 5.9 |
| 1000 | 0.275 | 0.842 | 0.842 | 4.5 |
| $T_{H\ in}$, °F | | | | |
| 360 | 0.226 | 0.556 | 0.61 | --- |
| 390 | 0.250 | 0.950 | 1.10 | --- |
| 410 | 0.200 | 1.05 | 1.14 | 5.3 |
| 420 | 0.255 | 1.05 | 1.25 | 7.4 |
| 430 | 0.231 | 1.08 | 1.43 | 3.92 |
| $P_{out}$, psia | | | | |
| 50 | -0.02 | 0.840 | 1.15 | 6.82 |
| 60 | 0.160 | 0.950 | 1.16 | 7.24 |
| 65 | 0.200 | 1.05 | 1.14 | 5.3 |
| 100 | 1.08 | 1.86 | 1.18 | --- |
| 130 | 1.41 | 1.81 | 0.50 | --- |
| $T_{in}$, °F | | | | |
| 95 | 0.213 | 0.980 | 1.24 | 4.04 |
| 120 | 0.195 | 0.961 | 1.17 | 4.61 |
| 140 | 0.200 | 1.05 | 1.14 | 5.30 |
| 160 | 0.171 | 0.890 | 1.11 | 6.68 |
| 185 | 0.155 | 0.900 | 1.02 | 6.80 |

TABLE 12

Boiler Parameters Required for Theoretical Transfer Function

$$\beta_1 = \left( \frac{\partial T_{SAT} / \Delta T_{P,o}}{\partial P / P_{P,o}} \right)$$

$$\beta_2 = \left( \frac{\partial T_{SAT} / \Delta T_{OUT}}{\partial P / P_{OUT,o}} \right)$$

$$\beta_3 = \left( \frac{\partial \Delta P_B / P_{P,o}}{\partial L_{SC} / L_{SC,o}} \right)$$

$$\theta_1 = \frac{h_{SC} P_{PM}}{\rho_L A_{SC} C_P}$$

$$\theta_2 = \frac{h_{SC} P_{PM}}{\rho_{PM} A_{PM} C_{PPM}}$$

$$\theta_{B1} = \frac{h_H P_{SM}}{\rho_H A_H C_{PH}}$$

$$\theta_{B2} = \frac{h_H P_{SM}}{\rho_{SM} A_{SM} C_{PSM}}$$

$$K = \frac{\partial \left( \int_0^{L_e} \rho A \, dL \right)}{\partial \left( \rho_L A_{SC} L_{SC} \right)}$$

$n_{SC}$ = DEFINED BY $U_{SC} \propto V_{SC}^{n_{SC}}$

$n_{SH}$ = DEFINED BY $U_{SH} \propto V_{SH}^{n_{SH}}$

TABLE 12 (continued)

Boiler Parameters Required for Theoretical Transfer Function

$$\phi_1 = \frac{T_{HP,0} - T_{IN}}{\Delta T_{P,0}}$$

$$\phi_2 = \frac{T_{HIN} - T_{SAT,0}}{\Delta T_{P,0}}$$

$$\phi_3 = \frac{\Delta T_{P,0}}{\Delta T_M}$$

$$\phi_4 = \frac{\Delta T_{OUT}}{T_{HIN} - T_{SAT,0}}$$

$$\phi_5 = \frac{\Delta T_{OUT}}{2\, T_{OUT,0}}$$

$\tilde{\tau}_B$ = transport time of liquid particle in boiling region

$\tilde{\tau}_{HB}$ = heating-fluid transport time in boiling region

$\tilde{\tau}_{HSC}$ = heating-fluid transport time in subcooled region

$\tilde{\tau}_{SC}$ = subcooled liquid transport time

$\tilde{\tau}_V$ = vapor transport time

$\tilde{\tau}_{SH}$ = vapor transport time in superheat region

$\tilde{\tau}_{HSH}$ = heating-fluid transport time in superheat region



NASA-Langley, 1969 —— 12 E-4608